SQT

RELATIVE RADIOMETRIC CALIBRATION OF LANDSAT TM REFLECTIVE BANDS

John L. Barker

LANDSAT ASSOCIATE PROJECT SCIENTIST

EARTH RESOURCES BRANCH, CODE 923

NATIONAL AERONAUTICS AND SPACE ADMINISTRATION

GODDARD SPACE FLIGHT CENTER

GREENBELT, MARYLAND 20771

(301) 344-8978

(Revised 26 April 1984)

FORWARD

This paper presents results and recommendations pertaining to the characterization of the relative radiometric calibration of the protoflight Thematic Mapper (TM/PF) sensor. TM/PF is the primary experiment on the Landsat-4 satellite, launched on July 16, 1982. Some preliminary pre-launch and in-orbit results are also included from the flight model (TM/F) on Landsat-5, which was launched on March 1, 1984. The goals of this paper are:

- Outline a common scientific methodology and terminology for characterizing the radiometry of both TM sensors
- Report on the magnitude of the most significant sources of radiometric variability
- Recommend methods for achieving the exceptional potential inherent in the radiometric precision and accuracy of the TM sensors.

The radiometric characteristics of TM digital imagery that are important for scientific interpretation include mean values of absolute and relative calibration constants, and estimates of the uncertainty in the relative and absolute post-calibration radiances. Mean values and uncertainties in the pre-launch absolute radiometric calibration are discussed elsewhere (Barker, Ball, et al., 1984). This paper focuses on characterizing variability and uncertainty of TM relative radiometry, including total variability as well as its systematic and random components. Emphasis is placed on identifying the magnitude and types of systematic error, since these have the potential for being reduced during ground processing. Estimates of innate random variability, such as the standard deviation or a signal of

its signal-to-noise ratio, are also important since they place limits on the inferences that can be drawn from single and multiple pixel radiances. However, accurate estimates of random error require the prior removal of all types of systematic variability.

While the recommendations contain ideas from many people, including scientific investigators on NASA's team for characterizing the quality of the imagery from the sensors on Landsat-4 and Landsat-5, they are the creation and sole responsibility of the author. These recommendations have not been approved by either the Landsat Science Office or the Landsat Project. Evaluation, and possible implementation, of the recommendations will pose significant difficulties both during the research period before the transition of the TM Image Processing System (TIPS) from NASA to NOAA near the end of 1984, and afterwards, during the operational period.

TABLE OF CONTENTS (Cont'd)

PAGE iv INTENTIONALLY BLANK

TABLE OF CONTENTS (Cont'd)

LIST OF ILLUSTRATIONS

Figure

LIST OF TABLES

Table

LIST OF TABLES (Cont'd)

LIST OF TABLES (Cont'd)

SECTION 1 - INTRODUCTION

The Landsat system for observing the land areas of the surface of the Earth is composed of three elements: 1) the spacecraft with the sensors; 2) the ground-processing facilities and the image-processing software of that facility; and 3) the image distribution facility in Sioux Falls, South Dakota. This paper characterizes some of the radiometric aspects of the first two.

The first three Landsat spacecraft were modified meteorological satellites, carrying "old-reliable" return-beam vidicon television sensors and "experimental" multispectral scanner (MSS) imaging radiometers. In this configuration, they provided images of the surface of the Earth that have received wide use in atlases (Short, et al., 1976; Sheffield, 1981) and research (Colwell, 1983; Williams and Carter, 1976).

The last two Landsat spacecraft contain instrument packages mounted on the Multimission Modular Spacecraft (MMS), which can be retrieved using the shuttle transportation system (STS) (Salomonson and Park, 1979). The Multispectral Scanner (MSS) provides data continuity with previous Landsat satellites (Engel et al., 1983). Thematic Mapper (TM) is a new experimental system which is being evaluated as a possible replacement for MSS-type systems (Engel, 1980).

The TM, which was the principal experiment on Landsat-4, was intended to be a second-generation land-scanning radiometer. Since launch on July 16, 1982, the protoflight (PF) instrument on Landsat-4 has provided about 6000 scenes of northern North America through X-band direct-readout ground facilities located at Goddard Space Flight Center, Greenbelt, MD, and at Prince Albert, Canada. Additional images have been acquired through indirect satellite communication networks and by other X-band ground stations.

Images from the TM/PF sensor have met or exceeded expectations, and are "... of excellent quality as examined in image or CCT /computer readable/ form. Besides the excellent geometric qualities of the data, the spatial, spectral, and radiometric qualities of the TM data represent a capability substantially advanced over that provided by the MSS" (Salomonson and Mannheimer, 1983).

The TM sensor is designed to provide increased spectral, radiometric, and geometric performance (Engel et al., 1983). The primary improvement of the TM over MSS is in spatial resolution (Salomonson and Park, 1979). Each TM pixel represents a 30m by 30m area on the ground, instead of the 80m by 80m instanteous field-of-view for MSS. A second major improvement is in new and more precisely located spectral bands. Finally, TM has higher radiometric resolution, namely 8-bit precision as compared to 6-bit for MSS. These improvements are expected to provide many new and improved capabilities (Salomonson and Park, 1979), including:

- Mapping of coastal water areas to water depths of 20-40 meters
- Differentiation between soil and vegetation
- Biomass surveys
- Differentiation between coniferous and deciduous vegetation
- Differentiation between plant species
- Differentiation between clouds and snow cover
- Discrimination of hydrothermal alteration zones in rock units
- Studies of plant heat stress and rock-unit thermal characteristics.

Preliminary evaluation indicate that TM image products have "... spectral and spatial detail clearly surpassing that provided by ... MSS" (Salomonson and Koffler, 1983).

1.1 RADIOMETRIC CHARACTERIZATION

The radiometric characteristics of TM digital imagery that are important for scientific interpretation include mean values of absolute and relative calibration constants, and estimates of the uncertainty in the relative and absolute post-calibration radiances. Mean values and uncertainities in the pre-launch absolute radiometric calibration are discussed elsewhere (Barker, Ball et al., 1984). This paper focuses on characterizing variability and uncertainty of TM relative radiometry, including total variability, as well as both the systematic and random components. Emphasis is

placed on identifying the magnitude and types of systematic error, since these have the potential for being reduced during ground processing. Estimates of innate random variability, such as the standard deviation of a signal or its signal-to-noise ratio, are also important since they place limits on the inferences that can be drawn from single and multiple pixel radiances. However, accurate estimates of random error require the prior removal of all types of systematic variability.

1.2 POST-CALIBRATION DYNAMIC RANGE

Pre-launch absolute radiometric calibration of the reflective bands on TM-Flight instrument (TM/F) were used to identify the pre-calibration range of sensitivity for each of these channels (Appendixes 9.3 and 9.4). These results were combined with similar pre-launch calibration ranges of sensitivity for TM/PF (Barker, Ball, et al., 1984), to provide a common post-calibration dynamic range for any TM imagery processed after 15 January 1984 on the TM Image Processing System (TIPS) (Appendix 9.1). This post-calibration dynamic range is defined by the minimum spectral radiance, RMIN, and the maximum, RMAX, given in Table 1-1. Equations are also given in Table 1-1 for relating RMIN and RMAX to the post-calibration offset, $O^{o}(B)$, and gain $G^{o}(B)$, for all channels in the band, as well as an equation for calculating the absolute spectral radiance, L_{λ}, from calibrated radiance on a digital image in units of DN (digital number), L_{cal}. RMIN and RMAX values, for the dynamic range after radiometric calibration on TIPS, are expected to be up-dated based on recalibration of the integrating sphere used for absolute calibration and on reduction of certain systematic errors in the raw digital data.

1.3 SOURCES OF RADIOMETRIC VARIABILITY

Radiometric variability in the final TM image can be divided into three components, based on origin:

- Scene variability (the source of potential information)
  - Solar irradiance
  - Atmospheric transmission, absorption and scattering (reflection)
  - Transmission, absorption and reflection (scattering) of the target, including shadows

Table 1-1. Post-Calibration Dynamic Range (TIPS processings after 15 January 1984)

	BAND 1	BAND 2	BAND 3	BAND 4	BAND 5	BAND 7
RMIN[a] AT $L_{cal} = 0$ DN	−0.15	−0.28	−0.12	−0.15	−0.037	−0.015
RMAX[b] AT $L_{cal} = 255$ DN	15.21	29.68	20.43	20.62	2.719	1.438

$$^{a}\text{RMIN} = \frac{-0^{\circ}\,(B)}{G^{\circ}\,(B)} \qquad ^{b}\text{RMAX} = \frac{\text{RANGE} - 0^{\circ}\,(B)}{G^{\circ}\,(B)}$$

$$L_{\lambda} = \frac{L_{cal} - 0^{\circ}\,(B)}{G^{\circ}\,(B)} = \text{RMIN} + \left[\frac{\text{RMAX} - \text{RMIN}}{\text{RANGE}}\right] L_{cal}$$

BARKER APR 84 GSFC

- Optical and electrical variability of the sensor
  - Reflected radiance from the TM scanning mirror
  - Radiance from the TM internal calibrator (IC)
- Variability introduced during processing
  - "Active-scan" imagery
  - "End-of-scan" shutter calibration data
  - Housekeeping telemetry

Once the total variability from all non-information sources is characterized, then an evaluation can be made as to the adequacy of the precision for specific requirements. If the sensor has already been placed in orbit, as with TM/PF and TM/F, then only the systematic errors from the sensor and any possible additional errors introduced by data processing can be reduced.

1.4 RESEARCH OBJECTIVES

This paper reports on the results of and recommendations from the scientific characterization of the relative radiometric performance for the "protoflight" Thematic Mapper sensor (TM/PF) carried on the Landsat-4 satellite. Emphasis is placed on the analysis of raw background and calibration data for the six reflective bands. These data consist of the detector responses to the internal calibrator (IC) system and to the surface of a shutter which passes in front of the detectors after each scan. The shutter surface is not illuminated, therefore responses to it are considered "background" data. These unprocessed data are not in products available to users. Specific objectives of this research effort to characterize TM radiometric performance included:

- Monitoring radiometric performance of TM sensor with time (Sections 2 and 3)
- Characterizing sources of within-scene variability and uncertainty in measuring radiance with the TM sensor (Section 4)
- Outlining possible pre-distribution methodologies for optimizing TM radiometric calibration parameters based on required scientific information extraction and on radiometric characteristics of the TM sensor (Section 5)

- Recommending changes in operational or processing procedures as well as areas for further calibration, experimentation, and research (Section 6)

Some results are also reported for the flight model of TM (TM/F) on Landsat-5, which was launched on March 1, 1984.

1.5 TM RADIOMETRIC CALIBRATION

Radiometric pre-processing for de-striping and calibration of TM digital images during both the Scrounge-era (prior to July 1983) and subsequently in the TIPS-era has been based on individually correcting each of the 100 channels by calculating a scene-specific radiometric look-up table (RLUT). This RLUT converts the potential range, L_R, of 256 raw digital numbers (DN) into a new set of 256 calibrated DN values, L_{cal}. Thus,

$$L_{cal} = \frac{L_R - NB_A}{NG_A} \quad . \qquad (1\text{-}1)$$

where L_R = raw radiance in DN

NB_A = applied normalized bias in DN; it is usually near zero (Barker, Abrams, et al., 1984b)

NG_A = dimensionless applied normalized gain; it is usually near unity

L_{cal} = radiometrically corrected radiance in DN.

Users of standard TM digital tapes, namely radiometrically corrected and geometrically resampled TM digital imagery from "CCT-PT" tapes, receive values of L_{cal} that can be converted from DN units to units of spectral radiance or in-band radiance using equations given in Table 1-1 (Barker, Ball, et al., 1984). Users of calibrated but unresampled TM digital imagery from "CCT-AT" tapes receive L_{cal} values and also have calibration constants from Equation 1-1, NB_A and NG_A, at the end of each line (Barker, Gunther, et al., 1984).

Procedures for creating these RLUTs are discussed elsewhere (Barker, Abrams, et al., 1984b, p. 27). In brief, the radiometric correction applied to almost all scenes has consisted of two steps:

- Calculation of the change in digital number based upon the on-board IC pulse for each channel

- Histogram equalization of the channels within a band to the mean and standard deviation of a subsampled set of the scene data in the band.

Normalized change for each channel has been determined from the regression of the measured and averaged IC pulse, $P(\ell,C)$ for each of eight lamp configurations (ℓ), for the reflective channels (C), on "nominal" reference values, $P_n(\ell,C)$, calculated to bring all channels in a single band, B, into a common dynamic radiance range from RMIN(B) to RMAX(B) (Barker, Abrams, et al., 1984b, p. 24):

$$\overline{P}(\ell,C) = NB_{IC}(C) + NG_{IC}(C) * P_n(\ell,C) \qquad (1\text{-}2)$$

where $NB_{IC}(C)$ = IC-measured normalized bias for channel C in DN

$NG_{IC}(C)$ = IC-measured normalized gain for channel C (dimensionless)

The absolute radiometric sensitivity of the sensor can be given by a least square fitting:

$$\overline{P}(\ell,C) = O(C) + G(C) * L^{\circ}_{\lambda,s,t,f}(\ell,C) \qquad (1\text{-}3)$$

where $O(C)$ = apparent offset in DN

$G(C)$ = apparent gain in DN per $mWcm^{-2}ster^{-1}\mu m^{-1}$

$L^{\circ}_{\lambda,s,t,f}(\ell, C)$ = reference spectral radiance of channel C in units of $mWcm^{-2}ster^{-1}\mu m^{-1}$ for lamp state ℓ based on three calibrations:
test s: sphere calibration
test t: channel calibration of TM
test f: IC calibration

$\overline{P}(\ell,C)$ = observed average IC pulse in DN of channel C for lamp state ℓ.

The above assumes constant "effective" spectral radiance, $L^{\circ}_{\lambda}(\ell,C)$, from the three IC lamps. The absolute radiometric accuracy of the $L^{\circ}_{\lambda}(\ell,C)$ values which

determine the TM dynamic range is specified to be within 10 percent of the full scale value of DN = 255 (Engel, 1980). Sections 2 and 3 of this paper summarize the average change in gain, for each band, $\overline{G}(B)$, with time since launch. This paper identifies sources and estimates the variability or uncertainty associated with measuring this radiance; i.e., the precision of the measurements. Assuming that the calibration measured in Equation 1-2, and applied in Equation 1-1, is correct, then the radiometrically calibrated digital data for every pixel in Band B, L_{cal}, can be converted to absolute spectral radiance, L_λ, by:

$$L_\lambda = \frac{L_{cal} - O^o(B)}{G^o(B)} \qquad (1\text{-}4)$$

where L_{cal} = calibrated radiance in DN

$O^o(B)$ = common offset for all channels in band B in DN

$G^o(B)$ = common gain for all channels in band B in DN per $mWcm^{-2}ster^{-1}\mu m^{-1}$

L_λ = spectral radiance in $mWcm^{-2}ster^{-1}\mu m^{-1}$

and values for $O^o(B)$ and $G^o(B)$ are determined in the absolute calibration experiments for TM/PF on Landsat-4 (Barker, Ball, et al., 1984).

A few of the absolute radiometric calibration numbers for TM/F on Landsat-5 are given in the appendices. The data in the appendices include: TIPS post-calibration dynamic range (Appendix 9.1), spectral radiances of twenty-one levels of 48" integrating sphere (Appendix 9.2), pre-launch radiometric gains of reflective channels of TM/F sensor on Landsat-5 (Appendix 9.3), and pre-launch offsets of TM/F for fit of raw midscan radiance versus IS spectral radiance (Appendix 9.4).

1.6 APPROACH TO RADIOMETRIC CHARACTERIZATION

In order to characterize and monitor TM radiometric performance, and to provide for possible changes in ground processing procedures, hundreds of tapes of raw video and calibration data have been and are being collected. These pre-launch and in-orbit tapes for Landsat-4 and -5 form the data base for these studies. Data on these tapes consist of 7400 minor frames (mf) for each scan; a minor frame is one sample of all 100 channels. General purpose collects

(GPC) of approximately 30 seconds each sampled 5 to 8 pre-launch collection windows (Table 1-2). Pre-launch data were stored on computer compatible tapes (CCTs) generated by the "BRU," back-up restore utility, program on the bench test equipment. In addition to the 30-second GPC, a few collects, called "BURST" collects, were also made of all data for the 100 channels from a single forward or reverse scan, consisting of about 7400 mf. During the Scrounge-era, 200 mf of in-orbit calibration data were archived a couple of times a week on "CCT-ADDS" tapes (Anon., 1982). A similar type of raw data, called a "CALDUMP" tape, is being planned for internal engineering evaluation during the TIPS-era.

This paper concentrates on an analysis of raw TM calibration data from prelaunch tests and from in-orbit acquisitions. A library of approximately one thousand pre-launch test tapes, each of which samples the equivalent of a scene, is currently maintained for characterization. About 25-50 percent have been examined. Most of the analyses on these tapes used a software program called TRAPP, TM Radiometric and Algorithmic Performance Program, which requires as input both the raw IC calibration data from the shutter region and the raw uncalibrated TM digital imagery. These raw data are not available to the general public. They are used primarily to characterize the sensor, rather than the performance of the ground processing system, for either the initial "Scrounge-era" prior to July, 1983, or for the current "TIPS-era".

Table 1-2. Illustration of an 8-Window General Purpose Collect (GPC) on a BRU Tape (used during ambient atmospheric prelaunch tests on Landsat-5 TM/F) These particular minor frame (mf) locations were taken for "droop" tests with the scanning mechanism locked

	FORWARD SCAN		REVERSE SCAN	
	START	STOP	START	STOP
TIME	1	5	1	5
VIDEO	3148	3172	3148	3172
LINE END	6315	6330	6315	6330
CAL LAMP	7060	7224	6496	6660
SHUTTER	6468	6492	6748	6776
SHUTTER	6924	6952	7204	7228
VIDEO	8	20	8	20
VIDEO	6200	6212	6200	6212

9122 1691/84

SECTION 2 - BETWEEN-SCENE CHANGES IN TM/PF GAIN

This section summarizes results on the radiometric stability of TM/PF with time. Multi-date, multi-sensor, and/or multi-band comparisons of digital images require known or constant radiometric characteristics for each image in order to allow conversion from digital brightness counts to relative radiance values measured in energy units. Therefore, intercomparable radiometric performance of a sensor requires that its sensitivity is either constant with time or that the raw radiance range in each channel can be corrected to a constant range of sensitivity within each band, namely its post-calibration dynamic range.

The use of Equation 1-2 to de-stripe individual images assumes that the TM sensor can be radiometrically corrected. One method of testing that assumption is to follow apparent changes with time. This has been done on TM/PF on approximately fifty sets of in-orbit calibration data. In particular, the apparent gain of each channel, G(C), from Equation 1-3, was calculated from the IC pulses for each image. An examination of the gains revealed systematic differences between the eight odd and eight even channels, but no single channel appeared to behave in a unique manner (Barker, Abrams, et al., 1984b, Appendix). Therefore, for convenience in summarizing all the data in a band, the odd and even average values have been averaged to give G(B) for Band B:

$$\overline{G}(B) = \frac{\overline{G}\ (\text{odd channels}) + \overline{G}\ (\text{even channels})}{2} \cdot \qquad (2\text{-}1)$$

Within-band TM radiometric trends can be characterized by plotting $\overline{G}(B)$ as a function of time. Points plotted in Figures 2-1 and 2-2 are representative of the available in-orbit data from Landsat-4. Figures of gain versus time for all six reflective bands on TM/PF are given in Appendix 9.5. Raw digital images, from which TRAPP runs for these plots of gain versus time were made, are listed in Appendix 9.6.

The nearly monotonically decreasing pattern shown in Figure 2-1, from the time of launch through the end of regular data acquisition by direct X-band link in February 1983, is the least noisy of what appear to be similar patterns for all four bands on the primary focal plane (PFP), namely Bands 1-4 (Appendix 9.5). One hypothesis is that this asymptotic drop of 3 to 6 percent in 300 days in

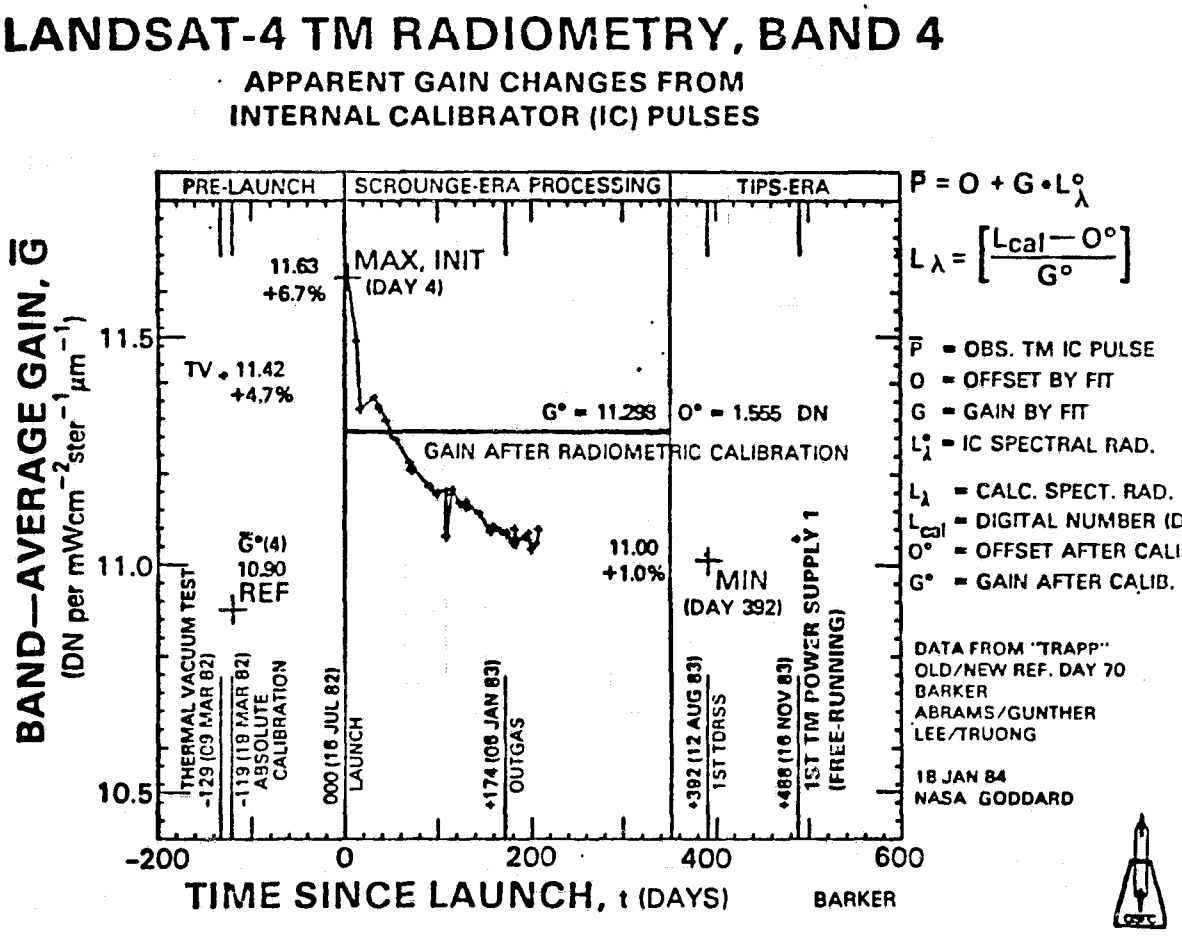

Figure 2-1. Apparent Change in IC-Determined PFP Gain (Gain with time for Band 4 on Landsat-4 TM/PF, as an example of monotonic decrease for the four bands on the Primary Focal Plane (PFP))

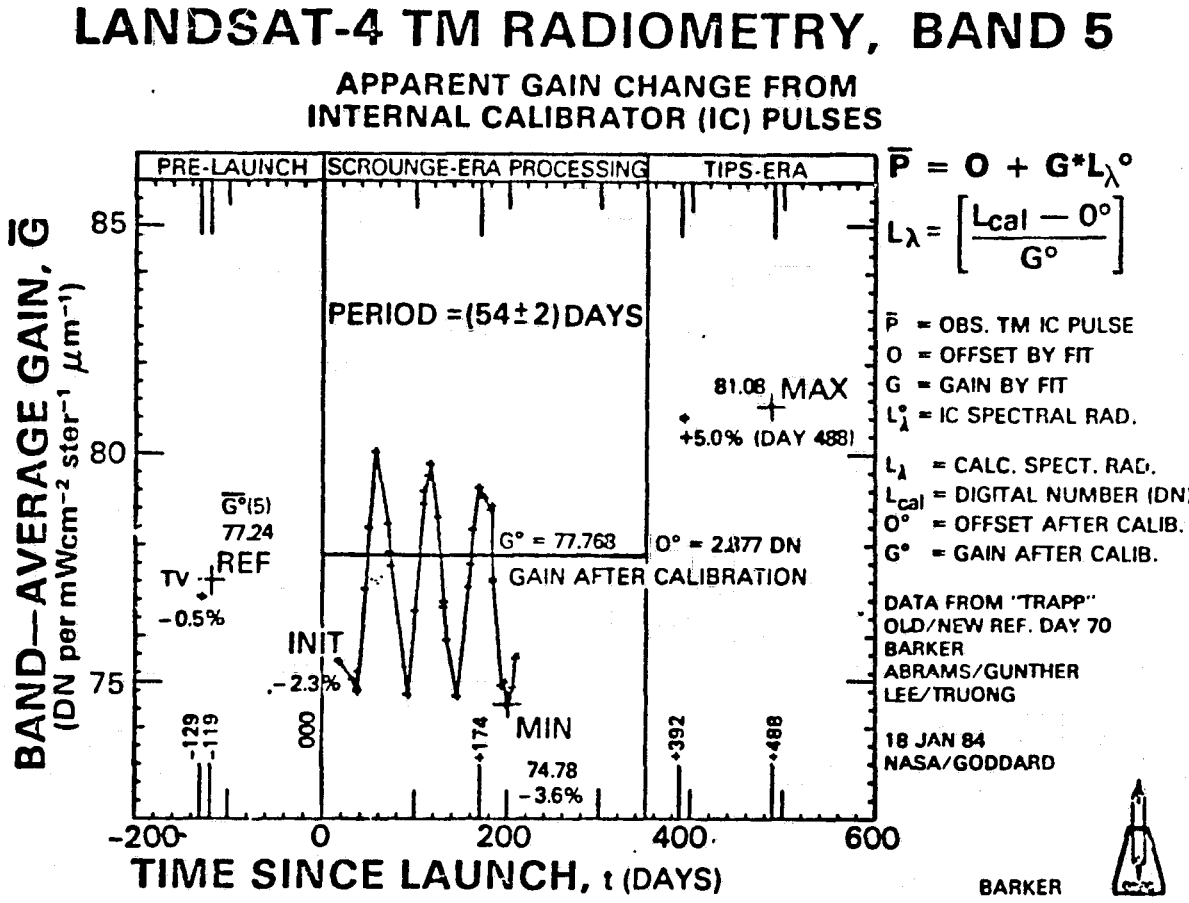

Figure 2-2. Apparent Change in IC-Determined SWIR Gain (Gain With Time for Band 5 on Landsat-4 TM/PF as an Example of Cyclic Pattern of Two SWIR Bands on the Cold Focal Plane (CFP))

orbit is the long-term curve of the "vacuum shift" between IC pulses measured during pre-launch absolute calibration under ambient atmspheric conditions and the IC pulse values observed during pre-launch thermal vacuum testing. This justifies the use of the IC pulses for radiometric calibration of the PFP under the assumption that the "vacuum shift" is due to an optical, physical, or electrical property of the detector and channel itself, rather than to some characteristic of the IC system.

The cyclic pattern in Figure 2-2 is the clearer of the two cyclic patterns for the short-wave infrared (SWIR) bands on the cold focal plane (CFP). Periods for the Band 5 and 7 cycles were estimated at (54 $\pm$ 2) and (75 $\pm$ 6) days, respectively. These periods are different at the 99 percent level of confidence. Prior to outgassing of the CFP on day 174, the peak-to-peak amplitudes of these cycles were approximately (6.5 $\pm$ .5) and (4.0 $\pm$ .5) percent for Bands 5 and 7, respectively. For all in-orbit observations, the range of gain changes was about 9 percent for Band 5 and 6 percent for Band 7.

The origin of these cyclic patterns on the CFP is not known. If the cyclic SWIR pattern is due to something independent of the detectors and their electronics, and external to the IC system, there are several possibilities:

- The composite filters over the detectors could be changing; thin film scattering can be both wavelength and thickness dependent

- The CFP itself is moving cyclically relative to the IC beams of light. One problem with this hypothesis is that it would seemingly produce identical periods for the two SWIR bands

- A monotonic, rather than cyclic, change in the opitcal path length inside the "relay optics," i.e., between the PFP and the CFP, might be consistent with the apparent direct relationship of the periods and the wavelengths of the SWIR bands. since the velocity of a wave is equal to its wavelength divided by its period, the observed periods for Bands 5 and 7 both imply a velocity of 11 nm/yr.

- The whole relay optics itself, CFP and all, could be moving at a fixed rate of 11 nm/yr relative to the lens on the shutter and the PFP. This alternative hypothesis is at least possible since the relay optics containing the CFP was designed to be moved in order to bring it into focus with the PFP.

An additional hypothesis is that the amplitude of the cyclic patterns is a function of how close the optics are to the difraction limit, where the amplitude will vary with phase. One test of these hypotheses would be to look for a cyclic pattern in the third band on the CFP, nameliy the Band 6 thermal band, and relate its period to its wavelength and its amplitude to the relative sizes and areas of the detectors on the CFP. Proof of this model for the cyclic pattern of the SWIR band would justify the continued use of the IC to calibrate these bands.

Conversely, the cyclic pattern may arise from a characteristic of the IC system that is unique to Bands 5 and 7. One such possibility is that the silicon photodiodes used to monitor the output of the three IC lamps may not be sensitive to some type of cyclic wavelength-dependence of the output of the three 1900^{o}K lamps or to the energy balance filters used to bring IC radiance into a range commensurate with the sensitivities of each of the six reflective bands. However, it is hard to imagine that these mechanisms for the IC system would produce such pronounced cycles on the SWIR bands and no observable effects on the PFP bands, except, perhaps, in the SWIR filters for the IC.

By process of elimination, the current assumption is that the cyclic patterns are unique characteristics of the detector systems for Bands 5 and 7. This justifies using the IC, as it was designed, to radiometrically correct them. In-orbit intercomparison of sensors and accurate simultaneous measurements of absolute radiance on the ground at White Sands and from TM at minimum and maximum times of these two cycles may provide enough sensitivity to resolve this question of absolute calibration. However, at this time, definitive origins of the monotonically decreasing or cyclic patterns are unknown.

Assuming perfect operation of the IC, all of these slowly varying trends in gain have been corrected out during the calibration of the TM imagery.

On August 22, 1983, the first TM digital imagery was received via the indirect transmission to the Tracking and Data Relay Satellite System (TDRSS) followed by relay to the receiving station at White Sands, New Mexico. All subsequent Landsat-4 TM acquisitions have been, and will be, via the TDRSS. On November 16, 1983, TM power supply 1 was turned on for the first time. Power supply 1 is "free-running," whereas power supply 2 is synchronized with the start of scan. Unlike Landsat-4, both power supplies on Landsat-5 are free-running.

The results of two Landsat-4 "pre-launch" tests for the absolute radiometric calibration are recorded on Figures 2-1, and 2-2, namely an average gain for a test in thermal vacuum (TV) on March 9, 1982 (test f = 9) and for a subsequent test (t = C) under ambient conditions on March 19, 1982 (Barker, Ball, et al., 1984). All data except the absolute reference (REF; $G^{o}(B)$) gain values of March 19 are referred to an IC reference test on March 20, 1982, called test f = 7, and to a recalibration of the sphere, namely test s = 2, in May 1982. TRAPP analyses that were run using the March 9 IC reference were normalized by band specific factors to the March 20 IC reference.

With the exception of some apparent outliers, the root-mean-square (rms) coefficient of variation for the gain measurements of the band averages, $CV_{\overline{G}(B)}$, as estimated from the range of variability around a smoothly varying curve, is approximately $\pm .05$ percent, for Bands 4 and 5:

$$CV_{\overline{G}(B)} \equiv \frac{\sigma_{\overline{G}(B)}}{\overline{G}(B)} 100 \simeq \pm 0.05\% \qquad (2\text{-}2)$$

where $\sigma_{\overline{G}(B)}$ = standard deviation of average gain for band B, namely $\overline{G}(B)$, in units of DN per $mWcm^{-2}ster^{-1}\mu m^{-1}$

$CV_{\overline{G}(B)}$ = coefficient of variation of $\overline{G}(B)$ in %

While the curves of IC-determined gain versus time for each individual channel appear to be even more well defined, the statistical square root of 16 channels indicates that the radiometric predictability of individual channels is at least better than an rms error of 0.2 percent. Therefore, the coefficient of variation is defined as:

$$CV_{G(C)} \equiv \frac{\sigma_{G(C)}}{G(C)} 100 \simeq \pm 0.2\% \qquad (2\text{-}3)$$

where $\sigma_{G(C)}$ = standard deviation of G(C)
$CV_{G(C)}$ = coefficient of variation of G(C) in percent.

There were changes in the TRAPP procedures used to calculate the gains and offsets. The smoothly varying patterns in Bands 4 and 5 validate the normalization scheme used in about half of the TRAPP outputs to the level of uncertainty

in the curves, namely ±0.05 percent. There is more variation in the other bands (Appendix 9.5). The total noise being lowest in Band 4 on Landsat-4, the other bands would be expected to show greater variability in gain versus time due to the lower precision of the estimation of gain. Alternatively, this greater variability in the gain with time in other bands may indicate that this normalization procedure is not as effective for them. Raw calibration data for these bands could be reprocessed to eliminate the need for this normalization.

The uncertainty in the least-squares calculation of the gain from individual IC pulse averages is greater than the uncertainty observed around the slowly varying patterns. This suggests that future analyses might provide a more quantitative systematic correction for gains and offsets by including trend analysis, or provide alternative radiometric correction procedures that do not show these systematic trends.

Regardless of the origin of this uncertainty, it means that there is the potential for estimating mean values of in-orbit TM radiometry to a precision of ±0.2 percent, at least for channels within Bands 4 and 5.

SECTION 3 - BETWEEN-BAND CHANGES IN TM/PF GAIN

In addition to maintaining scene-to-scene calibration of each band, it is also necessary to maintain band-to-band calibration. Current TIPS procedures do not provide for any between-band correlation of channels. If the IC system has been working as designed, then the radiometric calibration of TM imagery with the IC data will maintain the relative calibration of the channels in each band to ± 0.2 percent (Equation 2-3), and therefore will also maintain the samme precision for band-to-band calibration. If, on the other band, patterns of gain versus time reflect changes in the IC system, then they can be used to estimate the possible absolute error in the radiometrically calibrated TM imagery. Use of IC calibration implies faith in the IC system.

Between-band TM/PF radiometric trends can be characterized from apparent gain changes with time in all six reflective bands (Appendix 9.5). Gains for four specific times are tabulated in Table 3-1 for each band relative to the band-average absolute calibration reference gain, $\overline{G}^{o}$: (1) TV is the March 9 pre-launch thermal vacuum test; (2) INIT is the initial in-orbit data which occurred on day 4 for PFP bands and day 17 for the CFP bands; (3) MAX is the maximum observed in-orbit gain, which coincides with day 4 initial turn-on for Bands 1-4 and was day 488 for Band 5 and day 392 for Band 7; and (4) MIN is the minimum observed in-orbit gain which occurred on days 392, 200, 200, 392, 200, and 56 for Bands 1-5 and 7, respectively.

Several observations and inferences apply to more than one band and to the radiometric relations between bands:

- IC Temperature-Dependence. The difference between pre-launch gains measured under ambient REF and TV conditions ranged from -1 to +5 percent. While the 6 percent range of differences in gain may be related to the "vacuum shift" of the individual channel responsivity, it is also consistent with a recently-observed temperature-dependence of the IC pulse. Both need to be quantitatively understood to reduce this uncertainty in absolute radiometric calibration of TM digital imagery.

The "IC temperature-dependence" was observed on the PFP bands on Landsat-5 during thermal cycling and is unique for each channel in a band. The dependence can increase or decrease pulse values and appears to be linear with a slope of up to 1 percent per ^{o}C. REF and TV IC shutter

Table 3-1. Apparent Percentage Changes in Band-Averaged Gain (for four times relative to time of absolute radiometric calibration for six reflective bands on Landsat-4 TM/PF). The four times are the expected post-launch value from a pre-launch test in thermal vacuum (TV), the actual first calibration after launch (INIT), and highest (MAX) and lowest (MIN) values observed in-orbit, i.e., the range of change (MAX-MIN). This range is an indication of a possible uncertainty of 3 to 9 percent in the absolute radiometric calibration of the TM/PF reflective bands.

APPARENT CHANGES IN TM/PF GAIN

	RELATIVE CHANGE IN %, $100\left[\frac{\overline{G} - \overline{G^\circ}}{\overline{G^\circ}}\right]^*$					
BAND	**1**	**2**	**3**	**4**	**5**	**7**
REF, $\overline{G^\circ}$	15.78	8.10	10.62	10.90	77.24	147.12
TV (PRE-LAUNCH)	−1.2	−1.0	3.2	4.7	−0.5	−0.5
INIT (IN-ORBIT)	−1.1	−1.0	3.6	6.7	−2.3	−0.8
(INIT-TV)	0.1	0.0	0.5	2.0	−1.8	−0.3
MAX (IN-ORBIT)	−1.1	−1.0	3.6	6.7	5.0	3.3
MIN (IN-ORBIT)	−8.2	−4.5	−2.8	1.0	−3.6	−2.5
MAX-MIN	7.1	3.4	6.5	5.7	8.5	5.8

*GAINS CALCULATED FROM LANDSAT-4 TM/PF INTERNAL CALIBRATION (IC) PULSES, $\overline{P}$, REGRESSED AGAINST IC EFFECTIVE SPECTRAL RADIANCE, L°_λ:

$$\overline{P} = O + G \cdot L^\circ_\lambda$$

WHERE O IS FITTED OFFSET AND G IS FITTED GAIN FOR A CHANNEL.

BAND-AVERAGE GAINS, $\overline{G}$, ARE COMPARED TO AN AMBIENT ABSOLUTE CALIBRATION REFERENCE $\overline{G^\circ}$ OF 19 MARCH 1982, WHERE GAINS ARE IN DN per mWcm^{-2} ster $^{-1}\mu m^{-1}$.

BARKER
FEB 84

temperatures were approximately 25°C and 8°C, respectively.

One hypothesis for the origin of the IC temperature-dependence is a thermally induced physical movement of the IC shutter and its seven pencils of light. Higher pulse values for either odd or even channels would be observed if the pencil of light was not completely uniform across the two rows of detectors. This would be especially true if the optimized initial location of the peak radiant intensity was between the odd and even channels. If this hypothesis is true, then regular midscan image data would not be expected to show any temperature-dependence.

The TM/F midscan pulse on Landsat-5 has been observed to be nearly independent of temperature as measured under ambient conditions from the initial turn-on near 20°C to the automatic shutdown at the peak thermal threshold near 30°C. Data are needed under vacuum conditions to characterize possible in-orbit temperature-dependence, especially for the CFP bands for which no pre-launch data were collected. Therefore, it is recommended that TDRSS be used to take in-orbit data over a long duty cycle of Landsat-4 and -5 in order to calibrate the magnitude of the effect and to provide for possible normalization.

- Expected Gains. The difference between pre-launch TV and initial in-orbit (INIT) gains in Table 3-1 ranges from -2 to +2 percent. This is less than half of the -2 to +7 percent range between INIT and the pre-launch ambient REF. In-orbit Landsat-4 digital data have been acquired on a low duty cycle with an IC shutter temperature of 8 to 9°C. Therefore, one hypothesis is that the closer agreement of in-orbit INIT and TV, as compared to INIT and REF gains, is a reflection of at least partial normalization of the "IC temperature-dependence." The residual difference between INIT and TV gains may reflect a combination of measurement error and dependence of "vacuum shift" on length of time in vacuum.

- Vacuum Shift. The first INIT and highest MAX observed in-orbit gains are the same for the four PFP bands (Table 3-1). This would be consistent with an hypothesis of monotonic change in "vacuum shift" with time in vacuum since the maxima are near day 4 and the minima are near day 200 for all four of the PFP bands.

- Thermal Expansion or Contraction. The relative change in gain monotonically increases from band 1 to band 4 for both the MAX and MIN in-orbit observations. This suggests an hypothesis associated with differential thermal

expansion of the PFP from its one-sided place of attachment to the bulkhead. The place of attachment is located such that physical expansion of the PFP would move detectors for band 1 the most, and those for band 4 the least. Such a physical expansion would justify the current use of IC data for making radiometric correction, and might suggest a need for using the IC peak location to measure fractional mf movements with time, within the PFP, and between the PFP and CFP. If this expansion exists, it probably does not exceed 0.2 pixels.

Alternative hypotheses implicating the IC system are also possible, such as a different physical expansion or contraction out along the radial arm of the IC shutter. This latter hypothesis seems less likely since an assumption of similar patterns of light for each array suggests that radial movements would produce a related change across all six reflective band optics on the IC shutter; this change is not observed.

- Gain Increase After Outgassing. Band 7, and perhaps Band 5, showed an apparent increase in gain following the turning on of the heaters for about 12 house on the CFP to outgas the thermal band. Measurements of gain were resumed on January 13, 1983, after a period of approximately 26 hours to recool the CFP. An apparent 2 percent increase in gain at 2.2 μm (band 7) would be consistent with the hypothesis that ice on the dewar window for the CFP caused a 30 percent loss in gain for Band 6 at 10 μm after approximately 160 days of operation. Band 7 has the most difficult to interpret patterns and may have band specific dependencies that are as yet unrecognized. Observed maximum values of Band 5 gain at day 392 and 488 are consistent with projected maxima at day 384 and day 492. A possible 2 percent increase in gain in band 5 (1.6 μm) has been estimated.

- Power Supplies. There is no obvious change in any patterns with the first use of the free-running TM power supply on day 488. None were expected, since there is a high degree of regulation on the power supplies.

- Absolute Radiometric Uncertainty. The MAX-MIN range of observed relative in-orbit gain changes for the six reflective bands on Landsat-4 is from 3 to 9 percent. Part of that range is associated with extreme values in Band 1, which are probably not real differences in gain but uncertainties in the measurement. Nevertheless, these extreme limits imply that the uncertainty in the absolute calibration associated with using the IC for radiometric correction is no worse than the range in relative in-orbit

gain observed in that particular band. The apparent asymptotic decay of gain with time over the first year inorbit to a nearly constant value for the PFP bands is consistent with the proposed monotonic "vacuum shift" with time. The uncertainty associated with an understanding of these patterns of band-average gain change with time is a measure of the uncertainty in between-band absolute radiometry.

SECTION 4 - WITHIN-SCENE VARIABILITY IN TM RADIOMETRY

If radiometric calibration is done on one scene at a time, as in the case of Scrounge-era and TIPS-era processing, then any sources of systematic variation that occur during the 23 seconds it takes to acquire a scene will remain uncorrected. This section provides an overview of residual uncertainties after radiometrically correcting TM digital imagery. Emphasis is placed on relative errors within a band and within a scene, since between-band and between-scene variability were discussed in the previous sections and current procedures are scene- and band-specific. Even if it were possible to apply radiometric corrections perfectly for mean differences in relative bias and gain for each channel in a band, residual uncertainties, which are associated with the sensor itself, would still produce channel related striping or other patterns of noise in the corrected TM image.

In addition to the uncertainties in radiometric calibration associated with using the sensor's IC over time and with looking at a point source of constant radiance, rather than a full aperture source external to the entire optical path (Section 3), the TM scanning radiometer has the following six types of variability:

- bin-radiance dependence
- Within-line droop
- Bright-target saturation
- coherent noise
- scan-correlated shifts
- forward/reverse-scan differences.

These sources of "noise" range up to 2 DN in value and are channel-dependent. All six of these types of variability are presumably systematic, or slowly varying in nature. They are potential candidates for at least partial, or statistical, removal during ground processing to leave only inherent random noise.

During the process of building the TM sensor, sources of systematic variation or high random noise were removed or brought within specifications by improving the hardware at Santa Barbara Research Center (SBRC) in California. During pre-launch testing and calibration phases, some data were collected for potential future processing, but were not

completely analyzed. Subsequent and still partial analyses have revealed several instrumental sources of discontinuous or slowly varying signal changes. Since launch, it has been possible, because of availability of more data under the nearly constant environmental conditions in space, to identify additional types of signal modulation. It is important to characterize the signal modulation because the stability of the TM radiometer and sensitivity of image processing techniques mean that even when scene-specific radiometric correction procedures remove striping between channels down to a few DN, users can display the systematic residual striping by stretching or classifying images.

This section reports on the identification and relative significance of some of these sources of noise. Exact modeling of possible ground processing corrections are in progress. The modeling must precede questions as to whether or not it is feasible to recalibrate the absolute radiometry and incorporate such procedures into the TIPS system, and if so, whether the corrections significantly reduce the errors in value-added products derived from digital imagery. A discussion of the six types of variable noise in TM imagery that are sensor specific and independent of processing procedures is given below.

4.1 BIN-RADIANCE DEPENDENCE

Bin-radiance dependence is a TM noise type associated with error in the analog-to-digital (A/D) converter's bin size and location. This noise can result in any specific DN value being mislocated by up to two levels and varying in size from nearly zero to 2 DN values. The 8-bit A/D converters in both TM/PF and TM/F exhibit this error. While as yet unmodeled for dependence on time and temperature, it has been quantitatively characterized in pre-launch unit-level testing of the multiplexer and A/D converters. Sizes of the unequal bins and sizes of displaced locations are of the same magnitude in all bands since a common design was used for the six A/D converters in a TM sensor. There is an even higher degree of correspondence between the threshold bin voltages of channels within a band because the parallel signals are fed into a track-and-hold storage buffer and serially switched by the multiplexer into the A/D converter for that band. The unequal bin errors, as well as quantization errors, are probably significant sources of variability in the signal-to-noise and absolute radiometric calibration tests. While local variability can be up to two DN values, the full 255 level range of the A/D system is linear to an rms error of $\pm$.4 percent in the slope of raw radiance, L_R, versus known spectral radiance from the

integrating sphere, L_{IS}. However, this bin-radiance dependence does result in saw-toothed histograms of raw digital-image data. It has been demonstrated for one channel (Band 1 channel 1 for a Landsat-4 January 3, 1983, scene over White Sands, New Mexico) that normalization for bin size based on pre-launch A/D thresholds can produce a smoother histogram of frequency versus L_R (Figure 4-1). Saw-toothed histograms illustrating bin-radiance dependence have also been noticed on preliminary in-orbit data from Landsat-5 (a 4-band scene over the Atlantic Ocean taken on March 4, 1984) in which local minima corresponded to the narrow size of bins observed in unit-level tests of the A/D converter.

An approximate rms "noise" associated with this systematic A/D bin-radiance dependence is about ± 0.3 DN, and is therefore of the same order as the ± 0.3 DN noise from digital quantization. It remains to be demonstrated that a time-independent bin-radiance model can be developed that would take raw radiance values, L_R, and replace them with A/D corrected values, $L'_{RA}(C, L_R, t, T)$, which would depend on the channel (C), on time (t) and perhaps on the temperature (T) of the A/D converter for long-duty cycles of TM acquisitions. Such a mean-value correction model for bin-radiance dependence would be most valuable if applied before other types of corrections, or calibrations, and retained in more than 8-bit precision. One form for this correction for each channel would be:

$$L'_{RA} = L_R + CA(L_R) \qquad (4\text{-}1)$$

where $CA(L_R)$ = a function in DN units for making an arithmetic correction for the A/D bin-radiance dependence which is dependent on L_R but independent of t and T, i.e. identical for all occurrences at a given bin number.

L'_{RA} = raw radiance, in DN, which has been corrected for A/D bin-radiance dependence

The apparent correspondence between both pre-launch system-level tests and in-orbit Landsat-5 bin-radiance dependence from histograms, and the pre-launch unit level electronic measurements of the threshold voltage of each bin, suggests that the A/D voltage measurements taken on different dates and at different temperatures will be usable for making corrections for bin-radiance dependence.

HISTOGRAMS (BAND 1, CHANNEL 1)
Landsat-4 TM (ID 40171-17080, 3 JAN 84, White Sand, NM)

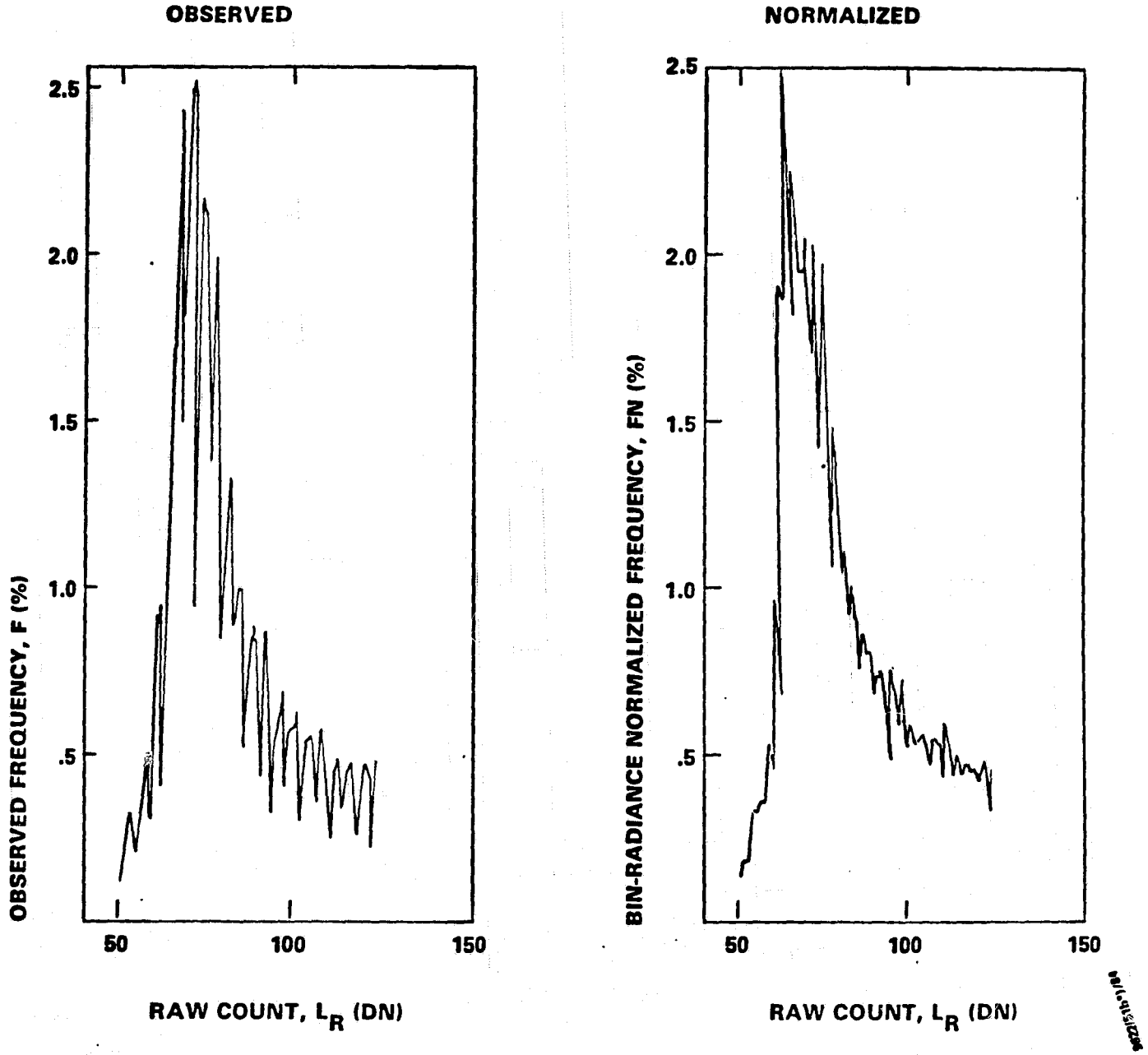

Figure 4-1. In-Orbit Landsat-4 TM/PF Frequency Histogram (Number of Pixels as a function of DN value, before and after normalization for bin-radiance dependence based on pre-launch measurements of bin size)

There are alternative ways to implement this correction, such as:

- Mean value of bin center
- Randomized distribution into bins based on proportion of overlap; this is preferred over the mean value method.

4.2 WITHIN-LINE DROOP

"Droop" is one of three types of "within-line, sample-location dependent noise." Malila et al. (1984) have characterized this noise as a sensor-related scan-angle artifact, partially because of the necessity to remove systematic atmospheric variations from the scene that are scan-angle dependent before observing this residual within-line droop. By comparing forward west-to-east scans to reverse east-to-west scans, a systematic droop of the signal was observed to be about 2 percent, or 1 DN, for Band 1 between the maximum value and the end of active scanning. This was the largest droop for the reflective bands.

The correction model (Malila et al., 1984) for the exponential decay constant required for a 1/e (63 percent decay) was approximately 10 msec, or 1000 samples, based on one Landsat-4 scene. Their model assumed a uniform scan-direction independent exponential decay of the difference, D^{∞}, between the true radiance before droop, L'_{RD} and the apparent radiance after drooping to infinity, L^{∞}_{RD}:

$$D^{\infty} \equiv L'_{RD} - L^{\infty}_{RD} \cdot \qquad (4\text{-}2)$$

Within-line "droop" can be positive or negative and is probably dependent on the time, t, or samples after the end of direct current (DC) restoration rather than on the pixels from the west edge of the scan, which was assumed in their model (Malila et al., 1984), and therefore:

$$CD(ADC, S) = D^{\infty} \exp [-KD*ADC] \qquad (4\text{-}3)$$

where ADC = # samples, at sample location S, after end of DC restoration

KD = within-line droop time constant for 1/e (63 percent) decay, in units of reciprocal samples or reciprocal msec. The half-time, $t_{1/2}$, for a drop, or increase, of 50 percent of D^{∞} is:

$$t_{1/2,D} = \frac{\ell n\ 2}{KD}$$

CD (ADC, S) = correction for within-line droop at sample S in DN.

Using nomenclature that is more consistent with this paper, their modified model is:

$$L'_{RD}(S) = \frac{L_R\ (S)}{1 - f_D^{\infty}\ [1 - \exp(-KD*ADC)]} \qquad (4\text{-}4)$$

where f_D^{∞} = fractional decay, or increase, at infinity of an undecayed radiance, L'_{RD}

$L_R(S)$ = observed raw radiance at S in DN

$L'_{RD}(S)$ = raw radiance at S in DN after correction for droop.

The additive correction term for within-line droop, CD (ADC), for each channel in a scan, is computed as follows:

$$L'_{RD}(S) = L_R(S) + CD(ADC, S) \qquad (4\text{-}5)$$

where CD(ADC, S) = correction for within-line droop at sample location S, which is ADC samples after DC restoration, in units of DN

$L'_{RD}(S)$ = raw radiance at S, in DN, corrected for within-line droop.

Equation 4-5 is the within-line droop equivalent of the linear correction applied for A/D bin-radiance dependence in Equation 4-1. One of the reasons for expressing corrections in this form is that the combined correction for both of these effects can then be viewed, under an assumption of separability, as the sum of two corrections, $CA(L_R)$ and CD(ADC,S). This linear formulation is also useful in the implementation of corrections to the image.

- Overshoot and Undershoot. Another type of within-line electronic "droop" is called overshoot or undershoot. It is most significant at boundaries between highly contrasted regions and can be as high as tens of DN values if the contrast is high enough. However, this is not expected to pose a problem since the multi-pole electronic filter on each channel is designed to damp the first most excessive swing of this recovery in a fraction of a sample, i.e. in less than 9.6 μsec (microseconds). Overshoot and undershoot were electronically characterized in analog unit-level tests prior to launch and would be hard to locate in digital imagery. There have been no reports of suspected overshoot or undershoot in any TM imagery. The less well characterized within-line droop referred to in Equation 4-3 appears to have a maximum amplitude of a couple of DN, and a time constant KD of the order of hundreds to thousands of samples, i.e. tens of milliseconds.

- Within-Line Droop in TM/F. Preliminary examinations of special pre-launch droop tests on Landsat-5 indicate up to 1.5 DN droop in the PFP bands, with a systematic decrease from the largest effect in Band 4 to the lowest in Band 1. Bands 5, 6 and 7 on TM/F do not seem to show significant within-line droop.

There is a possibility that droop is some form of bright-target saturation or vice versa. An alternative hypothesis is that these effects arise from independent electronic causes, such as droop being associated with the circuity trying to maintain a constant reference voltage and bright-target saturation being a characteristic of detector-type and pre-amplifier electronics.

4.3 BRIGHT-TARGET SATURATION

Bright-target saturation is a second type of "within-line sample-location dependent noise." It is characterized by a memory effect after exposure to a bright target, such as a cloud. The time constant of the hysteresis is such that the effect may last for thousands of samples. There may be two separate physical effects on the detectors, one which has a

shorter time constant and decreases the detector sensitivity, and the other, which has a longer time constant and increases the sensitivity.

- Broken-Cloud Saturation Effects. A qualitative observation of the effects of bright-target saturation was first seen by Fischel (1984) on a cloudy TM scene of Terrebonne Bay, LA (ID 40174-16011, 6 JAN 83). Clouds were scattered throughout, but were most prominent in the east and bottom of the scene. The effect was most noticeable as a change in the background observed on the shutter before and after DC restoration, with recovery made more observable by applying a radiometric correction for bias on a line-by-line basis. DN values in alternating sweeps of 16 lines were observed to be lower to the east of bright clouds on forward scans and to the west of bright clouds on reverse scans. After apparent saturation from several kilometers of clouds, there were depressed DN values for about a thousand samples (pixels). At the end of each active scan, the observed differences in averaged background before and after DC restoration were as high as 1 DN in Channel 4 of Band 1.

- Arithmetic Application of Correction. A correction for bright-target saturation can be expressed additively. For each channel in a scan:

$$L'_{RB}(S) = L_R(S) + CB(SB, S) \qquad (4\text{-}6)$$

where $CB(SB, S)$ = correction for bright-target saturation in DN at sample S after coming out of saturation SB samples earlier

$L_R(S)$ = observed raw radiance at S in DN

$L'_{RB}(S)$ = raw radiance at S in DN, which has been corrected for bright-target saturation.

- Exponential Form of Cloud Correction. One possibility is that the bright-target saturation effect has a recovery of the same analytical form as droop. By analogy to Equation 4-3, an equation for the expected additive correction term for bright-target saturation in Equation 4-6 would be:

$$CB(SB, S) = BD \exp [-KS*SB] \qquad (4\text{-}7)$$

where SB = samples since bright-target saturation at sample S

KS = time constant for bright-target saturation

BD = maximum initial drop in DN

CB(SB, S) = correction in DN at S for bright-target saturation

The exact form of the correction for bright-target saturation remains to be determined. Preliminary analyses of the "solid-cloud" example below indicate two independent physical phenonema may be occuring in the detectors. One causes a decreased sensitivity in the detectors and the correction for this depletion effect can be modeled by Equation 4-7. The other phenomenon gives the appearance of an increased sensitivity in the detectors after exposure to bright targets. This second phenomenon may have a similar correction, except that there would be a new amplitude constant with a changed sign to replace BD, perhaps BI for increased background. There would also be a new time constant to replace KS, perhaps KSI, and it is possible that this second term might require a displaced start from the end of saturation. The correction for bright-target saturation would then be the sum of these two opposing effects. An alternative interpretation of the deeper shorter undershoot and longer lower amplitude overshoot observed in the solid-cloud example below is an underdamped alternating oscillation of decreasing amplitude. This underdamped alternative was tentatively rejected because there was no evidence for a second undershoot and the period of overshoot and undershoot were not the same.

- "Solid-Cloud" Examples. In order to facilitate the interpretation of the data in terms of bright-target saturation, a TM scene was chosen which had one solid formation of clouds. The initial "solid-cloud" scene was of San Francisco, CA (ID 40392-18152, 12 AUG 83). A solid formation of clouds along the coast of the Pacific Ocean on the western edge of this scene starts at about scan 80 and reaches eastward until there is nearly 75% cloud-cover in the lower quarter of the scene. Backgrounds were taken from two shutter regions, "background 1" and "background 2", before and after DC restoration, respectively, namely B-BDC and B-ADC. Uncorrected raw scene-average backgrounds are given in Appendix 9.12. These averaged backgrounds were corrected on a line-by-line basis for scan-correlated shifts (Section 4.5). The corrected backgrounds were plotted separately versus scan number for forward and reverse scans in both regions for all reflective channels (Appendix 9.9),

giving four plots for each band, namely, BF-BDC, BR-BDC, BF-ADC and BR-ADC.

If there were no bright-target saturation effects, then four identically flat plots of the same constant background, independent of scan number would be expected. This is not the case. Slowly varying trends are visible in the PFP bands. These trends of the background as a function of scan number are most visible in Band 2 (Appendices 9.9.3 and 9.9.4), especially when related to the known patterns of cloud cover, and can be summarized as follows:

- A "1st transition" occurs between scans 80 and 120.
- All four PFP bands show a 1st transition.
- The 1st transition is correlated to cloud cover.

  Cloud cover is zero down to scan 80.

  About 30% of the western edge of the image is cloud covered by scan 120
- A "2nd transition" occurs between scans 290 and 320.
- The 2nd transition is correlated to cloud cover.

  Cloud cover increases toward the east from 30% to 75% between scans 120 and 290.

  Cloud cover is nearly constant at 75% of western side of image for last 80 scans.
- All channels change at approximately the same time.
- All channels have approximately the same change in DN.
- Band 2 backgrounds depend on region and scan direction.

Estimated <u>changes</u> in Band 2 at 1st transition:

Δ BR-ADC = -2.0 DN, From 2.0 to 0.0 DN
Δ BF-BDC = +1.4 DN, From 2.2 to 3.4 DN
Δ BF-ADC = +1.0 DN, From 2.2 to 3.2 DN
Δ BR-BDC = 0.2 DN, From 2.0 to 1.8 DN

Estimated changes in Band 2 at 2nd transition:

Δ BF-BDC = -0.7 DN, From 4.0 to 3.3 DN
Δ BR-ADC = +0.4 DN, From 0.0 to 0.4 DN
Δ BF-ADC = -0.2 DN, From 3.8 to 3.6 DN
Δ BR-BDC = +0.1 DN, From 1.8 to 1.9 DN

A specific channel was chosen from each band to test the background dependence on distance from the end of the exposure to the bright clouds, SB. For Channel 7 in Band 2, data from both regions can be combined to give a nearly self-consistent curve of B versus SB, starting at about 2.1 DN at the edge of the cloud, to a minimum of about 0.0 DN near pixel 800, and then to a maximum of about +3.8 DN near pixel 4000, followed by a decline to within 0.3 DN of the original background of 2.1 DN near SB = 7000 pixels. This slowly and smoothly varying curve of B versus SB is the justification for the two component bright-target correction model given above. There is a difference of about 0.3 DN between the maxima in forward scan backgrounds before and after DC restoration.

The estimates of actual backgrounds in the San Francisco example were uncertain to varying degrees because of an incomplete printing of the line-by-line backgrounds for any channel in Band 2. Furthermore, there were no normalizations for bin-radiance dependence, and the lower backgrounds are probably biased to the high side because values of L_R = 0 DN undoubtedly include real values that were below zero.

The model for bright-target saturation effects is that they are related to the distance from the end of bright target, or cloud. This hypothesis was tested in this study and the results are shown in Figure 4-2, where the backgrounds from all four regions on the shutter are plotted against the distance from the cloud edge. The initial 1000 mf undershoot and a 6000 mf overshoot suggests that all of the background data can be fit on a single slowly varying curve, thereby justifying the two component model mentioned above.

Some additional verification for this correction model is evident from an examination of the change in the shutter backgrounds in the bottom 100 scans of a Washington, DC scene (ID 40109-15140, 2 NOV 82), in which the eastern 10% is cloud covered at the bottom of the scene. Changes in the background of this eastern solid cloud example are in the opposite direction from the western case, as expected.

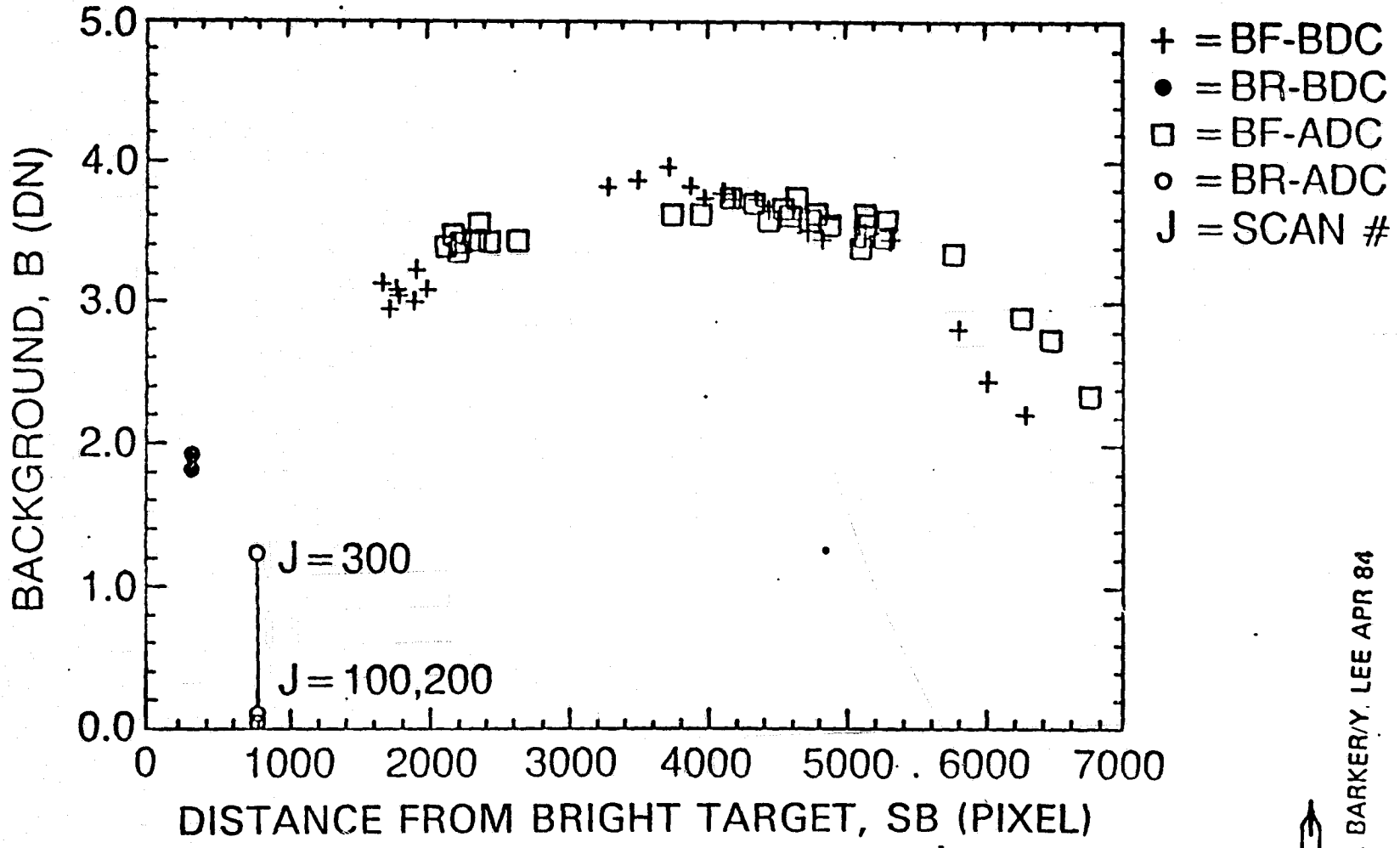

Figure 4-2. Bright-Target Saturation Effects on Background

- Cloud Mask. For real scenes, with single or multiple clouds, implementation of a bright-target correction will probably require initial creation of cloud mask. Corrections may need to be aggregated when there is more than one bright target either within a scan or within a couple of scans, unless it can be shown that the "clock" is reset each time the detector is exposed to a bright target.

- Between-Scan Correction. Because the DC restoration circuit, which is activated by switches on the shutter for about 3.1 milliseconds at the end of each scan, has a 1/e time constant of about 6.2 milliseconds, it is possible that there may be a "between-scan trend-dependent noise" from bright-target saturation effects. The nearly overlapping and smoothly varying curves of B versus SB for both regions suggest that changes which are independent of SB and due to changes during DC restoration are small, less than 0.3 DN.

- Bright-Target Drop-Out during Saturation. During pre-launch testing of Landsat-5 TM/F, occassional major drops in signal were observed in Band-4 during exposure to sources whose radiance was more than about 30% above the nominal limit at a DN value of 255. If such bright targets are observed over land, perhaps in a summer scene of a bright desert, then apparent holes may appear in the saturated imagery.

- Absolute Radiometric Recalibration. If the bright-target saturation effect is radiance-level dependent, then a re-examination of the absolute calibration methodology may be necessary. The re-examination would include the potential impact of the brightest 111 all-lamps-on IC state on video data for 40 scans out of every 360 scans, when the normal IC automatic sequencer mode is used. If the scan mirror is locked, the re-examination needs to include the effect of bright-target saturation in the video on background and calibration data.

4.4 COHERENT NOISE

Coherent noise is a "within-scan, sample-location dependent noise" which has been observed by Fourier analysis in TM scenes (Anuta et al., 1984). Peak-to-peak amplitudes at the 32 KHz peak are given in Table 4-1 for a similar analysis using a Fast Fourier Transform (FFT) on an in-orbit scene (ID 40037-16033, August 22, 1982, Memphis, TN). A scene-independent analysis was performed on 512 mf of in-orbit calibration data from the shutter region (ID 40171-17080, January 3, 1982, White Sands, NM). The

Table 4-1. 32 KHz Coherent Noise (every 3.2 pixels), measured by peak-to-peak amplitude in DN from midscan digital data for 96 reflective channels on Landsat-4 TM/PF (ID 40037-16033, 22 AUG 82, Memphis, TN)

IN-ORBIT LANDSAT-4 TM RADIOMETRIC COHERENT NOISE (DIGITAL COUNTS)

Channel No.	Peak-to-Peak Coherent Noise at 32 KHz (DN)					
	Band 1	Band 2	Band 3	Band 4	Band 5	Band 7
1	.54	.08	.09	.28	.25	.16
2	.98	.13	.13	.39	.50	.28
3	.74	.07	.07	.42	—	.20
4	.03	.15	.86	.77	.19	.37
5	.83	.15	.20	.76	.33	.35
6	1.02	.16	.19	.49	.25	.21
7	.39	.10	.15	.58	.59	.46
8	.93	.00	.80	.70	.34	.29
9	.44	.08	.16	.43	.38	.25
10	.33	.14	.08	.35	.19	.28
11	.54	.13	.17	.37	.29	.18
12	.47	.13	.10	.35	.41	.31
13	.52	.05	.21	.43	.20	.26
14	.76	.00	.12	.28	.25	.34
15	.57	.06	.09	.34	.32	.18
16	1.43	.06	.35	.37	.49	.20

Data Measured Peak-to-Peak, With Background Subtracted in Digital Counts
Data from Scene W023036 ID = 40037-16033 (22 Aug 82) Memphis, TN

TM/PF exhibits coherent noise in the PFP bands at two frequencies, f_2 = 32.8 KHz (a period of every 3.2 pixels) and at f_1 = 5.9 KHz (a period of 17.6 pixels). Results are tabulated in Tables 4-2 and 4-3 for the integrated area under the peaks in the Fourier domain, instead of peak-to-peak amplitudes. A standard method for reducing this noise would be to perform a FFT on each line, apply a notch filter at the two spikes, and apply an inverse Fourier Transform. Given the reproducibility of the frequencies, it might be possible to avoid the need for FFTs by applying a filter in the spatial domain. This could be done by using one channel with a high amplitude to calculate the phase location for all channels, SP, from the start of a period in the shutter region. For each channel in a scan:

$$L'_{RC}(S) = L_R(S) + CC(f, S, SP) \qquad (4\text{-}8)$$

where CC(f, S, SP) = correction in DN for coherent noise of frequency f, at sample S, and where the start of a cycle is at SP

$L'_{RC}(S)$ = raw radiance at S in DN after correction for coherent noise.

There are no observable coherent noise peaks for the SWIR bands, only a steadily rising amplitude with frequency.

Landsat-5 TM/F has a different coherent noise pattern. It does not have as significant a peak at 32 KHz. Most channels on the primary focal plane in TM/F have only one peak, or multiples of it, near 8.5 n KHz, where n is an integer, and the periods are about (12.5/n) pixels. Two tests on pre-launch data differed in apparent frequency of the coherent noise by about 10 percent. If this magnitude of variability is real, its origin might be traceable and modelable from engineering telemetry. Channel 1 in Band 3 appears to have the largest 8.5 KHz noise on Landsat-5 TM/F.

Systematic corrections for coherent noise are possible. If bin-radiance dependencies are removed first, then the characterization of the coherent noise will be more precise. Coherent noise corrections need to be made before characterizing the between-scan shifts and other types of systematic noise with periods longer than that for coherent noise. When fractional DN corrections are applied to

Table 4-2. In-Orbit Coherent Noise at Frequency 3.17 Pixels
White Sands (3 January 83)

CHANNEL	BAND 1	BAND 2	BAND 3	BAND 4	BAND 5	BAND 7
1	0.976 ± 0.258	0.230 ± 0.052	0.282 ± 0.056	0.556 ± 0.091	0.165 ± 0.333	0.080 ± 0.024
2	1.642 ± 0.346	0.345 ± 0.051	0.233 ± 0.037	0.288 ± 0.057	0.102 ± 0.010	0.233 ± 0.076
3	1.194 ± 0.243	0.166 ± 0.025	0.069 ± 0.013	0.401 ± 0.080	±	0.083 ± 0.017
4	0.253 ± 0.029	0.106 ± 0.037	1.193 ± 0.212	0.453 ± 0.085	0.043 ± 0.012	0.201 ± 0.024
5	1.116 ± 0.201	0.227 ± 0.033	0.057 ± 0.027	0.259 ± 0.029	0.127 ± 0.026	0.037 ± 0.003
6	1.908 ± 0.380	0.349 ± 0.074	0.338 ± 0.074	0.345 ± 0.074	0.187 ± 0.044	0.129 ± 0.042
7	0.569 ± 0.171	0.086 ± 0.008	0.077 ± 0.013	0.191 ± 0.025	0.176 ± 0.044	0.103 ± 0.018
8	1.787 ± 0.343	0.203 ± 0.026	1.609 ± 0.282	0.766 ± 0.132	0.247 ± 0.040	0.075 ± 0.008
9	0.722 ± 0.192	0.046 ± 0.003	0.136 ± 0.029	0.224 ± 0.017	0.035 ± 0.000	0.081 ± 0.022
10	0.601 ± 0.169	0.127 ± 0.018	0.275 ± 0.056	0.305 ± 0.038	0.157 ± 0.019	0.283 ± 0.041
11	1.054 ± 0.200	0.083 ± 0.017	0.049 ± 0.012	0.312 ± 0.023	0.084 ± 0.039	0.122 ± 0.041
12	0.861 ± 0.179	0.192 ± 0.027	0.078 ± 0.022	0.063 ± 0.015	0.039 ± 0.002	0.204 ± 0.030
13	0.787 ± 0.248	0.116 ± 0.024	0.155 ± 0.038	0.221 ± 0.024	0.052 ± 0.021	0.059 ± 0.025
14	1.683 ± 0.313	0.106 ± 0.027	0.416 ± 0.084	0.150 ± 0.010	0.096 ± 0.008	0.048 ± 0.000
15	0.995 ± 0.224	0.098 ± 0.010	0.151 ± 0.031	0.235 ± 0.034	0.259 ± 0.063	0.100 ± 0.016
16	2.626 ± 0.447	0.180 ± 0.039	0.918 ± 0.145	0.218 ± 0.017	0.168 ± 0.026	0.171 ± 0.041

Table 4-3. In-Orbit Coherent Noise at Frequency 17.6 Pixels
White Sands (3 January 83)

CHANNEL	BAND 1	BAND 2	BAND 3	BAND 4	BAND 5	BAND 7
1	0.352 ± 0.118	0.161 ± 0.050	0.469 ± 0.078	0.186 ± 0.078	0.012 ± 0.006	0.066 ± 0.015
2	0.103 ± 0.028	0.062 ± 0.000	0.256 ± 0.058	0.091 ± 0.012	0.114 ± 0.009	0.141 ± 0.018
3	0.374 ± 0.087	0.076 ± 0.014	0.213 ± 0.087	0.185 ± 0.024	±	0.022 ± 0.005
4	0.417 ± 0.237	0.082 ± 0.020	0.198 ± 0.051	0.045 ± 0.007	0.057 ± 0.011	0.119 ± 0.030
5	0.270 ± 0.103	0.111 ± 0.026	0.113 ± 0.038	0.059 ± 0.010	0.033 ± 0.008	0.134 ± 0.017
6	0.158 ± 0.028	0.061 ± 0.010	0.167 ± 0.070	0.115 ± 0.024	0.094 ± 0.029	0.045 ± 0.014
7	0.357 ± 0.081	0.082 ± 0.006	0.157 ± 0.023	0.101 ± 0.009	0.159 ± 0.018	0.223 ± 0.092
8	0.092 ± 0.031	0.017 ± 0.006	0.082 ± 0.031	0.146 ± 0.009	0.009 ± 0.000	0.114 ± 0.022
9	0.184 ± 0.063	0.049 ± 0.008	0.221 ± 0.053	0.126 ± 0.053	0.023 ± 0.000	0.012 ± 0.000
10	0.307 ± 0.060	0.043 ± 0.004	0.088 ± 0.050	0.044 ± 0.009	0.031 ± 0.000	0.003 ± 0.000
11	0.206 ± 0.094	0.049 ± 0.004	0.167 ± 0.023	0.035 ± 0.010	0.128 ± 0.022	0.046 ± 0.000
12	0.366 ± 0.188	0.047 ± 0.004	0.102 ± 0.030	0.092 ± 0.019	0.146 ± 0.016	0.067 ± 0.027
13	0.348 ± 0.143	0.110 ± 0.025	0.142 ± 0.069	0.052 ± 0.009	0.052 ± 0.012	0.138 ± 0.016
14	0.195 ± 0.044	0.032 ± 0.009	0.138 ± 0.047	0.015 ± 0.002	0.067 ± 0.032	0.141 ± 0.032
15	0.308 ± 0.090	0.122 ± 0.012	0.273 ± 0.069	0.060 ± 0.010	0.142 ± 0.016	0.212 ± 0.010
16	0.209 ± 0.106	0.074 ± 0.028	0.338 ± 0.109	0.267 ± 0.032	0.051 ± 0.014	0.116 ± 0.009

digital imagery to partially reduce coherent noise, a statistical randomization can be used to assure a zero mean quantization error (Section 5.2.4).

4.5 SCAN-CORRELATED SHIFTS

Scan-correlated shifts are one of two types of "between-scan, line-dependent noise." Malila et al., (1984) referred to them, on Landsat-4 TM/PF, as level-shift artifacts of Form 1 (exemplified by Channel 4 of Band 1) and Form 2 (exemplified by Channel 7 of Band 7). In this paper, these shifts will be called scan-correlated shifts of Type 4-1 and 4-7, respectively. Malila et al., (1984) observed these shifts most clearly in scenes of raw or geometrically unresampled data taken at night (ID 40037-02243 and ID 40161-02481) and over the clear waters of the Bahamas. Type 4-1 shifts were absent in many scenes but, when present, were largest for Channels 4, 12, 10 and 8 in Band 1, with respective amplitudes of approximately 2.2, 1.8, 1.0 and 0.75 DN. Type 4-7 shifts were present in all examined scenes and occurred with a higher within-scene frequency approaching every 2 sweeps. The largest amplitudes for Type 4-7 shifts were 1.0, 0.5 and 0.4 DN for Channels 7, 10 and 8, respectively, in Band 7. Murphy et al. (1984) have observed that these Type 4-1 shifts start and end at the beginning of a scan line. Their magnitude and consistency suggest a line-by-line radiometric correction procedure for each channel:

$$L'_{RS} = L_R + CS(T,J) \qquad (4\text{-}9)$$

where $CS(T,J)$ = correction in DN for scan-correlated shift of Type T in scan number J

L'_{RS} = raw radiance in DN corrected for scan-correlated shift

A procedure for correcting for scan-correlated shifts has been developed and tested as part of this study. Assumptions that were made include:

- Shifts are constant within a line; they are either present or absent
- If a shift is present in one channel, it is present in all channels

- The direction and magnitude of the shifts are constant within a scene for each channel (Appendices 9.8 and 9.11)

- There can be as many different types of shifts as there are bands. Two types are tested for Landsat-4 TM/PF (Type 4-1 and 4-7). Two types were also tested for Landsat-5 TM/F (Type 5-3 and 5-7), but only Type 5-3 was significant

- Backgrounds are not constant within a line or between lines because of effects such as bright-target saturation. In this study, the average of 24 or 28 mf on the shutter, before and after DC restoration, were used as background, B, for testing the procedures for correcting for shifts. Forward and reverse scans were calculated separately. Therefore, there were four distinct sets of backgrounds:

  BF-BDC = Background from a forward scan before DC restoration, i.e. from shutter region 1

  BF-ADC = Background from a forward scan after DC restoration, i.e. from shutter region 2

  BR-BDC = Background from a reverse scan before DC restoration, i.e. from shutter region 1

  BR-ADC = Background from a reverse scan after DC restoration, i.e. from shutter region 2.

The steps in the correction procedure were:

- Separately process forward and reverse scans

- Use a reference channel for each type of shift:

  Type 4-1 = Channel 4 in Band 1 on Landsat-4
  Type 4-7 = Channel 7 in Band 7 on Landsat-4
  Type 5-3 = Channel 1 in Band 3 on Landsat-5

- Use the line-averaged background to monitor for shifts

- Separate the backgrounds of the references into two states, thereby creating a binary mask for each type, indicating its presence or absence in each scan of the scene. In future tests, this step could be done for the most significant shift first,

and a correction applied for this shift before searching for a second type of shift

- For each channel, calculate the average size of the correction for scan-correlated shift, CS(T), of each type, by averaging the difference between the high and low states at each transition, i:

$$CS(T) = \frac{1}{t} \sum_{i=1}^{t} \left(B_H - B_L \right)_i \qquad (4\text{-}10)$$

- Apply corrections, CS(T), on a line-by-line basis. Illustrative results for all channels are given in Appendices 9.7 through 9.11, before and after backgrounds were corrected for both TM/PF and TM/F.

An initial test of this correction procedure was made for type 4-1 noise on a pre-launch single background collect of ambient data from March 22, 1982. A simultaneous test for Type 4-7 correction, CS, could not be made because the CFP was not cooled. Linear within-band correlations were run for all channels in forward and reverse scans, both with and without corrections from Equation 4-10. For uncorrected data, the apparent linear correlations from this binary level phenomenon were highest for pairs of channels which both had large Type 4-1 shifts. Correlation coefficients, R, were highest between forward and forward scans and lowest between adjacent forward and reverse scans, i.e.:

$$R^2_{FF}(B_i, B_j) \quad R^2_{RR}(B_i, B_j) >> R^2_{RF}(B_{i,F}, B_{i,F+1})$$

where

B_i = average background in DN on shutter for channel i for a single line

B_j = average background in DN on shutter for channel j where j and i are in the same band

$R_{FF}(B_i, B_j)$ = linear correlation coefficient for pairs (B_i, B_j) versus scan number, 2J, for 200 forward scans

$R_{RR}(B_i, B_j)$ = correlation of (B_i, B_j) versus $(2J + 1)$, for 200 reverse scans

$R_{RF}(B_{i,F}, B_{i,F+1})$ = correlation of 200 adjacent forward and reverse scan pairs for channel i.

All channels in all four bands appear to shift at the same time. This led to the original name of channel-correlated shifts, which was later broadened to scan-correlated shifts since all channels within a scan are affected. The low correlation of pairs of adjacent forward and reverse scans versus scan number is due to shifts occurring randomly at the start of any scan, forward or reverse. When comparing pairs within, rather than between, a scan, the pairs of channels always change states at the same time. Illustrative correlation coefficients for the backgrounds in two specified channels for these initial tests are summarized in Table 4-4, both before and after applying corrections for scan-correlated shifts, and for both TM/PF and TM/F. These results, especially the near-unity correlations of forward-to-forward backgrounds, justify the assumption that "if a shift is present in one channel, it is present in all channels in that band."

For Landsat-5 TM/F, the reference channel is Band 3 Channel 1 for Type 5-3, with the largest prelaunch shifts being 0.5, 0.5, 0.4 and 0.3 DN in Band 2 Channel 1, Band 3 Channel 1, Band 3 Channel 3 and Band 4 Channel 1, respectively, for the "Golden Tape," which was an ambient 7-band integrating sphere GPC collect on August 30, 1983 at 16:14:15, labeled as Goddard BRU tape #517 (GE/VF # CIS1B, Scene ID 5-198-10563). This scan-correlated shift is lower in magnitude in Landsat-5 (Appendix 9.11), however, it is more uniformly present in Band 3 than in any bands on Landsat-4 (Appendix 9.8).

For the Landsat-4 San Francisco scene on day 392 after launch, there were approximately 70 changes of state in 380 scans for Type 4-1 noise, and many more for Type 4-7. Type 4-1 shifts were present before and after DC restorations, which is consistent with the assumption that "shifts are constant within a line." This scene was acquired using the synchronized second or redundant TM/PF power supply, The presence of scan-correlated shifts of Landsat-5 TM/F, where both primary and redundant power supplies are free-running, exonerates the synchronization as the sole source of the shift.

The A/D converter is a possible source of this scan-correlated noise. Corrections were possible on Bands 5 and 7 for pre-launch Landsat-4 data even though these

detectors were turned off (Table 4-4, and Appendices 9.10 and 9.11). When the bands are off, a constant reference voltage is expected from the A/D converter. In fact, the reference voltage must have a small but finite variability relative to the size of the bin. Therefore, if such a reference signal happens to fall near the upper threshold of bin 2, then a mix of counts 2 and 3 would be expected from quantization error. Values other than 2 are indeed observed when the CFP bands are off. The observed correlation and correctability of these noise counts in Table 4-4, and in Appendix 9.10 and 9.11, suggests that a variable reference voltage in the A/D converter may be a source of scan-correlated shifts.

Observations of the shutter backgrounds lead to suggestions for least-noisy and most-noisy references. Results are given in Table 4-5. The largest shift was used to define the noisiest. Small shift, low random variability, and minimum differences between forward and reverse scans were used as criteria to identify the quiet references. These reference channels are used in preference to earlier ones, such as Channels 1 and 9. Channel 1 was the first reference but it also has the largest offset. Channel 9 was chosen because it was the middle of the focal plane. Criteria cited here provide a basis for choosing a reference channel, based on the stability of its signal.

Since the magnitude of the scan-correlated shifts range from zero to two DNs, uncorrected attempts to normalize gains and offsets will be uncertain by this amount when full-scene histogram-equalization procedures are used. This is also the reason that there are some values of relative biases in Equation 1-1 that are nearly a DN different from zero. Scan-correlated shifts are a large source of noise and are at least partially correctable.

Application of corrections for scan-correlated shifts needs to be scan-specific. It appears that this may have contributed to some residual errors in bias by Fischel (1984, Equation 4-12) and Kogut (1984, Equation 4-5). Estimating background by averaging between scans is not desirable, unless these corrections have been made.

A single unconfirmed case has been reported of a discontinuous change in sensitivity part way through the image. If such a discontinuous bias or gain change does occur, it has not been fully characterized. Such "multi-scan bands" are potentially subject to line-by-line application of the normal IC system radiometric calibration, except that the IC data has to be separated into as many separate calibration sets as there are multi-scan bands.

Table 4-4. Between-Channel Linear Correlation Coefficients, before and after making corrections for scan-correlated shifts in Landsat TM sensor, illustrating with two channels the fact that "if a shift is present in one channel, it is present in all channels of that band."

(TM/PF REF: BAND 1 CHANNEL 4 NOISE TYPE 4-1) (TM/F REF: BAND 3 CHANNEL 1, NOISE TYPE 5-3)

CHANNEL-TO-CHANNEL WITHIN-BAND FORWARD-FORWARD CORRELATIONS (R) BEFORE AND AFTER CORRECTIONS FOR SCAN-CORRELATED SHIFTS IN AVERAGE SHUTTER BACKGROUND

	BAND 1	BAND 2	BAND 3	BAND 4	BAND 5	BAND 7	BAND 6
LANDSAT-4 (TM/PF)					OFF	OFF	OFF
CHANNEL PAIR	4/12	1/14	1/15	6/16	2/4/12 13/14/15	14/16	1/3
$100R^2$, BEFORE	98	75	92	92	99	91	97 REV
$100R^2$, AFTER	10	5	15	18	15	2	98 REV
LANDSAT-5 (TM/F)					ON	ON	ON
CHANNEL PAIR	10/12	1/3	1/3	1/4	1/3	7/9	1/2
$100R^2$, BEFORE	60	84	90	72	47	55	78
$100R^2$, AFTER	5	3	4	0	0	0	78

9622 (501 84

Table 4-5. TM Radiometric Reference Channels

	BAND 1	BAND 2	BAND 3	BAND 4	BAND 5	BAND 7	BAND 6
LANDSAT-4 TM/PF							
LOWEST NOISE							
SHUTTER rms	**9**	**14**	**12**	**7**	**2**	**15**	**4F**
HIGHEST NOISE							
SHUTTER rms	16	2	1	8	7	7	1
SHIFT TYPE 4-1	4	—	1	16	15	—	—
SHIFT TYPE 4-7	—	1	16	—	10	7	—
32 KHz (3.2 mf)	16	6	8	8	[8]	[10]	—
6 KHz (18 mf)	4	1	1	16	[7]	[7]	—
LANDSAT-5 TM/F							
LOWEST NOISE							
SHUTTER rms	**15**	**10**	**2**	**1**	**2**	**15**	**4**
HIGHEST NOISE							
SHUTTER rms	4	1	12	3	10	9	1
SHIFT TYPE 5-3	10	1	1	1	3	—	—

5622 (54°1/84

This type of between-scan change is not called noise because its apparent correction involves processing of IC data. Multi-scan banding may also prove to be a gain-free offset shift, such as those associated with bright-target saturation or with the scan-correlated shifts discussed in this section.

4.6 FORWARD/REVERSE-SCAN DIFFERENCES

Forward/reverse-scan differences are the second type of "between-scan, line-dependent noise." If a forward/reverse-scan difference actually exists, it has not been definitively demonstrated to be independent of expected forward/reverse manifestations from one or more of the types of noise referred to above (Sections 4.2, 4.3, and 4.5). For background in the shutter region, the apparent magnitude of the average value of (BFWD-BREV) in Landsat-4 is 0.1 DN in the PFP bands, except for scenes with clouds (Appendix 9.12).

In most of the pre-launch tests, calculated values of forward/reverse-scan differences are nearly zero in all bands of Landsat-5, with the exception of a value for Band 4 Channel 16 of -0.1 DN (Appendix 9.12). In the worst cases with calculated DN values as large as 2, the test procedure called for a light source in front of the TM/F. This indicates that the forward/reverse difference is scene dependent. Indeed, initial in-orbit data indicate a background difference as high as 3 DN for band 1 on Landsat-5 TM/F.

It is necessary to process calibration pulses, P, separately in order to avoid scan-correlated shifts. For forward scans, each line has a corrected pulse value of:

$$P' = P - BF\text{-}ADC' \qquad (4\text{-}11)$$

and

$$BF\text{-}ADC' = BF\text{-}ADC + CS \qquad (4\text{-}12)$$

where BF-ADC = background on shutter after DC restoration, in DN

CS = correction for scan-correlated shift (see Equation 4-10).

For reverse scans:

$$P' = P - BR\text{-}BDC' \qquad (4\text{-}13)$$

and

$$BR\text{-}BDC' = BR\text{-}BDC + CS \qquad (4\text{-}14)$$

where BR-BDC = background of shutter before DC restoration, in DN.

These are net pulses rather than gross pulses. Useful net pulses cannot be created from the 000 all-lamps-off configuration of the IC unless corrected for between-scan shifts. In general, uncorrected or gross pulse values cannot be used. The same procedure applies to conversion of digital imagery values to net counts. For forward and reverse scans:

$$L_R' = L_R - BDC' \cdot \qquad (4\text{-}15)$$

When using shutter background, threshold checks are feasible for removing noise from sources such as resetting the scan-line corrector (SLC) and incomplete obscuration. This removal requires an outlier rejection strategy. All such possible forward/reverse-scan differences can be avoided if one chooses to calibrate forward and reverse scans separately. However, if a need to make this correction exists, it can take the form:

$$L_{RF}' = L_R + CF(J) \qquad (4\text{-}16)$$

where CF(J) = correction in DN for normalization to forward scans as a function of scan number, J.

Some authors (Engel et al., 1983) have chosen to use the term "banding" to distinguish this forward/reverse difference between adjacent sweeps of 16 channels and the repeated radiometric striping which is associated with a specific channel.

4.7 TOTAL NOISE

In earlier descriptions of absolute calibration, signal-to-noise values were calculated at two specific radiances (Barker, Bell et al., 1984). The rms noise of that signal can now be seen to be the upper limit on the rms random noise, since it contains a finite number of systematic noise components. For later use in error models, the random noise of each channel is defined as the standard deviation, σ_r.

An rms estimate of the apparent total background noise in the TM/PF sensor ranges from ± 0.4 to ± 1.3 DN, depending on the band (Table 4-6). If one assumes a range of plus or minus three standard deviations, then this implies that the range of uncertainty in DN values, prior to any systematic corrections outlined in this section, is from 2 to 8 DN. As expected from real sources, estimates of rms noise, for either a pre-launch flooding lamp or for an apparently homogeneous part of an ocean scene, have a slightly higher range from ± 0.5 to ± 1.7 DN, depending on the band (Table 4-7). This implies that the range of uncertainty in DN, prior to any systematic corrections outlined earlier in this section, is from 3 to 9 DN values.

One measure of the total noise is the standard deviation on shutter backgrounds (Appendix 9.12). The true random error can be estimated from shutter counts after correction for systematic errors.

4.8 WITHIN-SCENE ERROR MODELS

In order to incorporate the within-scene corrections mentioned above, the basic radiometric calibration equations have to be restructured for each channel. Equation 1-2, for regressing observed pulses against nominal pulses, becomes:

$$\overline{P'}(\ell) = NB'_{IC} + NG'_{IC}P'_n(\ell) \qquad (4\text{-}17)$$

Equation 1-1, for applying the normalized gain and bias to the raw image data, becomes:

$$L'_{cal} = \frac{L'_R - NB'_A}{NG'_A} \qquad (4\text{-}18)$$

Table 4-6. Apparent rms Noise in Background Data for Landsat-4 TM/PF

		BAND 1	BAND 2	BAND 3	BAND 4	BAND 5	BAND 7
ODD CHANNEL	FLOODING LAMP[1]	1.24	0.450	0.539	0.333	0.948	1.25
EVEN CHANNEL	FLOODING LAMP[1]	1.27	0.557	0.669	0.405	0.939	1.13
ODD CHANNEL	WATER[2]	1.12	0.393	0.518	0.496	0.872	1.03
EVEN CHANNEL	WATER[2]	1.33	0.523	0.657	0.575	0.818	1.01

Table 4-7. Apparent rms Noise in Image Data for Landsat-4 TM/PF

		BAND 1	BAND 2	BAND 3	BAND 4	BAND 5	BAND 7
ODD CHANNEL	FLOODING LAMP[1]	1.45	0.606	0.859	0.483	1.19	1.67
EVEN CHANNEL	FLOODING LAMP[1]	1.50	0.684	0.952	0.532	1.19	1.40
ODD CHANNEL	WATER[2]	1.51	0.589	0.842	0.462	0.921	1.13
EVEN CHANNEL	WATER[2]	1.71	0.655	0.942	0.461	0.840	1.06

[1]Flooding Lamp, March 1982.

[2]Boston Water Scene, September 10, 1982 (ID 40056-14541).

and Equation 1-4, for converting calibrated counts into spectral radiance, becomes:

$$L_\lambda = \frac{L'_{cal} - O^o(B)}{G^o(B)} \quad . \tag{4-19}$$

The construction of this correction model has proceeded from the fact that, in general, if the raw radiance, L_R, is corrected for v correction variables, C_i, then the corrected radiance, L'_R, is a function of all these variables:

$$L'_R = L'_R\ (L_R,\ C_1,\ C_2,\ \ldots\ C_i\ \ldots\ C_v) \tag{4-20}$$

and the standard deviation of this corrected radiance, $\sigma_{L'}$, is the square root of the variance:

$$\sigma^2_{L'} = \left(\frac{\partial L'_R}{\partial L_R}\right)^2 \sigma^2_{L_R} + \sum_{i=1}^{v} \left(\frac{\partial L'_R}{\partial C_i}\right)^2 \sigma^2_{C_i} \quad . \tag{4-21}$$

Assuming that the variables are separable, a formulation of the corrections in additive terms is:

$$L'_R = L_R + \sum_{i=1}^{v} C_i \tag{4-22}$$

which for the six currently identified sources of within-scene systematic variation could be written as:

$$L'_R = L_R + CA + CD + CB + CC + CS + CF \tag{4-23}$$

which are defined by Equations 4-1, 4-3, 4-7, 4-8, 4-10 and 4-16.

The variance in the corrected signal can be derived from Equations 4-21 and 4-22, and the assumption that the only variance in L_R is from the random noise, σ_r:

$$\sigma^2_{L'} = \sigma^2_r + \sum_{i=1}^{v} \sigma^2_{C_i} \qquad (4\text{-}24)$$

or more explicitly from Equation 4-23:

$$\sigma^2_{L'} = \sigma^2_r + \sigma^2_{CA} + \sigma^2_{CD} + \sigma^2_{CB} + \sigma^2_{CC} + \sigma^2_{CS} + \sigma^2_{CF}. \qquad (4\text{-}25)$$

One of the advantages of formulating the corrections linearly is that optimization of the fitting parameters can now be done in each correction term separately. Minimizing individual correction errors produces the minimum error for the fully corrected raw radiance. For the magnitude of systematic corrections for TM of less than 2 DN, the assumption of separability of primary causes implied by additive corrections in Equation 4-23 is a useful approximation if the coupling between these sources of radiometric variability is small relative to the uncertainties in making the corrections. Use of additive corrections also implies that the multiplicative corrections, such as droop, have an overall correction that is small relative to the size of the raw signal.

Time is one physical variable which can be used to quantify the degree of separability of individual types of systematic variations in the TM sensor's response to radiance. The period of a phenomenon, in pixels or seconds, or the frequency, in cycles per second (Hz), can be used as surrogates for time. For the currently-identified systematic corrections to TM data, an approximate order by frequency is:

$$f_A \gg f_C \gg f_D \quad f_B > f_{FR} > f_S \gg f_P \gg f_{BD} \qquad (4\text{-}26)$$

where the symbols are:

$>$ = greater than
$\gg$ = factor of more than ten greater than
$\approx$ = approximately equal

and the frequency, f, subscripts are:

A = A/D Bin-Radiance Dependence (Section 4.1)
C = Coherent Noise (Section 4.4)
D = Within-Line Droop (Section 4.2)
B = Bright-Target Saturation (Section 4.3)
FR = Forward/Reverse-Scan Differences (Section 4.6)
S = Scan-Correlated Shifts (Section 4.5)
P = Within-Path Smoothing (Section 5.1.7)
BD = Between-Date Smoothing (Section 5.1.8).

If a sufficient criterion for separability is a difference in period or frequency of more than a factor of ten, then Equation 4-26 is a guide to which corrections might not be separable.

Errors associated with applying systematic corrections will be reduced if the corrections are calculated in the order of their occurrence, as well as in the order of their absolute magnitude. Order of occurrence is given by Equation 4-26. If the phenomena cannot be uncoupled sufficiently by serial linear corrections, then iterative procedures can be used to reduce the random errors in applying these systematic corrections.

An additional use of error models is to decide whether or not to make a correction. Using the correction for scan-correlated shifts, calculated for t transitions, as an example, the variance of Equation 4-10 is:

$$\sigma_{CS}^2 = \frac{1}{t} \quad \sigma_{B_H}^2 + \sigma_{B_L}^2 \quad \frac{2}{t} \sigma_B^2. \qquad (4\text{-}27)$$

Since the corrected shutter background for a line is:

$$B' = B + CS \qquad (4\text{-}28)$$

then its variance is:

$$\sigma_{B'}^2 = \sigma_B^2 + \sigma_{CS}^2 \qquad (4\text{-}29)$$

which by substitution becomes:

$$\sigma_{B'}^2 = 1 + \frac{2}{t} \quad \sigma_B^2. \qquad (4\text{-}30)$$

Equation 4-30 illustrates the generically true statement that the random error in an arithmetically corrected raw radiance value will always be larger than the random error in the uncorrected value. However, Equation 4-30 also illustrates the fact that a correction for scan-correlated shifts can be made to as high a precision as desired by using a sufficient number of transitions, t, between high and low states. For certain channels, this assumption is adequately valid, while for others, there is a possibility that each of these states might themselves be split into two states. One empirical method to use in deciding the validity of the assumption is to use Equation 4-27 in a linear plot of observed variance in CS, σ_{CS}^2, versus the number of transitions within a pass and then between passes to check for systematic displacement of the lines.

At some value of t, the value of σ_{CS}^2 will stop decreasing linearly due to the start of some as yet unaccounted for variability, such as a further two-state splitting. The utility of deriving equations such as 4-27 and 4-30 is that they lead to methods for testing the validity of the assumptions in the model. Furthermore, they also provide a method for testing the statistical significance, at a given level α, of any correction C with a standard deviation σ_C. The correction is statistically significant if:

$$\frac{|C|}{\sigma_C} > t_\alpha \qquad (4\text{-}31)$$

where t_α = the student t distribution number for an α level of significance.

This has the implication for TM, that if the correction is constant with time, then a single experimental collection of data can be used to derive an average value for the correction to a specific level of precision for use on any scene.

This empirical formulation of a correction model might be usefully augmented by using the engineering model of TM that is still available to identify the causes of these radiometric variations.

A causitive engineering model of these systematic variations could produce a more stable set of correction procedures for radiometric ground processing, whether the corrections are done line-by-line between scans or sample-by-sample within scans.

Without within-scene corrections, the TM/PF sensor has a range of radiometric uncertainty of 3 to 8 DN, depending on the band (Table 4-6). This is a second order effect, as defined in Table 4-8. It is of the same order as the current uncertainty, or accuracy, of the absolute radiometry. Relative precision might be improved by an order of magnitude, and thereby reduced to a third order effect, by applying the systematic corrections suggested in this section.

Historically, scientists have wanted to start with raw data rather than processed or "corrected" digital imagery. This has led to a generation of discipline scientists in remote sensing being converted into self-made image processing scientists. The amount of computer capacity and time required to develop calibration procedures and analyze TM imagery no longer affords more than a small number of such scientists that luxury. For multidisciplinary general use of TM digital imagery, the preprocessing steps associated with radiometric and geometric resampling must be an accepted starting place. Ideally, the final corrected product needs to be ready for immediate use in scientific studies, i.e., the final systematically corrected product needs to have minimal errors in absolute and relative radiometry.

Table 4-8. Definition of Size of Uncertainty in TM Radiometry

SIZE OF EFFECT	RELATIVE UNCERTAINTY (%)	ABSOLUTE UNCERTAINTY (DN)
ZERO ORDER	∞	∞
1ST ORDER	10 TO 100	26 TO 255
2ND ORDER	1 TO 10	3 TO 26
3RD ORDER	0.1 TO 1	0.3 TO 3
4TH ORDER	0.01 TO 0.1	0.03 TO 0.3

SN-22 150) 84

4.9 SUMMARY OF WITHIN-SCENE VARIABILITY

The effect of bright-target saturation was shown as a function of the distance from the end of exposure to the bright target (see Figure 4-2). This means that the variability introduced into the background will be a function of the scene content and is not a fundamental characteristic of the sensor system. Tables 4-9 and 4-10 illustrate this point. In Table 4-9, per-band average forward-reverse differences are presented for "quiet" scenes (nighttime data for Landsat-4, integrating sphere data for Landsat-5). These measured differences are insignificant (near zero) especially when compared to the same per-band averages taken from Landsat-4 data of a cloudy scene, given in Table 4-10.

Total within-scene variability for individual detectors of Landsat-4 reflective bands is given in Tables 4-11 through 4-16, along with data on forward-reverse differences, scan-correlated shifts and coherent noise. Early data taken on within-scene variability for Landsat-5 (total shutter noise and scan-correlated shifts) is given in Table 4-17. Finally, in Table 4-18, lowest and highest noise measures are given for reference channels of Landsats-4 and 5 reflective bands. (Note, reference channels are identified in Table 4-5.)

Table 4-9

WITHIN-SCENE VARIABILITY
TM SHUTTER BACKGROUND IN "QUIET" SCENES
TM/PF ON LANDSAT-4 AND TM/F ON LANDSAT-5
(AVERAGE OF ALL CHANNELS IN A BAND)

	TOTAL VARIABILITY (SD)		(FWD-REV) DIFFERENCE	
BAND	TM/PF[a] (DN)	TM/F[b] (DN)	TM/PF[a] (DN)	TM/F[b] (DN)
1	±1.24	±0.89	0.20	0.04
2	±0.56	±0.29	0.12	0.06
3	±0.73	±0.51	0.13	0.03
4	±0.41	±0.37	0.09	0.01
5	±0.89	±0.93	0.01	0.08
7	±1.03	±0.93	0.03	0.10

[a]LANDSAT-4 IN-ORBIT NIGHT SCENE OF BUFFALO, NY (40037-02243, 22 AUG 82)

[b]LANDSAT-5 PRE-LAUNCH AMBIENT INTEGRATING SPHERE (5-198-10563, 30 AUG 83)

BARKER APR 84 GSFC

Table 4-10

WITHIN-SCENE VARIABILITY

TM SHUTTER BACKGROUND IN CLOUDY SCENE
CLOUDS ON WESTERN EDGE OF SCENE
SAN FRANCISCO, CA (40392-18152, 12 AUG 83)

(AVERAGE OF ALL CHANNELS IN A BAND)

	TOTAL VARIABILITY (SD) BEFORE AND AFTER DC RESTORE		(FWD-REV) DIFFERENCE BEFORE AND AFTER DC RESTORE	
BAND	B-BDC (DN)	B-ADC (DN)	B-BDC (DN)	B-ADC (DN)
1	±1.45	±1.42	−0.54	1.53
2	±1.11	±1.51	1.29	2.56
3	±1.24	±1.46	1.31	2.44
4	±0.71	±1.02	0.39	1.62
5	±0.93	±0.89	−0.21	0.02
7	±1.05	±1.01	−0.15	0.05

BARKER APR 84 GSFC

Table 4-11

BAND 1 ON LANDSAT-4 TM/PF, WITHIN-SCENE VARIABILITY (IN DN)

	TOTAL VARIABILITY STANDARD DEVIATION OF SHUTTER IN AND AROUND DC RESTORATION			(FWD-REV) DIFFERENCE BACKGROUND ON SHUTTER IN AND AROUND DC RESTORATION			SCAN-CORRELATED SHIFTS		COHERENT NOISE	
		CLOUDY SCENE[b]			CLOUDY SCENE[b]				32 KHz (3.2 mf)	6 KHz (18 mf)
CHANNEL	PM SCENE[a] SD(B)	SD(B-BDC)	SD(B-ADC)	PM SCENE[a] ΔBFR	ΔBFR (BDC)	ΔBFR (ADC)	TYPE 4-1.4 AVERAGE[b] CS(4-1)	TYPE 4-7.7 AVG[a,b] CS (4-7)	(area ± 2 mf of peak) CC (32)	CC(6)
16	±1.5	±1.7	±1.7	0.1	-0.6	1.2	0.1	0.0	2.6	0.2
15	±1.4	±1.5	±1.6	0.3	-0.1	2.5	0.0	0.1	1.0	0.3
14	±1.3	±1.5	±1.4	0.1	-0.6	1.6	0.2	0.0	1.7	0.2
13	±1.3	±1.4	±1.4	0.3	-0.2	2.0	0.1	-0.1	0.8	0.3
12	±1.1	±1.6	±1.4	0.2	-0.4	1.3	1.7	0.0	0.9	0.4
11	±1.3	±1.4	±1.4	0.3	-0.4	2.0	0.0	-0.1	1.0	0.2
10	±1.0	±1.4	±1.4	0.1	-0.6	1.8	1.0	0.0	0.6	0.3
9	±1.1	±1.2	±1.2	0.2	-0.5	1.4	0.0	0.0	0.7	0.2
8	±1.2	±1.5	±1.5	0.1	-1.1	1.3	0.8	-0.1	1.8	0.1
7	±1.3	±1.4	±1.3	0.2	-0.5	1.4	0.0	-0.1	0.6	0.4
6	±1.3	±1.6	±1.5	0.1	-1.3	1.2	0.2	0.0	1.1	0.2
5	±1.1	±1.2	±1.0	0.2	-0.4	1.0	0.0	-0.1	1.1	0.3
4	±1.2	±1.8	±1.6	0.2	-0.5	1.6	2.0	0.0	0.3	0.4
3	±1.1	±1.2	±1.2	0.2	-0.6	1.4	0.0	-0.1	1.2	0.4
2	±1.3	±1.6	±1.6	0.2	-0.7	1.7	0.1	-0.1	1.6	0.1
1	±1.3	±1.4	±1.3	0.2	-0.4	1.3	0.3	0.1	1.0	0.4

[a]PM BUFFALO, NY (40037-02243), [b]SAN FRANCISCO, CA (40392-18152), [c]WHITE SANDS, NM (40171-17080)

BARKER APR 84

Table 4-12

BAND 2 ON LANDSAT-4 TM/PF, WITHIN-SCENE VARIABILITY (IN DN)

	TOTAL VARIABILITY STANDARD DEVIATION OF SHUTTER IN AND AROUND DC RESTORATION			(FWD-REV) DIFFERENCE BACKGROUND ON SHUTTER IN AND AROUND DC RESTORATION			SCAN-CORRELATED SHIFTS		COHERENT NOISE	
		CLOUDY SCENE[b]			CLOUDY SCENE[b]				32 KHz (3.2 mf) (area ± 2 mf of peak)	6 KHz (18 mf)
CHANNEL	PM SCENE[a] SD(B)	SD(B-BDC)	SD(B-ADC)	PM SCENE[a] ΔBFR	ΔBFR (BDC)	ΔBFR (ADC)	TYPE 4-1.4 AVERAGE[b] CS(4-1)	TYPE 4-7.7 AVG[a,b] CS (4-7)	CC (32)	CC(6)
16	±0.5	±1.7	±1.6	0.1	1.5	2.9	0.0	0.0	0.2	0.1
15	±0.6	±1.5	±1.5	0.3	1.3	2.6	0.0	0.0	0.1	0.1
14	±0.4	±1.5	±1.5	0.1	1.2	2.5	0.0	0.0	0.1	0.0
13	±0.6	±1.4	±1.6	0.3	1.5	2.8	0.0	0.0	0.1	0.1
12	±0.5	±1.6	±1.5	0.2	1.3	2.7	0.0	0.0	0.2	0.0
11	±0.5	±1.4	±1.4	0.3	1.3	2.4	0.0	0.0	0.1	0.0
10	±0.4	±1.4	±1.4	0.1	1.2	2.5	0.0	0.0	0.1	0.0
9	±0.5	±1.2	±1.5	0.2	1.3	2.6	0.0	0.0	0.0	0.0
8	±0.5	±1.5	±1.5	0.1	1.3	2.7	0.0	0.0	0.2	0.0
7	±0.5	±1.4	±1.4	0.2	1.2	2.3	0.0	0.0	0.1	0.1
6	±0.5	±1.6	±1.5	0.1	1.3	2.7	0.0	0.0	0.3	0.1
5	±0.5	±1.2	±1.4	0.2	1.3	2.4	0.0	-0.1	0.2	0.1
4	±0.7	±1.8	±1.4	0.2	1.1	2.2	0.1	0.0	0.1	0.1
3	±0.6	±1.2	±1.5	0.2	1.3	2.6	0.0	-0.1	0.2	0.1
2	±1.0	±1.6	±1.7	0.2	1.1	2.6	0.0	0.0	0.3	0.1
1	±0.7	±1.4	±1.5	0.2	1.3	2.6	0.1	-0.2	0.2	0.2

[a]PM BUFFALO, NY (40037-02243), [b]SAN FRANCISCO, CA (40392-18152), [c]WHITE SANDS, NM (40171-17080)

BARKER APR 84 GSFC

Table 4-13

BAND 3 ON LANDSAT-4 TM/PF, WITHIN-SCENE VARIABILITY (IN DN)

	TOTAL VARIABILITY STANDARD DEVIATION OF SHUTTER IN AND AROUND DC RESTORATION			(FWD-REV) DIFFERENCE BACKGROUND ON SHUTTER IN AND AROUND DC RESTORATION			SCAN-CORRELATED SHIFTS		COHERENT NOISE	
		CLOUDY SCENE[b]			CLOUDY SCENE[b]				32 KHz (3.2 mf)	6 KHz (18 mf)
CHANNEL	PM SCENE[a] SD(B)	SD(B-BDC)	SD(B-ADC)	PM SCENE[a] ΔBFR	ΔBFR (BDC)	ΔBFR (ADC)	TYPE 4-1.4 AVERAGE[b] CS(4-1)	TYPE 4-7.7 AVG[a,b] CS (4-7)	(area ±2 mf of peak) CC (32)	CC(6)
16	±1.0	±1.5	±1.6	0.1	1.3	2.7	0.1	0.6	0.9	0.3
15	±0.9	±1.4	±1.4	0.2	1.4	2.3	0.2	-0.3	0.2	0.3
14	±0.5	±1.2	±1.6	0.0	1.6	2.7	0.0	0.0	0.4	0.1
13	±0.8	±1.3	±1.4	0.2	1.4	2.3	0.1	-0.1	0.2	0.1
12	±0.4	±1.1	±1.6	0.1	1.4	2.8	0.0	0.0	0.1	0.1
11	±0.7	±1.2	±1.4	0.1	1.3	2.3	0.0	-0.1	0.0	0.2
10	±0.5	±1.1	±1.7	0.1	1.4	3.0	0.0	0.0	0.3	0.1
9	±0.8	±1.3	±1.6	0.2	1.5	2.8	0.0	0.0	0.1	0.2
8	±0.9	±1.2	±1.6	0.1	1.2	2.6	0.0	0.0	1.6	0.1
7	±0.7	±1.2	±1.4	0.1	1.2	2.3	0.0	-0.1	0.1	0.2
6	±0.5	±1.0	±1.5	0.1	1.4	2.6	0.0	0.0	0.3	0.2
5	±0.8	±1.2	±1.4	0.2	1.2	2.4	0.1	-0.2	0.1	0.1
4	±0.7	±1.1	±1.4	0.1	1.0	2.2	0.0	0.0	1.2	0.2
3	±0.8	±1.2	±1.2	0.2	1.1	2.0	0.1	-0.2	0.1	0.2
2	±0.6	±1.0	±1.3	0.1	0.9	2.1	0.0	0.1	0.2	0.3
1	±1.3	±1.7	±1.3	0.3	1.4	2.0	0.3	0.5	0.3	0.5

[a]PM BUFFALO, NY (40037-02243), [b]SAN FRANCISCO, CA (40392-18152), [c]WHITE SANDS, NM (40171-17080)

BARKER APR 84 GSFC

Table 4-14

BAND 4 ON LANDSAT-4 TM/PF, WITHIN-SCENE VARIABILITY (IN DN)

	TOTAL VARIABILITY STANDARD DEVIATION OF SHUTTER IN AND AROUND DC RESTORATION			(FWD-REV) DIFFERENCE BACKGROUND ON SHUTTER IN AND AROUND DC RESTORATION			SCAN-CORRELATED SHIFTS		COHERENT NOISE	
	PM	CLOUDY SCENE[b]		PM	CLOUDY SCENE[b]				32 KHz (3.2 mf)	6 KHz (18 mf)
CHANNEL	SCENE[a] SD(B)	SD(B-BDC)	SD(B-ADC)	SCENE[a] ΔBFR	ΔBFR (BDC)	ΔBFR (ADC)	TYPE 4-1.4 AVERAGE[b] CS(4-1)	TYPE 4-7.7 AVG[a,b] CS (4-7)	(area ± 2 mf of peak) CC (32)	CC(6)
16	±0.3	±0.7	±0.9	0.0	0.5	1.4	0.2	0.0	0.2	0.3
15	±0.4	±0.6	±1.1	0.1	0.4	1.7	0.1	0.0	0.2	0.1
14	±0.3	±0.8	±1.2	0.1	0.6	1.9	0.0	0.0	0.2	0.0
13	±0.4	±0.6	±0.8	0.1	0.4	1.3	0.0	0.0	0.2	0.1
12	±0.3	±0.7	±1.1	0.1	0.4	1.8	0.1	0.0	0.1	0.1
11	±0.3	±0.6	±0.9	0.1	0.3	1.4	0.1	0.0	0.3	0.1
10	±0.3	±0.7	±1.0	0.1	0.4	1.6	0.0	0.0	0.3	0.0
9	±0.3	±0.6	±1.1	0.1	0.3	1.8	0.0	0.0	0.2	0.1
8	±0.6	±0.9	±1.1	0.1	0.3	1.6	0.0	−0.1	0.8	0.1
7	±0.3	±0.6	±0.9	0.1	0.4	1.5	0.0	0.0	0.2	0.1
6	±0.5	±0.7	±1.1	0.1	0.4	1.8	0.0	0.0	0.3	0.1
5	±0.4	±0.7	±1.0	0.1	0.5	1.7	0.0	0.0	0.3	0.1
4	±0.5	±0.8	±1.0	0.1	0.2	1.6	0.0	−0.1	0.5	0.0
3	±0.6	±0.7	±1.1	0.2	0.4	1.9	0.0	0.0	0.4	0.2
2	±0.4	±0.8	±1.1	0.1	0.3	1.7	0.0	−0.1	0.3	0.1
1	±0.6	±0.7	±0.8	0.1	0.5	1.3	0.2	−0.1	0.6	0.2

[a]PM BUFFALO, NY (40037-02243), [b]SAN FRANCISCO, CA (40392-18152), [c]WHITE SANDS, NM (40171-17080)

Table 4-15

BAND 5 ON LANDSAT-4 TM/PF, WITHIN-SCENE VARIABILITY (IN DN)

	TOTAL VARIABILITY STANDARD DEVIATION OF SHUTTER IN AND AROUND DC RESTORATION			(FWD-REV) DIFFERENCE BACKGROUND ON SHUTTER IN AND AROUND DC RESTORATION			SCAN-CORRELATED SHIFTS		COHERENT NOISE	
		CLOUDY SCENE[b]			CLOUDY SCENE[b]				32 KHz (3.2 mf)	6 KHz (18 mf)
CHANNEL	PM SCENE[a] SD(B)	SD(B-BDC)	SD(B-ADC)	PM SCENE[a] ΔBFR	ΔBFR (BDC)	ΔBFR (ADC)	TYPE 4-1.4 AVERAGE[b] CS(4-1)	TYPE 4-7.7 AVG[a,b] CS (4-7)	(area ±2 mf of peak) CC (32)	CC(6)
16	±0.8	±0.9	±0.8	0.1	-0.3	0.2	0.0	0.1	[0.2]	[0.1]
15	±0.9	±0.9	±0.9	0.1	-0.3	0.1	0.1	0.1	[0.3]	[0.1]
14	±0.9	±0.9	±0.9	0.0	-0.1	0.0	0.0	-0.1	[0.1]	[0.1]
13	±0.9	±0.9	±0.9	0.0	-0.1	0.0	0.0	0.0	[0.1]	[0.1]
12	±0.9	±0.9	±0.9	0.0	-0.1	0.0	0.0	0.0	[0.0]	[0.1]
11	±0.9	±1.0	±0.9	0.0	-0.1	0.0	0.0	0.0	[0.1]	[0.1]
10	±0.9	±1.0	±0.9	0.0	-0.1	0.0	0.0	0.6	[0.1]	[0.0]
9	±0.9	±0.9	±0.9	0.0	-0.1	-0.1	0.0	0.0	[0.0]	[0.0]
8	±0.9	±0.9	±0.8	0.0	-0.1	0.0	0.0	-0.2	[0.2]	[0.0]
7	±1.1	±1.1	±1.1	0.0	0.1	0.0	0.0	0.1	[0.2]	[0.2]
6	±0.9	±0.9	±0.9	0.0	-0.1	0.0	0.0	-0.1	[0.2]	[0.0]
5	±0.9	±0.9	±0.9	0.0	-0.1	-0.1	0.1	0.0	[0.1]	[0.0]
4	±0.8	±0.9	±0.9	0.0	-0.1	0.0	0.1	0.1	[0.0]	[0.1]
3	—	—	—	—	—	—	0.0	0.0	—	—
2	±0.8	±0.9	±0.8	0.1	-0.7	0.1	0.1	0.1	[0.1]	[0.1]
1	±0.8	±0.9	±0.9	0.0	-0.7	-0.1	0.0	0.1	[0.2]	[0.0]

[a]PM BUFFALO, NY (40037-02243), [b]SAN FRANCISCO, CA (40392-18152), [c]WHITE SANDS, NM (40171-17080)

BARKER APR 84 GSFC

Table 4-16

BAND 7 ON LANDSAT-4 TM/PF, WITHIN-SCENE VARIABILITY (IN DN)

	TOTAL VARIABILITY STANDARD DEVIATION OF SHUTTER IN AND AROUND DC RESTORATION			(FWD-REV) DIFFERENCE BACKGROUND ON SHUTTER IN AND AROUND DC RESTORATION			SCAN-CORRELATED SHIFTS		COHERENT NOISE	
		CLOUDY SCENE[b]			CLOUDY SCENE[b]				32 KHz (3.2 mf)	6 KHz (18 mf)
CHANNEL	PM SCENE[a] SD(B)	SD(B-BDC)	SD(B-ADC)	PM SCENE[a] ΔBFR	ΔBFR (BDC)	ΔBFR (ADC)	TYPE 4-1.4 AVERAGE[b] CS(4-1)	TYPE 4-7.7 AVG[a,b] CS (4-7)	(area ±2 mf of peak) CC (32)	CC(6)
16	±1.0	±1.0	±1.0	0.1	-0.2	0.2	0.1	-0.2	[0.2]	[0.1]
15	±0.8	±0.8	±0.8	0.1	-0.2	0.1	0.0	0.2	[0.1]	[0.2]
14	±1.1	±1.1	±1.1	0.0	-0.1	0.0	0.1	-0.1	[0.0]	[0.1]
13	±0.8	±0.9	±0.8	0.0	-0.1	0.0	0.0	0.2	[0.1]	[0.1]
12	±1.0	±1.0	±1.0	0.0	0.0	0.0	0.1	-0.2	[0.2]	[0.1]
11	±1.0	±1.0	±0.9	0.0	0.0	0.0	0.0	-0.2	[0.1]	[0.0]
10	±1.1	±1.1	±1.1	0.0	0.0	0.0	0.1	-0.4	[0.3]	[0.0]
9	±1.0	±1.0	±1.0	0.0	-0.1	0.0	-0.1	0.2	[0.1]	[0.0]
8	±1.0	±1.0	±0.9	0.0	-0.1	0.0	0.0	-0.3	[0.1]	[0.1]
7	±2.0	±1.8	±1.8	0.0	-0.2	0.2	-0.1	0.9	[0.1]	[0.2]
6	±1.0	±1.0	±1.0	0.0	0.0	0.0	0.1	-0.3	[0.1]	[0.1]
5	±0.9	±1.0	±0.9	0.0	0.0	0.0	0.0	0.2	[0.0]	[0.1]
4	±1.0	±1.0	±1.0	0.0	-0.1	0.0	0.1	-0.2	[0.2]	[0.1]
3	±0.9	±0.9	±0.9	0.0	-0.1	0.0	-0.1	0.3	[0.1]	[0.0]
2	±1.0	±1.0	±1.0	0.1	-0.6	0.1	0.0	-0.3	[0.2]	[0.1]
1	±1.0	±1.0	±1.0	0.0	-0.6	0.1	0.0	0.3	[0.1]	[0.1]

[a]PM BUFFALO, NY (40037-02243), [b]SAN FRANCISCO, CA (40392-18152), [c]WHITE SANDS, NM (40171-17080)

Table 4-17

LANDSAT-5 TM/F WITHIN-SCENE VARIABILITY (IN DN)

	BAND 1		BAND 2		BAND 3		BAND 4		BAND 5	BAND 7
CHANNEL	TOTAL SHUTTER NOISE[a] SD(B)	SHIFT TYPE 5-3.1 AVERAGE[b] CS (5-3)	TOTAL SHUTTER NOISE[a] SD(B)	SHIFT TYPE 5-3.1 AVERAGE[b] CS (5-3)	TOTAL SHUTTER NOISE[a] SD(B)	SHIFT TYPE 5-3.1 AVERAGE[b] CS (5-3)	TOTAL SHUTTER NOISE[a] SD(B)	SHIFT TYPE 5-3.1 AVERAGE[b] CS (5-3)	TOTAL SHUTTER NOISE[a] SD(B)	TOTAL SHUTTER NOISE[a] SD(B)
16	±0.9	-0.2	±0.3	0.7	±0.5	0.3	±0.5	0.0	±0.8	±0.9
15	±0.8	0.0	±0.3	0.3	±0.4	0.3	±0.3	0.1	±0.8	±0.8
14	±1.0	-0.3	±0.2	0.2	±0.4	0.3	±0.4	0.0	±0.8	±0.9
13	±0.8	0.0	±0.3	0.4	±0.5	0.3	±0.3	0.2	±0.9	±0.8
12	±0.9	-0.2	±0.2	0.1	±0.7	0.3	±0.3	0.0	±1.0	±1.0
11	±0.9	0.0	±0.3	0.3	±0.5	0.5	±0.4	0.1	±0.8	±0.9
10	±0.9	-0.3	±0.2	0.0	±0.4	0.4	±0.3	0.0	±1.3	±1.0
9	±0.8	0.0	±0.3	0.2	±0.6	0.4	±0.4	0.1	±1.0	±1.3
8	±1.0	-0.1	±0.2	0.1	±0.5	0.2	±0.4	0.0	±0.9	±1.0
7	±0.8	0.0	±0.3	0.3	±0.5	0.3	±0.3	0.1	±1.3	±0.9
6	±0.9	-0.1	±0.2	0.1	±0.4	0.6	±0.4	0.0	±0.8	±0.9
5	±0.8	0.0	±0.3	0.3	±0.6	0.4	±0.3	0.1	±0.9	±0.8
4	±1.0	-0.1	±0.3	0.0	±0.5	0.5	±0.4	0.3	±0.9	±0.9
3	±0.9	0.0	±0.4	0.4	±0.6	0.5	±0.5	0.1	±0.9	±0.9
2	±1.0	-0.1	±0.4	0.0	±0.5	0.2	±0.4	0.1	±0.8	±1.0
1	±1.0	0.0	±0.5	0.7	±0.6	0.5	±0.2	0.4	±0.8	±0.9

[a]PRE-LAUNCH "IS GOLDEN TAPE" (5-198-10563, 16:14 30 AUG 83)

[b]AVERAGED (5-596-13285), (5-198-10563) AND (50005-16221)

BARKER APR 84 GSFC

Table 4-18

TM RADIOMETRIC VARIABILITY (IN DN)

	BAND 1	BAND 2	BAND 3	BAND 4	BAND 5	BAND 7
LANDSAT-4 TM/PF						
LOWEST NOISE						
SHUTTER rms	±1.1	±0.4	±0.4	±0.3	±0.8	±0.8
HIGHEST NOISE						
SHUTTER rms	±1.5	±1.0	±1.3	±0.6	±1.1	±2.0
SHIFT TYPE 4-1	2.0	—	0.3	0.2	−0.1	—
SHIFT TYPE 4-7	—	−0.2	0.6	—	0.6	0.9
32 KHz (3.2 mf)	2.6	0.3	1.6	0.8	[0.2]	[0.3]
6 KHz (18 mf)	0.4	0.2	0.5	0.3	[0.2]	[0.2]
LANDSAT-5 TM/F						
LOWEST NOISE						
SHUTTER rms	±0.8	±0.2	±0.5	±0.2	±0.8	±0.8
HIGHEST NOISE						
SHUTTER rms	±1.0	±0.5	±0.7	±0.5	±1.3	±1.3
SHIFT TYPE 5-3	−0.3	0.7	0.5	0.4	—	—

BARKER APR 84 GSFC

SECTION 5 - PROCESSING EFFECTS ON RADIOMETRY

In addition to the impact of innate sensor-induced uncertainties, information derived from TM imagery can also be affected by the processes used to calibrate the sensor, to apply the calibration to imagery, and to extract information. Procedures for radiometrically pre-processing of TM data used during the Scrounge-era are described elsewhere (Barker, Abrams et al., 1984b). The residual uncertainty associated with applying a single correction for gain and bias for each channel to a whole TM scene were discussed in Section 4 above. Some of the uncertainties of using the TM internal calibrator for absolute calibration in space were discussed in Section 3. This section focuses on additional uncertainties associated with:

- Existing and proposed procedures for calibration of individual channels with the TM internal calibrator
- Procedures for applying calibration to TM digital imagery
- Procedures for converting from radiance to reflectance
- Procedures for converting radiance or reflectance data into information

It is assumed that corrections to the raw data from sensor-related anomalies discussed previously have been performed prior to the processing procedures discussed here. However, repeated introduction of the $1/\sqrt{12}$ quantization error is to be avoided. Every time the digital numbers are changed, there is the potential for the introduction of additional error. Therefore, it is better to maintain corrected values in floating point notation, or in 16-bit bins, rather than their original 8-bit bins, through as many changes as possible; ideally, through to the finally derived information or value-added product.

5.1 CALIBRATION WITH INTERNAL CALIBRATOR

The random error associated with the use of the internal calibrator (IC) can be reduced by more than a factor of two by optimizing processing parameters. The random error can perhaps be reduced further by modeling trends. Factors

which need to be examined for obtaining a high precision on the measurement of the calibration pulses include:

- Where in the data stream to measure background
- Whether or not to use net signals
- What portion of the calibration data to use as a collect window
- How to perform the calibration pulse integration step
- How to average the calibration pulses which are calculated for each line
- What regression strategy to use in terms of lamps and lamp configurations
- How to perform within-scene smoothing to correct for temperature-dependence of the pulse, odd-even shifts, and within/and between-band correlations
- How, or if, to smooth within a pass
- How, or whether, to model for between-date smoothing.

Data exist, or can be collected, to model these effects.

The radiometric stability of the TM sensor makes it likely that the reproducibility of the calibration can be improved by more than a factor of five once the above factors are understood and incorporated into improved ground-processing procedures. The increased precision from these improvements could become particularly important if procedures are developed for creating images of estimated at-surfaces reflectances for a whole pass by peeling off atmospheric effects.

Potential corrections and additional calculations using the calibration data are not likely to significantly impact the computer-processing time for applying the calibration to an image, as long as such calibrations require at least two passes over the raw TM digital data.

5.1.1 BACKGROUND CALCULATION

Proper background data are needed for calculation of net signal for both calibration data and image data. Whether background is considered as a variable to be calculated by

line, or within a line, or whether the background is considered as a constant to be estimated from the shutter or a no-lamp-on 000 configuration, it is important to use an appropriate background. There have not been sufficient studies to date to definitively answer either key question, namely, where is the appropriate background, and how is it to be measured.

Current use by TIPS of lamp-state 000 values for background radiometric calibration is not sufficiently precise. Four reasons for this insufficiency are:

- Some high biasing of the background from negative DN values being stored in bin zero
- High values of background from an image-dependent light leak in part of the 148 mf collect window for Landsat-5 (Section 5.1.3)
- Insufficient data to make a line-by-line correction for scan-correlated shift (Section 4.5) or unrepresentative averaging for this shift over a whole scene from 40 consecutive scans of lamp-state 000
- Variations in background throughout the scene due to factors such as bright target saturation over clouds (Section 4.3).

TM was the first sensor in the Landsat series in which a positive non-zero offset of approximately 2 DN was used so that random variations about this mean would not result in values below this mean being stored collectively in bin zero. While this 2 DN offset was not large enough to prevent some negative values from occurring in Bands 1, 5 and 7 on TM/PF, nevertheless it may have prevented overestimating of background, except in a few particularly noisy channels; this effect can be quantitatively assessed. Use of uncorrected lamp-state 000 values introduces variability from scan-correlated shifts that is of the same order as the offset itself. Whether or not lamp-state 000 values, taken for 40 scans with the IC automatic sequencer, could provide appropriate backgrounds, after correction (Section 4), for all 360 scans in a repeating cycle remains to be determined from corrected data.

In any case, use of the shutter for some backgrounds will be necessary. First, it was always necessary for calibration of the emissive thermal IR Band, Band 6, since two points are necessary for calculating gain and bias; the black body temperature requires approximately 20 minutes to equilibrate

and therefore has not been operated at more than one of its two temperatures during a single pass. Second, it is probably desirable to change the normal operating mode of the Mapper from automatic sequencer to manual use of a single lamp in order to preserve the absolute calibration on two of the three lamps, in which case a shutter value for background would be needed in order to avoid manually switching the settings back and forth from lamp-state 000 to one-lamp-on within a pass.

Verification of the region on the shutter to be measured for background remains to be done on both TM sensors. During the Scrounge-era, there was an initial collection of 52 mf from one region of the shutter before DC restoration in the forward scan and after DC restoration in the reverse scan. Final Scrounge-era calibration data tapes, CCT-ADDS, contained background collects from two regions on the shutter on both sides of expected DC restoration in each scan direction; each region was required to be a multiple of four minor frames, and to start with a minor frame containing the initial unrepeated value for Band 6. Currently TIPS-era processing is making only one 52 mf background (shutter) collect from the shutter region and it appears to be inside the region of DC restoration. Outlier rejection algorithms need to be used to remove severe noise and to see if systematic noise is present, such as from the resetting of the scan-line corrector (SLC).

An attempt was made to position these two 24 and 28 mf Scrounge-era collect windows before and after the period of electronic DC restoration, which occurs during obscuration of the optical axis by the shutter. This was necessary because the initial 52 mf background within the DC restore region was found to be changing in some bands, perhaps due to recovery from droop and bright-target saturation effects. It appears that some of these Scrounge-era collect windows may have incomplete obscuration because they were set too close to the edge of the shutter, especially in Band 6; this can be corrected by excluding some minor frames from the calculations, at the cost of a reduced precision in the mean value of the background. It is also possible to use regions within the 148 mf calibration collect window, immediately adjacent to the 40-50 mf calibration pulse. This possibility is more feasible in the TIPS-era now that calibration collects are set individually for each channel so as to put the peak in the center of the 148 mf window.

5.1.2 PULSE WINDOW LOCATIONS

During the Scrounge-era processing, the 148 mf collect windows of calibration data could not be adjusted for

each channel. Pulse locations varied continuously from channel 1 through channel 16 for each reflective band, and the 50 mf wide pulses spread over all but about 20 mf of the collect window. Prior to December 1982, the collect window clipped part of some peaks of pulses in channels 1 through 4 of Band 1 (Barker, Abrams, et al. 1984). The processing algorithms did not adjust for this clipping and therefore the calculated gain for Band 1 Channel 1 was over estimated by about 5 percent. Clipping was also a problem in Band 6. Clipping is not as critical a problem in the TIPS-era because the peaks are individually centered for each channel, and therefore the margin for error in a priori knowledge of the peak location is approximately 50 mf, instead of 10 mf. Variations in line length are up to 10 mf.

5.1.3 PULSE INTEGRATION PARAMETERS

During the calibration of both TM/PF and TM/F, the IC pulse-integration methodology for pre-launch absolute radiometric calibration was a 31 mf "Hughes" algorithm. Various peak-location algorithms proved to be adequate to a precision of better than one minor frame. However, the IC pulses do not have flat tops, especially in the case of Landsat-5 TM/F (Figure 5-1). Therefore, the peak integration methodology affects the precision of the measurement.

A light leak in the shutter, which interferes with current procedures for pulse integration, has been observed as a secondary pulse in the calibration region on Landsat-5 TM/F (Figure 5-1, 2nd of 2). This leak has the following characteristics:

- Fixed Location. The center of the secondary peak is always a fixed distance from the center of the calibration pulse:

  $+(53 \pm 2)$ mf in forward scans

  $-(53 \pm 2)$ mf in reverse scans

- Always Present. A single secondary peak is always present, even in the 000 no-lamp-on state.

- Variable Intensity and Shape. Intensities and shape of the secondary peaks are a function of the light source being imaged along the optical axis during obscuration by the shutter. Actual values for radiant intensity are unknown since the imaging is 2 Km (reverse) or 20 Km (forward) outside the 180 Km field-of-view, except for

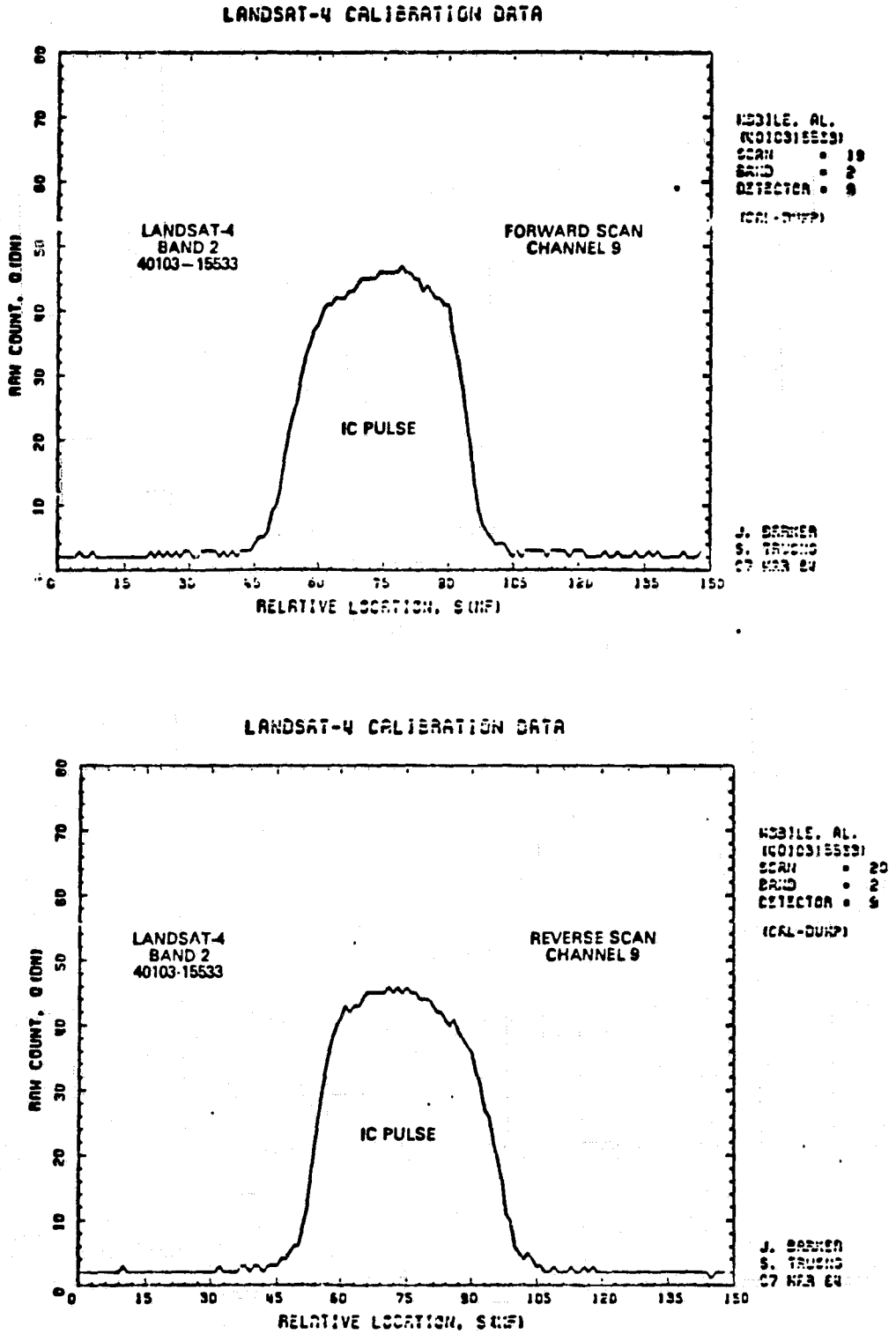

Figure 5-1. Landsat-4 and -5 Calibration Pulse and Light Leak (1 of 2)

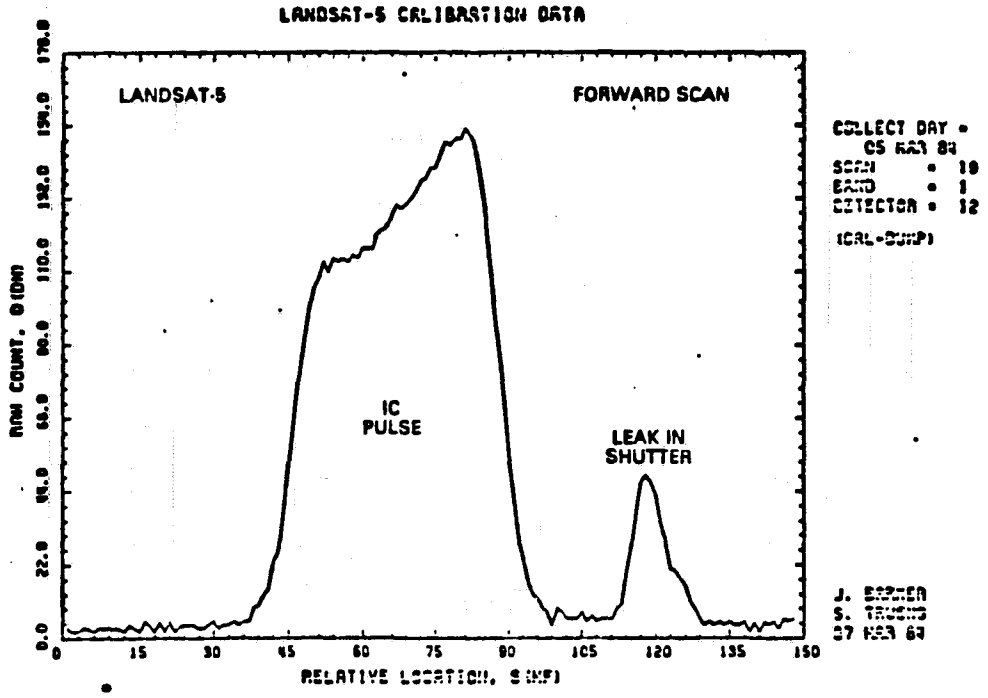

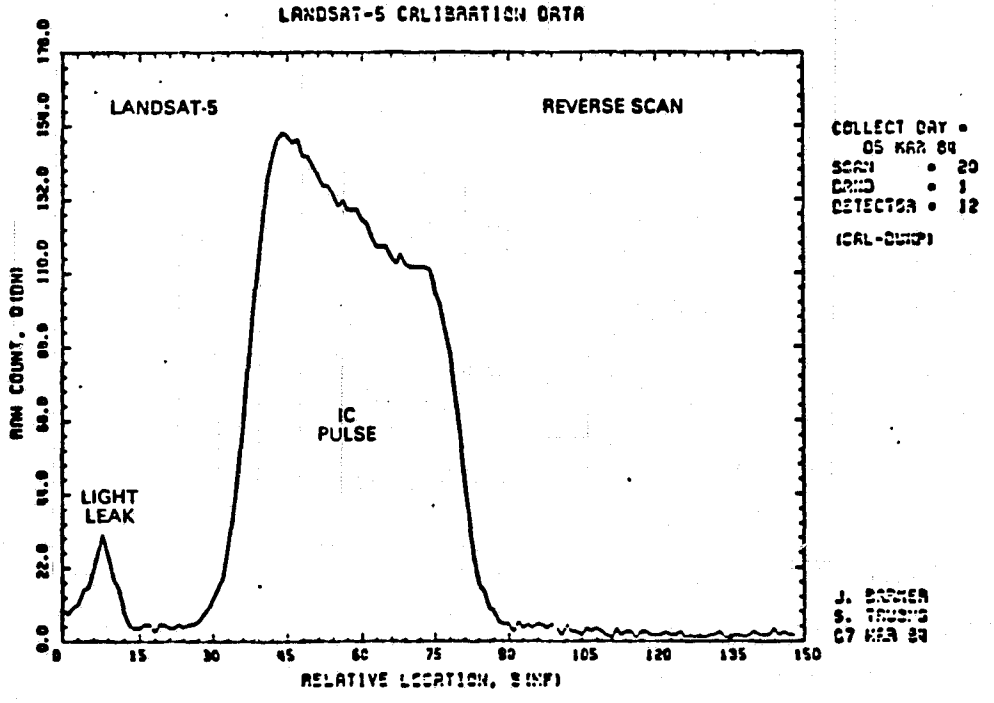

Figure 5-1. Landsat-4 and -5 Calibration Pulse and Light Leak (2 of 2)

the observed peaks when the scan mechanism was locked during "droop" tests. However, cloudy scenes have given the highest values in the PFP bands and clear scenes over land have given much lower secondary peaks. For a pre-launch flooding lamp test (9 Oct 82), the intensity of all secondary peaks differed by about a factor of two in the forward and reverse directions. The width of the secondary peak is as great as 24 mf in Band 5 and 16 mf in Band 4.

The origin of this light leak appears to be an incomplete masking of the lens on the shutter. Recommendations for reducing the impact of this light leak during TIPS processing are given in Section 6.3.2.

A few parametric studies on pulse integration width have been done. Results of a plot of σ_p versus pulse-integration width, w, is given in Figure 5-2 for one lamp state for one channel in each reflective band on TM/PF. A plot of the logarithm of $(100\sigma_p/P)$ versus w is given in Figure 5-3 for three channels in TM/F. Both plots illustrate the non-optimum nature of a w = 31 mf Hughes pulse-integration width. Severely non-flat IC pulses in Landsat-5 can result in this coefficient of variation (% error), CV, which is a factor of 2 to 4 higher than optimum for the current TIPS-era constant width of w = 65 mf.

The optimum pulse-integration width appears to be between 32 and 42 mf, before the slopes are reached on each side of the peak, and is channel dependent. A width of 39 mf is being used for both TM/PF and TM/F for current TRAPP processing. Parametric studies taken on different dates for all channels and for all lamp configurations need to wait until the largest systematic errors have been reduced, and the parametric analysis will be more sensitive.

5.1.4 PULSE AVERAGING PARAMETERS

Averaged pulse, $\bar{P}$, values are more precisely determined if the within-line pulse values, P, which are not too close to a change in lamp configuration are used to calculate the average. When the IC automatic sequencer is used, a set of pulses need to be chosen which show no trend with scan number. If there is a trend, it needs to be normalized out if it is characteristic of the IC system, or incorporated into a line-by-line calibration if it is a reflection of a real change in the gain and offset of the individual channels. Because of the slow cool down of the IC lamps in

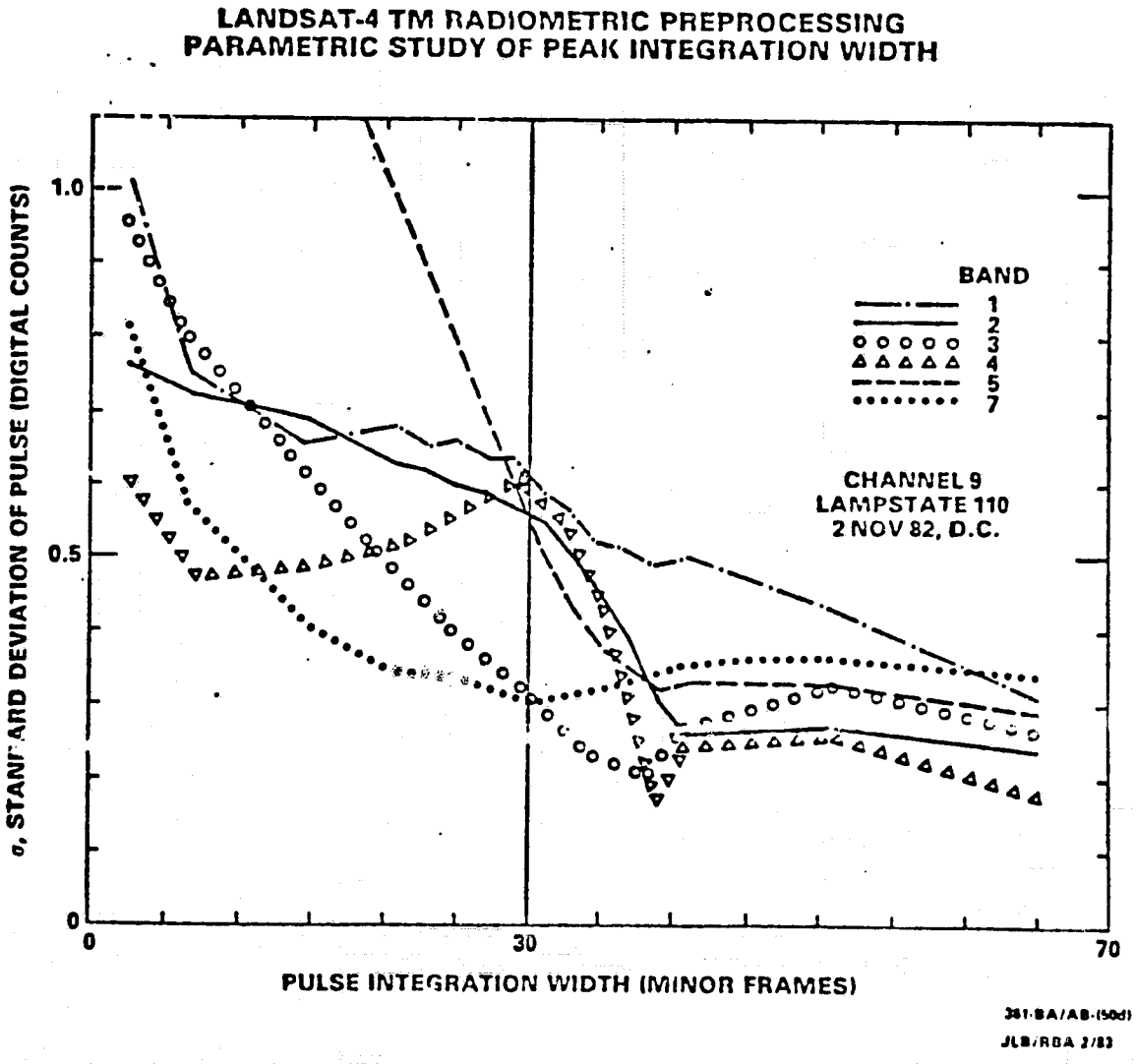

Figure 5-2. Parametric Study on Landsat-4 TM/PF Calibration-Pulse Integration Width

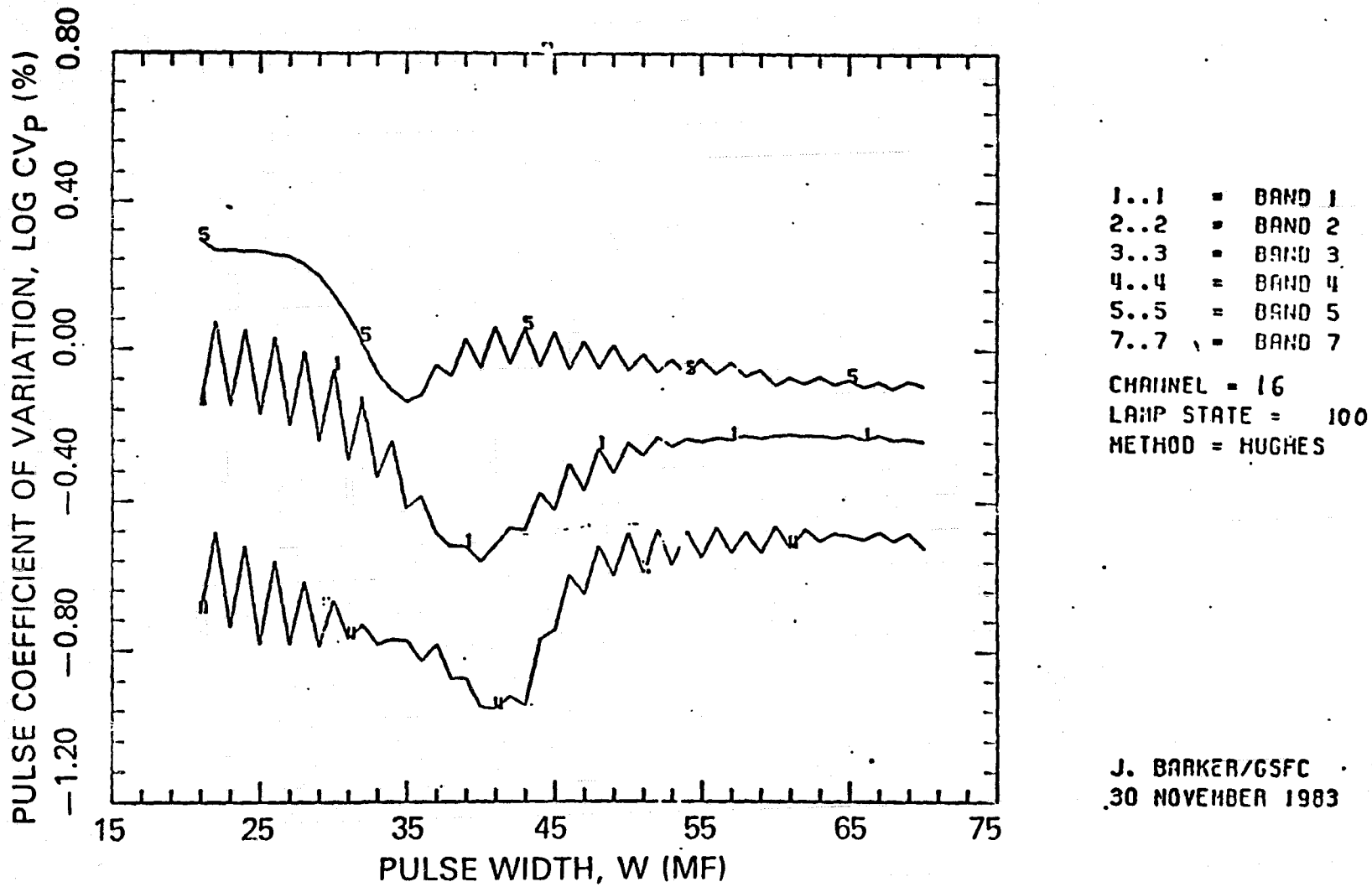

Figure 5-3. Parametric Study of Landsat-5 TM/F Calibration-Pulse Integration Width

the SWIR region, and the difficulty of identifying exactly where a lamp was turned on, parametric studies show that reduced errors resulted from omitting calibration-pulse data 4 scans before transitions and 10 scans after transitions between different lamp configurations. Dropping 4 scans preceding a transition improved precision for the SWIR bands by 35 percent. This has not been done during pre-launch or operational processing to date. Calibration needs to separate forward and reverse scans in order to avoid scene-dependence differences. Again, optimization of averaging parameters will be more efficient if it is done after reduction of the largest systematic errors.

5.1.5 REGRESSION STRATEGY

The choice of which IC lamp configurations to use in the regression of P versus L_λ^Q can affect the uncertainty of the fitting parameters. In pre-launch calibration and in operational TM processing, all eight states have been used. This has resulted in a probable error in the calculation of the gain and effective spectral radiance when using lamp-state 111 for Band 4 (TM/PF) and Band 1 (TM/F), where maximum values of 255 were present, indicating that some signals may be in excess of the dynamic range of these channels. Values of gain calculated in Figures 2-1 and 2-2, by TRAPP, do not contain the 111 lamp-state. Self-consistency checks made in all TRAPP runs showed that the difference between the net 111 pulse and the sum of the net pulses of the individual lamp were always negative. DN values of 255 should not be used in calculations because they may represent higher unknown values. Furthermore, values of 255 cannot be removed as outliers without introducing a systematic under-estimate of P.

Selective use of different lamp states on different dates would also be likely to lead to systematic errors. Therefore, states that have the potential for saturation at any time should be excluded from all calculations, including the transfer of the absolute calibration from the integrating sphere to the lamps. Raw data exist on CCT tapes to permit this recalculation for Landsat-5 TM/F, but not for Landsat-4. Recalibration of the absolute radiometry from these integrating sphere tests would be better if it awaited development of correction procedures for the largest systematic errors and the optimization of pulse integration and pulse averaging parameters.

The IC lamp brightness values have not been constant with time. Test results indicate that TM/PF IC lamp 2 has changed its effective radiant output between pre-launch and

in-orbit tests, as judged by comparisons with lamps 1 and 3. For any given band, the estimates of in-orbit changes of gain are the same to within 0.5 percent for all three lamps when compared to an in-orbit reference (2 NOV 82, ID 40109-15140). When pre-launch 9 March 1982 thermal-vacuum test data are used as a reference, lamps 1 and 3 have the same change to within 0.8 percent, while lamp 2 differs from lamp 1, on the average, by 2.2 percent. If this effect is real, it implies a change in something unique to that lamp, such as a change in the photodiode monitor system on that lamp or in the folding prism optics of the IC system prior to the point of merging the output of the three lamps; such a change might be the movement of the neutral-density filter on lamp 2, or in the sensitivity of the photodiode used to monitor the radiance of lamp 2.

One of the advantages of the three-lamp IC system is redundancy. It was designed to give 8 values for regression fitting. The observed linearity of the responses may allow for sufficient precision with fewer points for a regression. A comparison of single and multiple lamp regression fittings for a single scene indicates that, with appropriate independent calibration of manual-mode operation and corrections for background, single lamps could provide the necessary gains and offsets for routine calibration. This means that the two filtered lamps could be used as a monitor of long term, multi-year drift or change in spectral distribution of the unfiltered lamp. This would be particularly advantageous in an attempt to maintain absolute radiometric calibration. For monitoring of lamps, the automatic sequencer mode could be used about once a week. Furthermore, the presence of three lamps means that a discontinuous change in any one of them, such as noted above, can be considered as evidence of failure, and its values normalized to the pre-failure calibration. It appears that a 2-point fit with 7-point monitoring is preferred to the current 8-point regression fitting.

5.1.6 WITHIN-SCENE SMOOTHING

The redundancy associated with 100 channels of independently acquired calibration data on a single sensor offers unique opportunities for smoothing out random errors within and between bands. It also provides a built-in logic for isolating possible sources of discontinuous changes. The informational need for spectral transforms involving more than one band places a high value on the introduction of an explicit between-band step in the calibration process.

As one example of redundant information, odd and even channels have shown dissimilar changes in pulse values on

TM. It is currently assumed that these changes in odd/even channels are associated with how the six pencils of light from the edge of the IC shutter are played across the focal planes to produce the pulses, i.e., the pencils of light change position with changes of position or orientation of the shutter. Since movement of the shutter must affect all six IC lenses and the Band 6 mirror, this source of variability is subject to potential modeling by comparing multi-band data. To continue to calibrate each band in isolation of the others runs the risk of unnecessary loss of between-band calibration.

Another example of the potential for within-scene smoothing involves the temperature-dependence of the IC pulses. Pre-launch data on temperature-dependence were collected for TM/F PFP bands and only in ambient conditions at temperatures near 20°C, or 10°C above the conditions in space. This effect appears to be sufficiently linear that changes in the most sensitive channels could be used to make smaller changes in the effective spectral radiance for other, less sensitive channels. This might be desirable if the measurements of the appropriate temperature in the telemetry was less precise than the error associated with using the observed changes. This temperature-dependence needs to be measured in-orbit by sampling of 7-Band TM IC data from immediate turn-on through thermal shut down. Such an in-orbit calibration test (Section 6.2.2) might also empirically answer the question of which temperatures are related to this temperature-dependence.

5.1.7 WITHIN-PATH SMOOTHING

Original TIPS processing designs called for blending the calibration between scenes by creating segments and subsegments within a scene for separate transitional calibration. Initial attempts to do this to a scene during Scrounge-era processing produced demonstrably striped products. It appears that the TM sensor is sufficiently stable over a single scene that less error is introduced by assuming a constant set of calibration parameters for the whole scene than by blending. TM is a very stable radiometer. However, the possibility of multi-scene digital-image processing of a single pass (path) still calls for a search for trends. Examples of such trends are the temperature-dependence of the IC pulses, and multi-scan bright-target recovery of the background from exposure to solid fronts of clouds or snow. It is anticipated that such corrections for trends can be absorbed more continuously in a line-by-line calibration procedure rather than in segmented blending, if they are necessary at all.

5.1.8 BETWEEN-DATE SMOOTHING

Smoothly varying day-to-day trends in calibration parameters, as implied by Figures 2-1 and 2-2, perhaps from time-dependent vacuum-shift, can be corrected by modeling these trends and including them in the fitting required for calibration. It is desirable for radiometric accuracy to correct all known sources of systematic variation.

5.2 IMAGE CALIBRATION

Radiometric calibration of the raw digital imagery is computer-intensive. Calculation of the analytical expressions for the corrections discussed in Sections 4 and 5.1 are, for the most part, not computer-intensive. Exceptions include corrections that are image-dependent, such as bright-target saturation. This section discusses some of the uncertainties in the precision and accuracy of the radiometry that are associated with manipulating digital imagery. In particular, the following processes are discussed:

- Histogram equalization to reduce within-band striping by normalizing to a common mean and standard deviation for all channels in a band
- Replacement of bad channels
- Post-calibration dynamic-range options to retain a greater fraction of the acquired data
- Unbiased pixel calibration procedures for applying calculated corrections to individual pixels
- Geometric resampling of radiometrically-corrected imagery for registration to a reference image or rectification to a specific map projection.

5.2.1 HISTOGRAM EQUALIZATION

Scene-dependent normalization of channels to each other, such as histogram equalization or ratioing, is one method of radiometrically calibrating images from scanners. Scrounge-era and TIPS-era processing for Landsat-4 TM imagery have collected frequency histograms by DN level for each channel from the first pass through the raw high density tapes (HDT-RT). During the Scrounge-era, histograms were created from every fourth pixel (sample). Means and standard deviations derived from these histograms were used to bring all channels within a band to a common mean and standard deviation through application of a gain and bias

for relative de-striping. Absolute radiometry was maintained by modifying this set further for the band-average apparent change in gain and offset based on the IC pulses. These were the radiometric corrections applied in Equation 1-1. Three assumptions are implicit in this calibration methodology:

- Within-scene variations in sensor characteristics are insignificant
- IC calibration is inadequate, since otherwise histogram equalization would not be needed
- Histogram equalization is more precise than IC calibration for destriping.

Neither IC nor histogram calibration currently correct for continuous or discontinuous within-scene variations or trends such as those outlined in Section 4. However, both methods can be used after reduction of systematic within-scene variations. Without these systematic corrections, phenomena such as between-scan striping will be inherent in the use of histogram equalization from raw data.

Pre-launch absolute calibration was based on the assumption that the individual channels are stable enough over a period of hours to a few days that they can be used as a transfer mechanism for calibrating the IC lamps from the known radiance of different levels of the integrating sphere. The use of histogram equalization implies that there was a significant imprecision in this transfer or that the effective radiance of the IC system has changed since it was calibrated, especially in regards to the relative gains and offsets of the channels in a single band. It is possible to examine this assumption quantitatively by measuring the residual between-channel standard deviation of a homogeneous scene after radiometric calibration using the IC data without histograming. Residual striping from IC calibration alone has not been quantitatively summarized.

The assumption that histogram equalization can and does produce less striping in a TM image than IC calibration has also not been evaluated quantitatively. Equalization techniques assume that each histogram has a sufficiently representative sample to be identical with that from other channels. This is dependent on the variability of scene content and will differ from scene to scene. Histogram equalization also assumes that the counts observed by each channel in a band cover the same dynamic range. This assumption can be evaluated from the range of gains and offsets in the absolute calibration of each channel, when

combined with the histograms of the scene to be used for equalization. Histogram equalization also assumes a normal frequency distribution, which is not a good assumption, and is also scene-dependent. Finally, the use of histogram equalization on every scene assumes that the range of scene-dependent radiances is sufficiently great to provide the required sensitivity. Histogram equalization is used because it has worked on MSS digital imagery, it produces acceptable film products, and it has not yet been demonstrated that it does not work for analysis of TM digital imagery.

Iterative calibration algorithms have been suggested by Fischel (1984). The use of scene histograms to implement these equations means that the proposed iterative algorithm is subject to the same limitations as the direct use of histogram equalization.

The use of some type of iterative technique following systematic corrections such as those outlined in Section 4 may prove to be effective, assuming that a rapidly converging formulation can be made; ideally, it needs to be independent of scene content.

If histogram equalization continues to be used, it is probably better to use a weighted average based on observed variability for both histogram equalization and for the absolute calibration to the IC data. If this is not possible, then a reference to one or two quiet channels (Table 4-5) in both cases would be better than the reference to the band average, whose uncertainty is driven by the noisiest channels. If reliable full-scene error estimates could be made for both methods of calibration, then the best method would be to use an average weighted by the inverse of the variance for within-band destriping.

Inherent in the use of histogram equalization is the assumption that the TM sensor is stable during the period of data acquisition for histograms. If within-scene corrections are made for each channel, this appears to be a reasonable assumption to the extent that Figures 2-1 and 2-2 indicate a slowly-varying, smooth between-scene IC trend of band-averages with time. If a similar trend of histogram calibration constants, corrected for within-scene systematic errors, is found over many scenes, then the scene-dependent portion of histogram equalization can be taken out to any required level of statistical accuracy by calculating a functional relationship for within-band change with time.

This suggests a potentially powerful way of combining apparent within-band variations from separate IC calibration and histogram equalization or ratioing in order to reduce the random error in both. Changes with time might provide a means of modeling out systematic within-band trends associated with the IC system only. With sixteen-channel redundancy in every reflective band, histogram equalization may have some new applications for radiometric calibration when used as a slowly varying modifier with time on the internal calibrator system.

5.2.2 REPLACEMENT OF CHANNELS

A multichannel scanner, such as TM, requires replacement of channels that fail. Without replacement, the image would have a break every 16 lines (Barker, Gunther, et al., 1984 Figure 2-7). Failure can be of two types, complete or partial. Complete failure is a zero order effect (Table 4-8), i.e., data are missing from a dead channel, and the radiometric uncertainty in its correct value cannot be estimated. There is one such channel on Landsat-4 TM/PF, namely, Channel 3 of Band 5. Partial failure also implies partial success, therefore failures of this type are inherently different. Because of the potential for blurring boundaries, the out-of-specification modulation transfer function (MTF) of Channel 4 in Band 2 led to this channel being considered a failure on TM/PF. There are no failed channels on Landsat-5 TM/F.

During Scrounge-era and TIPS-era processing of Landsat-4 digital imagery, both bad channels were replaced by duplicating data from an adjacent channel (Barker, Guther, et al., 1984). In Band 5, Channel 3 was replaced with a duplicate line of Channel 4 data. In Band 2, Channel 4 was replaced by Channel 5. This is the simplest type of replacement.

A routine monitoring of Channel 4 of Band 2 by TRAPP has indicated that this channel has been as radiometrically stable as others in that band. It is therefore recommended that TIPS procedures be modified to stop replacing this channel. From a scientific point-of-view, it is better to use a partially-deficient channel than to not use it at all. This is especially true on the TM sensor where there is no significant overlap of the effective instantaneous field-of-view for adjacent channels.

Within-band algorithms for replacing bad channels are still being evaluated. In general, the trade-off is between the lower probability of an error by using as many neighbors as possible in an estimate and the increased computations

inherent in multi-neighbor algorithms. The simplest strategy is one-for-one line replacement either by an adjacent line or by a more representative pattern such as alternating back and forth between the channels on either side of the dead channel. Averaging of two adjacent channels is the next easiest. Weighted averaging by position requires more intensive computation but allows for a nearly complete encirclement of the missing pixel with a probability of the radiance value being driven by the pixels which are geometrically closest to the one being replaced. For channels that have only partially failed, one has the additional possibility of a weighted average of the original pixel value itself and the value that would have been used if the channel had completely failed. For MTF deficiencies such as those in channel 4 of Band 2, the weighting could depend on the probable distance from a boundary, since the pure pixel value, while slightly averaged with its neighbors, will be best without additional averaging with data from other channels. Replacement algorithms can be evaluated by using several adjacent channels that have not failed to compare the proposed replacement value with either the observed value or the calculated partially-deficient value.

Between-band replacement algorithms, applied after radiometric calibration, are potentially better than within-band ones. They are better from a spatial perspective because they use imagery which is viewing the area that was missed by one band and from a radiometric perspective because there is a high degree of correlation between bands. Possible multi-band substitution algorithms also range from spatially simple single-pixel replacement to multi-neighbor resampling. Weighting algorithms for averaging within-band and between-band estimates of missing data could place higher weight on the spatial information from outside bands and on the radiometry from neighboring pixels within the band. If tests are run on the error in information content from alternative replacement algorithms, perhaps by optimizing the ratio of random error to computation cost, a likely replacement candidate is a single-pixel replacement where the new value is produced by calculations based upon correlation to another band.

Any replacement will lead to additional errors. For example, the sensitivity and accuracy of texture or contextual classifiers will be reduced by the implicit rather than explicit use of the same data in more than one pixel. To the extent that information of this type is important, it is desirable to limit the geometric extent of the pixels used for replacement and, if possible, to retain the ability to identify pixels that are calculated rather

than observed. For TM imagery, tagging of replaced pixels is not warranted since, prior to geometric resampling, replaced data can be located by line number, and after resampling, especially after rotation of the image to north, all of the pixels are likely to contain some redundant data. One method to avoid the use of redundant data is to make the replacement step an inherent part of a non-uniform geometric resampling algorithm that behaves well in the presence of missing data.

Most applications of digital imagery of land place a high value on boundary location and/or mensuration. Both these requirements favor using some type of between-band replacement algorithm.

5.2.3 POST-CALIBRATION DYNAMIC RANGE

For a given and fixed resolution, such as TM's 8-bit radiometric precision, the total amount of information in digital imagery is reduced by radiometric calibration, since it either compresses data from more than one bin into a single inseparable bin, or it cuts off some data at the low or high ends of the post-calibration dynamic range. The graph of Band 5 gain versus time, Figure 2-2, illustrates that Scrounge-era processing did result in some loss of data by compression for those days when the raw channel gain was above the post-calibration gain. For TIPS-era processing after January 15, 1984, this post-calibration dynamic range has been raised, in part to avoid compressing data (Appendix 9.1).

Relative between-channel, between-band, and between-scene calibration is essential for information extraction. One data-intensive solution to this dilemma is to increase the radiometric resolution of the calibrated products. Another solution is to consider alternatives to the single gain options of the current calibration procedures.

A three-sectioned dynamic range is a possible future option for TIPS (Section 6.3.5). A small number of bins, perhaps b = 15, at both ends of the dynamic range would be calibrated separately from the central portion of (256 - 2b) bins. The dynamic range for the linear central portion would be a common range for both TM/PF and TM/F that would assure that, during the life-time of these sensors, calibration would result in information-retentive expansion in this, the most important part of the band. The overall dynamic range would be from a zero radiance to an upper limit of the most sensitive channel in a specific band. This would mean that one or both of these two less-important sections on either end would contain some compressed data.

The advantage of this three-section calibration scheme is that some out-of-range data (high radiance values from deserts, snow and clouds) would be retained in a less compressed manner. The fact that TM data are characterized by an absence of high radiance values means that shifting and expanding of the central portion will push very little data into the more compressed region at the top, while at the same time retaining the full range of data in those less frequent cases where there is saturation. Still more information would have been retained if these schemes could have been applied on the sensor to the selection of bits for transmission from the A/D converter. Calibration of these end sections could be linear, piece-wise linear, or use a more smoothly varying function for these regions. While it might be some time before users are able to demonstrate the utility of the less compressed data in these end regions, this three-section scheme would provide potential information that would otherwise be lost.

5.2.4 UNBIASED PIXEL CALIBRATION

Conventional calibration of a digital image introduces its own "nearest integer" striping. It can be made visible by differencing a TM image before and after radiometric calibration and noticing the stripes along lines on the resultant difference image (Barker and Gunther, 1983, Figure 9). This differencing of TM/PF images also makes the peaks of the coherent noise somewhat more visible every 3 and 17 pixels. The solid striping arises because of the additional discontinuous quantization error in converting from a raw 8-bit integer to a calibrated 8-bit integer. As Bernstein and Lotspiech (1983) have pointed out, this would occur even if the calibration step was a perfect inversion of the different responses that the channels have to a COMMON input radiance. Whether the radiometric corrections to the digital imagery are being applied by a conventional mainframe computer using a one-to-one replacement in a radiometric look-up table (RLUT) or by an array processor using calculations of a specific formula on many pixels in parallel, this "nearest integer" striping will occur.

Bernstein and Lotspiech (1983) have proposed a "probabilistic" approach to replace the "nearest integer" procedure. A modified version of that proposal would replace the RLUT generation, or parallel processing

implementation of the corrected calibration from Equation 1-1:

$$\text{INT } L'_{cal} = \text{INT} \quad \frac{L'_R - NB'_A}{NG'_A} \tag{5-1}$$

where INT = rounded integer value of its argument with a probabilistic choice between the nearest two integers,

$$\text{INT } L'_{cal} = \text{TRUN } L'_{cal} \tag{5-2}$$

with a probability of

$$p = 1 - [L'_{cal} - \text{TRUN } (L'_{cal})]$$

or (5-3)

$$\text{INT } L'_{cal} = 1 + \text{TRUN } L'_{cal}$$

with a probability of (1-p)

where TRUN = truncated integer value of its argument.

The advantages of this probabilistic approach are that visual striping is removed, and the accumulated error over all pixels is zero, i.e., it is an unbiased estimator of the correct value. The disadvantage is that the implicit quantization error has been entered explicitly as $1/\sqrt{12}$ salt-and-pepper noise into the imagery. This probabilistic approach could improve the radiometry sufficiently to produce less-biased estimates in multipixel information extraction algorithms such as boundary delineation, region growing, texture measures and contextural and textural classifiers. As with all radiometric corrections, a smaller error due to rounding will occur if this probabilistic approach is applied once and only once at the last geometric resampling required for "P" products. If separate "A" products are required, then this probabilistic approach could be used each time an 8-bit image is generated.

5.2.5 GEOMETRIC RESAMPLING

While several potential sources of radiometric error exist in the geometric pre-processing of TM data, Fischel (1984)

has found that the "geometric correction algorithm for TM works exceedingly well". A quantitative comparison of the difference between alternative resampling algorithms remains to be done, partially because of the computational difficulty of implementing even a single resampling algorithm for TM digital imagery.

Between-scan fitting due to overlap or underlap between sweeps has not been a problem due to the excellent performance of the scan-line-corrector (SLC). The periscope-type mirrors of the SLC rotate to correct out the effect caused by the movement of the spacecraft during the period of a single scan. The SLC repositions the start of each scan relative to the end of the last scan (Engel, 1980). It is reset at the end of each sweep. Since the SLC is set for a specific altitude and latitude of operation, acquisitions at the current orbital altitude near the poles will result in as much as a three pixel overlap or underlap at the ends of lines 1 and 16 between sweeps. Landsat-4 TM/PF images of North America have shown less than a one pixel gap or overlap.

Rounding introduces some radiometric uncertainty during the geometric correction process. Procedures used during the Scrounge-era and current TIPS-era involve two steps:

1. Equal interval along-scan (within-scan) 4-point cubic convolution resampling

2. Unequal interval along-track (between-scan) 4-point cubic spline resampling, to create lines by "sweep extension" as necessary at the end of each sweep.

Fischel (1984) has recommended a single-pass resampling procedure to replace the current two-pass cubic spline in the second step in order to avoid the loss of as much as 40 DN levels from a bright pixel at the bottom of a scan. It is also desirable to change the current procedure and use raw data (HDT-RT) as input to this geometric process rather than radiometrically corrected data (HDT-AT); this could avoid one rounding error by applying radiometric and geometric corrections in the same process.

Smoothing of adjacent pixels is a characteristic of these resampling algorithms, and therefore there is an inherent loss of peaks and valleys. There is also a ringing from spatial filters that resample with the intention of maximizing the retension of extreme values. Appropriate scenes need to be identified for quantifying the extent of this smoothing or ringing by comparing the particular

combining fractions of each of six bands to account for the maximum amount of total variance is at the core of attempts to convert spectral axes into orthogonal informational axes via image-independent "spectral transforms". It is important to develop quantitative measures of how much useful information is in each of these transforms since it is desirable to reduce the TM dimensionality if this can be done without the loss of significant information. When principle component analysis has been applied to TM scenes, significant non-random non-noise patterns are visible in the sixth component, which accounts for less than a percent of the total variance of the six bands (Bernstein and Lotspiech, 1983). However, the mathematical linear orthogonality of this computation has not necessarily created informationally independent transformations. In particular, all six transforms of TM data reveal some similarity in spatial patterns. If the electronic, vibrational, rotational, and other energy transitions could be modeled from reflectance spectra of targets, then it might be possible to establish a physically meaningful functional form for an informational spectral transformation.

Any transform of independently measured radiances will have a larger associated error than the original observations. Current linear spectral transforms have the following form:

$$T_i = \sum_{B=1}^{6} E_i(B)\ L_{cal}(B) \qquad (5\text{-}4)$$

where $L_{cal}(B)$ = calibrated radiance in one of the six TM Bands, B, DN

$E_i(B)$ = factor for the ith transform for Band B

T_i = one of six TM spectral transforms.

Coefficients for one such set of spectral transforms are given in Table 5-1 (Crist and Cicone, 1984). The first three are called "brightness", "greenness", and "wetness" transforms, implying a relationship to physical variables. Some biophysically meaningful variables that might be inferable from such transforms include albedo, green biomass, soil moisture and canopy thickness. Some of these transforms increase the contrast as compared to the original single bands. Such increased separability can reduce the errors associated with single band "per pixel" classifiers and spatial correlation such as that required for ground

C-2 5-23 — 5-30

Table 5-1. Thematic Mapper Tasseled Cap Transformation Coefficients From In-Orbit Data (Crist and Cicone, 1984)

FEATURE	TM BAND					
	1	2	3	4	5	7
BRIGHTNESS	0.3037	0.2793	0.4743	0.5585	0.5082	0.1863
GREENNESS	−0.2848	−0.2435	−0.5436	0.7243	0.0840	−0.1800
WETNESS	0.1509	0.1973	0.3279	0.3406	−0.7112	−0.4572
FOURTH	−0.8242	0.0849	0.4392	−0.0580	0.2012	−0.2768
FIFTH	−0.3280	0.0549	0.1075	0.1855	−0.4357	0.8085
SIXTH	0.1084	−0.9022	0.4120	0.0573	−0.0251	0.0238

9622 (691/84

control point (GCP) registration of one image to a reference image. One reason for using spectral transforms rather than 6 bands is that they may lead more quickly to definitions of scientifically useful spectral information.

The variances of these transforms are:

$$\sigma^2_{T_i} = \sum_{B=1}^{6} E_i(B)^2 \, \sigma^2_{L_{cal}(B)} \qquad (5\text{-}5)$$

where $\sigma_{L_{cal}(B)}$ = The rms error in the calibrated radiance in Band B, which has as it's minimum value the variability of the sensor.

The error in the spectral transform will usually be dominated by the largest errors in the individual bands. For the 6 TM bands, the uncorrected non-informational variance from the total noise background in the shutter region from Table 4-6 indicates that bands 1, 5, and 7 contribute approximately 80 percent of the variance. This suggests several alternative methods for reducing the errors associated with using spectral transforms:

1. Radiometric correction procedures could emphasize reduction in the largest uncertainties

2. Spectral transforms could be weighted by the inverse of the variance of their individual bands

3. Spectral transforms might be developed using only the low noise bands namely TM bands 2, 3 and 4.

These suggestions are particularly important in the use of spectral transforms, where all but the "brightness" component have mixed positive and negative terms, which can lead to larger errors in the calculated transforms. Since these spectral transforms appear to be informationally richer, or at least more focused, than the original bands, optimization of radiometric calibration parameters needs to minimize the variance in the spectral transforms.

5.4.2 RADIOMETRY

Entropy is one measure of the within-band informational content of discrete data such as 8-bit TM digital imagery. An advantage of using entropy is that it places a quantitative upper limit on the potential information that can be derived from the frequency and radiometric range of observed counts in a single band. Five

limitations on the use of entropy as a measure of information include the absence of:

- Normalization for non-informational sensor variabilities (Section 4)
- Any measure of spatial information (Section 5.4.3)
- Subsets of useful information such as partitioning of atmospheric and terrestrial variability (Section 5.3.2)
- Potentially higher radiometric resolution information from the smaller bins of the bin-radiance variability (Section 4.1)
- Innate properties for associative or cumulative between-band aggregation without correction for factors discussed under spectrometry (Section 5.4.1).

Future radiometric calibration parameters could be derived by maximizing a per-pixel entropy-based correction for one or more of the above factors, especially the normalization for sensor variability. This radiometric optimization using entropy in processing steps might help in defining a three-sectioned post-calibration dynamic range (Section 5.2.3), or in definition of the dynamic range to be collected or transmitted from future land-observing satellite systems. One objective of such a formulation of per-pixel entropy would be to retain its thermodynamic property as a state function, which depends only on the state of the target, not on the path by which it was achieved.

5.4.3 GEOMETRY

Spatial information could be optimized in two steps. Radiometric parameters used for calibration could be optimized on unresampled corrected and radiometrically calibrated digital imagery. Parameters for geometric pre-processing could be optimized on spatially resampled data.

Texture is another measure of within-band information. Various measures of texture can be used to place upper limits on the combined radiometric and spatial information. If both the random and systematic contributions from the sensor variability can be removed from the measures of texture, then a figure-of-merit (FOM) could be calculated

for the spatial information above by combining these normalized measures of texture with the normalized per-pixel entropy. Such a spatial FOM would still be an intensive property of the digital image and not an extensive property of the size of the image.

Intensive variables that quantify the point, line and regional spatial information of a digital image move closer to characterizing useful information than do total measures such as texture. Modified texture measures would then be used on binary masks of within-region "pure" pixels. It is likely that a "spatial stability theorem" will emerge from scientific and informational research in land remote sensing stating that pointed, linear, and areal features of two dimensional images remain invariant to spatial resolution. If this theorem is true, then research on information extraction techniques, which may involve artificial intelligence methodology, may separate the spectral and radiometric informational content of "pure pixels" from the spatial informational content of points, lines and regions on the whole scene for each specific sensor. Reproducible unsupervised methods using matrix filters are being developed for calculating these intensive spatial variables. Once such variables are found, they can be used to compare and optimize parameters in different resampling algorithms.

The geometric utility of digital imagery is related to two characteristics of a system's performance, the sensor's instantaneous-field-of-view (IFOV) for each pixel and the accuracy with which a resampled pixel can be located on a reference data set, usually a map. A more quantitative description of the nominal 30m IFOV for TM can be given in space as two line-spread functions, one along scan and one across scan, or as some other 2-dimensional spatial-distribution function. The nominal 30m IFOV for TM can be described in the time domain as frequency in a modulation transfer function (MTF) (Markham, 1984).

These measured spatial-distribution functions can be inverted to more accurately resample the original imagery. This is one method to reduce the loss of information during resampling. Such de-convolving will also provide more accurate resampling of imagery from different sensors to a common spatial data base.

SECTION 6 - RECOMMENDATIONS

The TM sensor is the most sensitive and best calibrated radiometer that has ever been flown for land remote sensing. If procedures can be developed and implemented for correcting its systematic radiometric variability (Section 4), then the TM sensor might contribute even more useful synoptic data. In addition to the improved utility of TM images over MSS images in agriculture (Pitts et al., 1983), natural resource mapping (Haas and Waltz, 1983), forestry (Hill, 1983), and geologic exploration (Everett et al., 1983), properly calibrated TM images could be used for modeling global habitability with a precision and accuracy unmatched by previous sensors. Some of the capabilities of the Landsat system suggest that the TM sensor might also be used experimentally to define requirements for future land observing satellite systems. A listing of the recommendations discussed below is provided in Appendix 9.13.

6.1 ENGINEERING CHARACTERIZATION

6.1.1 ABSOLUTE RADIOMETRIC CALIBRATION

Original specifications for absolute radiometric TM calibration required that the radiometric error be less than 10 percent. If the actual errors in the various bands had been this large, then a significant limitation would have existed on:

- The accuracy and precision of arithmetically and geometrically peeling off the atmospheric component of the at-satellite reflected radiance (Section 5.3.2)
- The between-band spectral transforms required for information extraction (Section 5.4.1)
- The ability to make precise and accurate comparisons to other sensors.

The slowly varying, or near-constancy, of radiometric gain with time (Sections 2 and 3), and the reproducibility of the absolute calibration with the external integrating sphere (Barker, Ball, et al., 1984), suggest that the TM sensor and the integrating sphere are stable enough to reduce the systematic errors of absolute calibration by more than a factor of two. This would be accomplished through recalibrating the integrating sphere against National Bureau of Standards (NBS) references.

The recommended experimental design for absolute radiometric recalibration involves three sets of cross-comparisons:

- Independent but co-ordinated spectral radiance measurements of the TM integrating sphere need to be made by the sensor's manufacturer, by the NASA calibration engineers, and by NBS scientists using absolute photon standards. These measurements need sufficient spectral resolution to avoid introducing errors when convolving them with the TM spectral response curves for each band. Errors resulting from variations across the aperture and with distance also have to be quantified.

- Recalibration of the two MSS integrating spheres for Landsat-4 and -5 by one or more of the above three groups calibrating the TM integrating sphere.

- Simultaneous calibration of one or more portable 8-Band Barnes Modular Multispectral Radiometer (MMR) TM field radiometers to serve as a radiometric transfer standard. The radiometers would be used in absolute radiometric calibration experiments at White Sands, New Mexico, and elsewhere. Accurate absolute calibration measurements taken from the ground on different dates provide one method for resolving whether the 8 percent cyclic behavior of the SWIR bands with time is a characteristic of the sensor only or of the internal calibration system (Section 2). This calibrated MMR would also be used at integrating sphere tests to measure the variability of sphere characteristics under different test conditions, as was done during the last set of pre-launch tests. Thermal band calibration needs to be done along with the reflective bands.

These recalibration data are needed for reprocessing of the pre-launch TM integrating sphere data for Landsat-5 TM/F after the tapes have been corrected for known sources of systematic variations. Such data on the TM and MSS integrating spheres will also enhance cross-comparisons of near-simultaneous acquisitions of MSS and TM digital imagery from Landsat-4 and -5.

6.1.2 RELATIVE RADIOMETRIC CALIBRATION

During pre-launch experiments using the TM sensors, it was not possible to record noise-free data on the 28-track tapes required as input to the TIPS system. Some 5-window collects were made on BRU tapes for Landsat-4 TM/PF, and a more extensive set was collected for Landsat-5 TM/F, especially during the special ambient tests at GE/Valley Forge, PA in August and September 1983.

Subsequent analysis has indicated a need for more data from the calibration region, especially from the shutter background. The raw data from these pre-launch collects are needed for within-scene correction prior to processing for absolute and relative recalibration of the detectors and the IC systems and to characterize the "double peak" in the calibration region of Landsat-5 TM/F. While corrections based on the absolute recalibrations recommended in Section 6.1.1 could be performed on the reduced data from the pre-launch "AC02" tests, a higher precision would be obtained if the raw data were used after correction for systematic variations.

Existing pre-launch 42-track HDTs, if noise free, need to be duplicated onto noise-free 28-track tapes for the critical pre-launch experiments on TM/PF and TM/F. 8-Window GPC are also needed on BRU tapes. Time needs to be made available on one of the TIPS strings to create appropriate "CALDUMP" tapes used as input to TRAPP processing, and to provide some specialized processing not available elsewhere. Computer resources are also needed for these recalibrations, especially for within-scene corrections as defined by analysis of in-orbit data and of the 1983 special collects.

6.1.3 MODELING OF SYSTEMATIC VARIABILITIES

Several types of systematic variations have been found during TM radiometric characterization (Section 4.8). The empirical corrections proposed for the systematic variations might be improved if the underlying causes could be identified and modeled. One way of identifying and quantifying these temperature-dependent causes would be to put heaters in specific locations on the existing engineering model of TM in order to run parametric sensitivity studies on temperature effects. Additional monitoring points for electronic noise isolation might also be required.

Specific engineering tasks are recommended to develop models for correcting systematic radiometric variations. These tasks might include obtaining quantitative explanations for the following:

- Vacuum shift (Section 2)
- Cyclic SWIR patterns (Section 2), apparent change in gain with time-in-orbit, presumably due to shutter position change

- IC pulse dependence on temperature, from a high change in Band 1 to a low change in Band 4
- Systematic changes of IC pulse values between dates, possibly due to thermal expansion of the primary focal plane from its one-sided line of attachment, as an additional or alternative cause of IC pulse temperature-dependence
- "Double peaks" in the calibration region of Landsat-5, apparently from incomplete obscuration of the optical path by the mask with a hole for the IC lens on the shutter
- Channel-correlated shifts
- Coherent noise
- Droop
- Bright-target saturation.

6.1.4 TM SENSOR REPORT

A report is recommended for the characterizing of the sensor performance from pre-launch engineering tests on TM/PF, TM/F and the engineering model of TM. This report needs to be prepared primarily by the sensor manufacturer and the TM system's engineer. The report needs to focus on the potential interpretation of digital imagery by scientists. The absence of such a single set of summarized volumes of test data and interpretation currently limits the ability to formulate quantitative algorithms for monitoring or correcting observations from the TM sensors. Examples of a few specific needs are:

- A schematic diagram of optical and electronic logic in order to build between-channel monitoring programs
- Prints of the exact locations of all the telemetry monitors, especially the temperature sensors
- A systematic summary of emissive band tests, characteristics, and scientific characterization
- A listing of optional tests that could be run in-orbit, such as the refocus of CFP relative to PFP.

A complete report on the spectral, radiometric, and geometric characterization of the TM sensor is needed from the engineers.

6.2 FLIGHT SEGMENT OPERATIONS

After the TM Research and Development (R&D) period ending in January 1985, or earlier, the operation of the Landsat satellites will be a NOAA responsibility. For scientific characterization, operational assistance, and experimentation, the following recommendations are made:

- Calibration and characterization tests need to be developed and performed prior to January 1985. The emphasis needs to be on possible changes in operational configuration and on implementing recommendations from the scientific investigations workshop in September, 1984.

- A memo-of-understanding (MOU) needs to be prepared between NASA and NOAA for NASA to provide technical and scientific assistance in the monitoring of Landsat normal performance and to help with potential problems. NOAA could provide operational time and access for occasional research experiments by NASA engineers and scientists. The NOAA/NASA MOU might include some compilation of conditions under which NOAA will turn back control of a Landsat satellite to NASA for possible de-boost since this might be an important time for higher-risk pre-defined calibration experiments (Section 6.4).

6.2.1 CHANGES IN OPERATIONAL PROCEDURES

Some options exist for changes in the configuration of the TM sensor during image acquisitions. Other options exist for changes in the operation of the MSS sensor and the spacecraft. Possible changes in the mission profile are suggested as scientific experiments in Section 6.2.4. This section recommends three changes in the current TM operations. Evaluation of TM data during its research and development (R&D) phase will probably lead to additional recommendations.

- Stop routine operation of the IC automatic sequencer, by operating the IC with only one of the lamps on, in order to preserve the pre-launch absolute radiometric characteristics of two of the three lamps throughout a possible multi-year mission. While each of the silicon photo-diodes, which monitor the three IC lamps, might keep the radiance output adjusted over long time periods by changes in the lamp temperature, the color balance between bands would be changed in this process. More than forty

tests on Landsat-4 scenes using each of the one-lamp-on configurations individually in processing by TRAPP have demonstrated the feasibility of using one lamp state and the background from the shutter in place of the eight-lamp-state regression used for calculating gain and offset. The recommendation is that several seven-band test images be acquired at night to obtain the required data for modifying and testing the operational TIPS programs.

The automatic sequencer could be used once a week to monitor and possibly to correct changes in the characteristics of the single lamp. An alternative operating procedure would be to turn the automatic IC sequencer on for a short time at the beginning and end of each pass, in order to verify by interpolation that the single-lamp calibration was correct. A log needs to be kept of the total number of hours of operation of each lamp.

The linearity of the TM sensors and the redundancy supplied by the three-lamp IC system provides a unique opportunity to monitor absolute radiometric calibration with time for changes such as clouding from filament evaporation and discontinuous filament movements.

- Change the operational procedure to alternate between black body temperatures "T2" and "T3" instead of always using "T3." Currently, there is no in-orbit test of linearity of gain with time for the emissive band. By alternating between two-point monitoring of the gain and offset with T3/shutter and T2/shutter, the degree of linearity can be evaluated quantitatively. Initial testing might involve use of T2 on a night scene. One long-pass test under constant operating conditions might involve bringing up T2 at the beginning of a pass, followed by switching to T3 with at least twenty minutes of subsequent IC data acquisition in order to determine whether the T3 temperature equilibrium had been reached and to measure the time needed for equilibration in space. These initial tests are also needed to verify whether the lower T2 temperature will provide sufficient sensitivity for calibration. Alternating use of T2 and T3 black-body temperature states would use the full TM calibration capability for Band 6.

- Establish a specific outgassing strategy for Band 6. A trade-off exists between loss of Band 6 sensitivity with time and the loss of all data from the CFP while it is outgassed and subsequently cooled down to restore the initial Band 6 sensitivity. Presumably, the criterion is the percentage loss in gain for Band 6; such loss might be acceptable until the gain drops between 20 and 30 percent.

6.2.2 IN-ORBIT CALIBRATION TESTS

Where possible, in-orbit calibration tests are desirable because:

- The pre-launch environmental test conditions are not exactly the same as those in space.
- Some characteristics of the sensor may have changed during launch.
- Some parameters may have been incompletely characterized prior to launch.

These radiometric-calibration tests place the emphasis on characterizing the normal operational mode of the sensor. Highest priority is needed on tests providing the required data for operational processing, or for modification of preprocessing or special-correction algorithms. Only one such test is currently recommended namely the calibration of the temperature-dependence of the IC pulses.

Calibration of the IC temperature-dependence is essential to the maintenance of absolute radiometry as well as to relative de-striping when scene histograms are not used. Ambient tests on Landsat-5 TM/F showed a 1 percent per ^{o}C change for some channels (Section 3). No tests were run for the IC temperature-dependence of the CFP, or during pre-launch thermal vacuum testing. Furthermore, temperatures of the TM shutter in space are up to 15^{o}C cooler than during the 15^{o}-25^{o}C ambient IC calibration tests, calling for in-orbit calibration. This can be done by taking calibration data (CALDUMP) from the initial TM turn-on for as long a pass as possible to permit warming up of the TM. The most sensitive series of data would be obtained if TDRSS could be used to transmit TM data for more than one orbit without turning off the sensor.

In the absence of such a long pass, it is possible that a shorter 30-minute pass would work. These data could be acquired at night since no imagery is needed. The pass might be of some value in acquiring real imagery over Artic regions, which are not normally viewed by Landsat.

6.2.3 IN-ORBIT CHARACTERIZATION TESTS

For certain critical types of radiometric variability it may be possible to suggest alternative configurations of the TM sensor to verify the noise model, and perhaps to generate the necessary data for applying corrections during ground

processing. Several suggestions are made for verification and characterization:

- Redundant Power Supply. Verify the constancy of IC pulses using the redundant power supply and compare the coherent noise of the two primary and redundant supplies on night scenes

- Manual IC Operation. Verify the agreement between IC pulses obtained with the automatic sequencer both on and off

- Back-up IC Operation. Verify the pre-launch relationship of "override" "constant-current" pulse values to normal "constant-radiance" IC pulses as a potential method for monitoring silicon photodiode performance with time

- Coherent Noise Phasing. Turn the midscan pulse on during a nighttime acquisition to look for the phasing relationship of coherent noise between scans. Midscan location information is always available in the Payload Correction Data (PCD), and therefore the midscan pulse is more of a convenience than a necessity.

6.2.4 IN-ORBIT SCIENTIFIC MISSION TESTS

Both the Landsat-4 and Landsat-5 spacecraft have mission capabilities that extend beyond the normal acquisition mode. Special tests have been and will be requested by the Landsat Science Office for sensor and image quality characterization. These tests gather representative normal nadir-looking data at night. In the daytime the tests gather data from homogeneous scenes of water, deserts, snow and clouds, and over selected calibration test sites, such as White Sands, New Mexico. In addition, several low-risk calibration and feasibility tests are proposed, which utilize additional capabilities of the TM sensor, or which provide between-sensor calibrations. Some higher risk experiments that test the extremes in TM capability are suggested elsewhere (Section 6.4).

Several characterization experiments for the TM sensor alone are recommended. They involve minimal changes in the mission profile, i.e., changes in configuration or pointing, but with no orbital adjusts.

They could be attempted on Landsat-4 TM/PF, and if successful, possibly used on Landsat-5.

- Subsampled Extension of Swath Width--By taking calibration data at the beginning and end of each pass and turning the internal IC shutter off, a 20 percent extension of imagery would be obtained to the east on forward scans and to the west on reverse scan, since the shutter would no longer be obscuring the optical axis at the end of each scan. Processing of such data would require special software because the scan-line-corrector resets during these acquisitions. One scientific use for such data might involve the creation of 40-percent larger swaths of lower spatial-resolution imagery for global monitoring of averaged biophysical variables, such as green biomass, temperature, and albedo. Obscuration by the resting shutter is a problem.

- Bidirectional Reflectance--By rotating the entire spacecraft to point the TM sensor off-nadir, either fore or aft, or to either side, bidirectional information could be collected over the same targets at different times. Such a data set could be used to test and/or modify radiance transfer models of the atmosphere and canopy models of specific sites.

- Intensive Single Site Acquisitions--Pointing the TM sensor from side-to-side could provide nearly daily coverage of a given path on the ground. Such an experimental set of acquisitions would help to define the mission requirements for overpass frequency, and demonstrate the limitations on the ability of Sun-synchronous satellites to monitor anomalous events, such as floods, for sites of various types of ground cover and with differing cloud-cover. Intensive sampling of several specific sites over several years could provide quantitative information on the feasibility of acquisition of cloud-free data by future-land observing satellite systems, and on the usefulness of such data.

- Single Sensor Stereo--Two ways to prepare stereo pictures from TM imagery are fore/aft pointing in the same pass or side-to-side pointing on different days. Both are technically feasible. The fore/aft is preferable because it provides nearly constant illumination.

Several in-orbit intercalibration and characterization experiments for comparing the TM sensor to other sensors are given below. They also appear to be within the operational capabilities of Landsat. By using known spectral response

curves and assuming a flat spectral response within each band for the ground targets, atmospheric absorption, and scattering, radiometric calibration can be made for acquisitions at nearly the same time of overpass for:

- TM/F to TM/PF--This 7-band to 7-band comparison can be done by pointing both spacecraft. This creates a between-sensor stereo data set. Either a simultaneous TDRSS acquisition or an X-band acquisition for TM/F and a TDRSS relay for TM/PF could be used to acquire the data set. A test of this intercomparison was done on 15-16 March, 1984, when the CFP bands on Landsat-5 TM/F were being activated. This was a unique opportunity provided by adjustment of the Landsat-5 orbit to put it on the Landsat-4, -5 World Reference System (WRS). During these movements, Landsat-5 passed underneath Landsat-4

- TM/F to MSS/F (High Gain)--The high-gain MSS acquisition needs to be taken over a clear-water area like the Bahamas, where ground observations exist for comparing the capability of the sensors to produce bathymetric charts

- TM/F to GOES E/W to NOAA-7/8--GOES-East or -West could be used to transfer spectral data between TM and the NOAA-7 and -8 polar orbiting satellites since the latter do not go over a specific location at the same time as TM.

Experiments such as these might provide better intercomparisons of absolute radiometry than calculation from aircraft and ground measurements, which usually use single-photon scattering atmospheric models. Such models are prone to high errors, especially at low sun angles. Mixed-sensor data collections have potential utility in many scientific experiments in addition to radiometric calibration.

6.3 TIPS GROUND PROCESSING

The TM Image Processing System (TIPS) consists of two computer strings, TIPS-1 and TIPS-2, located at Goddard Space Flight Center. TIPS is scheduled to be turned over to NOAA in February, 1985. In the TM R&D period prior to turn-over, TIPS needs to be brought up to the highest level of performance possible. From a radiometric perspective, that would mean implementing corrections and changes suggested in the preceding sections. Realistically, the number of changes that can be tested and implemented is significantly smaller than desirable. Therefore, this section will focus on a subset of recommendations that seem most feasible, including updates of calibration parameters, several proposed changes in radiometric processing, changes

in geometric processing, some new digital products, and R&D tasks for which TIPS is uniquely suited.

6.3.1 RADIOMETRIC CALIBRATION PARAMETERS

As a result of on-going research, a parameter file for TIPS processing is periodically updated. This was the mechanism for implementing a change in the post-calibration dynamic range on 15 January 1984. This change was a trade-off between the desire for recoverable raw data by use of expansion only during radiometric calibration and avoidance of pushing real high-radiance observations off-scale. Two further updates in calibrated dynamic range are scheduled. The first change is planned for late Spring, 1984, to assure a common range for in-orbit TM/PF and TM/F data. The second change is planned for the Fall, 1984, to implement any improved estimates of the absolute radiometric range from sources such as:

- Recalibration of the integrating spheres (Section 6.1.1)
- Sensor-to-sensor in-orbit cross comparisons (Section 6.2.4)
- Ground and aircraft absolute calibrations at the time of TM overpass over selected homogeneous areas.

Absolute radiometric calibrations from the ground using passive atmospheric sensing, rather than aircraft, are difficult. Repeated measurements over an area such as White Sands, NM under different atmospheric conditions will be needed to demonstrate greater reproducibility than pre-launch calibration tests.

It is also recommended that the absolute calibration parameters supplied to TIPS by NASA scientists and engineers be recalculated to separate effects of time and temperature during TM/IS calibration, and to remove as many sources as possible ot systematic variability discussed in Sections 4 and 5.1.

The above discussion means that a capability has to be retained by TIPS for updating the following quantities:

- Post-calibration dynamic range for each band, RMIN (B) and RMAX (B) (Appendix 9.1)
- Pre-launch values for spectral radiance for each of the twenty-one integrating sphere levels, $L_{\lambda,IS}$ (Appendix 9.2)

- Pre-launch gain and offset for each channel calculated from the regression of raw radiance L_R against $L_{\lambda,IS}$ for the sphere levels inside the dynamic range of the detector (Appendix 9.3 and 9.4).

- Pre-launch average IC pulse values of each channel for each of the eight lamp configurations, ℓ; namely, $P^o(\ell, C)$.

An alternative to updating the pre-launch gain and offset of each channel, is to update the calculated nominal IC pulse, $P_n(\ell, C)$ in Equation 1-2. Still another alternative is to provide the effective spectral radiances, $L^o_\lambda(\ell)$, for each of the IC lamp configurations, ℓ, which are calculated from the observed pre-launch averaged IC pulse, $P^o(\ell)$, and the offset, O_{IS}, and gain, G_{IS}; this is Equation 1-3, solved for $L^o_\lambda(\ell)$. In any case, TIPS needs to retain the ability to calculate these values from improved estimates over the next several years, or to provide for a direct replacement of the critical values in its parameter file.

6.3.2 IC SYSTEMATIC RADIOMETRIC CORRECTIONS

It is recommended that TIPS-era radiometric processing be optimized for the minimum striping using stand-alone IC processing, without histograms. One reason for this is that any residual destriping from histogram equalization guarantees an increased between-channel variability in the absolute radiometric calibration, even if the correct reference histogram is applied. TIPS-specific recommendations, primarily from experience with Scrounge-era processing and analysis with TRAPP software, are given below for some of the corrections implied in Sections 4.0 and 5.1.

- Two-Background Shutter Collects. In the middle of Scrounge-era processing, the single 52mf background was replaced with a double background collect of 24mf and 28mf, in the stable regions before and after DC restoration (Section 5.1.1). The same needs to be done for TIPS-era processing until a better method of background estimation is determined, such as using regions directly adjacent to the pulse. In particular, the raw data collected for calibration and that used for engineering analysis (CALDUMP) should be taken from the same region. The Canadians have incorporated these two background collects into their TM preprocessing (Murphy et al., 1984).

- Within-Scene IC Corrections. As many of the systematic sources of variability as possible need to be removed from the raw calibration values before calculating relative gains and offsets (Section 4). This is an easier requirement for the pulse or average background calibration data for each line than for individual raw radiance values at each pixel location in the image.

- Background Outliers. Outliers need to be rejected by using a threshold on raw radiance values, or by using a lower thresholding on a traveling average, in the shutter region in order to avoid noise pulses from the sensor (e.g., scan-line correction reset, or incomplete obscuration), from transmission loss, or from tape drop-outs during processing (Section 5.1.1). Retention of high values in the background region will result in bias values which are too high. This background value will become essential to radiometric calibration of the reflective bands if a single lamp state is used, even though it is currently used only for band 6 calibration.

- "Pulse" from Light Leak. There is a secondary or double pulse in the calibration region due to a light leak around the IC shutter mask on Landsat-5 TM/F (Section 5.1.3). The algorithms in TIPS need to be examined to be sure that they will not be affected by this leak pulse, especially during the 000 no-lamps-on configuration. It is possible that this is contributing to the high 4-DN values for the IC-only relative bias in some PFP channels on TIPS, although the high initial values of bias in TIPS were probably from incomplete obscuration in the shutter collect window for the background. One possible method to remove the potential interference of the light leak is to take advantage of the observed reproducible location of a few mf for the pulse with time, the fixed 52 mf distance between the center of the pulse and the center of the leak, and use a subset of the 148 mf calibration region which always excludes the 24 mf wide leak, namely, a window less than 80 mf [2(52-(24/2))] centered at the calculated center of the pulse. The existing algorithms could then continue to be used on this 80 mf subset of the original 148 mf collect window. An implementation that has been verified, using TRAPP, is to restrict the acceptable region for the center of the pulse to a fixed subset, namely from 40 to 100 mf, of the 148 mf collect region. The location and size of this secondary peak needs to be monitored to be assured that there is no change with time.

- Pulse Integration. TIPS parameters should be modified to include a variable IC pulse-integration width

for each channel in order to reduce the random error in the pulse by a factor of 2 (Section 5.1.3). It is also necessary to either recalculate the pulses used for absolute calibration the same way as TIPS, or to definitively demonstrate that a multiplication factor can be used for the conversion of a 31 mf to a 65 mf summation, in order to avoid additional error in absolute radiometric calibration.

- Pulse Averaging. The methodology used for averaging pulses in TIPS needs to be reviewed to assure that trends or transitional pulses between lamp state configurations are not included (Section 5.1.4). If a single lamp is used, then both calibration and trending errors can probably be reduced compared with the use of central pulses in the 40-scan periods of the IC automatic sequencer. An option is also needed for separate processing of forward and reverse scans.

- Lamp State Options. TIPS software needs to be modified to accept calibration data from any single lamp configuration, or from the automatic sequencer, instead of only from the automatic sequencer. The software also has to allow for omission of any particular lamp configurations in a "regression" with as few as one lamp state and the background from a shutter region (Section 5.1.5). TIPS currently uses a nine-state regression, i.e., the shutter background is used as a separate zero-level lamp-state configuration. Each of the nine states has an a priori inverse weighting factor which was set at maximum for shutter data on Landsat-4. The weighting factors are potentially valuable, although the current set of a priori "noise" could be reviewed in light of the known sources of variations (Section 4). These a priori weighting factors could be used as threshold defaults for comparison to observed "noise" on the corrected data.

- IC Temperature-Dependence. The temperature-dependence of the IC pulse is the single largest systematic error that needs to be quantified and normalized in order to preserve absolute radiometric calibration and to provide for relative within-band de-striping without histograms (Sections 5.1.6 and 6.2.2). Judging from a couple of twenty-plus scenes in a single pass for both Landsat-4 and -5, the rate of temperature increase with TM operating time is lower in space than it was in pre-lauch tests. This may mean that a single transformation to the temperature in space is all that is necessary to correct for the IC-temperature-dependence, i.e., within-pass smoothing may not be needed.

- Between-Channel Correlations. An algorithm needs to be developed to assure between-band absolute radiometric calibration for atmospheric correction and spectral transformation. In principle, the redundancy of the correlation of all 100 channels can be used if a method is developed which does not introduce significant additional error. A "shading factor" of the pulse value divided by the band average is one method for normalizing within-band correlations, which are often odd/even channel effects, that are presumably associated with characteristics of the IC system. This multiplicative gain-type shading factor correction has been used in pre-launch calculations. Correlation is a better method for between-band within-scene smoothing (5.1.6), because it can apply both an arithmetic and a multiplicative correction.

- Within-Pass Smoothing. Intervals of several scenes or a whole pass need to be smoothed to account for effects such as the continuous increase in the temperature along the path (Subsection 5.1.7). These effects need to be corrected in the floating point mode of calibration in order to avoid the addition of any rounding error associated with either segmentation or blending of subsegments.

- Between-Date Smoothing. If physical explanations can be used to reliably predict change with time, then provision could be made for utilizing this information during calculation of gains and biases (Section 5.1.8).

- Referencing or Weighting. Some channels are more noisy than others. When averages are used in calculations, it is desirable to use averages weighted by the inverse of the variance. If good estimates of the variance are not available, then it is better to use a quiet reference channel (Table 4-5) than an average.

- Quality Indices. Statistical measures of the uncertainty in the calculations, such as standard error of the estimate for regression, could be explicitly included in the TIPS reports as quality indices.

6.3.3 HISTOGRAM EQUALIZATION

It is recommended that histogram equalization by TIPS be used primarily as a quality control measure. The reasons for this are given in Section 5.2.1. Histogram equalization would be used for TIPS radiometric calibration if the striping, calculated after IC calibration by comparing the histograms of different channels, is above a threshold level, and then only as a slowly varying weighting with

the gain and offset calculated from the IC system. Possible modifications to the TIPS processing, which appear to be appropriate to accomplish this recommendation, are given below.

- First Pass HDT-RT Histogram File. One option that would reduce the operational processing time is to drop histogramming from the first pass through the raw data on the HDT-RT. If this option is implemented operationally, a less frequently used engineering capacity is needed to calculate and retain a file for a histogram of each scene and for the cumulative pass. This engineering option for histogramming the HDT-RT would be used for creating files for the long term monitoring of the constancy of "bin-radiance dependence" and for monitoring the magnitude of the radiometric corrections by comparing the normalized gains and biases calculated from histogram equalization of this raw data to the actual normalized gains and biases that were calculated after applying a radiometric calibration.

- Calculation of Systematic Corrections. Normalized gains and biases need to be calculated for every line in the HDT-RT based on the corrections outlined in Section 6.3.2. The alternative of continuing to calculate a single RLUT for a whole scene, or segments of an interval, is almost unacceptable.

- Second Pass HDT-RT 11-Bit Histogram. An archival HDT-AT needs to be created, during the second pass through the raw HDT-RT, that is equivalent to the current HDT-AT with unity RLUT. The respective "relative" and "applied" gain and biases at the end of every line of the HDT-AT would be replaced, respectively, with systematically corrected normalized IC gains and biases, and normalized gains and biases calculated by histogram equalization. This histogram equalization would be calculated from a centrally defined common radiance region for all channels, presumably identical to the middle section of the three section dynamic range proposed in Section 6.3.5. The histogram used for this histogram equalization would be a cumulative 11-bit histogram of radiometrically corrected pixels from both the scene and the calibration region for all preceding scenes from this second pass through the HDT-RT. The 11-bit, rather than 8-bit, histogram is necessary to avoid loss of the accuracy gained by sub-DN systematic corrections. Some of the additional benefits of this proposed histogramming procedure include:

    - Absolute radiometric calibration would be retained because the common radiance range for histogramming is chosen after radiometric calibration

- A higher sensitivity is obtained on low radiance scenes because a nearly full range of DN values can be guaranteed by the inclusion of IC data in the histogram

- The current HDT-AT format is unchanged

- Raw observations become routinely available to any investigator requesting either an HDT-AT or a CCT-AT. This is a high priority for scientific investigators, who are the principle users of non-P data

- Well averaged constants for both IC and histogram calibration become directly available from an -AT tape

• HDT-AT Histogram File. If the 11-bit scene histograms and the cumulative 11-bit histogram for all the scenes in a given pass are retained on a history file, as well as the normalized gains and offsets calculated from them, then it will be possible to systematically monitor the TM radiometric performance as a function of time, as required for making within-path or between date corrections (Sections 5.1.7 and 5.1.8). A history file of the systematically corrected IC normalized gains and offsets for each line, and an average for each scene and the whole pass, would provide the complementary data for monitoring and modeling the absolute radiometric performance of the TM internal calibrator.

• Histogram Reference. When the normalized gains and biases are calculated by histogram equalization, use the quietest channel in the band as the reference (Table 4-5), or the band-average weighted by the variance, in order to avoid the larger potential error in absolute radiometry associated with using the equally weighted band-average.

• Histogram Monitoring of IC Quality. Ideally, the residual striping will be sufficiently small, after appropriate calibration with the IC system alone, that there will be no justification for the use of histogram equalization. In that case, histogram equalization can be used as a monitor of residual striping, and only used if the striping is greater than some a priori value. This quality index could be calculated automatically in real-time just before geometric resampling.

• Weighting of IC and Histogram Constants. A less satisfactory procedure than using IC alone, but one that incorporates histogramming, is to calculate a set of

weighting factors for the gains and offsets from the separate IC and histogram calculations and apply them in 16-bit or floating point calculations during the geometric resampling process. A set of weights could be calculated as the inverse of the square of the differences between the calculated gains and offsets and their values as predicted by an empirical fit of their slowly varying behavior with time. If it is not possible to modify TIPS to allow for radiometric calibration during the geometric resampling, then the raw values suggested above for the HDT-AT would have to be replaced with radiometrically calibrated values.

- HDT-PT Histogram File for Each Band. An 11-bit summary histogram for each band, for each scene and for the whole pass, from the geometrically resampled P-tapes, would provide the data necessary to monitor the overall operational radiometric performance of TIPS during P-processing by comparison to A-histograms for the same scene. P-histograms would also provide a research and development tool for quantitatively assessing the effect of difference resampling algorithms.

6.3.4 GEOMETRIC PROCESSING

In general, geometric processing on TIPS is excellent. Improvements would be useful in several areas, if possible.

- Single Pass Geodetic Product. At present, TIPS can not use its ground control points, GCPs, to produce a geodetically rectified image of the reference scene from which the GCPs are taken. This means that if there is only one cloud-free TM scene of an area, that it can not be geodetically rectified. A TIPS capability is needed for producing geodetically rectified scenes from a single TM pass.

- Map Compatibility by Rotation to North. A TIPS resampling option is needed for directly creating a north-pointing projection without resampling of the P-product, in order to provide greater compatibility to most maps, e.g., 1:24,000 scale USGS maps. The Canadians at CCRS are planning on providing this type of projection as a normal TM product, which will also be more easily compatible with information extraction procedures using GIS, Geographic Information Systems. An additional benefit of such a resampling is that residual channel-related striping remaining after radiometric calibration would be less visible. Since a UTM option exists in TIPS, a recommendation is made that all geodetic P products be in a UTM projection.

- Single Pass Cubic Spline Resampling. Fischel (1984) has suggested that it would be better to use a single pass, rather than a double pass, in the second part of the TIPS resampling procedure (see Section 5.2.5).

- Image Co-ordinates of GCPs. It would be useful to have the image co-ordinates (start line and sample) for each of the 33 by 33 pixel GCP chips that were used in a specific image.

- Relative GCPs. After the required geodetic accuracy has been achieved by use of map-referenceable GCPs, it is suggested that these cloud-free reference images be searched for additional "relative" 32 by 32 pixel GCP chips, even though they may represent features which are not present on current maps. Since many scenes are more than 50 percent cloud-covered, it is desirable to have two-to-four times as many GCP chips as are needed in a cloud-free scene. Excellent GCPs are being rejected by some operators in the current building of the TIPS GCP library because they can not be located on maps.

- GCP Methodology. Spectral transforms (Section 5.4.1) such as "greenness" and "brightness" are suggested as replacements for the two raw spectral bands, in order to provide potentially higher contrast in a one or two band correlation of the chip to the 128 by 128 pixel ground control point neighborhood. It is also recommended that these spectral transforms be examined for use, in conjunction with the thermal band, for automatic cloud cover assessment (ACCA). Up to four sets of GCPs are recommended for each scene so that the GCPs can be selected on the basis of season.

- Schedule for Global GCP Library Build. With the current TIPS methodology for building the GCP library, it will probably take one or two decades to complete it on a global scale, even if appropriate maps were available, which they are not. Therefore, it is recommended that an alternative methodology be proposed, perhaps using a factor of fifty fewer GCPs in the initial building of the library for each interval.

6.3.5 THREE-SECTIONED POST-CALIBRATION DYNAMIC RANGE

A proposal is requested for implementing the three-sectioned RLUT on TIPS in a manner similar to that discussed in Section 5.2.3. The Canadians at CCRS attempt to accomplish the same objective of retaining non-saturated data in all channels by widening the post-calibration dynamic range to

include the lowest RMIN and the highest RMAX, with a linear fit in between. This single section procedure has the disadvantage, for a fixed 8-bit RLUT, of lowering the sensitivity for all channels, i.e., some data are compressed from two bins into one bin; this does not happen if the post-calibration radiometric resolution is increased, as CCRS accomplishes in intermediate steps by going to a 16-bit RLUT, or by dropping the most significant bit in the lower radiance scenes of the North and replacing it with one more bit in a shifted 8-bit RLUT.

Since DN values of 0 and 255 may represent values outside of the dynamic range, it is recommended that settings of the dynamic range be from DN values 1 through 254. DN values of 0 to 255 would then be used explicitly for values outside the post-calibration dynamic range.

6.3.6 IMAGE CALIBRATION

A TIPS procedure needs to be developed for replacing bad channels (Section 5.2.2), other than the current procedure of replacement with an adjacent channel. TIPS needs to retain, rather than replace, the imagery and calibration from Channel 4 of Band 2 in future processing of data from Landsat-4 TM/PF.

TIPS needs to implement an unbiased 8-bit probabilistic approach, using an individual bias and gain for each line, to replace the current 8-bit integer RLUT approach for the whole scene (Section 5.2.4). It is desirable to provide a mechanism for within-line calibration. The most desirable procedure to avoid quantization errors is to combine radiometric and geometric calibration and to use 16-bit arithmetic until the final stage of resampling, as CCRS will do. Here again, the final rounding can be done with zero bias by using the probabilistic approach.

6.3.7 PRODUCTS

TIPS, and other facilities with ground receiving stations or an ability to process high density tapes, are in a unique position to produce special, and potentially operational, products because they can start with raw data on an HDT-RT without introducing unnecessary additional quantization errors. The HDT-RT tapes are also the only source of raw calibration data. Some recommendations for current and future special products are given below.

- Semi-Weekly Tapes of Raw Calibration Data. A recommendation is made that raw TM data from the calibration region of the HDT-RT, which are used in TIPS processing, be

made available as an optional part of an operational TIPS string. Currently, it is necessary to have dedicated use of a TIPS string to produce three files of data and an analysis file on an engineering tape, called CALDUMP. No changes in tape format are requested; what is needed is access to the raw calibration data from the background and calibration regions of the shutter (Section 5.1). It is recommended that it be possible to put any or all of the calibration collect files from a single TIPS processing interval of scenes onto such a CALDUMP tape. Such CALDUMP tapes are need approximately twice a week for TRAPP.

- Semi-Weekly "Unity" CCT-AT. An operational option is also needed to be able to produce a CCT-AT with "unity" RLUT to accompany the CALDUMP tape for input to TRAPP. This is the mechanism for accessing raw data and it needs to be part of the operational TIPS procedure. If the recommendation is accepted to normally use only one lamp (Section 6.2.1), whether the IC automatic sequencer is on or off, then it is anticipated that one monitoring tape a week would be with three lamps sequencing and one tape a week would be with only one lamp on.

- Special "Unity" CCT-AT. It is recommended that special collections of raw data on CCT tapes be occasionally accessible from anywhere on the HDT-RT, not just the current background collect regions. One method for implementing this request is to make a CCT-AT with a unity RLUT, with a different starting and ending minor frame; this worked in the Scrounge-era processing. It is not anticipated that these products would be standard products, they are viewed as necessary for engineering and scientific studies during the research and development period, and for subsequent monitoring and trouble-shooting by scientists in the Landsat Science Office.

- Reprocessed Internal Reference Scenes. A recommendation is made that ten 7-band reference scenes be chosen for both Landsat-4 TM/PF and Landsat-5 TM/F. When changes are made in the TIPS processing algorithms, it is recommended that the most appropriate reference scene be rerun and the following products submitted for examination to the Landsat Science Office: CALDUMP, unity CCT-AT, CCT-AT, CCT-PT, black and white prints of A-product in all bands, black and white prints of P-product if the resampling process was modified, and copies of appropriate quality assessment printouts. To the extent that such products are identical to previous submissions, they do no have to be

resubmitted. These are also the scenes that need to be used for testing special processing options, such as nearest neighbor (NN) and different implementations of cubic convolution (CC) resampling.

- History Tapes of Calibration Constants. A recommendation is made that TIPS maintain a history file of calibration results for operational processing of TM imagery. Such a file would provide the data for trend analysis and possible smoothing (Sections 5.1.6, 5.1.7, and 5.1.8). Some of the suggested contents for a history file were outlined with recommendations for histogram equalization (Section 6.3.3). These files need to be made available periodically on tape to the Landsat Science Office for analysis. Possible contents for these files include tabulation by scene center and time of:

  - Average IC pulses
  - Average shutter background and standard deviation
  - 8-bit histograms of raw data
  - 11-bit radiometrically calibrated A-histograms
  - 11-bit P-histograms by band
  - IC offsets and gains
  - Applied offsets and gains
  - Corrections by type and channel
  - TIPS "TIG" Quality Assessment files
  - TIPS "TAG" Quality Assessment files.

- Selected HDT-RT Copies. If research efforts are started to separate information about the atmosphere and the land (Section 5.3.2), then it is assumed that copies of HDT-RT tapes will be needed as direct input to computers such as the MPP or Cyber. It is recommended that official intercomparisons of products from common HDT-RTs be made with other facilities, such as those in Canada and Italy.

- Extra Band(s) of Binary Data. Certain types of information that would increase the utility of TM imagery are extractable as part of the TIPS processing, especially the ground control-point geodetic resampling. Much of this type of information, such as boundary maps, can be

summarized with single bit binary masks. Once a boundary map is prepared as part of the building of the GCP library, it can be used for all subsequent scenes at the same location. The addition of an 8th band to the TM digital imagery would permit the addition of eight such binary masks. It is recommended that a feasibility study be made of adding such a band with the following types of binary masks:

- Political boundaries from GCP maps
- "Infrastructure" of important features, such as roads and railroads, that are below the spatial resolution of the TM sensor
- Topographic boundaries for watersheds
- Boundaries for major ecosystems
- Clouds from ACCA
- Calculated edges of cloud shadows
- Outlines of locations of used and unused GCP chips
- Points and boundaries from texture analysis.

- Extra Bands of 8-Bit Data. Several types of 8-bit data are of potential value to users and are producible prior to quantization error during TIPS-type processing. It is recommended that the feasibility of preparing such registered P-products be examined for:

  - Spectral transforms (Section 5.4.1)
  - Texture measures
  - Digital topographic maps
  - Slope and aspect
  - Irradiance
  - Atmospheric variables
  - Surface bidirectional reflectance.

- Tapes at Reduced Spatial Resolution. It is recommended that the feasibility of operational production of TM imagery at reduced spatial resolution be examined. Historically, it has been easier to acquire imagery from space than to analyze it. This proposal is designed to:

  - Make the product less expensive to the user
  - Take advantage of the multi-temporal synoptic strength of the Landsat system

- Provide a maximum of cloud-free data by resampling only cloud-free pixels at resolutions of 120 m and 1 Km (Section 5.3.2)

- Provide a reason for acquiring more imagery, both globally and at night, because of the presumed increase in the number of applications

- Provide fewer bands, such as bands 3 and 4, and spectral transforms, such as brightness and greenness

- Provide more multi-temporal data

- Provide less data to process

- Provide the user community with the opportunity to examine quantitative data, with the knowledge that if it proves useful, the full resolution of the TM data is available for exactly the same scene.

- Cloud-free Global TM Archive. It is recommended that a cloud-free archive of seasonal TM digital imagery be acquired and maintained on a medium, or with error correction capability, that can guarantee error-free recovery of this data over the next several decades.

6.3.8 RESEARCH AND DEVELOPMENT

Many of the proposed operational recommendations and suggestions in the preceding sections will require examination during the research and development period of TIPS. In addition, some effort needs to be made to examine other topics, such as:

- Within-line processing
- Band 6 processing
- Ingestion of foreign TM tapes
- Full interval radiometric processing
- Creation and processing of pre-launch 28-tracks
- Global Positioning System tests to reduce required control point neighborhood from 128 x 128.

6.4 CONTINGENCY EXPERIMENTS

It is recommended that a contingency plan of scientific and engineering experiments be prepared for acquisition of TM and MSS digital imagery when these sensors are not being used operationally. This requires agreement of NASA and NOAA on flight segment operation (Section 6.2). Advanced planning is important since opportunities for these experiments may be lost, or go unrecognized, if the need and feasibility are not understood. In the final stages of spacecraft operation, there may be very little time between loss of power, or some other failure, and the need to de-boost in order to attempt a recovery by a polar-orbiting shuttle mission at a lower altitude.

6.4.1 SCIENTIFIC EXPERIMENTS

Scientific needs are particularly great for space-acquired imagery to help define sensor and mission requirements for future land-observing satellite systems. Scientific experiments would be aimed at acquiring data that cannot be acquired in the normal modes or in the special in-orbit scientific mission tests (Section 6.2.4). Some experiments could be done with pointing or minor orbital adjusts while at current altitude, others could occur during or after de-boost to a lower altitude. Illustrative experiments include:

- Radiometric Calibration with Moon. The Landsat spacecraft is capable of pointing at the Moon, and this might provide a means of long-term multi-decade absolute radiometric calibration between sensors
- Stereo and Bidirectional Reflectance
- Time-of-Day Orbital Changes
- Revisit Frequency Requirements
- Utility of Mixed Spatial Resolution.

6.4.2 ENGINEERING EXPERIMENTS

Engineering experiments would be designed to characterize the best performance that could be achieved by the sensor, as a complement to the normal in-orbit calibration and

characterization tests (Sections 6.2.2 and 6.2.3). Illustrative experiments might include:

- Band 6 Sensitivity at 70 Degrees Kelvin
- Focus Tests of Inchworms Over GCPs
- Tests of Global Positioning System Utility
- Tests of On-Board Computer Options
- Alternative Lamp and Power Supply Tests

SECTION 7 - ACKNOWLEDGMENTS

One of the reasons that a paper like this, which attempts to bridge part of the gap between the engineering and the scientific characterization of the TM sensor, can be written, is because of the initiative shown by key NASA engineers in inviting active participation of NASA scientists in the various phases of the Landsat program, especially in the pre-launch testing of both the MSS and TM sensors. Particular appreciation is expressed to Oscar Weinstein and Jon Busse, the instrument manager and the Project Manager, respectively, at the time of critical scientific involvement with the engineers. The complementary part of this successful working relationship was the encouragement from the Project Scientist, Vince Salomonson, to maintain a nearly full-time involvement with the engineers over a period of several years. The generous co-operation of many engineers at Santa Barbara Research Center (SBRC) and General Electric at Valley Forge (GE/VF), especially during on-site testing, was invaluable. Some of the engineers were: Jack Engel (SBRC), Jack Lansing (SBRC), Eric Beyer (GE/VF), and Nick Koepp-Baker (GE/VF). This was a marvelous opportunity to see first-hand the literally hundreds of people who, by personal dedication, have made the TM sensor on the Landsat spacecraft such a success. This co-operation between engineers and scientists has continued with the current Project Manager, Lou Gonzales, and the Mission Opeations Manager, Bill Webb.

Two teams of contractors have supported the computing and analysis efforts associated with this scientific characterization over the last three years, one from Computer Sciences Corporation (CSC) and the other, more recently, from Science Applications Research (SAR). Key scientists and analysts from these companies were Rochelle Abrams (CSC), Dave Ball (CSC), Fred Gunther (CSC), Yung Lee (SAR), and Son Truong (SAR). All of these people, and the supporting staff, have been extremely conscientious and devoted in designing, coding, maintaining and running the many versions of TRAPP software on the computers at Goddard Space Flight Center, and then assisting in the months of analysis of the library of TRAPP books upon which most of the conclusions in this paper are based.

A special note of appreciation goes to Fred Gunther who has assisted extensively in the preparation of this manuscript, and to those people who reviewed earlier versions of this paper, namely, Winona Barker, Jack Lansing, Yung Lee, Loren Linstrom, and Brian Markham.

A portion of data processing was performed under the National Oceanic and Atmospheric Administration, Contract Number NA-83-SAC-00600.

SECTION 8 - SELECTED BIBLIOGRAPHY

Anonymous, "Scrounge Interface Control Document," LANDSAT-D PROJECT, ADDS/LAS, Goddard Space Flight Center, Greenbelt, Maryland, February 1982

Anuta, P., L. Bartolucci, E. Dean, F. Lozano, E. Malaret, C. McGillen, J. Valdez and C. Valenzuela, "Landsat-4 data quality analysis,". PROCEEDINGS, PECORA 8 REMOTE SENSING SYMPOSIUM. Sioux Falls, South Dakota, 1983

Anuta, P. E., L. A. Bartolucci, M. E. Dean, D. F. Lozano, E. Malaret, C. D. McGillem, J. A. Valdez, and C. R. Valenzuela, "Landsat-4 MSS and Thematic Mapper data quality and information content analysis," IEEE TRANSACTIONS ON GEOSCIENCE AND REMOTE SENSING, Vol. GE-22, May 1984

Barker, John L., and Fred J. Gunther, "Landsat-4 sensor performance," PROCEEDINGS, PECORA 8 REMOTE SENSING SYMPOSIUM, Sioux Falls, South Dakota, 1983

Barker, J. L., R. B. Abrams, D. L. Ball, and K. C. Leung, "Characterization of radiometric calibration of Landsat-4 TM reflective bands," PROCEEDINGS, LANDSAT-4 SCIENTIFIC CHARACTERIZATION, EARLY RESULTS SYMPOSIUM, Greenbelt, Maryland, April 1984

Barker, J. L., R. B. Abrams, D. L. Ball, and K. C. Leung, "Radiometric calibration and processing procedure for reflective bands on Landsat-4 protoflight Thematic Mapper," PROCEEDINGS, LANDSAT-4 SCIENTIFIC CHARACTERIZATION, EARLY RESULTS SYMPOSIUM, Greenbelt, Maryland, April 1984

Barker, J. L. , D. L. Ball, K. C. Leung, and J. A. Walker, "Prelaunch absolute radiometric calibration of the reflective bands on the Landsat-4 protoflight Thematic Mapper," PROCEEDINGS, LANDSAT-4 SCIENTIFIC CHARACTERIZATION, EARLY RESULTS SYMPOSIUM, Greenbelt, Maryland, April 1984

Barker, J. L. F. J. Gunther, R. B. Abrams, and D. L. Ball, "TM digital image products for applications," PROCEEDINGS, LANDSAT-4 SCIENTIFIC CHARACTERIZATION, EARLY RESULTS SYMPOSIUM, Greenbelt, Maryland, April 1984

Bernstein, R., and J. B. Lotspiech, "Landsat-4 Thematic Mapper-results of advanced digital image processing experiments," PROCEEDINGS, PECORA 8 REMOTE SENSING SYMPOSIUM, Sioux Falls, South Dakota, 1983

Bernstein, R., J. B. Lotspiech, J. J. Myers, H. G. Kolsky, and R. D. Lees, "Analysis and processing of Landsat-4 data using advanced image processing techniques and technologies," IEEE TRANSACTIONS ON GEOSCIENCE AND REMOTE SENSING, Vol. GE-22, May 1984

Castle, K. R., R. G. Holm, C. J. Kastnev, J. M. Palmer, P. N. Slater, M. Dinguivard, C. E., Ezra, R. D. Jackson, and R. K. Savage, "In-flight absolute radiometric calibration of the Thematic Mapper," IEEE TRANSACTIONS ON GEOSCIENCE AND REMOTE SENSING, Vol. GE-22, May 1984

Chavez, P., Jr., S. C. Guptill, and J. Bowell, "Image processing techniques for Thematic Mapper data," TECHNICAL PAPERS OF THE 50TH ANNUAL MEETING OF THE AMERICAN SOCIETY OF PHOTOGRAMMETRY, Washington, D.C., 1984

Colvocoresses, A. P., "Mapping of Washington, D.C. and vicinity with the Landsat-4 Thematic Mapper," TECHNICAL PAPERS OF THE 50TH ANNUAL MEETING OF THE AMERICAN SOCIETY OF PHOTOGRAMMETRY, Washington, D.C., 1984

Engel, J. L., "Thematic Mapper: An interim report on anticipated performance," AIAA SYSTEMS FOR THE 80'S CONFERENCE, Colorado Springs, Colorado, 1980

Colwell, R. N. (Editor), "Manual of Remote Sensing," AMERICAN SOCIETY OF PHOTOGRAMMETRY, Falls Church, Virginia, 1983

Crist, E. P., and R. C. Cicone, "A physically-based transformation of Thematic Mapper Data - the TM Tasseled Cap," IEEE TRANSACTIONS ON GEOSCIENCE AND REMOTE SENSING, Vol. GE-22, May 1984

DeGloria, S. D., "Spectral variability of Landsat-4 Thematic Mapper and Multispectral Scanner data for selected crop and forest cover types," IEEE TRANSACTIONS ON GEOSCIENCE AND REMOTE SENSING, Vol. GE-22, May 1984

Dozier, J., "Snow reflectance from Landsat-4 Thematic Mapper," IEEE TRANSACTIONS ON GEOSCIENCE AND REMOTE SENSING, Vol. GE-22, May 1984

Engel, J. L., J. C. Lansing, Jr., D. G. Brandshaft, and B. J. Marks, "Radiometric performance of the Thematic Mapper," PROCEEDINGS, 17th INTERNATIONAL, ENVIRONMENTAL RESEARCH INSTITUTE OF MICHIGAN. Ann Arbor, Michigan, May 1983

Everett, J. R., J. D. Dykstra, and C. A. Sheffield, "The contribution of Landsat-4 Thematic Mapper data to geologic exploration," PECORA 8 REMOTE SENSING SYMPOSIUM. Sioux Falls, South Dakota, 1983

Fischel, D., "Validation of the Thematic Mapper radiometric and geometric correction algorithms," IEEE TRANSACTIONS ON GEOSCIENCE AND REMOTE SENSING, Vol. GE-22, May 1984

Fusco, L., "Thematic Mapper: The ESA-Earthnet ground segment and processing experience," IEEE TRANSACTIONS ON GEOSCIENCE AND REMOTE SENSING, Vol. GE-22, May 1984

Gunther, Fred J., "A new principal components procedure to aid the analysis of Landsat MSS digital data," PROCEEDINGS, 1982 CONFERENCE ON PATTERN RECOGNITION AND IMAGE PROCESSING IEEE Computer Society, Las Vegas, Nevada, 1982

Haas, R. H., and F. A. Waltz, "Evaluation of Thematic Mapper data for natural resource assessment," PECORA 8 REMOTE SENSING SYMPOSIUM, Sioux Falls, South Dakota, 1983

Hill, C. L. "Analysis of Landsat-4 Thematic Mapper data for classification of forest stands in Baldwin County, Alabama," PECORA 8 REMOTE SENSING SYMPOSIUM, Sioux Falls, South Dakota, 1983

Kogart, J., E. Larduinat, and M. Fitzgerald, "An Analysis of New Techniques for Radiometric Correction of Landsat-4 Thematic Mapper Images," Contractor Report, Contract No. NAS 5-27371, Research and Data Systems, Inc., Lanham, Maryland, October 1983

Malila, W. A., M.D. Metzler, D.P. Rice, and E. P. Crist, "Characterization of Landsat-4 MSS and TM digital image data," IEEE TRANSACTION ON GEOSCIENCE AND REMOTE SENSING, Vol. GE-22, May 1984

Masuoka, P. M., "Availability of Landsat-4 Thematic Mapper data," TECHNICAL PAPERS OF THE 50TH ANNUAL MEETING OF THE AMERICAN SOCIETY OF PHOTOGRAMMETRY, Washington, D.C., 1984

Murphy, J. M., T. Butlin, P. F. Dutt, and A. J. Fitzgerald, "Revised radiometric calibration technique for Landsat-4 Thematic Mapper data," IEEE TRANSACTION ON GEOSCIENCE AND REMOTE SENSING, Vol. GE-22, May 1984

Palmer, J. M., "Effective bandwidths for Landsat-4 and Landsat-D' Multispectral Scanner and Thematic Mapper subsystems," IEEE TRANSACTIONS ON GEOSCIENCE AND REMOTE SENSING, Vol. GE-22, May 1984

Pitts, D. E., G. D. Bahhwar, D. R. Thompson, K. E. Henderson, S. Shen, C. Sorensen, and J. G. Carnes, "Evaluation of corn/soybeans separability using Thematic Mapper and Thematic Mapper simulator data," IEEE TRANSACTIONS ON GEOSCIENCE AND REMOTE SENSING, Vol. GE-22, May 1984

Price, J. C., "Comparison of the information content of data from the Landsat-4 Thematic Mapper and the Multispectral Scanner," IEEE TRANSACTIONS ON GEOSCIENCE AND REMOTE SENSING, Vol. GE-22, May 1984

Salomonson, V. V., and A. B. Park, "An Overview of the Landsat-D Project with Emphasis on the Flight Segment," PROCEEDINGS, 5th SYMPOSIUM ON MACHINE PROCESSING OF REMOTELY SENSED DATA, PURDUE UNIVERSITY, Lafayette, Indiana, June 1979

Salomonson, V. V., and R. Koffler, "An Overview of Landsat-4 status and results from Thematic Mapper data analysis," SUMMARIES, 17th INTERNATIONAL SYMPOSIUM ON REMOTE SENSING OF THE ENVIRONMENT, ENVIRONMENTAL RESEARCH INSTITUTE OF MICHIGAN, Ann Arbor, Michigan, May 1983

Salomonson, V. V., and H. Mannheimer, "An Overview of the evolution of Landsat-4," PECORA 8 REMOTE SENSING SYMPOSIUM, Sioux Falls, South Dakota, 1983

Sheffield, C., "Earthwatch - A Survey of the World from Space," MacMilan, New York, 1981, 160 pages

Short, N. M., P. D. Lowman, Jr., S. C. Freden, and W. A. Finch Jr., "Mission to Earth: Landsat Views the World," NASA Special Publication 360, Washington, D.C. 1976, 362 pages

Thompson, D. R. and K. E. Henderson, "Evaluation of Thematic Mapper for detecting soil properties under grassland vegetation," IEEE TRANSACTIONS ON GEOSCIENCE AND REMOTE SENSING, Vol. GE-22, May 1984

Walker, R. E., A. I. Zobrist, N. A. Bryant, B. Gohkman, S. Z. Friedman, and T. L. Logan, "An analysis of Landsat-4 Thematic Mapper geometric properties," IEEE TRANSACTIONS ON GEOSCIENCE AND REMOTE SENSING, Vol. GE-22, May 1984

Walker, R. E., A. I. Zobrist, N. A. Bryant, B. Gohkman, S. Z. Friedman, and T. L. Logan, "An assessment of the geometry of Thematic Mapper data," TECHNICAL PAPERS OF THE 50TH ANNUAL MEETING OF THE AMERICAN SOCIETY OF PHOTOGRAMMETRY, Washington, D.C., 1984

Welch, R. and E. Lynn Usery, "Cartographic accuracy of Landsat-4 MSS and TM image data," IEEE TRANSACTIONS ON GEOSCIENCE AND REMOTE SENSING, Vol. GE-22, May 1984

Williams, D. L., J. R. Irons, B. L. Markham, R. F. Nelson, D. L. Toll, R. S. Latty, and M. L. Stauffer, "A statistical evaluation of the advantages of Landsat Thematic Mapper data in comparison to Multispectral Scanner data," IEEE TRANSACTIONS ON GEOSCIENCE AND REMOTE SENSING, Vol. GE-22, May 1984

Williams, R. S., Jr., and W. D. Carter (Editors), "ERTS-1, A New Window on Our Planet," U.S. Geological Survey, Professional Paper 929, Washington, D.C., 1976, 362 pages

Wrigley, R. C., D. H. Card, C. A. Hlavka, J. R. Hall, F. C. Mertz, C. Archwamety, and R. A. Schowengerdt, "Thematic Mapper image quality: registration, noise and resolution," IEEE TRANSACTIONS ON GEOSCIENCE AND REMOTE SENSING, Vol. GE-22, May 1984

APPENDIX 9.1 - TIPS POST-CALIBRATION DYNAMIC RANGE

Copy of Memo that Established Significant Figures of Post-Calibration Dynamic Range Constants for TIPS Calibration, as of 20 January 1984.

January 20, 1984

TO: Distribution

FROM: 923/Landsat Associate Project Scientist/J. Barker

SUBJECT: Significant Figures for TM Dynamic Range Constants

At a working meeting on January 16, 1984 at Goddard Space Flight Center, it was agreed that the following specific and exact values shall be used for calibration of Landsat-4 and Landsat-5 Thematic Mapper (TM) image data:

Table 1) Spectral Radiance (in $mWcm^{-2}ster^{-1}\mu m^{-1}$)

BAND	1	2	3	4	5	7
RMIN	-0.15	-0.28	-0.12	-0.15	-0.037	-0.015
RMAX	15.21	29.68	20.43	20.62	2.719	1.438

Table 2) TM Band-Width (in μm)

BAND	1	2	3	4	5	7
L-4	.066	.081	.069	.129	.216	.250
L-5	.066	.082	.067	.128	.217	.252

Table 3) In-Band Radiance for Landsat-4 (in $mWcm^{-2}ster^{-1}$)

BAND	1	2	3	4	5	7
RMIN	-0.0099	-0.0227	-0.0083	-0.0194	-0.00799	-0.00375
RMAX	1.004	2.404	1.410	2.660	0.5873	0.3595

Table 4) In-Band Radiance for Landsat-5 (in $mWcm^{-2}ster^{-1}$)

BAND	1	2	3	4	5	7
RMIN	-0.0099	-0.0230	-0.0080	-0.0192	-0.00803	-0.00378
RMAX	1.004	2.434	1.369	2.639	0.5900	0.3624

It is the intention of this memo to provide the data necessary to assure that these particular numbers be explicitly entered into computer calibration programs as written and not be calculated from each other. The expectation is that these numbers will be used by TIPS until another recommendation is made, presumably after the launch of Landsat-5. By using these numbers, self-consistency and intercompariability of software or processed data will be more likely without differences due to significant digits, rounding or truncation on different computers

The meeting was attend by J. Barker (GSFC, chair), F. Gunther (CSC), T. Keller (GE), Y. Lee (SAR) and S. Truong (SAR). The numbers agreed to at this meeting represent a slight change in a few numbers of the second table of the RMIN and RMAX in units of In-Band radiance included in the required CSC/GSFC delivery of Landsat-5 TM calibration constants to GE/VF on December 16, 1983. These recommendations do not change any numbers in the other twelve tables of spectral radiance, sphere radiance, channel gain, channel offset, or reference DN values for eight lamp configurations for all 96 channels.

John L. Barker

APPENDIX 9.2 - INTEGRATING SPHERE SPECTRAL RADIANCES

Integrating Sphere (IS) calibration data in spectral radiance, $L_{\lambda,IS}$ ($mWcm^{-2}ster^{-1}\mu m^{-1}$) for each IS lamp level, furnished by NASA/GSFC to GE/VF on 15 December 1983 for TIPS-era calibration of Landsat-5 TM/F instrument. These data were from a recalibration of the 48"IS in May, 1982.

LANDSAT-5
ABSOLUTE CALIBRATION
122cm INTEGRATING SPHERE RADIANCE LEVELS BY LAMP

LAMP STATE		SPECTRAL RADIANCE ($mWcm^{-2}ster^{-1}\mu m^{-1}$)					
STATE	WATTS	BAND 1	BAND 2	BAND 3	BAND 4	BAND 5	BAND 7
624	1500	11.4834	24.1872	37.5986	50.6061	20.1763	6.3701
524	1300	9.8813	20.8205	32.1692	43.7448	17.5040	5.5233
424	1100	8.2954	17.4969	27.1895	36.8790	14.7894	4.6894
324	900	6.7193	14.2517	22.1644	30.2746	12.1894	3.8490
224	700	5.1586	10.9343	17.1686	23.4835	9.5213	3.0056
224	700	5.1586	10.9343	17.1686	23.4835	9.5213	3.0056
214	600	4.4518	9.3815	14.6944	19.9793	8.0239	2.5277
124	500	3.7441	7.9530	12.4919	17.1592	6.9848	2.2071
114	400	3.0373	6.4002	10.0175	13.6547	5.4877	1.7296
024	300	2.1426	4.6344	7.3691	10.3740	4.3563	1.3797
023	275	1.9565	4.2449	6.7506	9.5372	4.0193	1.2723
022	250	1.7872	3.8795	6.1670	8.7236	3.6875	1.1680
014	200	1.4357	3.0817	4.8942	6.8696	2.8593	0.9021
012	150	0.0804	2.3267	3.6919	5.2192	2.1907	0.6903
011	125	0.9113	1.9641	3.1168	4.4225	1.8651	0.5881
010	100	0.7396	1.5924	2.5233	3.6058	1.5373	0.4912
004	100	0.6961	1.4898	2.3710	3.2634	1.3223	0.4109
003	75	0.5100	1.1003	1.7525	2.4264	0.9853	0.3036
002	50	0.3407	0.7348	1.1687	1.6134	0.6535	0.1991
001	25	0.1717	0.3722	0.5938	0.8164	0.3278	0.0970
000	0	0.0	0.0	0.0	0.0	0.0	0.0

617-GUN-161

APPENDIX 9.3 - TM/F GAINS

TM/F instrument calibration data (gain) are presented for each channel of each reflective band, as furnished by NASA/GSFC to GE/VF on 15 December 1983 for TIPS-era processing of Landsat-5 in-orbit image data. These pre-launch gains, G_{IS}, in units of DN per $mWcm^{-2}ster^{-1}\mu m^{-1}$ were calculated from the regression of averaged midscan counts in DN, L_R, against the known spectral radiance of the integrating sphere, $L_{\lambda,IS}$ (Appendix 9.2), in units of $mW\ cm^{-2}ster^{-1}\mu m^{-1}$: $L_R = O_{IS} + G_{IS} * L_{\lambda,IS}$.

CHANNEL	BAND					
	1	2	3	4	5	7
1	15.5973	7.8781	10.2083	10.8950	78.9797	147.5916
2	15.4837	7.8485	10.2852	10.8421	78.0460	146.2116
3	15.6616	7.8402	10.1852	10.7759	78.5030	147.3723
4	15.4738	7.8432	10.2747	10.7317	78.2444	146.5488
5	15.7131	7.8543	10.1887	10.8196	78.6471	148.8685
6	15.4406	7.8187	10.1612	10.8094	78.6875	146.3335
7	15.6139	7.8374	10.0438	10.7961	78.1700	148.4280
8	15.4797	7.9195	10.2459	10.8916	79.4837	147.9753
9	15.5082	7.8128	10.0956	10.7254	78.7218	147.6473
10	15.5686	7.8753	10.2281	10.9348	78.8279	147.3096
11	15.6141	7.8932	10.1053	10.8019	79.3421	148.6744
12	15.5868	7.9215	10.2798	10.8098	79.2062	148.4549
13	15.5822	7.8748	10.1573	10.7987	78.7834	148.4755
14	15.4218	7.8431	10.2711	10.8591	78.3314	148.3712
15	15.5370	7.9122	10.2169	10.7782	78.9255	147.4282
16	15.5579	7.7793	10.3020	10.8595	79.1123	147.8104

9622:1691/84

APPENDIX 9.4 - TM/F OFFSETS

TM/F instrument calibration data (offset) are presented for each channel of each reflective band, as furnished by NASA/GSFC to GE/VF on 15 December 1983 for TIPS-era processing of Landsat-5 in-orbit image data. These pre-launch offsets, O_{IS}, in DN were calculated from the regression of raw midscan radiance, $\overline{L}_R$, in DN, usually averaged over 25mF and 100 scans, L_R, against the twenty known settings of spectral radiance of the integrating sphere, $L_{\lambda,IS}$ (Appendix 9.2), in units of $mWcm^{-2}$ $ster^{-1}$ μm^{-1}. For each channel: $\overline{L}_R = O_{IS} + G_{IS} * L_{\lambda,IS}$.

CHANNEL	BAND					
	1	2	3	4	5	7
1	2.2965	2.2691	2.4569	2.6652	3.5727	3.8231
2	1.9313	1.5379	1.9920	2.1440	3.2601	3.2194
3	1.8734	1.8693	1.9709	2.4287	3.2736	3.3549
4	1.8895	1.5357	1.7282	1.9523	3.2701	3.2758
5	1.7628	1.5069	1.8442	2.2046	3.1314	3.1052
6	1.9744	1.8161	1.7437	2.3107	3.2506	3.2558
7	1.7435	1.5605	1.8571	2.6408	3.1252	3.0121
8	2.1147	1.7427	1.8852	2.2091	3.5024	3.2427
9	1.6412	1.7117	2.0105	2.1524	3.2843	3.1006
10	1.8049	1.5873	1.8130	2.0022	3.3784	3.1922
11	1.5761	1.8789	1.8650	2.4152	3.2440	3.1158
12	1.7649	1.6117	1.7688	2.0702	3.2882	3.0190
13	1.6324	1.5945	1.7462	2.1371	3.1520	3.0402
14	1.8487	1.5986	1.8063	2.1669	3.3691	3.2440
15	1.6416	1.6357	1.7881	2.1682	3.1806	3.1068
16	1.8337	1.5766	1.8836	2.1291	3.3460	3.2790

9622 1169/84

APPENDIX 9.5 - TM/PF APPARANT GAIN CHANGE WITH TIME

Landsat-4 TM/PF apparent gain changes with time, by band, under the assumption that the TM internal calibration (IC) has effective spectral radiances, L_λ^Q, which do not change with time. Gain, G(c), in units of DN per $mWcm^{-2}ster^{-1}\ \mu m^{-1}$, is a measure of absolute radiometric sensitivity for each channel, C. These post-launch gains, G(C), were calculated from the regression of an averaged IC pulse, P (ℓ, C), in DN against the pre-launch values of L_λ^Q (ℓ, C), in $mWcm^{-2}\ ster^{-1}\ \mu m^{-1}$. For each channel, the least squares values for O and G were calculated from data for the lowest seven lamp configurations, ℓ:

$$\overline{P}\ (\ell) = O + G * L_\lambda^{\cdot}\ (\ell)$$

Averaged gains values for odd channels and even channels were averaged together to give G (B):

$$\overline{G}\ (B) = \frac{\overline{G}\ (odd) + \overline{G}\ (even)}{2}$$

O^o (B) and G^o (B) are the offset and gain after calibration to a common post-calibration dynamic range from RMIN to RMAX, for the Scrounge-era prior to August, 1983. Plots of apparant gain change with time are given in this appendix as follows:

9.5.1	Band 1
9.5.2	Band 2
9.5.3	Band 3
9.5.4	Band 4
9.5.5	Band 5
9.5.6	Band 7

LANDSAT-4 TM RADIOMETRY, BAND 1

APPARENT GAIN CHANGE FROM INTERNAL CALIBRATION (IC) PULSES

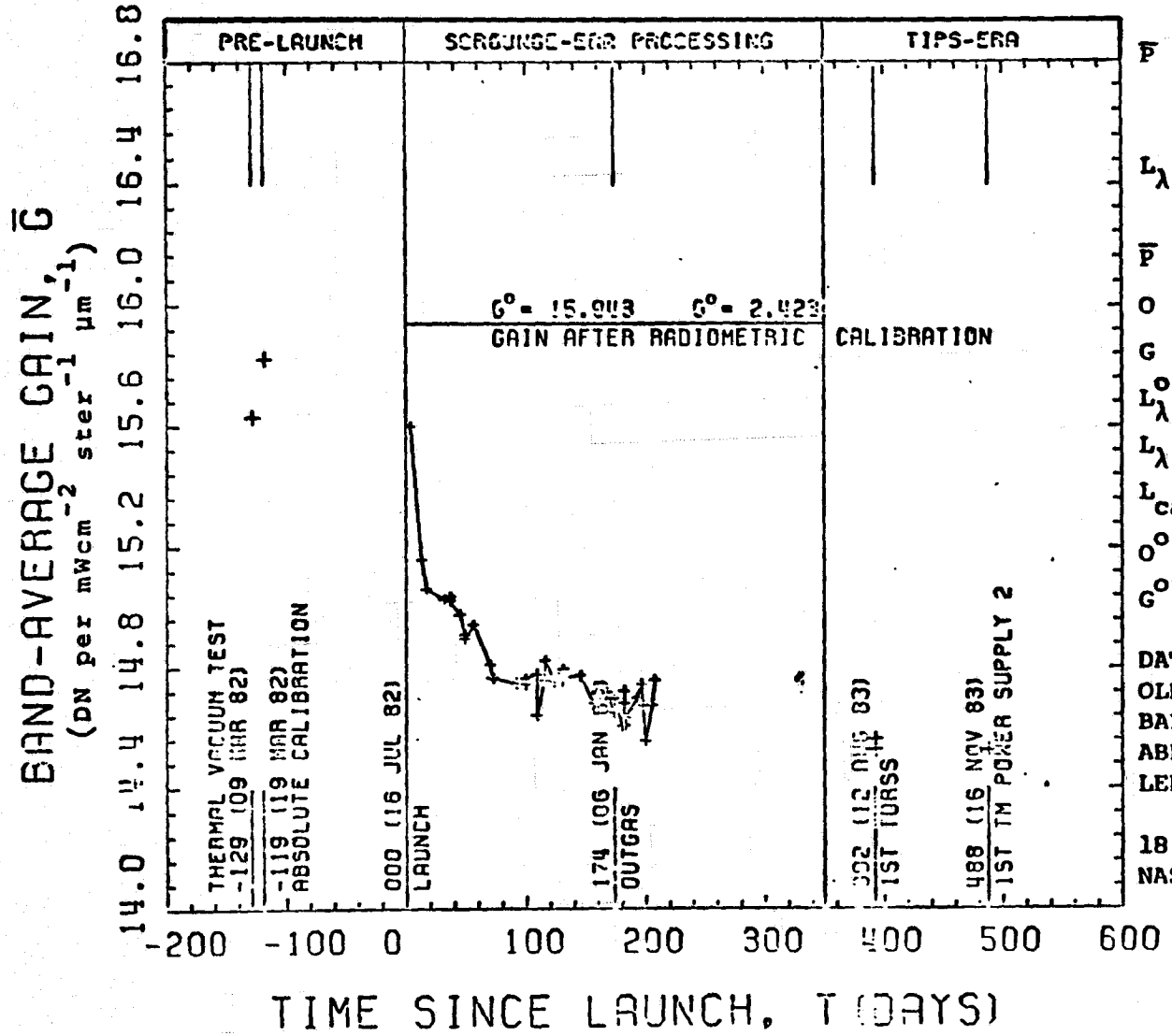

$\bar{P} = O + G^{*}L^{o}_{\lambda}$

$L_{\lambda} = \left[\frac{L_{cal} - O^{o}}{G^{o}}\right]$

$\bar{P}$ = OBS. TM IC PULSE

O = OFFSET BY FIT

G = GAIN BY FIT

L^{o}_{λ} = IC SPECTRAL RAD.

L_{λ} = CALC. SPECT. RAD.

L_{cal} = DIGITAL NUMBER (DN)

O^{o} = OFFSET AFTER CALIB.

G^{o} = GAIN AFTER CALIB.

DATA FROM "TRAPP"
OLD/NEW REF. DAY 70
BARKER
ABRAMS/GUNTHER
LEE/TRUONG

18 JAN 84
NASA/GODDARD

LANDSAT-4 TM RADIOMETRY, BAND 2

APPARENT GAIN CHANGE FROM INTERNAL CALIBRATION (IC) PULSES

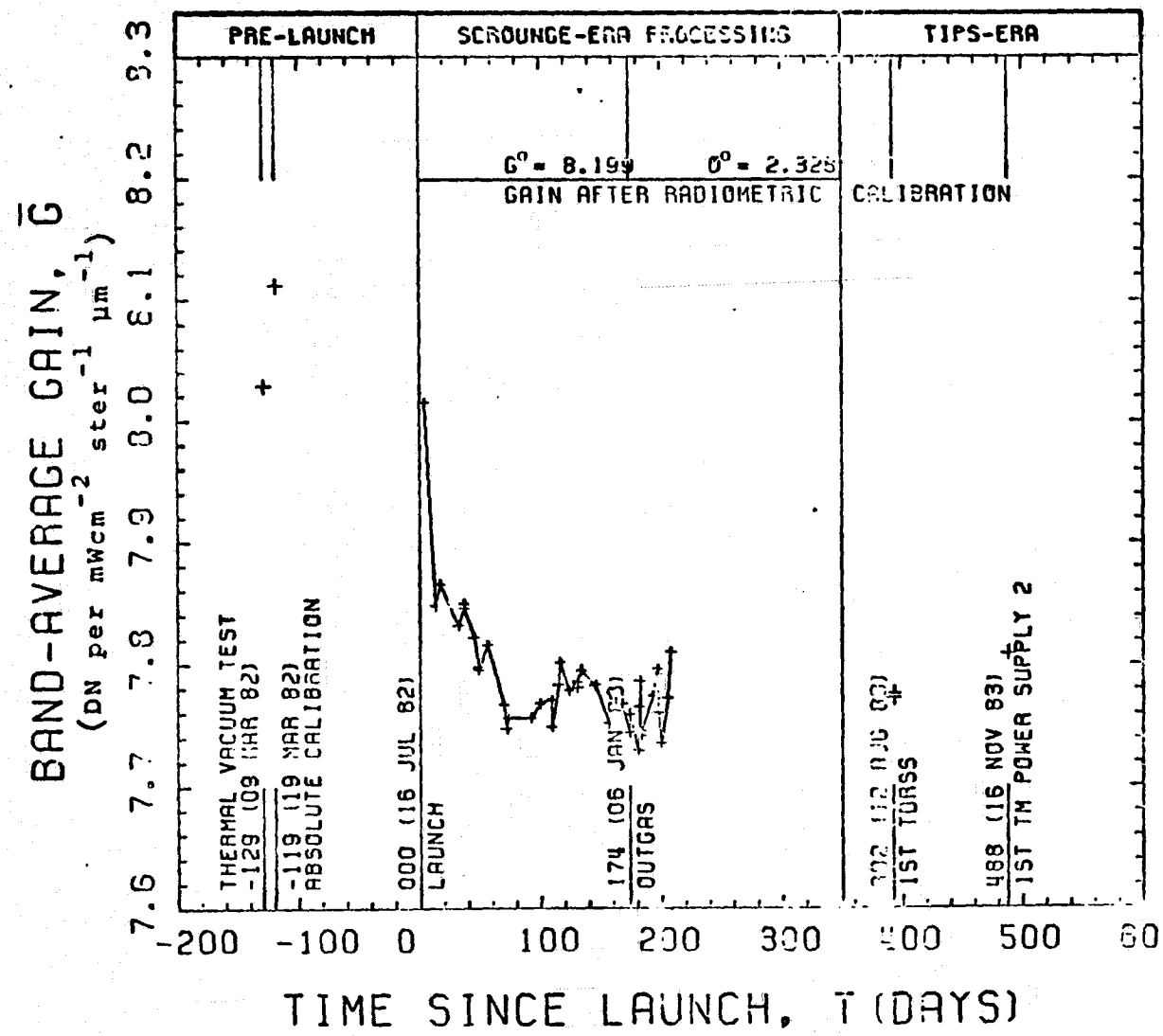

$\bar{P} = O + G * L_\lambda^o$

$L_\lambda = \left[\frac{L_{cal} - O^o}{G^o}\right]$

$\bar{P}$ = OBS. TM IC PULSE

O = OFFSET BY FIT

G = GAIN BY FIT

L_λ^o = IC SPECTRAL RAD.

L_λ = CALC. SPECT. RAD.

L_{cal} = DIGITAL NUMBER (DN)

O^o = OFFSET AFTER CALIB.

G^o = GAIN AFTER CALIB.

DATA FROM "TRAPP"
OLD/NEW REF. DAY 70
BARKER
ABRAMS/GUNTHER
LEE/TRUONG

18 JAN 84
NASA/GODDARD

LANDSAT-4 TM RADIOMETRY, BAND 3

APPARENT GAIN CHANGE FROM INTERNAL CALIBRATION (IC) PULSES

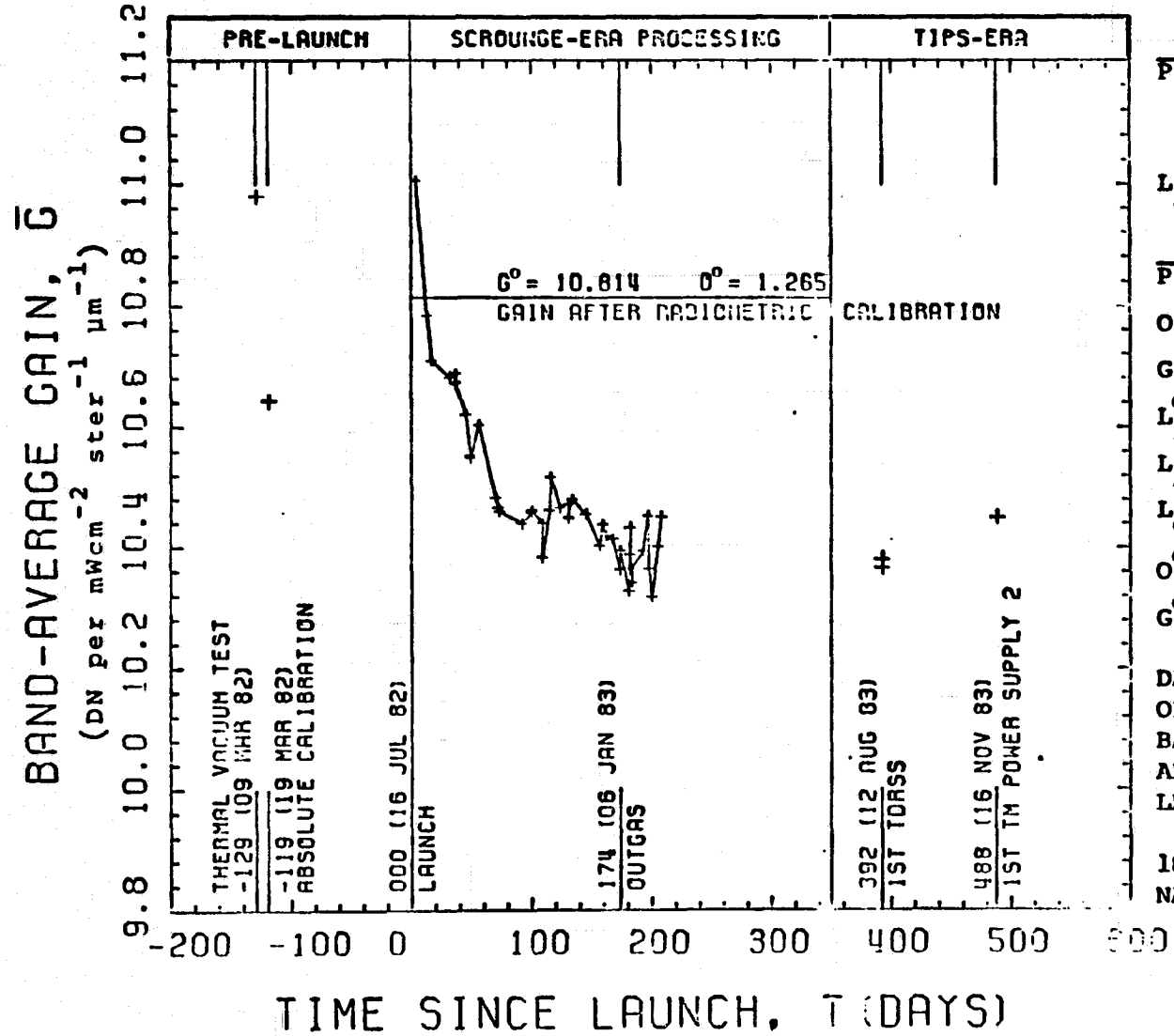

$\bar{P} = O + G * L^{o}_{\lambda}$

$L_{\lambda} = \left[\frac{L_{cal} - O^{o}}{G^{o}}\right]$

$\bar{P}$ = OBS. TM IC PULSE
O = OFFSET BY FIT
G = GAIN BY FIT
L^{o}_{λ} = IC SPECTRAL RAD.
L_{λ} = CALC. SPECT. RAD.
L_{cal} = DIGITAL NUMBER (DN)
O^{o} = OFFSET AFTER CALIB.
G^{o} = GAIN AFTER CALIB.

DATA FROM "TRAPP"
OLD/NEW REF. DAY 70
BARKER
ABRAMS/GUNTHER
LEE/TRUONG

18 JAN 84
NASA/GODDARD

LANDSAT-4 TM RADIOMETRY, BAND 4

APPARENT GAIN CHANGE FROM INTERNAL CALIBRATION (IC) PULSES

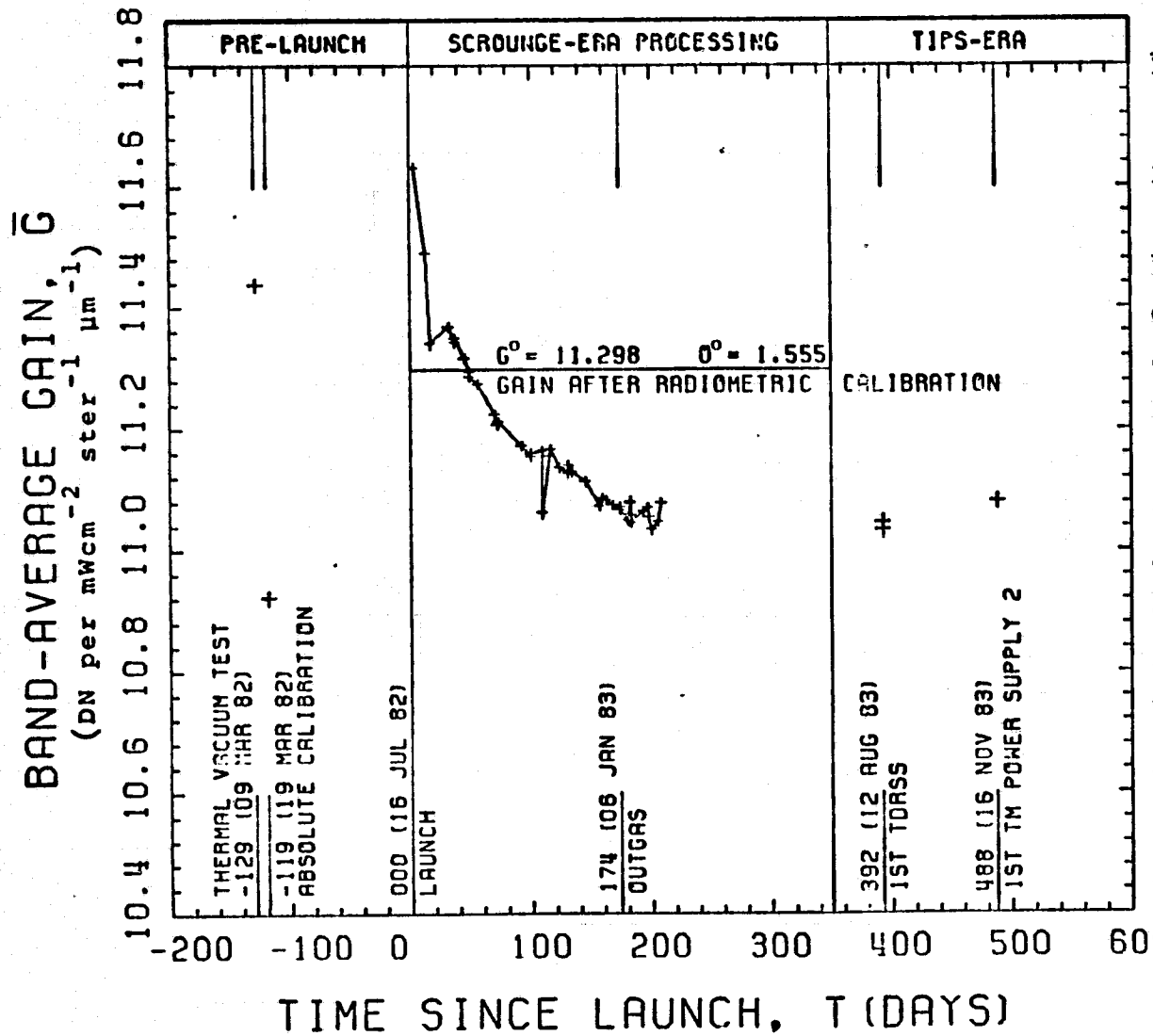

$\bar{P} = O + G^*L_\lambda^o$

$L_\lambda = \left[\frac{L_{cal} - O^o}{G^o}\right]$

$\bar{P}$ = OBS. TM IC PULSE
O = OFFSET BY FIT
G = GAIN BY FIT
L_λ^o = IC SPECTRAL RAD.
L_λ = CALC. SPECT. RAD.
L_{cal} = DIGITAL NUMBER (DN)
O^o = OFFSET AFTER CALIB.
G^o = GAIN AFTER CALIB.

DATA FROM "TRAPP"
OLD/NEW REF. DAY 70
BARKER
ABRAMS/GUNTHER
LEE/TRUONG

18 JAN 84
NASA/GODDARD

ORIGINAL PAGE IS
OF POOR QUALITY

LANDSAT-4 TM RADIOMETRY, BAND 5

APPARENT GAIN CHANGE FROM INTERNAL CALIBRATION (IC) PULSES

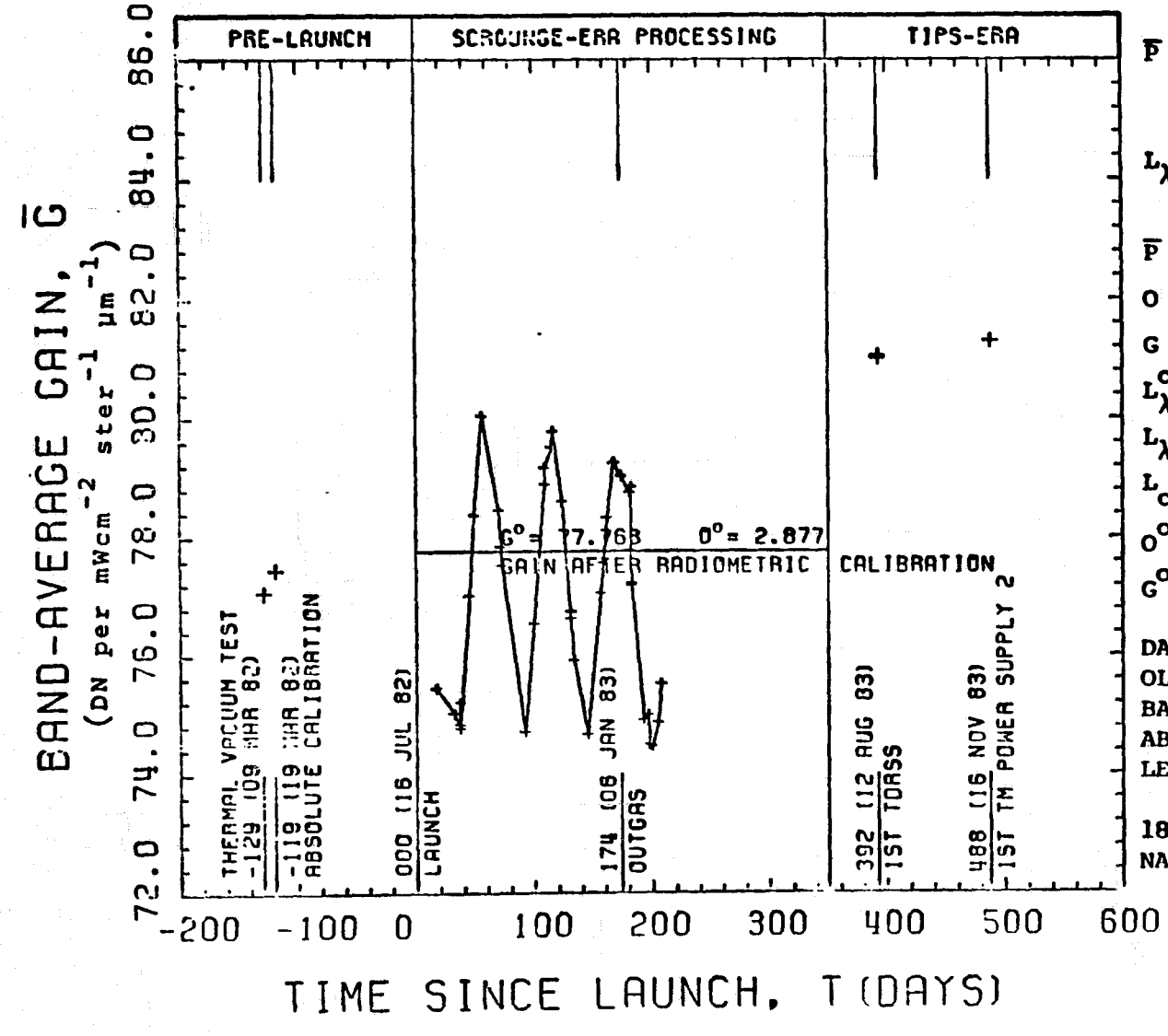

$\bar{P} = O + G * L_\lambda^o$

$L_\lambda = \left[\frac{L_{cal} - O^o}{G^o}\right]$

$\bar{P}$ = OBS. TM IC PULSE
O = OFFSET BY FIT
G = GAIN BY FIT
L_λ^o = IC SPECTRAL RAD.
L_λ = CALC. SPECT. RAD.
L_{cal} = DIGITAL NUMBER (DN)
O^o = OFFSET AFTER CALIB.
G^o = GAIN AFTER CALIB.

DATA FROM "TRAPP"
OLD/NEW REF. DAY 70
BARKER
ABRAMS/GUNTHER
LEE/TRUONG

18 JAN 84
NASA/GODDARD

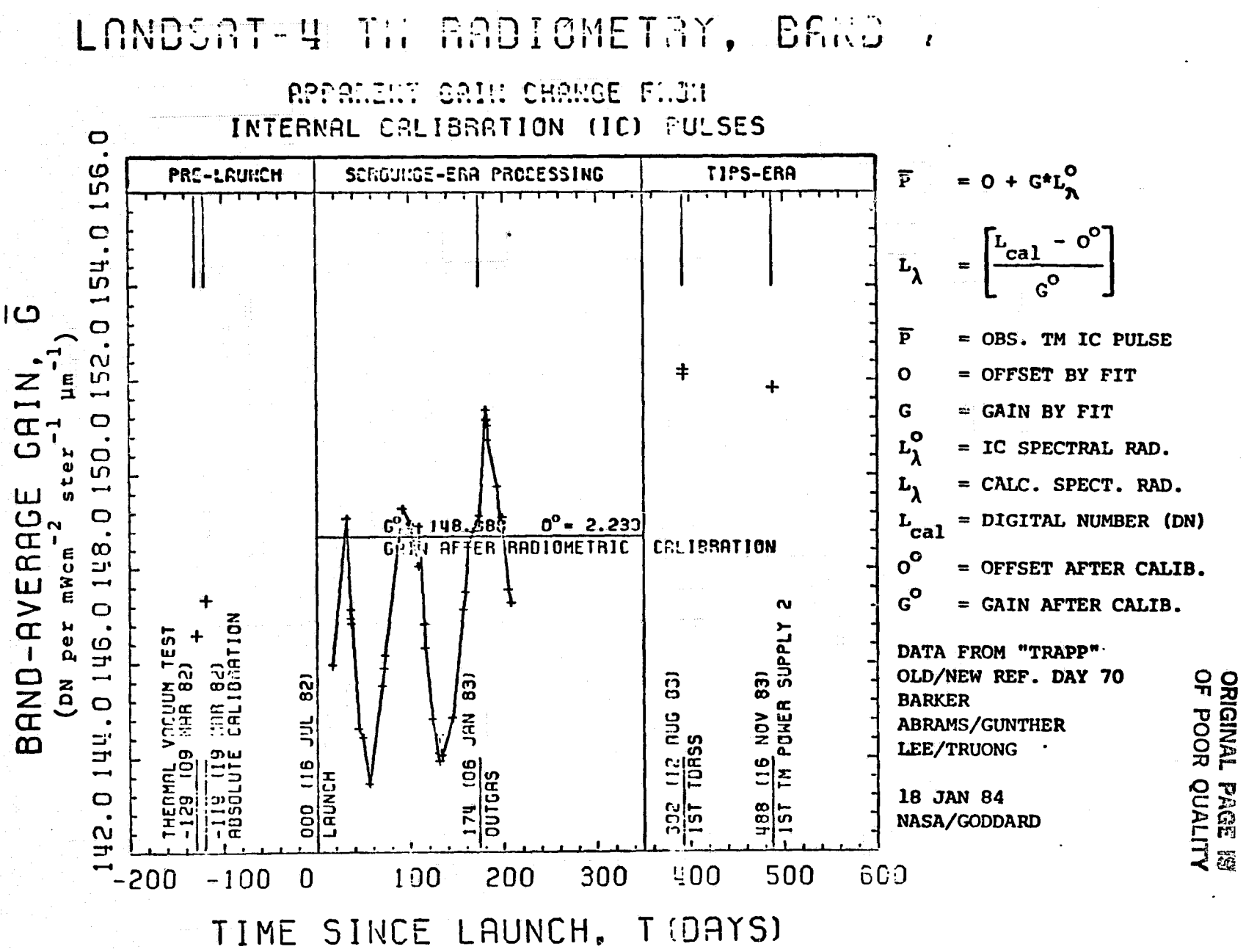

$\bar{P} = O + G * L_\lambda^o$

$L_\lambda = \left[\frac{L_{cal} - O^o}{G^o}\right]$

$\bar{P}$ = OBS. TM IC PULSE
O = OFFSET BY FIT
G = GAIN BY FIT
L_λ^o = IC SPECTRAL RAD.
L_λ = CALC. SPECT. RAD.
L_{cal} = DIGITAL NUMBER (DN)
O^o = OFFSET AFTER CALIB.
G^o = GAIN AFTER CALIB.

DATA FROM "TRAPP"
OLD/NEW REF. DAY 70
BARKER
ABRAMS/GUNTHER
LEE/TRUONG

18 JAN 84
NASA/GODDARD

ORIGINAL PAGE IS OF POOR QUALITY

APPENDIX 9.6 - LANDSAT-4 IMAGES PROCESSED BY TRAPP

The catalog of Landsat-4 Images processed at Goddard Space Flight Center using the TM Radiative and Algorithm Performance Program (TRAPP) is provided herein.

Appendix 9-6
CATALOG OF LANDSAT-4 IMAGES PROCESSED BY TRAPP

WRS	SCENE	DATE	LOCATION
012031	4005614541	091082	BOSTON
012031	4005614541	091082	WATER OF BOSTON
028030	4004016321	082582	FT. DODGE, IOWA
015033	4010915140	110282	GODDARD
015033	4010916140	110282	WASH, DC
022039	4005215591	091682	NEW ORLEANS
W041028	4013117533	112482	HAMILTON MONTANA
W043034	4014518082	120882	MODESTO CALIF.
W015041	401571514	122082	FT. PIERCE
W017038	4015515292	121882	JACKSON-VILLE, FLOR
W016028	4010015182	122482	OTTAWA, CANADA
W016028	4010015184	102482	KINGSTON CANADA
S030028	4007016442	092482	FORMAN, ND
W002002	4000915413	092582	DETROIT 2
W001001	4002515341	072082	DETROIT 3
W084025	4011618350	110982	VANCOUVER
W013036	4015915032	122282	CAPE HATTERAS
W014032	4002215061	080782	N.Y./PHILA
B015033	4001315125	072982	WASH, D.C.
W037308	4018317332	011583	LUKEVILLE ARIZONA
W0040035	5012517495	111782	DEATH VALLEY CALIF.
J033038	UNKNOWN	010383	WHITE SANDS
J020031	4003215425	081782	TOLEDO, OH
J041033	4013117530	112482	KIMVERLY
J028030	4007216325	092682	N.W. IOWA
J019037	4007315400	092782	ATLANTA
J031025	4020526512	020683	WINNIPEG
J111213	4019002204	012283	WELLSBORO PENN.--PM
J041036	4013117564	112482	L.A., CAL
J112114	4003702243	082282	BUFFALO PM
J022040	4017416011	010683	TERREBONNE BAY, LOUISIANA
J119207	4018293073	011483	BIRMINGHAM, ALA. PM
J027027	4019316272	012583	GILBERT, MONTANA
J037036	4018317323	011583	CLARKDALE ARIZONA
J034036	4017817135	011083	QUEMADO, NM
J015032	4010915134	110282	HARRISBURG
J025039	4011516182	110882	LIBERTY, TEX
J034027	4016217094	122582	GRASSY BUTTE, ND
J014042	4018215125	010483	GRAND BAHAMA ISL
J044034	4020018152	020183	SAN FRANCISCO
K023035	4003716031	082282	N.E. ARK
J023029	4018116071	011383	BATON ROUGE
K046028	4019818251	013083	MT. ST. HELENS
J027030	4004916262	090382	N. CENTRAL IOWA
J014036	4007015084	092482	CAPE LOOKOUT NORTH CAROLINA
K028035	4039216365	081283	OKLAHOMA
K044034	4039218152	081283	SAN FRANCISCO
K027031	4009716273	112783	FT. DODGE IA
K014032	4013415082	112783	N.Y./PHILA
K028035	4048816362	111683	OKLAHOMA
K028034	4048816360	111683	WICHITA KANSAS
K028033	4048816353	111683	SALINA KANSAS
W033037	4017117180	010383	WHITE SANDS
P021039	4010315503	102782	MOBILE ALABAMA
P031025	4039216365	081283	WINNIPEG CANADA
P112211	4019702261	010683	WASH, D.C. PM
P024032	4009216092	101682	GALESBURG
P001001	4000415401	072082	DETROIT 1
P026035		030784	TULSA, OKL

APPENDIX 9.7 - TM/F PLOTS OF SHIFTED BACKGROUND VERSUS SCAN

Landsat-4 TM/PF averaged shutter backgrounds before DC restoration are plotted versus scan number of illustrative reverse scans before and after being corrected (as described in Section 4.5) for scan-correlated shifts of type 4-1 (Landsat-4 Band 1, Channel 4) and type 4-7 (Landsat-4 Band 7, Channel 7) for San Francisco, 12 AUG 83 (Scene ID 40392-18152). Before-and-after-correction comparative plots are included in this Appendix as follows:

9.7.1 Band 1
9.7.2 Band 2
9.7.3 Band 3
9.7.4 Band 4
9.7.5 Band 5
9.7.6 Band 7
9.7.7 Band 6 (uncorrected).

SCENE ID=40392-18152, BAND 1 (REVERSE)
SHUTTER BACKGROUND 1 SPECTRA BEFORE CORRECTION

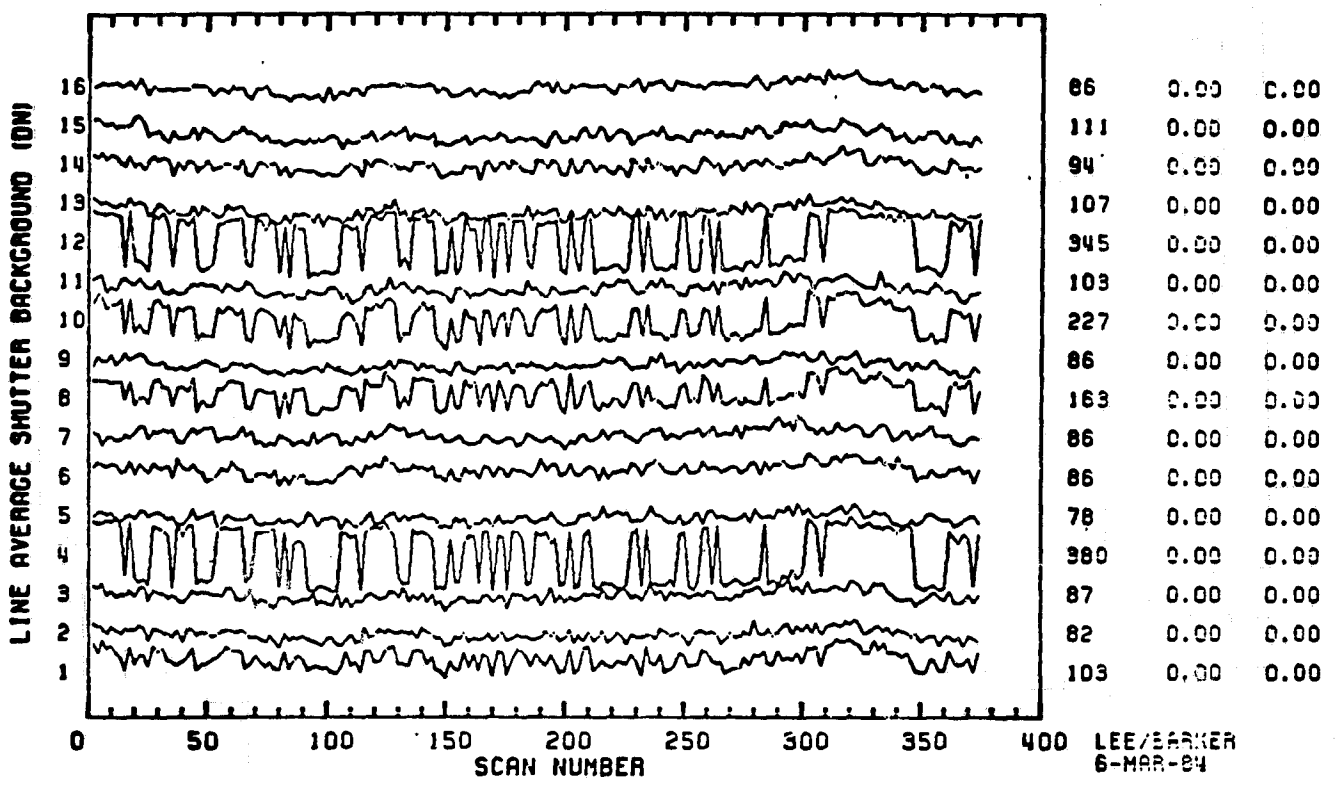

SCENE ID=40392-18152, BAND 1 (REVERSE)
SHUTTER BACKGROUND 1 SPECTRA AFTER CORRECTION

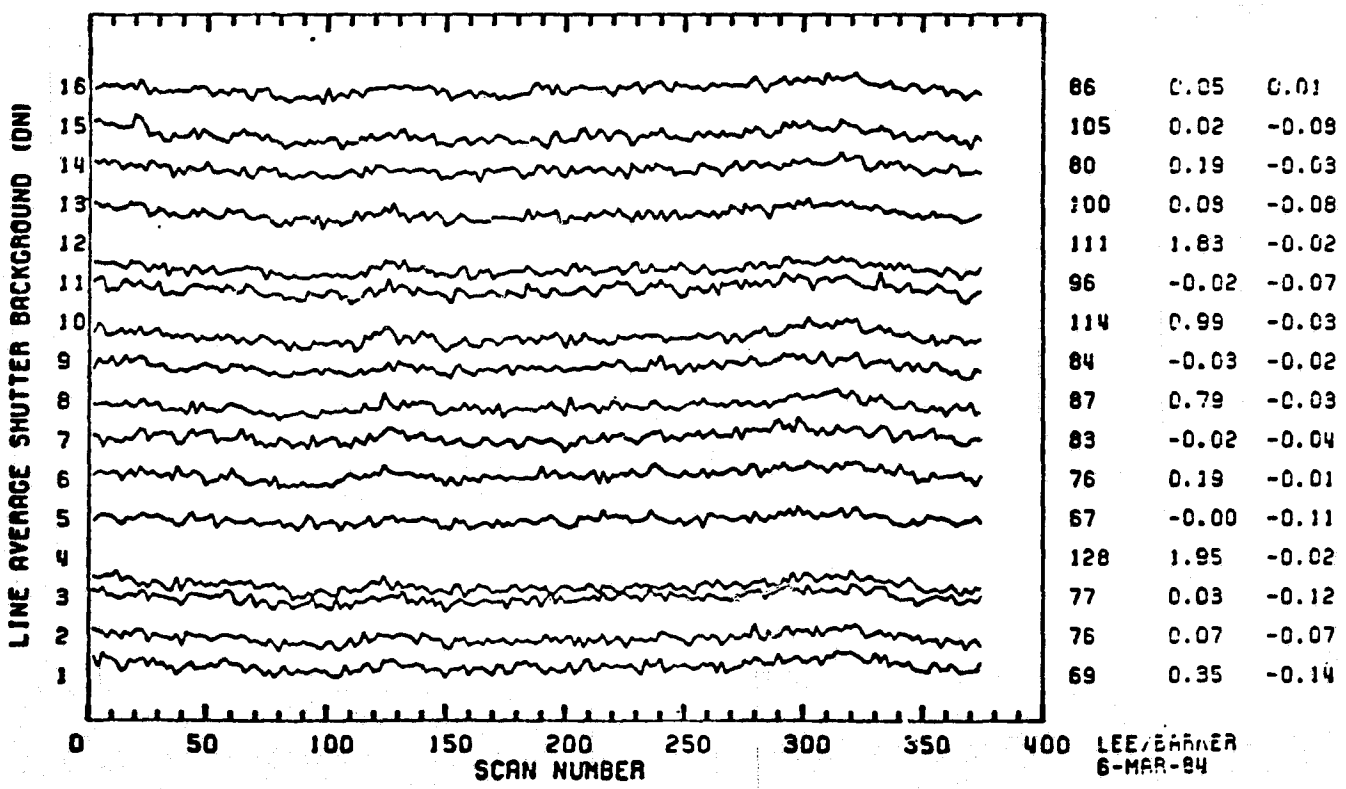

SCENE ID=40392-18152, BAND 2 (REVERSE)
SHUTTER BACKGROUND 1 SPECTRA BEFORE CORRECTION

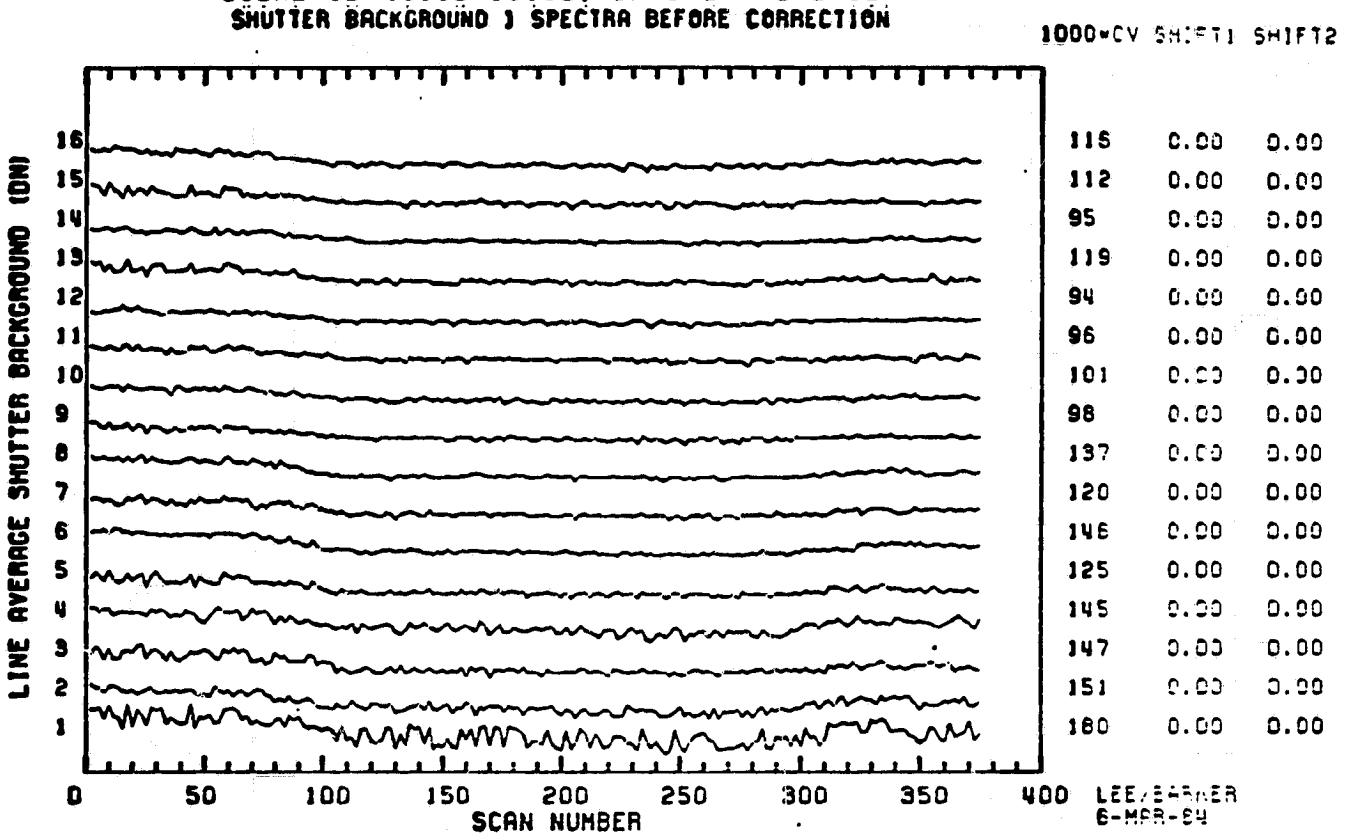

SCENE ID=40392-18152, BAND 2 (REVERSE)
SHUTTER BACKGROUND 1 SPECTRA AFTER CORRECTION

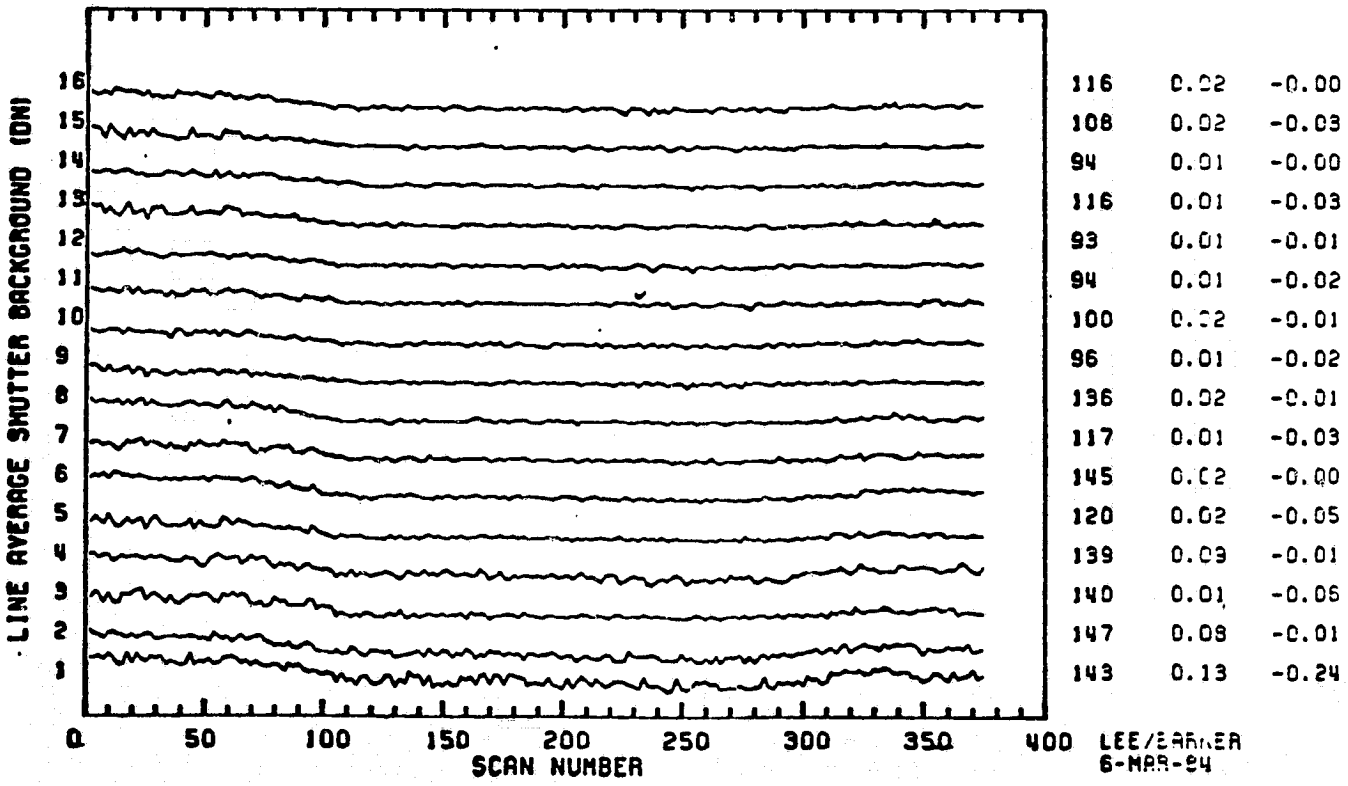

SCENE ID=40392-18152, BAND 3 (REVERSE)
SHUTTER BACKGROUND 1 SPECTRA BEFORE CORRECTION

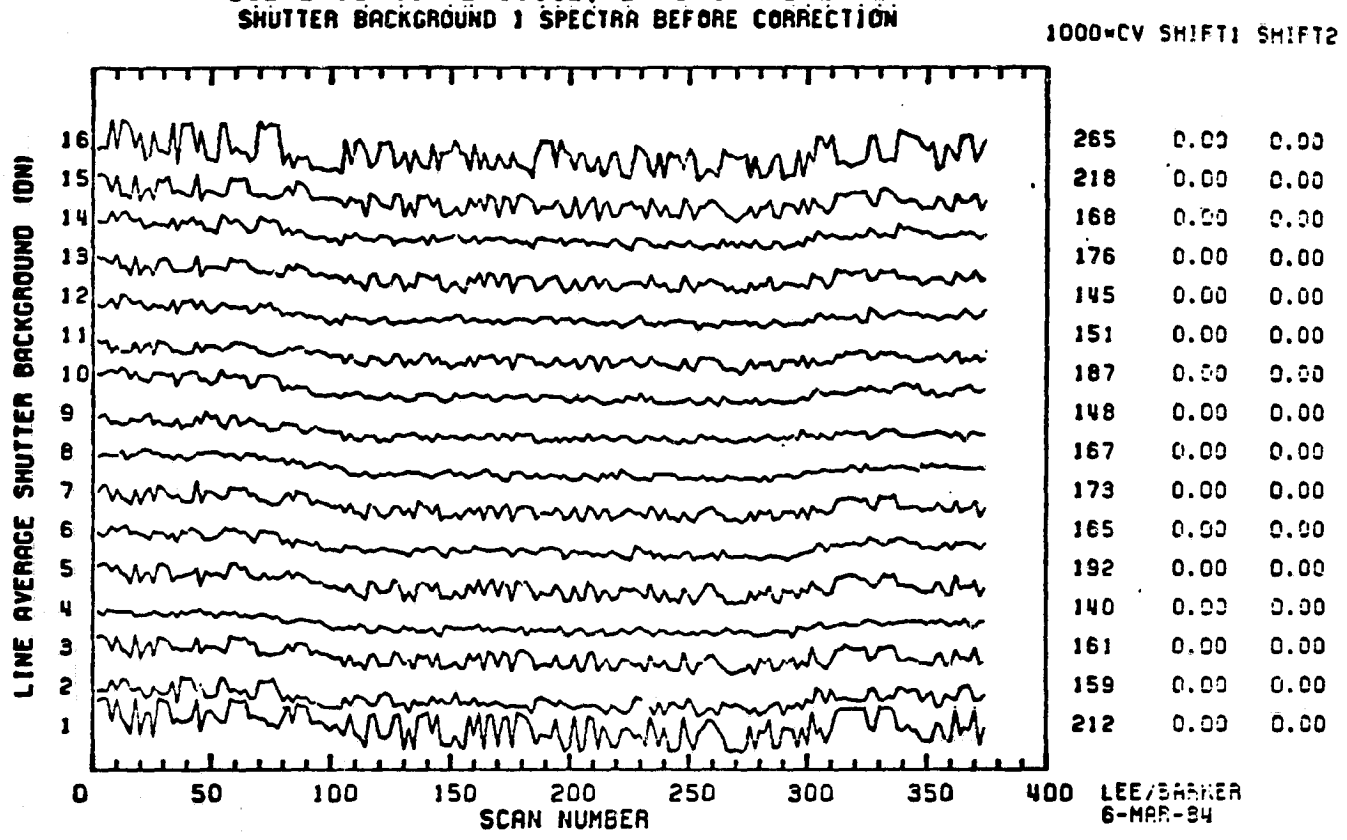

SCENE ID=40392-18152, BAND 3 (REVERSE)
SHUTTER BACKGROUND 1 SPECTRA AFTER CORRECTION

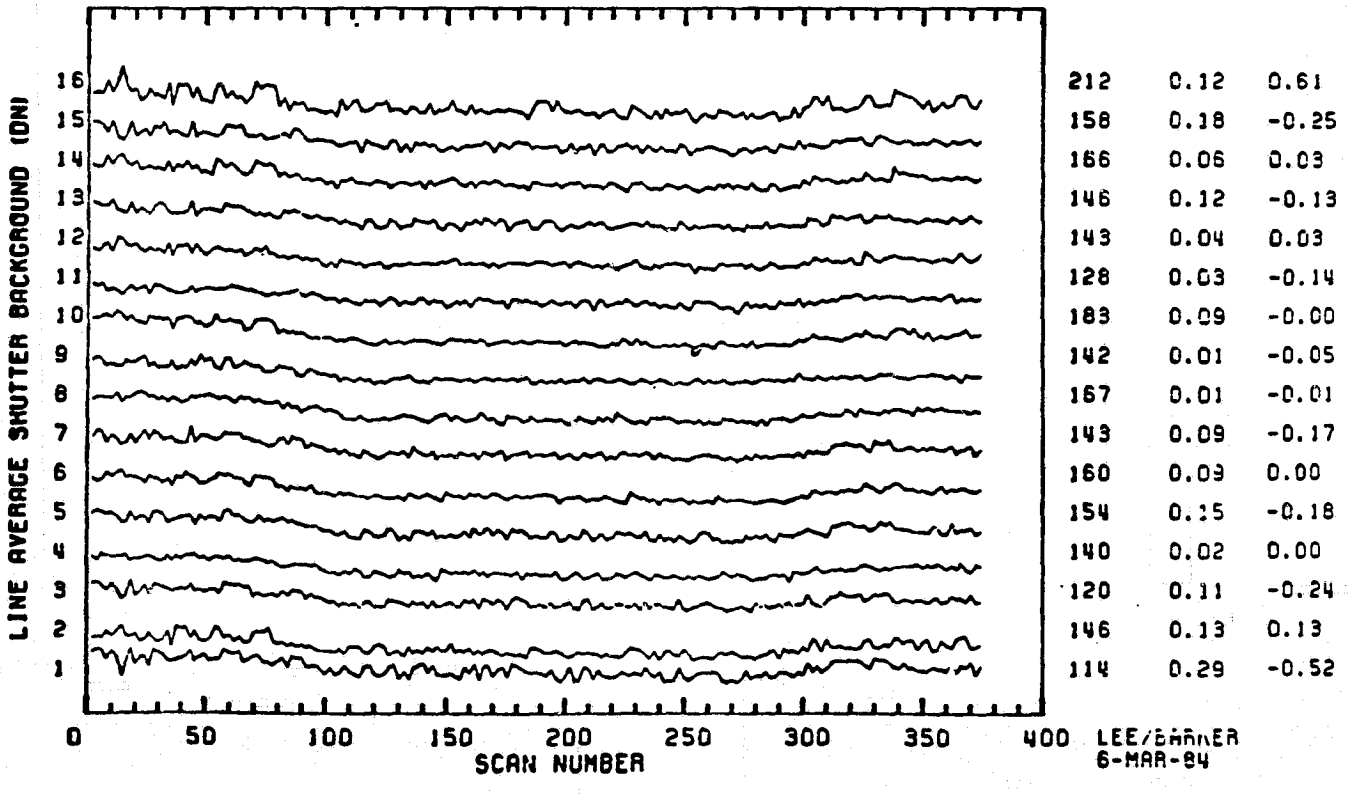

SCENE ID=40392-18152, BAND 4 (REVERSE)
SHUTTER BACKGROUND 1 SPECTRA BEFORE CORRECTION

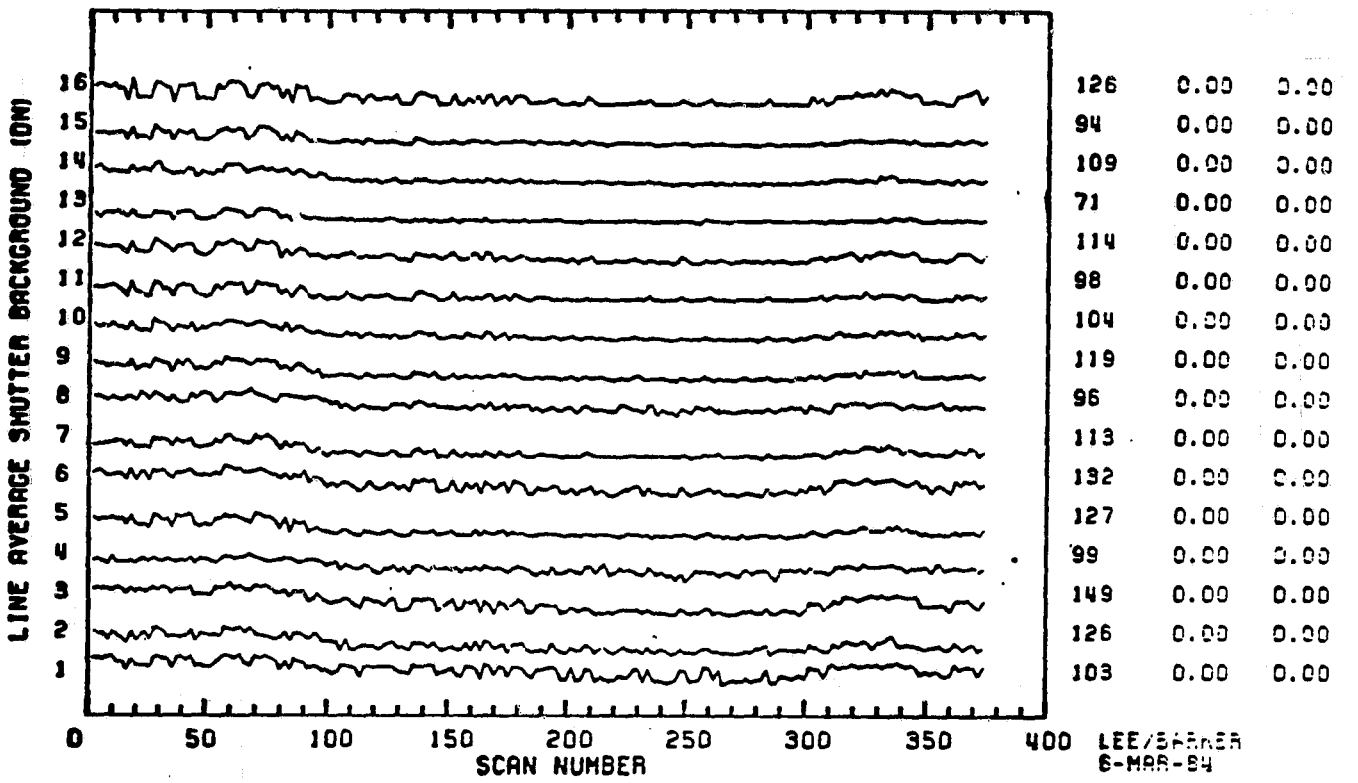

SCENE ID=40392-18152, BAND 4 (REVERSE)
SHUTTER BACKGROUND 1 SPECTRA AFTER CORRECTION

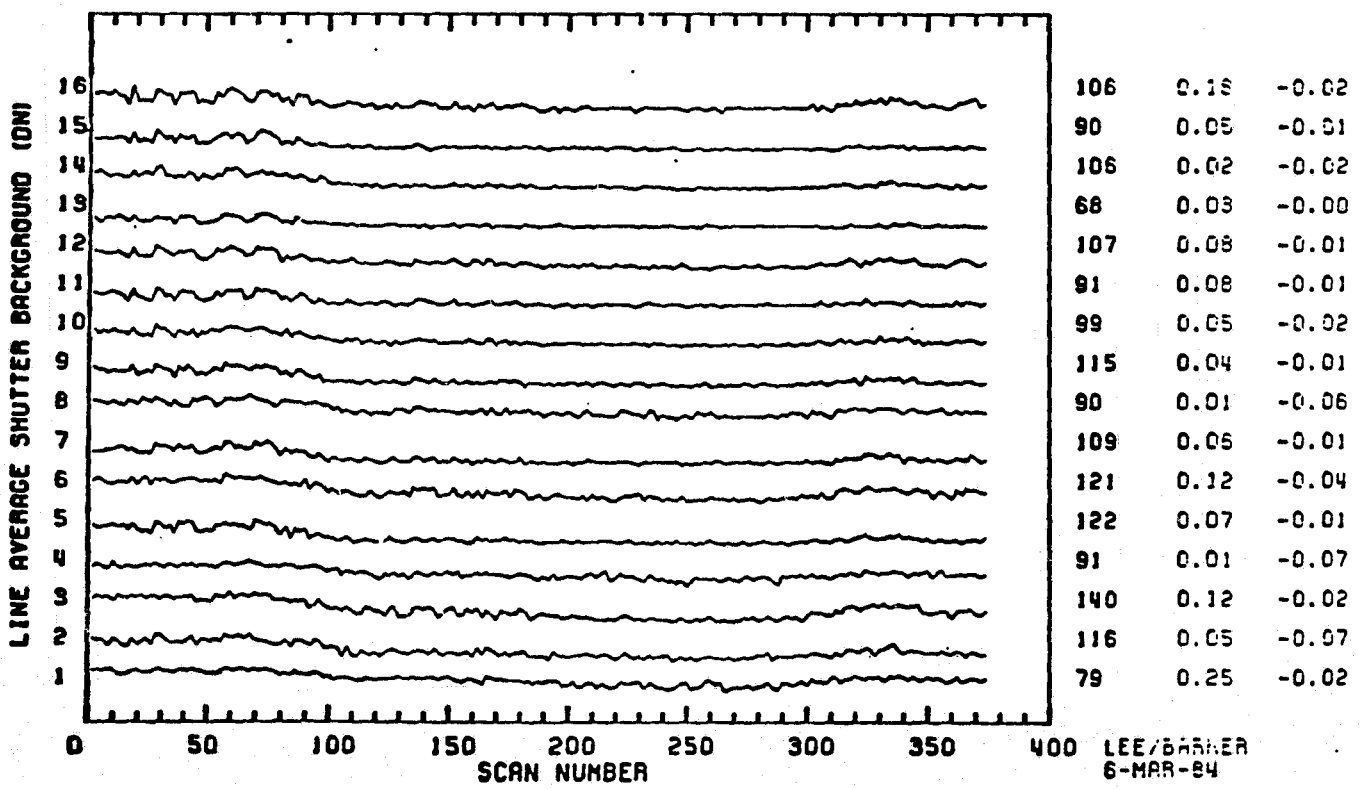

SCENE ID=40392-18152, BAND 5 (REVERSE)
SHUTTER BACKGROUND 1 SPECTRA BEFORE CORRECTION

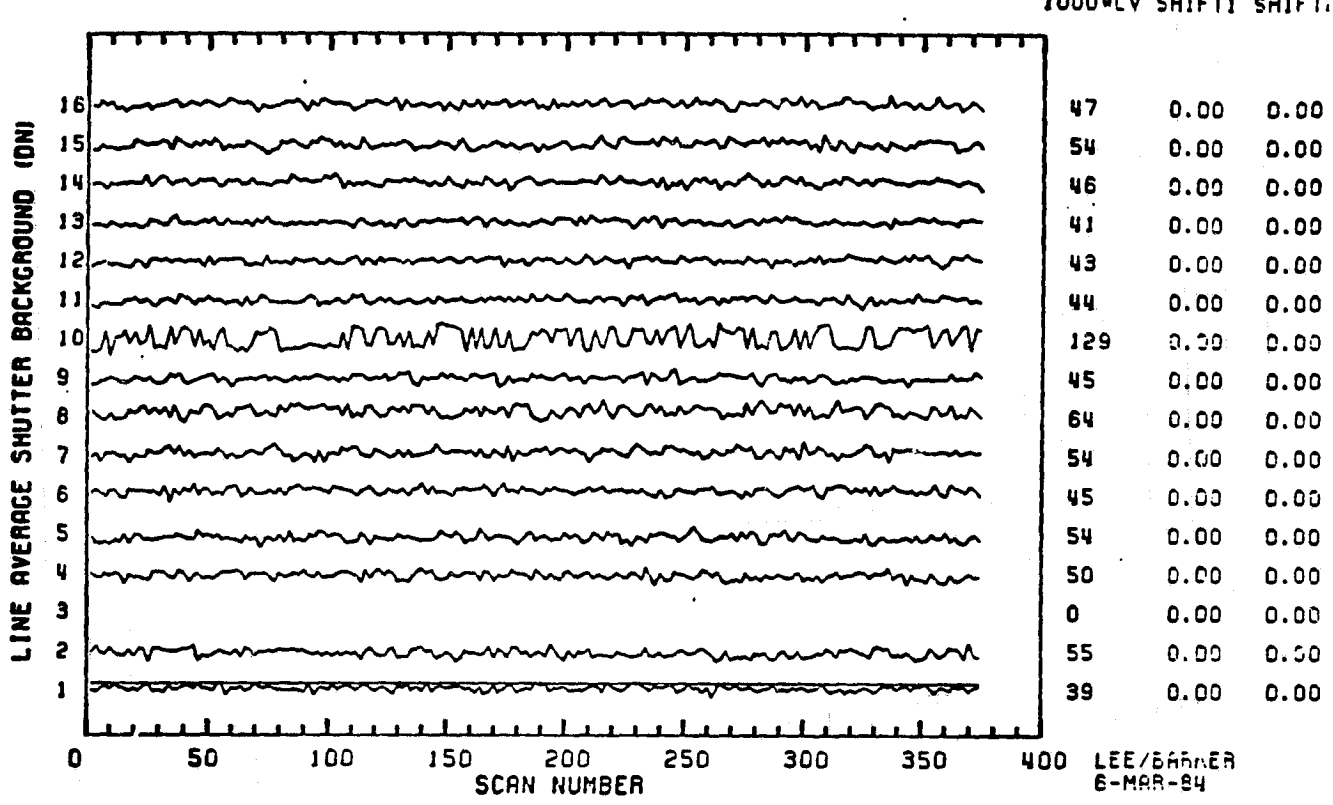

SCENE ID=40392-18152, BAND 5 (REVERSE)
SHUTTER BACKGROUND 1 SPECTRA AFTER CORRECTION

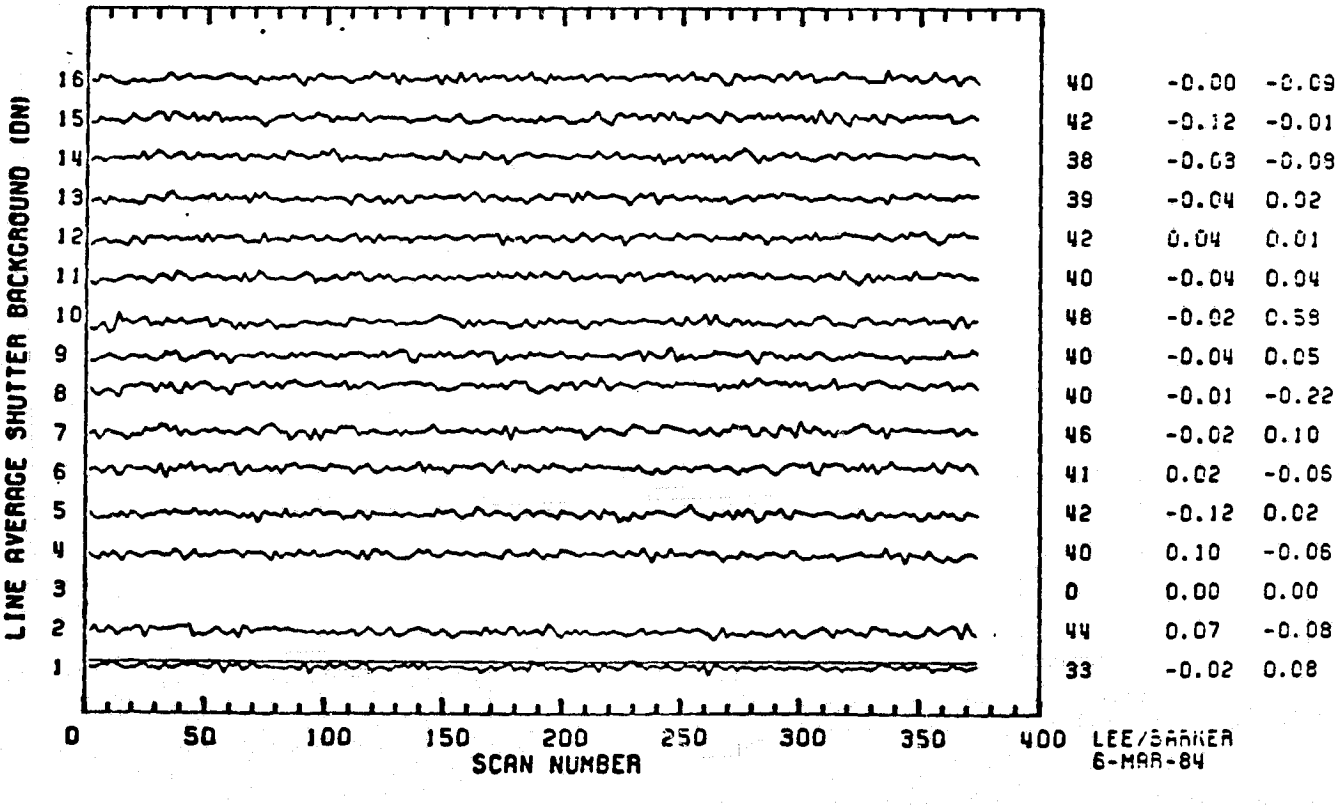

SCENE ID=40392-18152, BAND 7 (REVERSE)
SHUTTER BACKGROUND) SPECTRA BEFORE CORRECTION

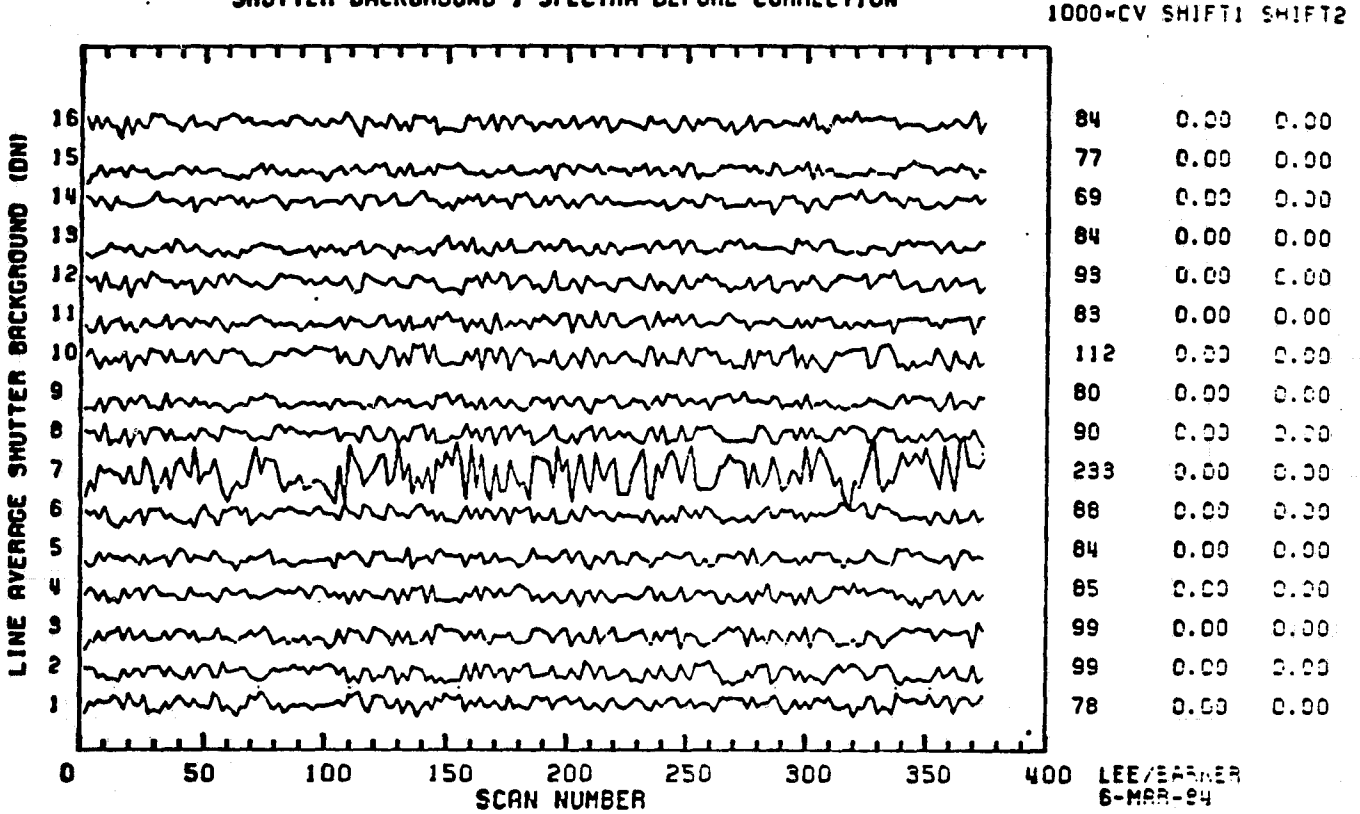

SCENE ID=40392-18152, BAND 7 (REVERSE)
SHUTTER BACKGROUND) SPECTRA AFTER CORRECTION

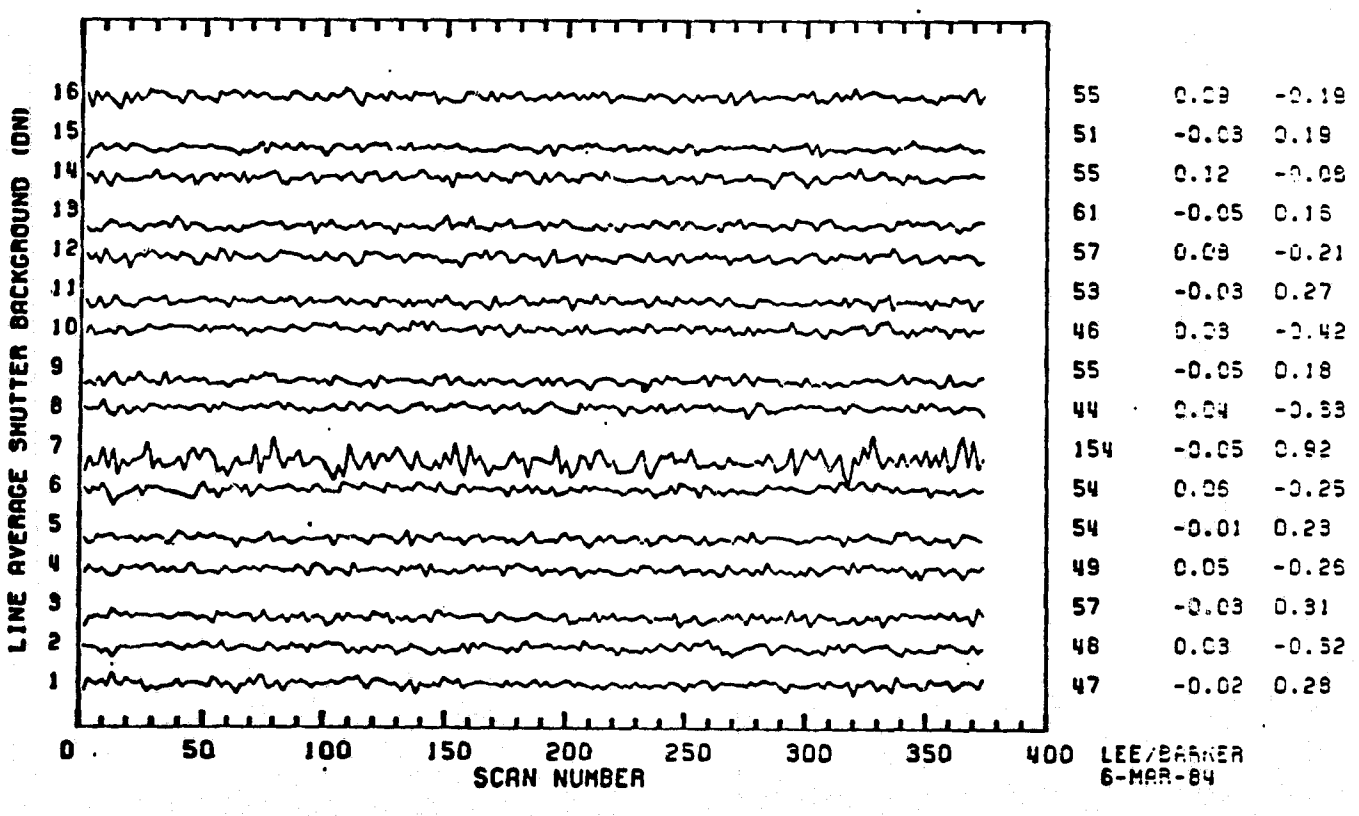

SCENE ID=40392-18152, BAND 6 (FORWARD)
SHUTTER BACKGROUND 1 SPECTRA BEFORE CORRECTION

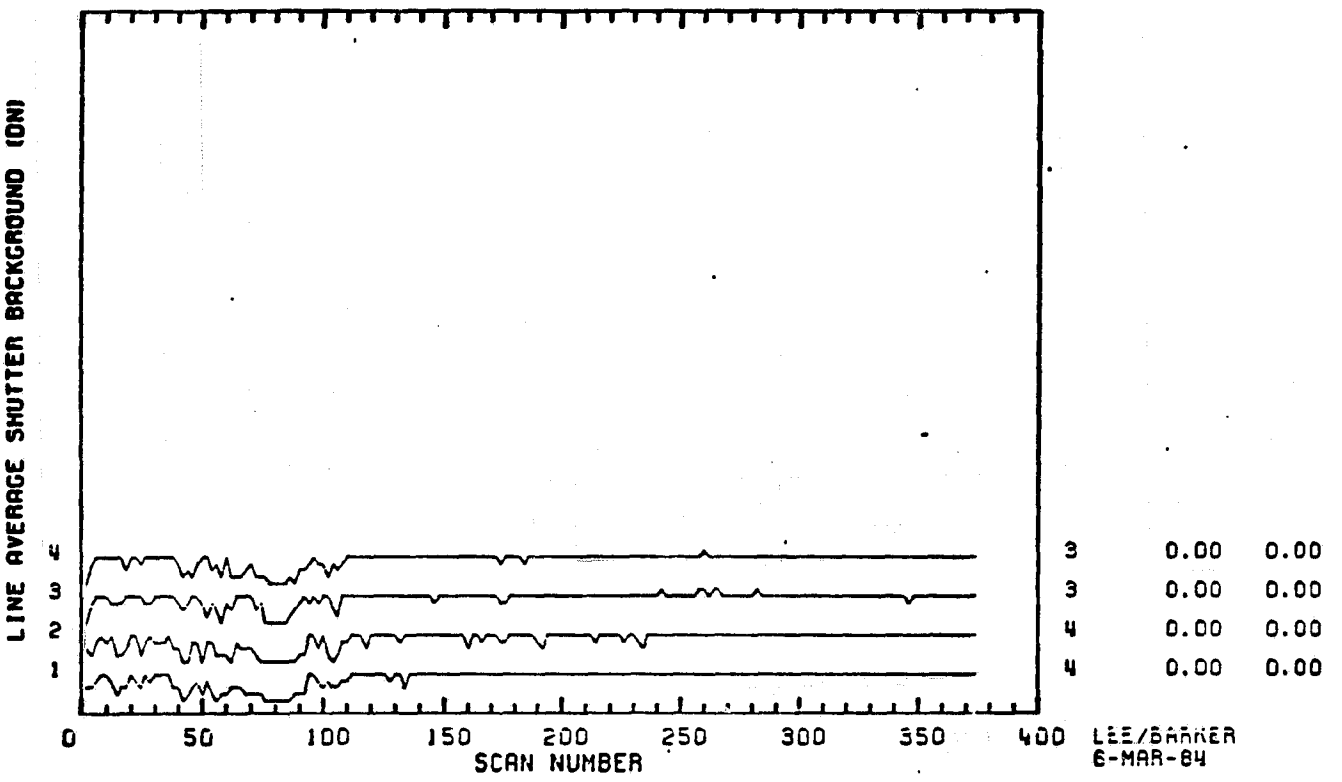

SCENE ID=40392-18152, BAND 6 (REVERSE)
SHUTTER BACKGROUND 1 SPECTRA BEFORE CORRECTION

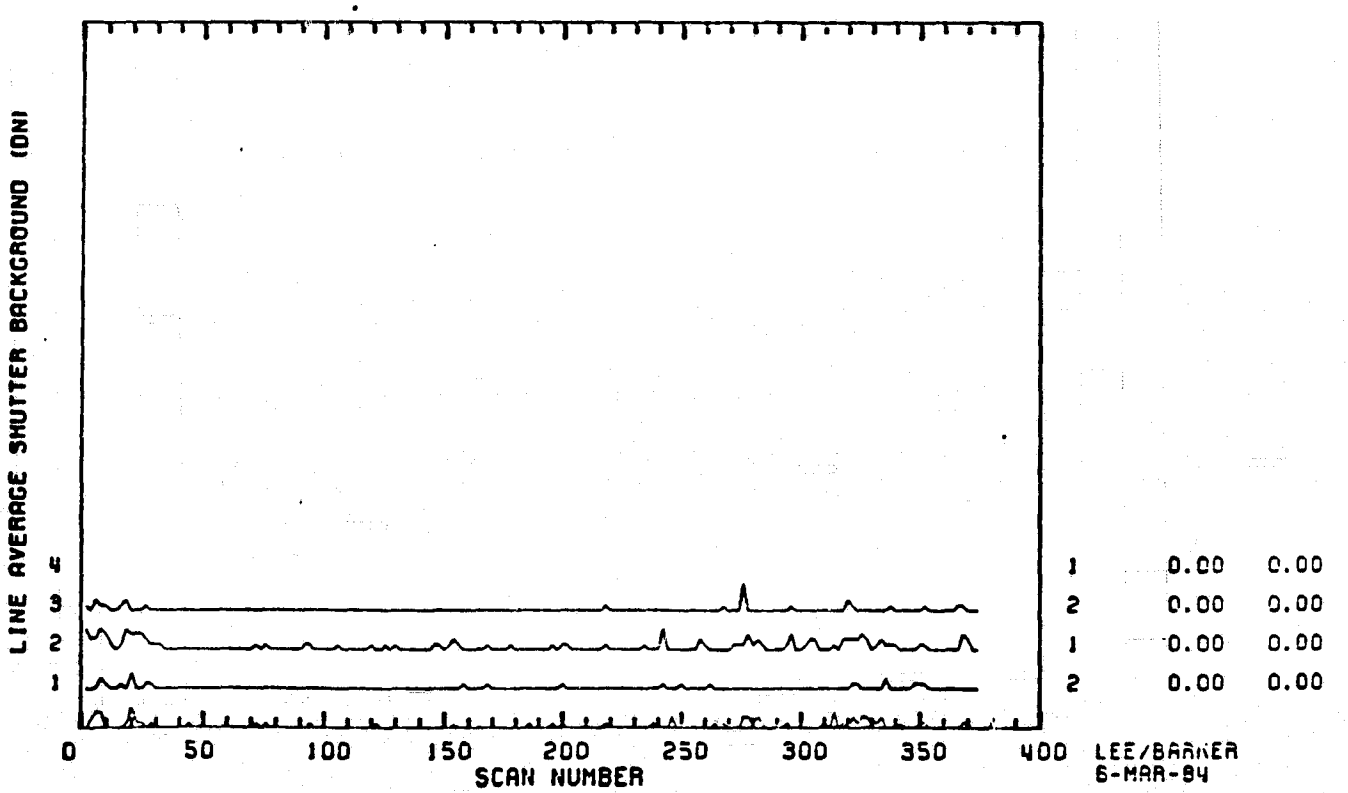

APPENDIX 9.8 - TM/PF TABLE OF SCAN-CORRELATED SHIFTS

Landsat-4 TM/PF within-scene tabulations (Section 4.5) of scan-correlated shifts by forward and reverse scans for type 4-1 (Landsat-4 Band 1, Channel 4) and type 4-7 (Landsat-4 Band 7, Channel 7) in shutter regions before and after DC restoration for San Francisco, 12 AUG 83 (Scene ID 40392-18152) and Buffalo PM, 26 SEP 82 (400037-02243) are included in this Appendix as follows:

9.8.1 TM/PF Band 1 Shifts (4-1, 4-7)
9.8.2 TM/PF Band 2 Shifts (4-1, 4-7)
9.8.3 TM/PF Band 3 Shifts (4-1, 4-7)
9.8.4 TM/PF Band 4 Shifts (4-1, 4-7)
9.8.5 TM/PF Band 5 Shifts (4-1, 4-7)
9.8.6 TM/PF Band 7 Shifts (4-1, 4-7).

Appendix 9.8.1

SCAN-CORRELATED SHIFTS (DN)
BAND 1 LANDSAT-4 TM/PF

	TYPE 4-1 NASA ID 40392-18152				TYPE 4-7 NASA ID 40037-02243				TYPE 4-7 NASA ID 40392-18152				
	SHUTTER 1		SHUTTER 2		SHUTTER 1		SHUTTER 2		SHUTTER 1		SHUTTER 2		
CH	FWD	REV	FWD	REV	FWD	REV	FWD	REV	FWD	REV	FWD	REV	CH
16	.05	.05	.04	.02	−.03	−.02	−.01	−.02	.03	.01	.01	−.02	16
15	.03	.02	.02	.02	−.06	−.08	−.14	−.10	−.02	−.08	−.07	−.04	15
14	.16	.19	.24	.11	−.05	−.05	−.05	−.05	−.01	−.03	−.01	−.03	14
13	.07	.08	.05	.03	−.05	−.08	−.10	−.05	−.02	−.08	−.04	−.04	13
12	1.62	1.83	1.88	1.52	−.03	−.03	−.04	−.02	−.02	−.02	−.02	−.04	12
11	.02	−.02	−.02	−.01	−.08	−.09	−.09	−.06	−.01	−.07	−.02	−.05	11
10	.93	.99	.09	.64	−.03	−.05	−.05	−.03	−.02	−.03	−.03	−.04	10
9	.01	−.03	−.02	−.02	.00	−.02	−.04	−.02	.02	−.02	.01	−.01	9
8	.75	.79	.84	.56	−.06	−.07	−.07	−.05	−.01	−.03	−.02	−.05	8
7	.01	−.02	−.01	.01	−.05	−.07	−.07	−.08	−.02	−.04	−.04	−.05	7
6	.17	.19	.18	.07	−.02	−.03	−.02	−.03	.02	−.01	.00	−.02	6
5	.04	−.00	.02	.01	−.12	−.13	−.12	−.14	−.03	−.11	−.13	−.07	5
4	1.70	1.95	2.05	1.50	.01	.01	−.01	.01	−.01	−.02	−.02	−.03	4
3	.03	.03	.03	.02	−.11	−.13	−.11	−.12	−.04	−.12	−.08	−.07	3
2	.07	.07	.06	.03	−.10	−.11	−.09	−.11	−.02	−.07	−.04	−.05	2
1	.33	.35	.38	.17	−.14	−.14	−.15	−.14	−.07	−.14	−.14	−.10	1

J. Barker/Y. Lee MAR 84 GSFC

Appendix 9.8.2

SCAN-CORRELATED SHIFTS (DN)
BAND 2 LANDSAT-4 TM/PF

	TYPE 4-1 NASA ID 40392-18152				TYPE 4-7 NASA ID 40037-02243				TYPE 4-7 NASA ID 40392-18152				
	SHUTTER 1		SHUTTER 2		SHUTTER 1		SHUTTER 2		SHUTTER 1		SHUTTER 2		
CH	FWD	REV	FWD	REV	FWD	REV	FWD	REV	FWD	REV	FWD	REV	CH
16	−.00	.02	−.00	.01	.08	.09	.09	.05	−.00	−.00	.00	−.01	16
15	.00	.01	.01	.01	−.10	−.08	−.14	−.05	−.06	−.03	−.10	−.02	15
14	−.01	.01	−.00	.02	.01	.01	.02	.01	−.01	−.00	−.00	−.01	14
13	−.00	.01	.01	.01	−.12	−.06	−.11	−.06	−.04	−.03	−.07	−.01	13
12	−.01	.01	−.01	.01	.01	−.00	.01	.01	−.01	−.01	−.01	−.00	12
11	−.00	.01	.00	.01	−.08	−.07	−.10	−.05	−.03	−.02	−.05	−.02	11
10	−.01	.02	−.00	.02	.00	.00	.00	.01	−.01	−.01	−.00	−.01	10
9	−.00	.01	.00	.01	−.06	−.03	−.05	−.02	−.04	−.02	.05	−.01	9
8	−.00	.02	.00	.01	.01	−.01	.00	.01	−.01	−.01	−.01	−.01	8
7	−.01	.01	−.01	.02	−.10	−.09	−.09	−.06	−.03	−.03	−.05	−.03	7
6	−.00	.02	−.00	.02	.01	.01	.00	.01	−.01	−.00	.00	−.01	6
5	−.00	.02	.00	.03	−.12	−.12	−.14	−.09	−.04	−.05	−.08	−.04	5
4	.01	.09	.03	.06	.01	.03	.02	.02	−.01	−.01	−.01	−.01	4
3	−.01	.01	−.02	.01	−.20	−.22	−.25	−.17	−.06	−.06	−.09	−.06	3
2	.00	.08	.00	.03	.04	.02	.02	.02	−.01	−.01	−.00	−.01	2
1	.05	.13	.07	.10	−.34	−.38	−.34	−.39	−.17	−.24	−.20	−.18	1

J. Barker/Y. Lee MAR 84 GSFC

9622(51*1)/84

Appendix 9.8.3

SCAN-CORRELATED SHIFTS (DN)
BAND 3 LANDSAT-4 TM/PF

	TYPE 4-1 NASA ID 40392-18152				TYPE 4-7 NASA ID 40037-02243				TYPE 4-7 NASA ID 40392-18152				
	SHUTTER 1		SHUTTER 2		SHUTTER 1		SHUTTER 2		SHUTTER 1		SHUTTER 2		
CH	FWD	REV	FWD	REV	FWD	REV	FWD	REV	FWD	REV	FWD	REV	CH
16	.03	.12	.06	.08	.78	.78	.81	.78	.41	.61	.15	.58	16
15	.09	.18	.12	.17	−.25	−.24	−.26	−.24	−.25	−.25	−.15	−.39	15
14	.00	.06	.05	.01	.15	.12	.13	.12	.01	.03	−.01	.03	14
13	.05	.12	.10	.09	−.17	−.15	−.18	−.14	−.11	−.13	−.09	−.18	13
12	−.00	.04	.02	−.00	.11	.09	.12	.08	.02	.03	−.01	.04	12
11	.01	.03	.03	.01	−.14	−.12	−.13	−.10	−.13	−.14	−.08	−.21	11
10	.01	.09	.03	.02	.03	.02	.03	.02	−.00	−.00	−.01	−.00	10
9	−.01	.01	.01	−.02	−.12	−.09	−.11	−.07	−.04	−.05	.02	−.04	9
8	−.02	.01	.01	−.02	−.05	−.02	−.04	−.03	−.01	−.01	−.01	−.01	8
7	.02	.09	.05	.03	−.21	−.20	−.21	−.19	−.12	−.17	−.10	−.17	7
6	.01	.09	.06	.02	.03	.04	.04	.03	.00	.00	−.01	.00	6
5	.06	.15	.10	.08	−.19	−.18	−.21	−.16	−.12	−.18	−.09	−.18	5
4	−.01	.02	.01	−.01	.01	.01	.01	.01	.00	.00	−.01	.00	4
3	.05	.11	.05	.09	−.30	−.32	−.32	−.27	−.20	−.24	−.12	−.28	3
2	.02	.13	.06	.04	.25	.23	.24	.18	.07	.13	.01	.13	2
1	.20	.29	.19	.27	−.54	−.59	−.59	−.53	−.41	.52	−.29	−.52	1

J. Barker/Y. Lee MAR 84 GSFC

Appendix 9.8.4

SCAN-CORRELATED SHIFTS (DN)
BAND 4 LANDSAT-4 TM/PF

	TYPE 4-1 NASA ID 40392-18152				TYPE 4-7 NASA ID 40037-02243				TYPE 4-7 NASA ID 40392-18152				
	SHUTTER 1		SHUTTER 2		SHUTTER 1		SHUTTER 2		SHUTTER 1		SHUTTER 2		
CH	FWD	REV	FWD	REV	FWD	REV	FWD	REV	FWD	REV	FWD	REV	CH
16	.12	.18	.29	.17	.00	.00	−.00	−.00	−.03	−.02	−.03	−.02	16
15	.06	.05	.12	.07	−.01	−.00	−.01	−.00	−.02	−.01	−.01	−.01	15
14	−.01	.02	−.00	.03	−.02	−.00	−.01	−.00	−.03	−.02	−.04	−.02	14
13	.04	.03	.08	.03	−.01	−.00	−.00	−.00	−.01	−.00	−.01	−.01	13
12	.06	.08	.13	.06	.00	.01	.01	.00	−.02	−.01	−.01	−.02	12
11	.07	.08	.10	.04	−.01	−.00	−.01	−.00	−.02	−.01	−.02	−.01	11
10	.01	.05	.05	.04	−.01	−.01	−.01	−.01	−.03	−.02	−.03	−.03	10
9	.00	.04	.03	.03	−.02	−.00	−.01	−.00	−.01	−.01	−.01	−.01	9
8	−.01	.01	−.01	.01	−.07	−.07	−.09	−.06	−.05	−.06	−.05	−.04	8
7	.01	.06	.03	.02	−.01	−.00	−.01	−.00	−.02	−.01	−.01	−.01	7
6	.01	.12	.03	.01	−.05	−.05	−.06	−.04	−.02	−.04	−.04	−.02	6
5	.02	.07	.07	.04	−.02	−.01	−.02	−.00	−.02	−.01	−.02	−.01	5
4	−.01	.01	−.01	.02	−.06	−.07	−.07	−.05	−.04	−.07	−.10	−.04	4
3	.01	.12	.06	.03	−.02	−.02	−.05	−.02	−.02	−.02	−.02	−.02	3
2	−.00	.05	.01	.02	−.06	−.05	−.06	−.03	−.06	−.07	−.08	−.03	2
1	.10	.25	.17	.10	−.06	−.05	−.06	−.04	−.02	−.02	−.02	−.01	1

J. Barker/Y. Lee MAR 84 GSFC

9622151*al/84

Appendix 9.8.5

SCAN-CORRELATED SHIFTS (DN)
BAND 5 LANDSAT-4 TM/PF

	TYPE 4-1 NASA ID 40392-18152				TYPE 4-7 NASA ID 40037-02243				TYPE 4-7 NASA ID 40392-18152				
	SHUTTER 1		SHUTTER 2		SHUTTER 1		SHUTTER 2		SHUTTER 1		SHUTTER 2		
CH	FWD	REV	FWD	REV	FWD	REV	FWD	REV	FWD	REV	FWD	REV	CH
16	.01	−.00	.01	.01	−.09	−.08	−.09	−.07	−.07	−.09	−.10	−.06	16
15	−.18	−.12	−.13	−.15	−.04	−.04	−.07	−.09	−.01	−.01	−.02	−.04	15
14	−.03	−.03	−.02	−.02	−.07	−.08	−.07	−.05	−.08	−.08	−.06	−.04	14
13	−.06	.04	.04	.02	.02	.01	.00	.02	−.00	−.01	.01	.01	13
12	.05	.04	.04	.02	.02	.01	.00	.02	−.00	−.01	−.01	−.01	12
11	−.04	−.04	−.01	−.04	.06	.06	.02	.04	.03	.04	.04	.02	11
10	−.04	−.02	−.03	−.04	.59	.63	.61	.59	.52	.58	.52	.60	10
9	−.05	−.04	−.02	−.04	.06	.05	.04	.02	.08	.05	.05	.00	9
8	−.02	−.01	−.01	−.05	−.17	−.20	−.20	−.13	−.19	−.22	−.17	−.13	8
7	−.01	−.02	.00	−.03	.10	.14	.08	.14	.10	.10	.10	.11	7
6	.03	.02	.03	.02	−.06	−.08	−.06	−.04	−.09	−.06	−.09	−.08	6
5	−.12	−.12	−.11	−.13	.01	−.02	−.01	−.01	.02	.02	.01	−.01	5
4	.06	.10	.07	.10	−.05	−.04	−.06	−.06	−.07	−.06	−.05	−.04	4
3	.00	.00	.00	.00	.00	.00	.00	.00	.00	.00	.00	.00	3
2	.07	.07	.10	.07	−.09	−.10	−.09	−.07	−.09	−.08	−.10	−.08	2
1	.00	−.02	−.01	−.02	.07	.04	.04	.04	.07	.08	.05	.04	1

J. Barker/Y. Lee MAR 84 GSFC

Appendix 9.8.6

SCAN-CORRELATED SHIFTS (DN)
BAND 7 LANDSAT-4 TM/PF

	TYPE 4-1 NASA ID 40392-18152				TYPE 4-7 NASA ID 40037-02243				TYPE 4-7 NASA ID 40392-18152				
	SHUTTER 1		SHUTTER 2		SHUTTER 1		SHUTTER 2		SHUTTER 1		SHUTTER 2		
CH	FWD	REV	FWD	REV	FWD	REV	FWD	REV	FWD	REV	FWD	REV	CH
16	.03	.09	.11	.09	−.23	−.19	−.21	−.19	−.23	−.19	−.19	−.19	16
15	−.03	−.03	−.04	−.02	.20	.17	.17	.13	.18	.19	.16	.12	15
14	.10	.12	.13	.14	−.07	−.06	−.05	−.07	−.12	−.08	−.08	−.05	14
13	−.03	−.05	−.04	−.06	.15	.20	.21	.17	.26	.16	.20	.17	13
12	.07	.08	.09	.09	−.23	−.26	−.22	−.21	−.22	−.21	−.21	−.23	12
11	−.02	−.03	−.03	−.04	.21	.18	.17	.17	.23	.27	.21	.17	11
10	.04	.03	.07	.06	**−.41**	**−.41**	**−.40**	**−.36**	**−.39**	**−.42**	**−.38**	**−.41**	10
9	−.06	−.05	−.06	−.06	.14	.16	.18	.13	.17	.18	.21	.10	9
8	.03	.04	.04	.02	−.29	−.29	−.30	−.30	−.27	−.33	−.27	−.29	8
7	−.02	−.05	.09	−.07	**1.03**	**1.07**	**.69**	**.80**	**1.09**	**.92**	**.76**	**.11**	7
6	.06	.06	.07	.06	−.29	−.29	−.28	−.26	−.29	−.25	−.25	−.28	6
5	−.01	−.01	−.02	−.02	.23	.25	.22	.22	.23	.23	.24	.23	5
4	.04	.05	.06	.04	−.23	−.24	−.19	−.20	−.25	−.26	−.23	−.05	4
3	−.05	−.03	−.04	−.05	.30	.30	.31	.22	.28	.31	.34	.32	3
2	.04	.03	.03	.02	−.27	−.28	−.28	−.24	−.24	−.32	−.24	−.26	2
1	−.00	−.02	−.02	−.03	.28	.28	.26	.27	.25	.28	.30	.25	1

J. Barker/Y. Lee MAR 84 GSFC

9822(51*e)/84

APPENDIX 9.9 - TM/PF PLOTS OF SHUTTER BACKGROUND VERSUS SCAN

Landsat-4 TM/PF averaged shutter backgrounds before and after DC restoration are plotted versus scan number for forward and reverse scans after being corrected (Section 4.5) for scan collerated shifts of type 4-1 (Landsat-4 Band 1, Channel 4) and type 4-7 (Landsat-4 Band 7, Channel 7) for 2 AUG 83 scene of San Francisco (NASA ID 40392-18152) in which lower half is cloud-covered. These plots are included as follows:

9.9.1	Band 1, Shutter 1
9.9.2	Band 1, Shutter 2
9.9.3	Band 2, Shutter 1
9.9.4	Band 2, Shutter 2
9.9.5	Band 3, Shutter 1
9.9.6	Band 3, Shutter 2
9.9.7	Band 4, Shutter 1
9.9.8	Band 4, Shutter 2
9.9.9	Band 5, Shutter 1
9.9.10	Band 5, Shutter 2
9.9.11	Band 7, Shutter 1
9.9.12	Band 7, Shutter 2.

SCENE ID=40392-18152, BAND 1 (FORWARD)
SHUTTER BACKGROUND 1 SPECTRA AFTER CORRECTION

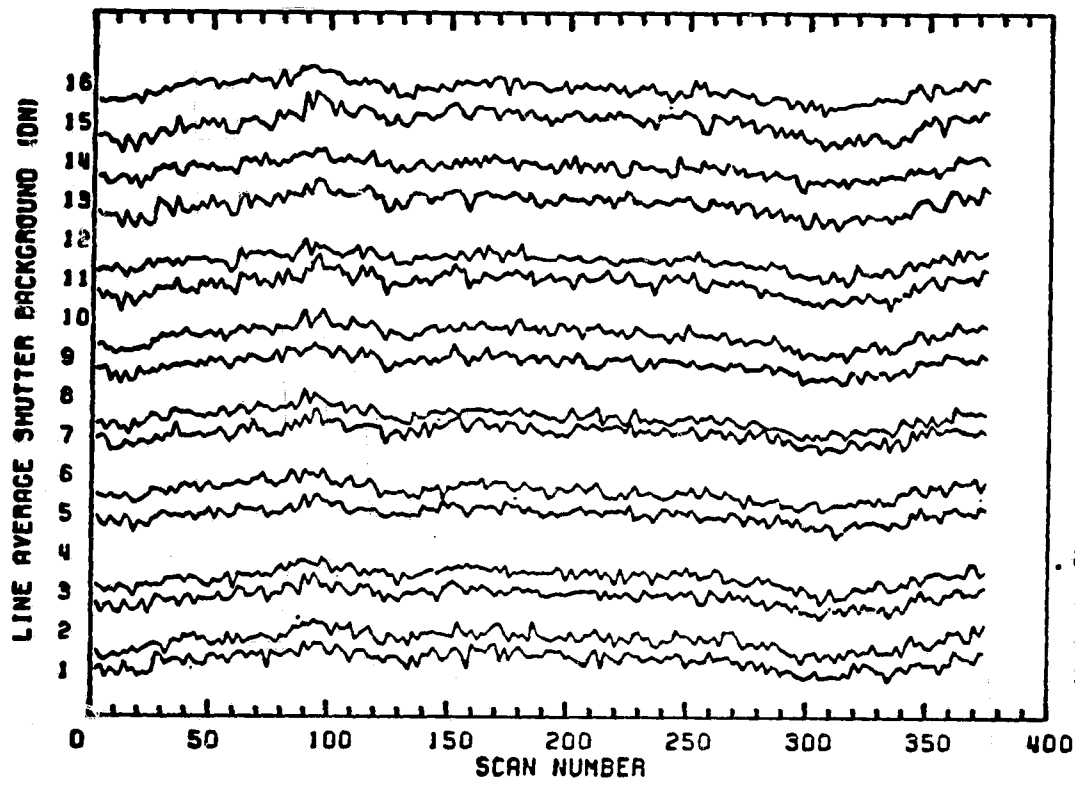

1000*CV	SHIFT1	SHIFT2
176	0.05	0.03
199	0.03	-0.02
158	0.16	-0.01
184	0.07	-0.02
213	1.62	-0.02
191	0.02	-0.01
230	0.93	-0.02
159	0.01	0.02
237	0.75	-0.01
195	0.01	-0.02
199	0.17	0.02
124	0.04	-0.03
244	1.70	-0.01
151	0.03	-0.04
178	0.07	-0.02
122	0.33	-0.07

LEE/BARKER
6-MAR-84

SCENE ID=40392-18152, BAND 1 (REVERSE)
SHUTTER BACKGROUND 1 SPECTRA AFTER CORRECTION

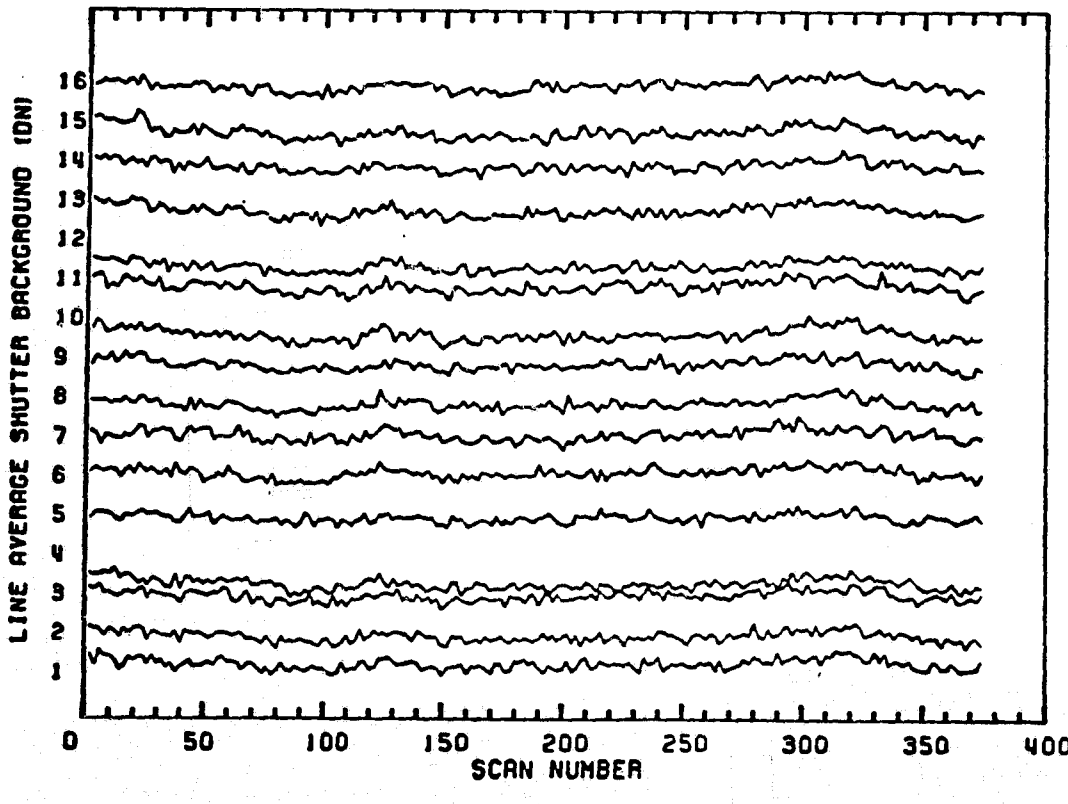

1000*CV	SHIFT1	SHIFT2
86	0.05	0.01
105	0.02	-0.03
80	0.19	-0.03
100	0.08	-0.03
111	1.63	-0.02
96	-0.02	-0.07
114	0.99	-0.03
84	-0.03	-0.02
87	0.79	-0.03
83	-0.02	-0.04
76	0.19	-0.01
67	-0.00	-0.11
128	1.95	-0.02
77	0.03	-0.12
76	0.07	-0.07
69	0.35	-0.14

LEE/BARKER
6-MAR-84

SCENE ID=40392-18152, BAND 1 (FORWARD)
SHUTTER BACKGROUND 2 SPECTRA AFTER CORRECTION

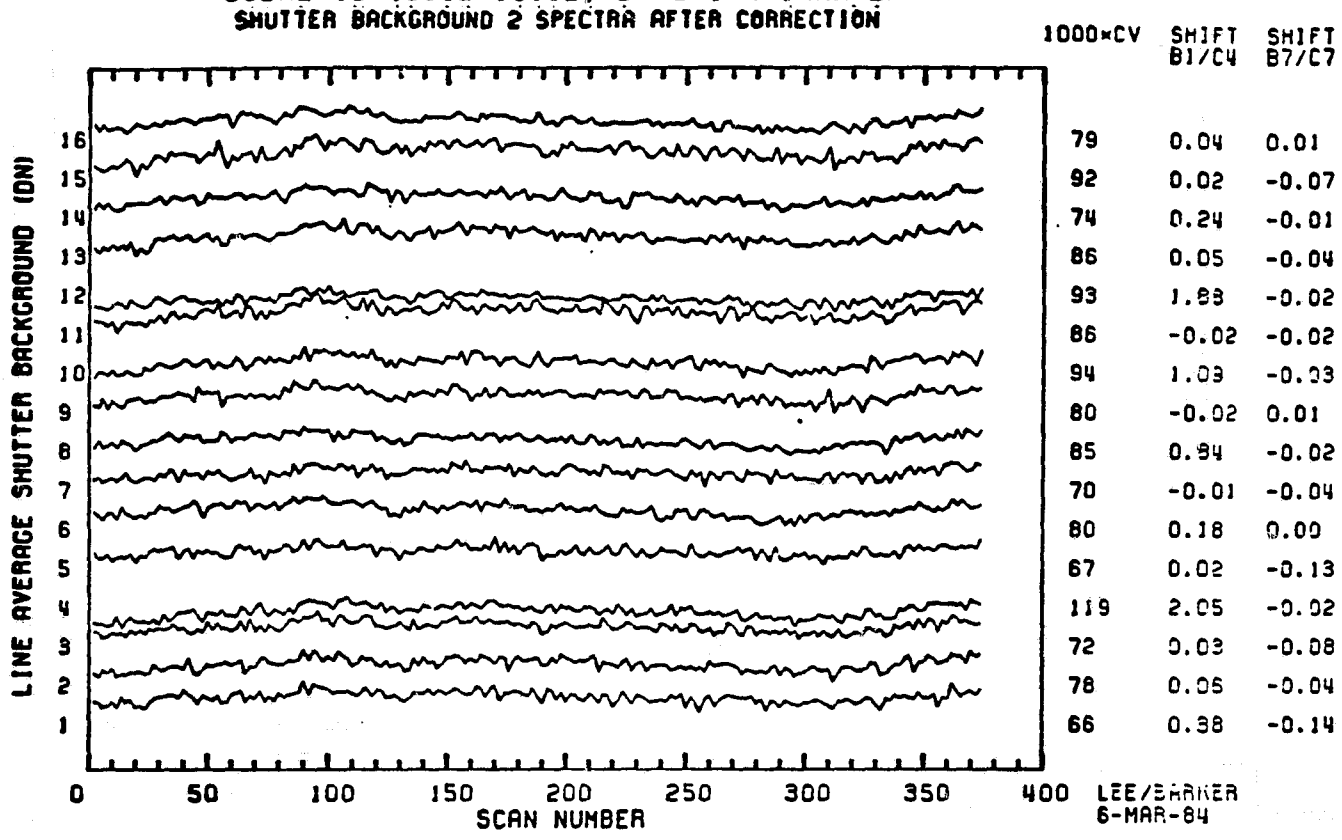

SCENE ID=40392-18152, BAND 1 (REVERSE)
SHUTTER BACKGROUND 2 SPECTRA AFTER CORRECTION

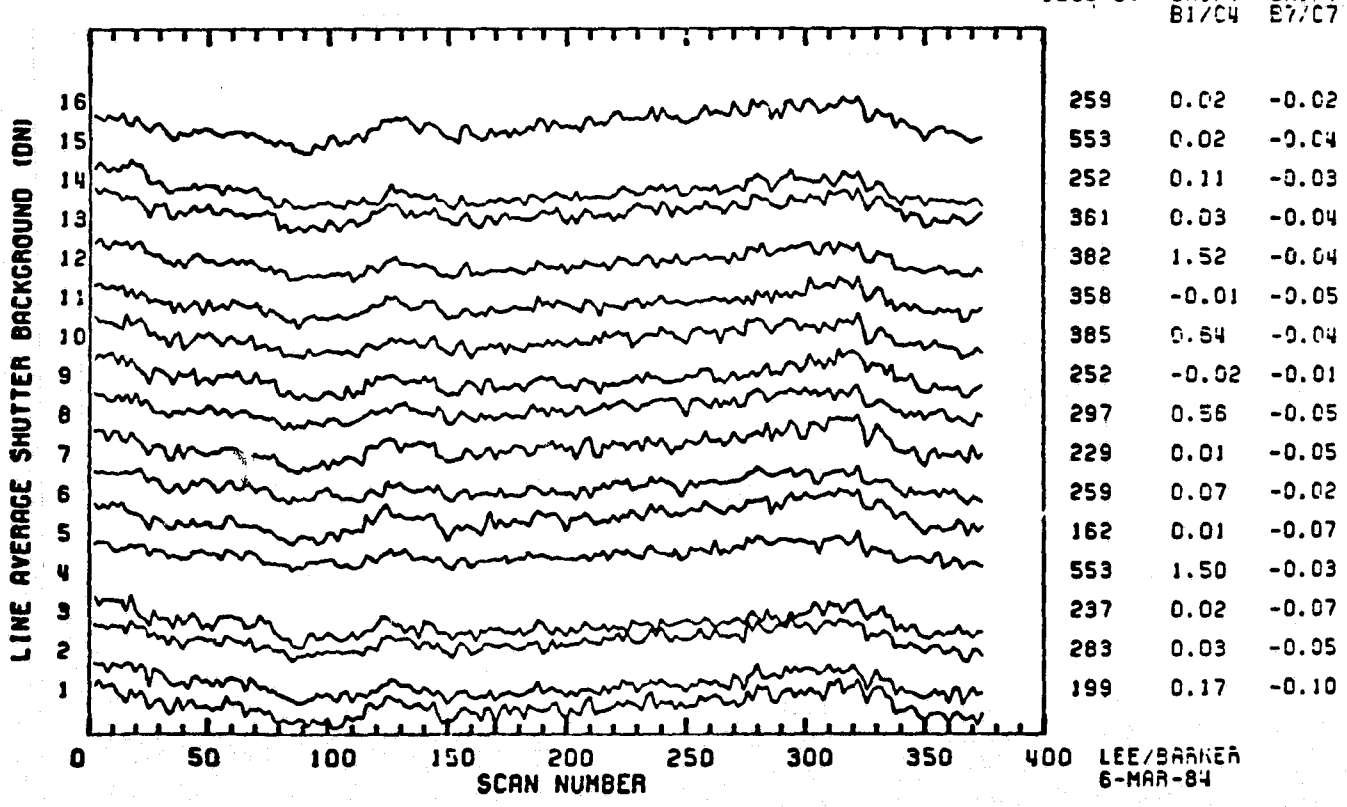

SCENE ID=40392-18152, BAND 2 (FORWARD)
SHUTTER BACKGROUND 1 SPECTRA AFTER CORRECTION

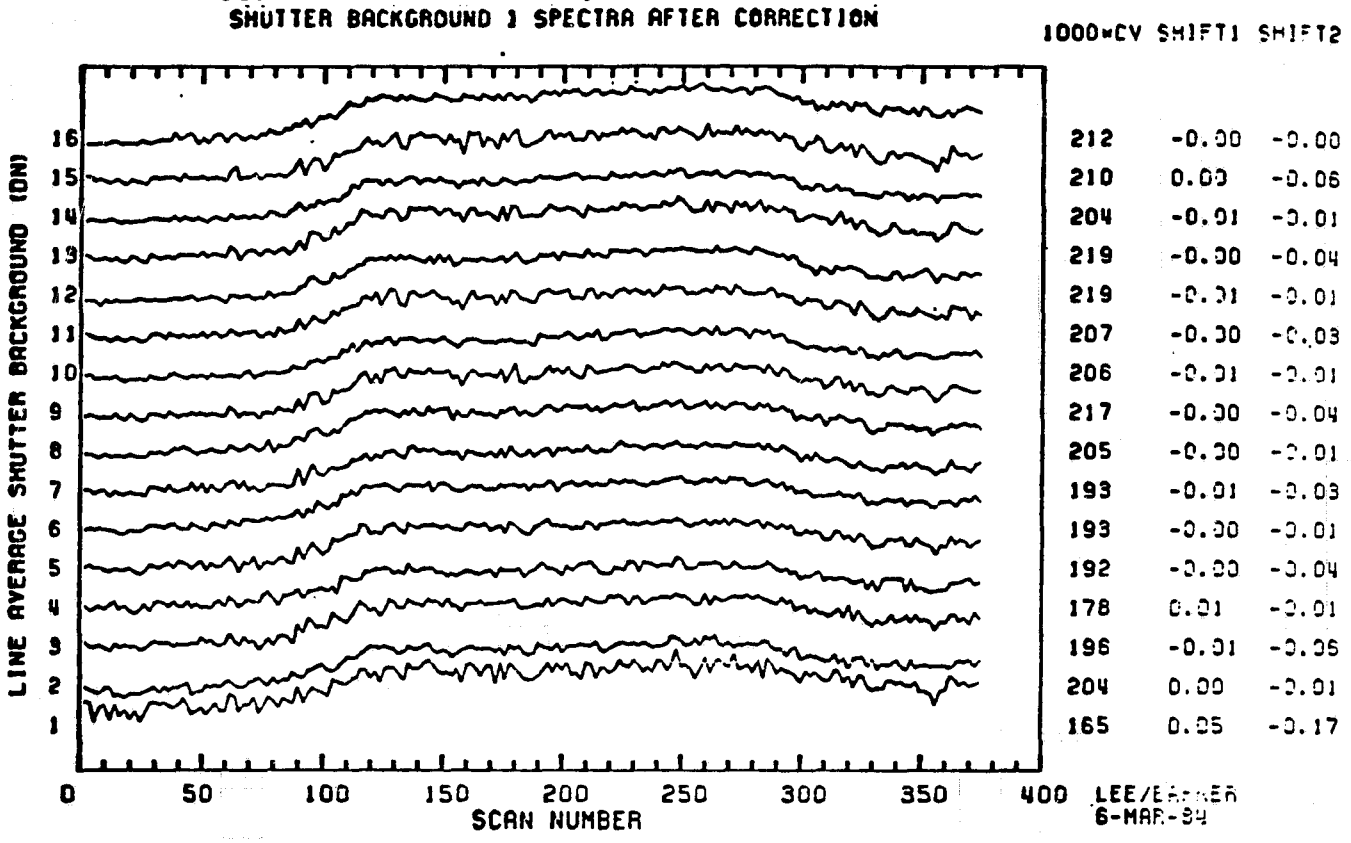

SCENE ID=40392-18152, BAND 2 (REVERSE)
SHUTTER BACKGROUND 1 SPECTRA AFTER CORRECTION

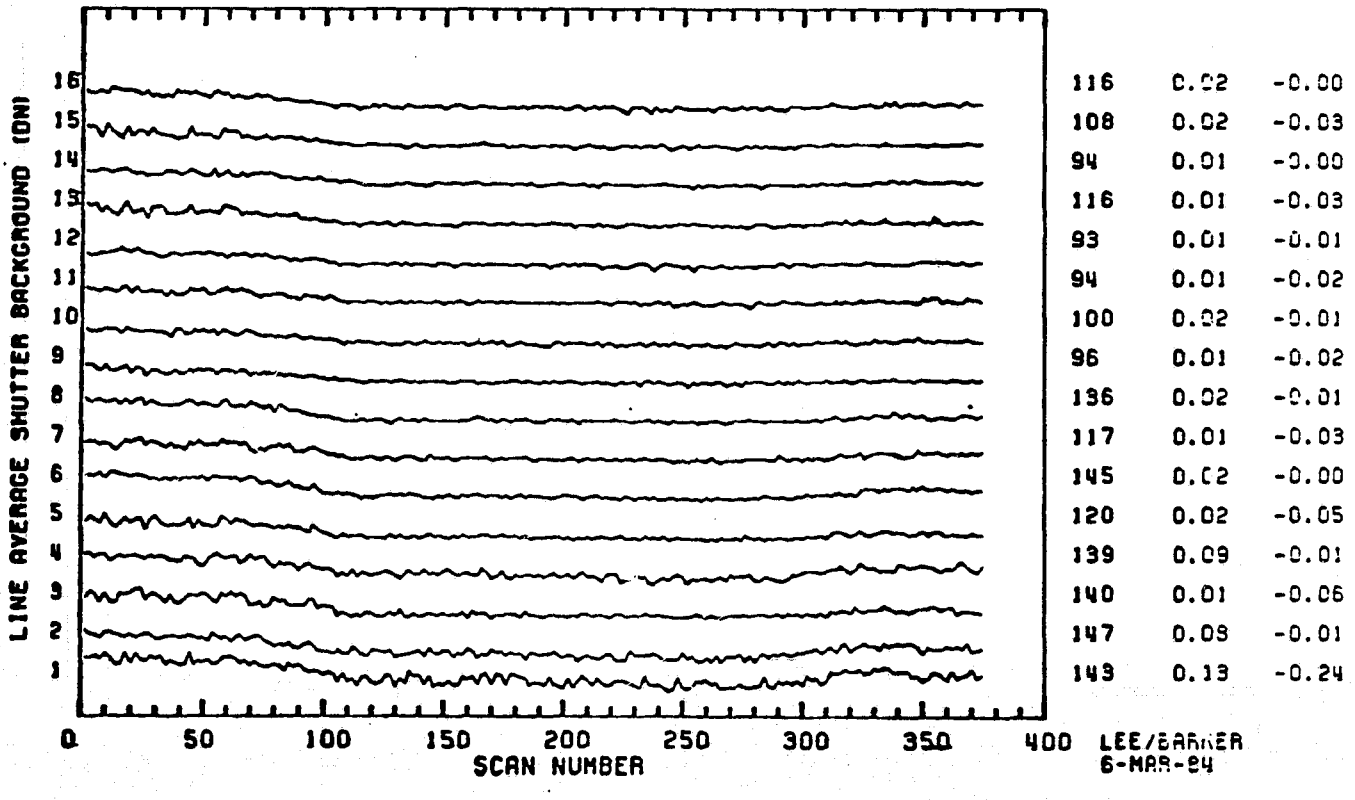

SCENE ID=40392-18152, BAND 2 (FORWARD)
SHUTTER BACKGROUND 2 SPECTRA AFTER CORRECTION

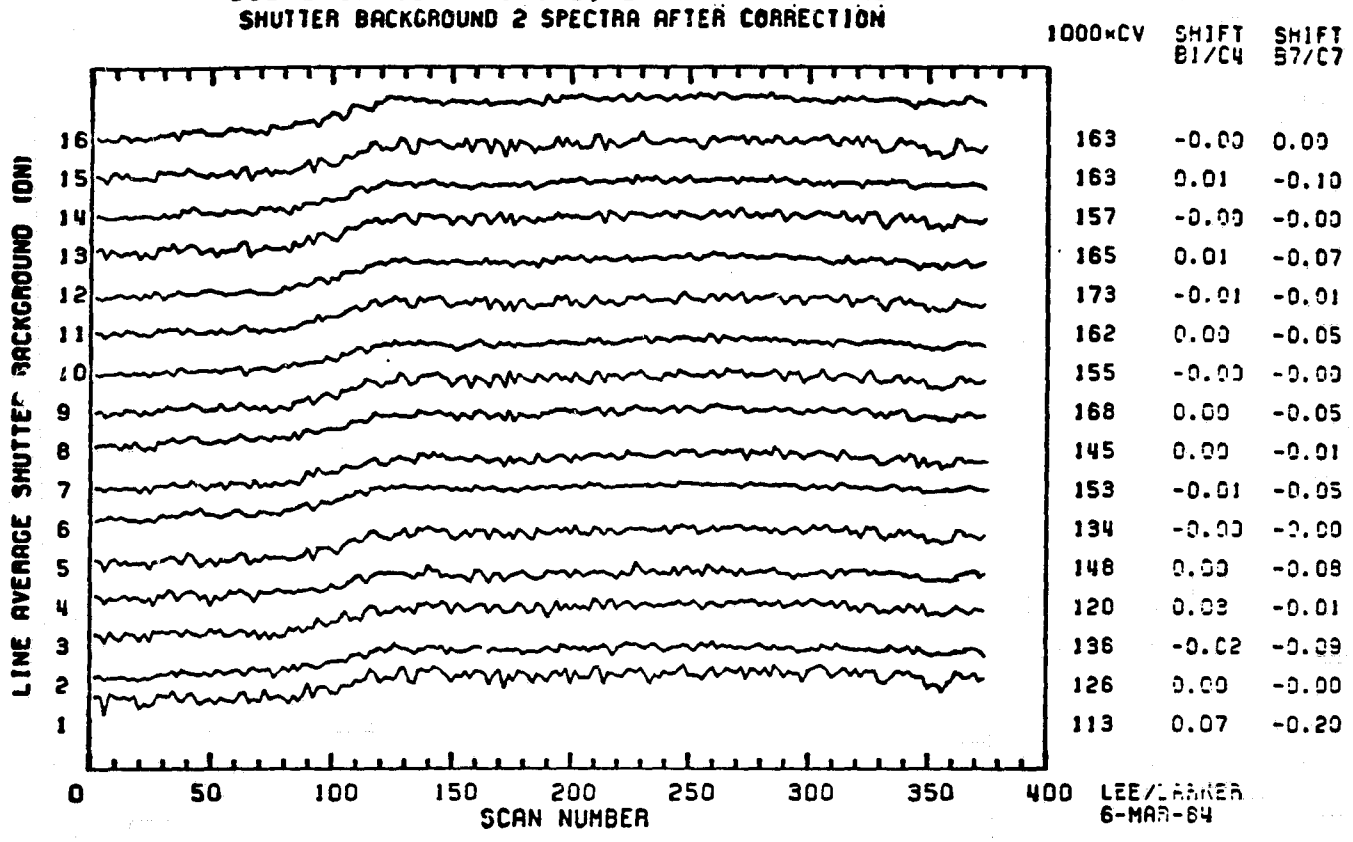

SCENE ID=40392-18152, BAND 2 (REVERSE)
SHUTTER BACKGROUND 2 SPECTRA AFTER CORRECTION

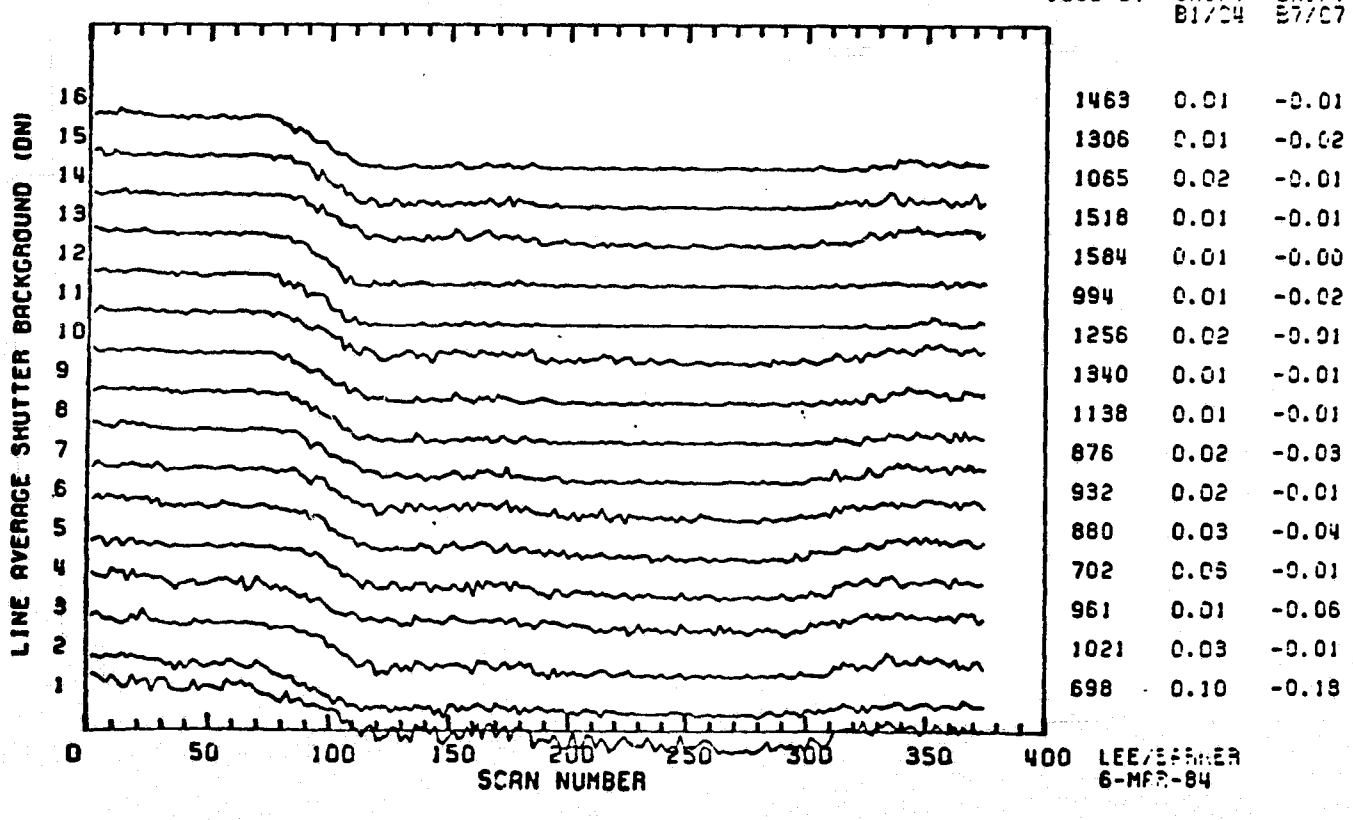

Appendix 9.9.5

SCENE ID=40392-18152, BAND 3 (FORWARD)
SHUTTER BACKGROUND 1 SPECTRA AFTER CORRECTION

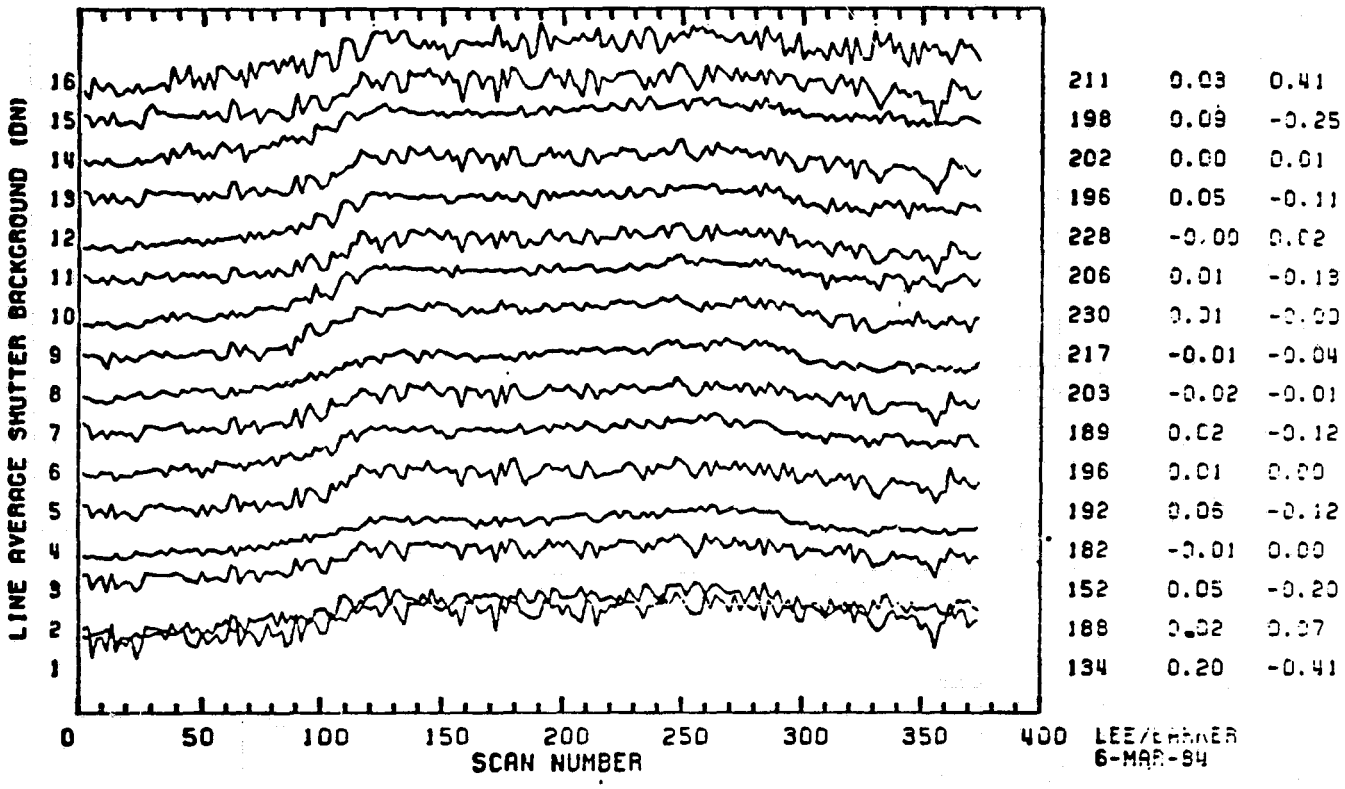

SCENE ID=40392-18152, BAND 3 (REVERSE)
SHUTTER BACKGROUND 1 SPECTRA AFTER CORRECTION

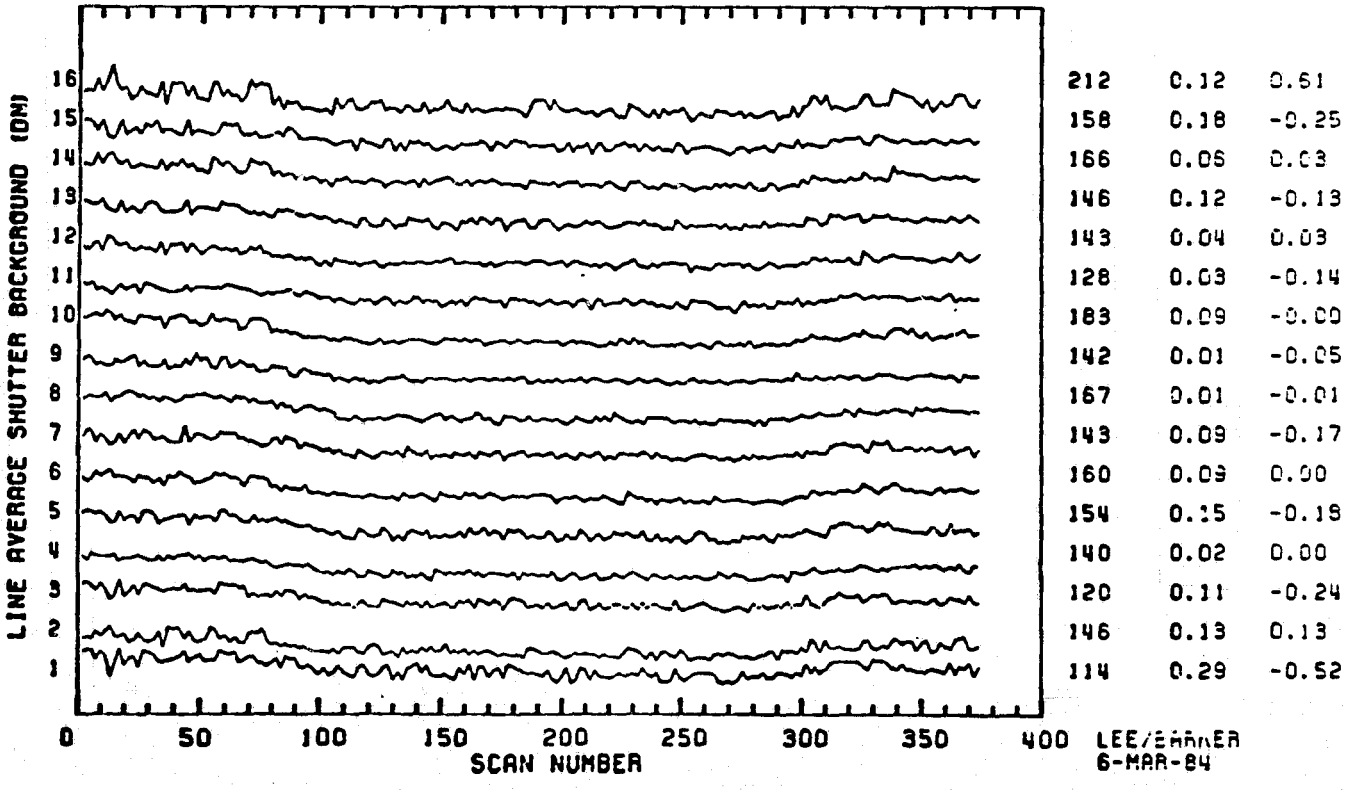

Appendix 9.9.6

SCENE ID=40392-18152, BAND 3 (FORWARD)
SHUTTER BACKGROUND 2 SPECTRA AFTER CORRECTION

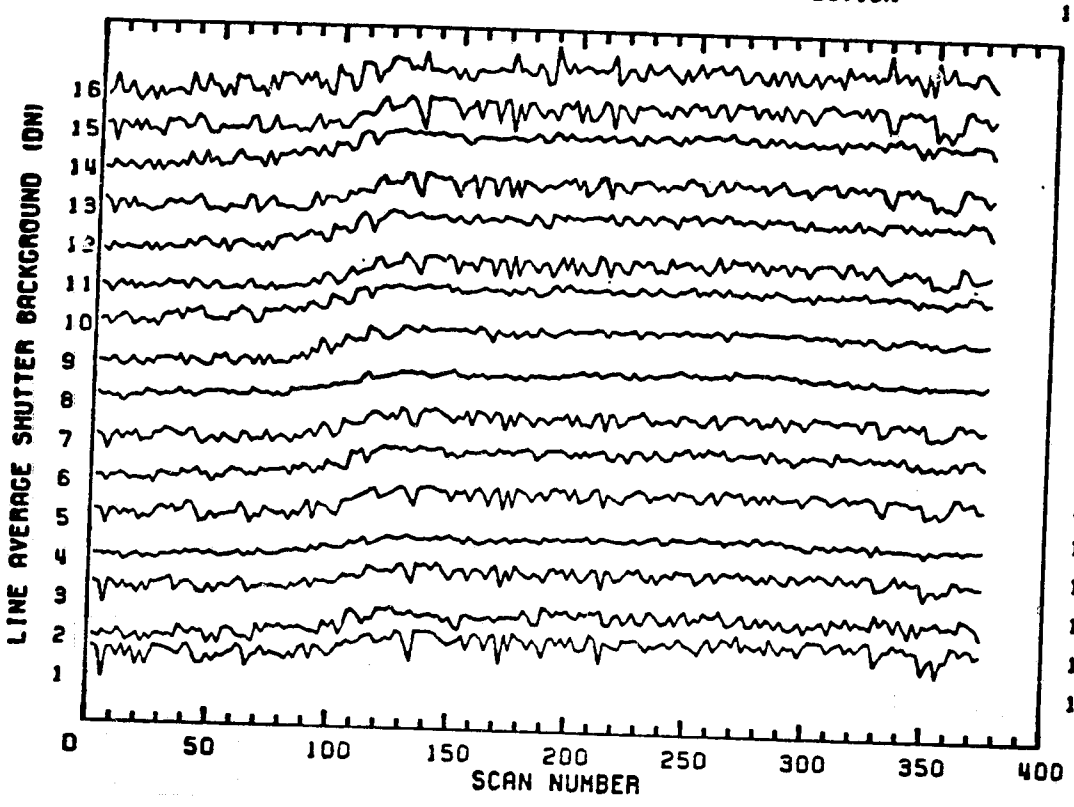

1000×CV	SHIFT B1/C4	SHIFT B7/C7
155	0.08	0.58
158	0.17	-0.39
152	0.01	0.03
161	0.09	-0.18
169	-0.00	0.04
164	0.01	-0.21
153	0.02	0.00
172	-0.02	-0.04
131	-0.02	-0.01
146	0.03	-0.17
147	0.02	0.00
141	0.08	-0.18
120	-0.01	0.00
112	0.09	-0.28
138	0.04	0.13
108	0.27	-0.52

LEE/BARNER
6-MAR-84

SCENE ID=40392-18152, BAND 3 (REVERSE)
SHUTTER BACKGROUND 2 SPECTRA AFTER CORRECTION

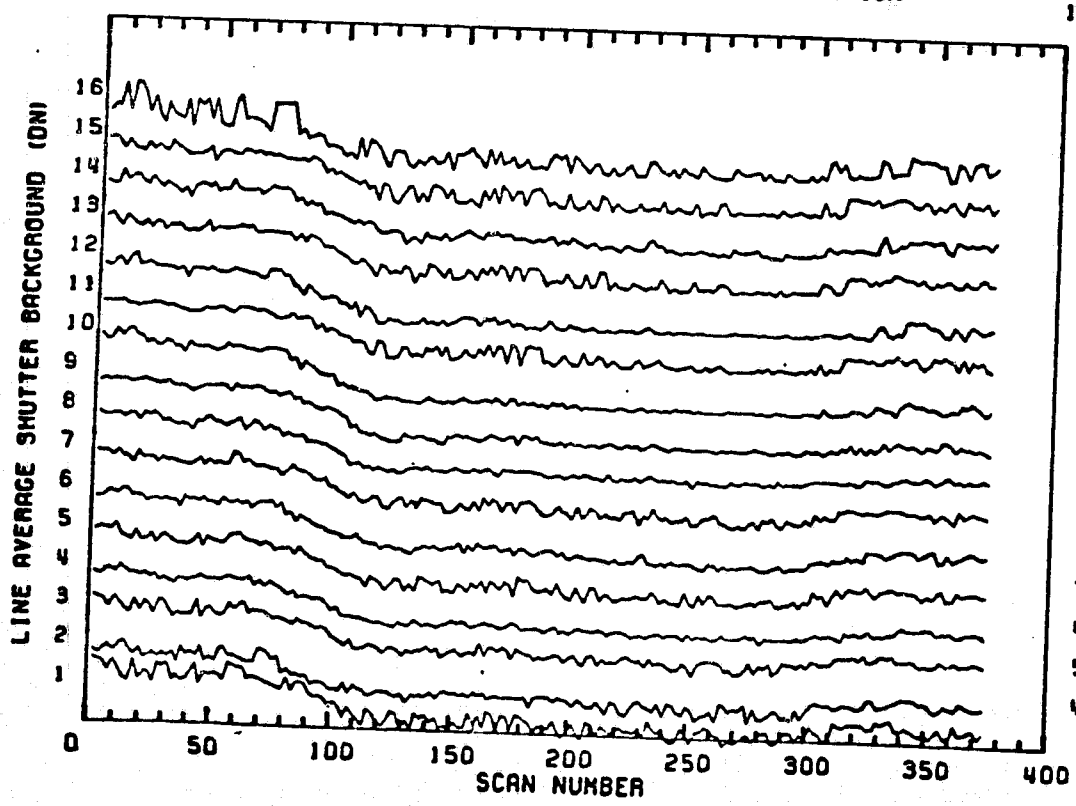

1000×CV	SHIFT B1/C4	SHIFT B7/C7
1016	0.06	0.15
814	0.12	-0.15
933	0.05	-0.01
804	0.10	-0.09
1264	0.02	-0.01
827	0.03	-0.08
1299	0.03	-0.01
1158	0.01	-0.02
820	0.01	-0.01
680	0.05	-0.10
873	0.06	-0.01
754	0.10	-0.09
711	0.01	-0.01
469	0.05	-0.12
550	0.06	0.01
417	0.19	-0.29

LEE/BARNER
6-MAR-84

SCENE ID=40392-18152, BAND 4 (FORWARD)
SHUTTER BACKGROUND 1 SPECTRA AFTER CORRECTION

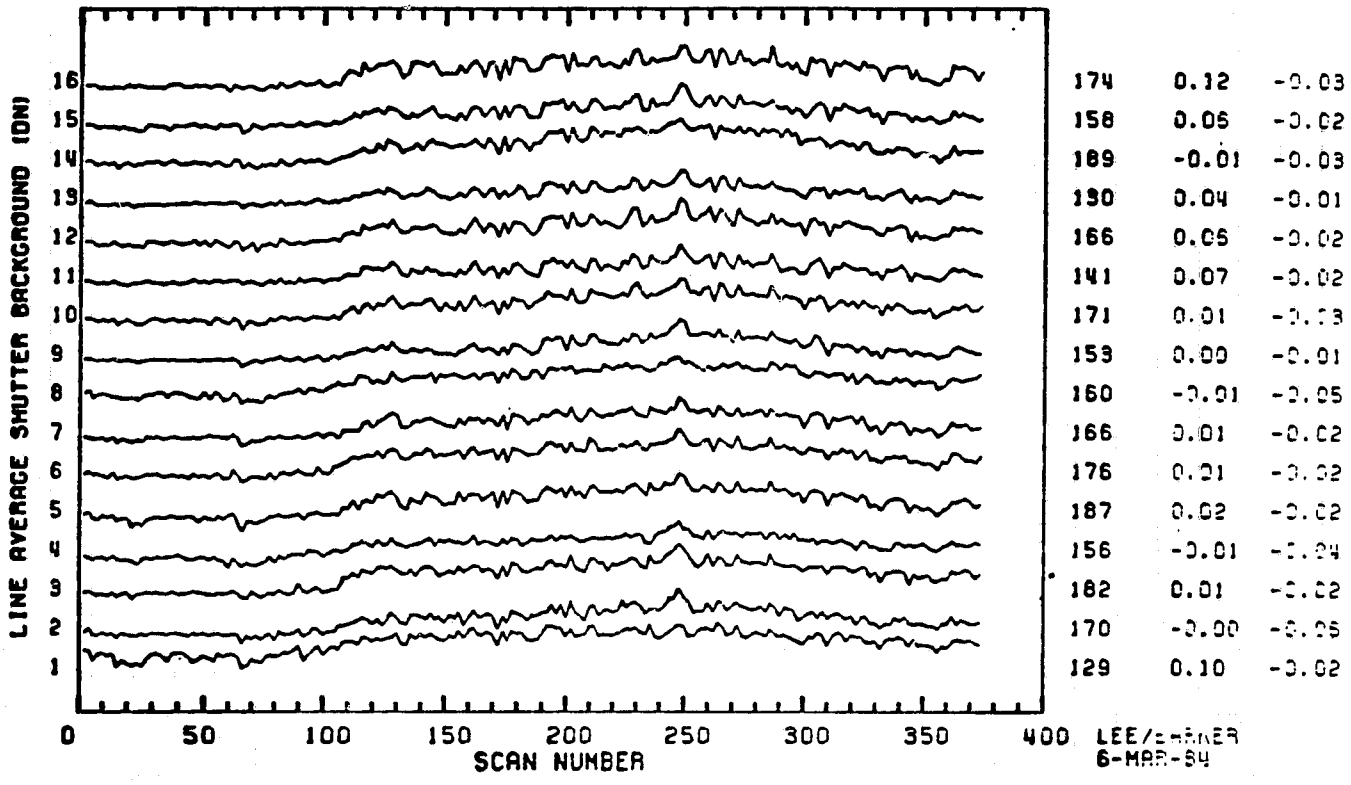

SCENE ID=40392-18152, BAND 4 (REVERSE)
SHUTTER BACKGROUND 1 SPECTRA AFTER CORRECTION

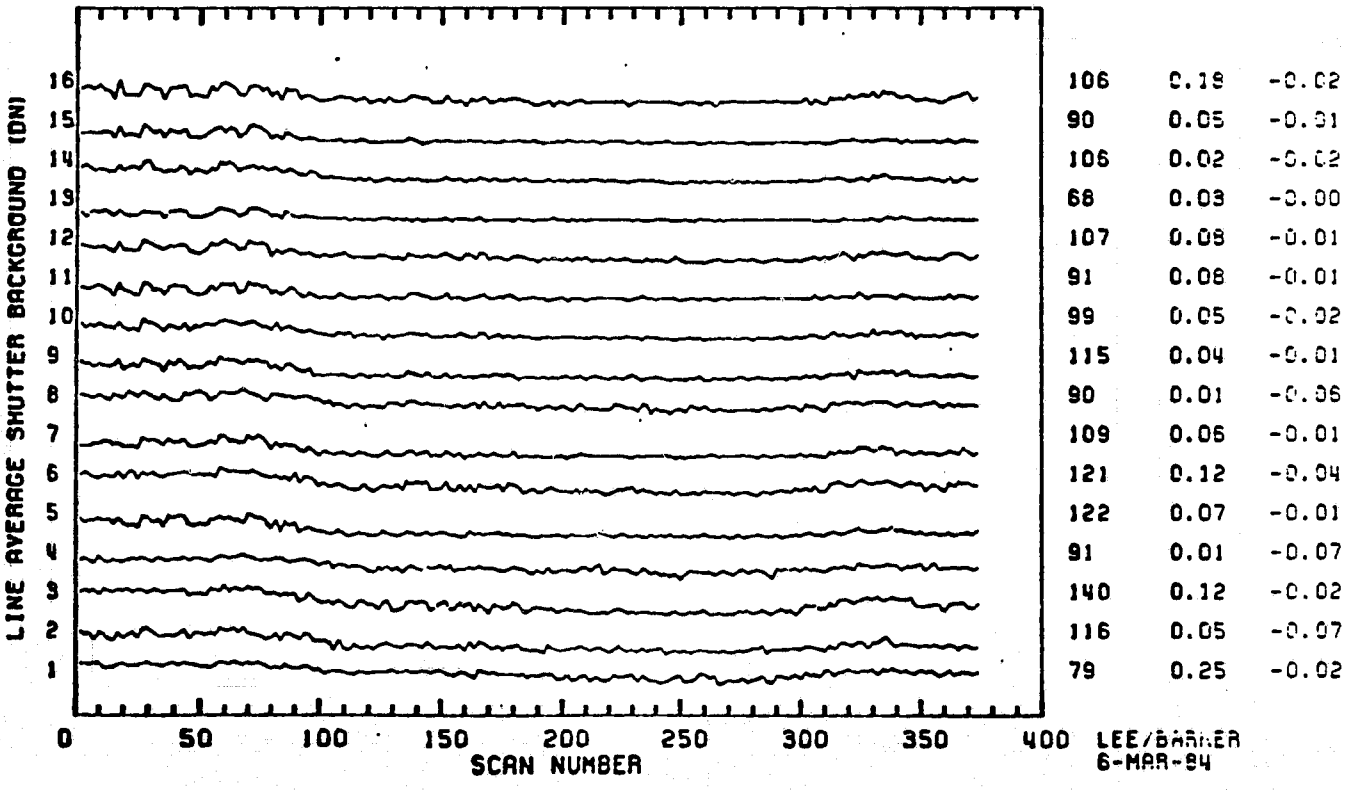

SCENE ID=40392-18152, BAND 4 (FORWARD)
SHUTTER BACKGROUND 2 SPECTRA AFTER CORRECTION

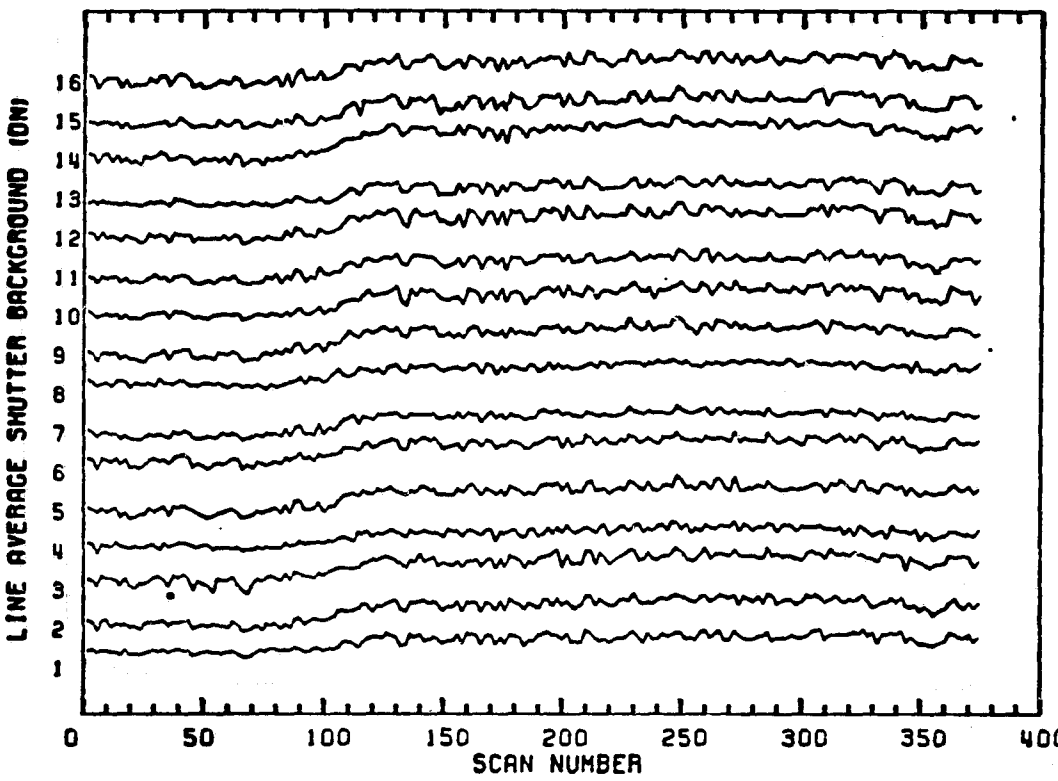

	1000×CV	SHIFT B1/C4	SHIFT B7/C7
16	141	0.29	-0.03
15	160	0.12	-0.01
14	174	-0.00	-0.04
13	135	0.09	-0.01
12	151	0.13	-0.01
11	140	0.10	-0.02
10	149	0 05	-0.03
9	156	0.03	-0.01
8	107	-0.01	-0.05
7	136	0.03	-0.01
6	121	0.03	-0.04
5	148	0.07	-0.02
4	108	-0.01	-0.10
3	132	0.06	-0.02
2	134	0.01	-0.08
1	87	0.17	-0.02

LEE/BARNER
6-MAR-84

SCENE ID=40392-18152, BAND 4 (REVERSE)
SHUTTER BACKGROUND 2 SPECTRA AFTER CORRECTION

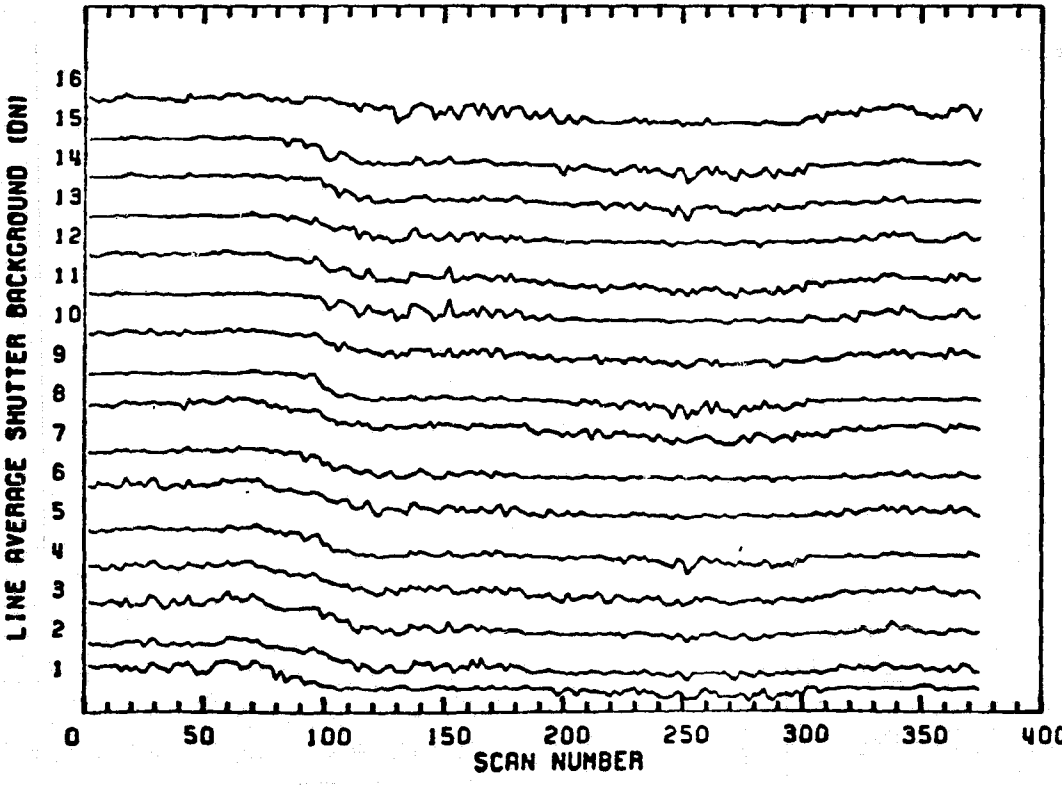

	1000×CV	SHIFT B1/C4	SHIFT B7/C7
16	250	0.17	-0.02
15	426	0.07	-0.01
14	388	0.03	-0.02
13	308	0.03	-0.01
12	421	0.05	-0.02
11	296	0.04	-0.01
10	328	0.04	-0.03
9	429	0.03	-0.01
8	323	0.01	-0.04
7	330	0.02	-0.01
6	338	0.01	-0.02
5	402	0.04	-0.01
4	394	0.02	-0.04
3	383	0.03	-0.02
2	340	0.02	-0.03
1	198	0.10	-0.01

LEE/BARNER
6-MAR-84

SCENE ID=40392-18152, BAND 5 (FORWARD)
SHUTTER BACKGROUND 1 SPECTRA AFTER CORRECTION

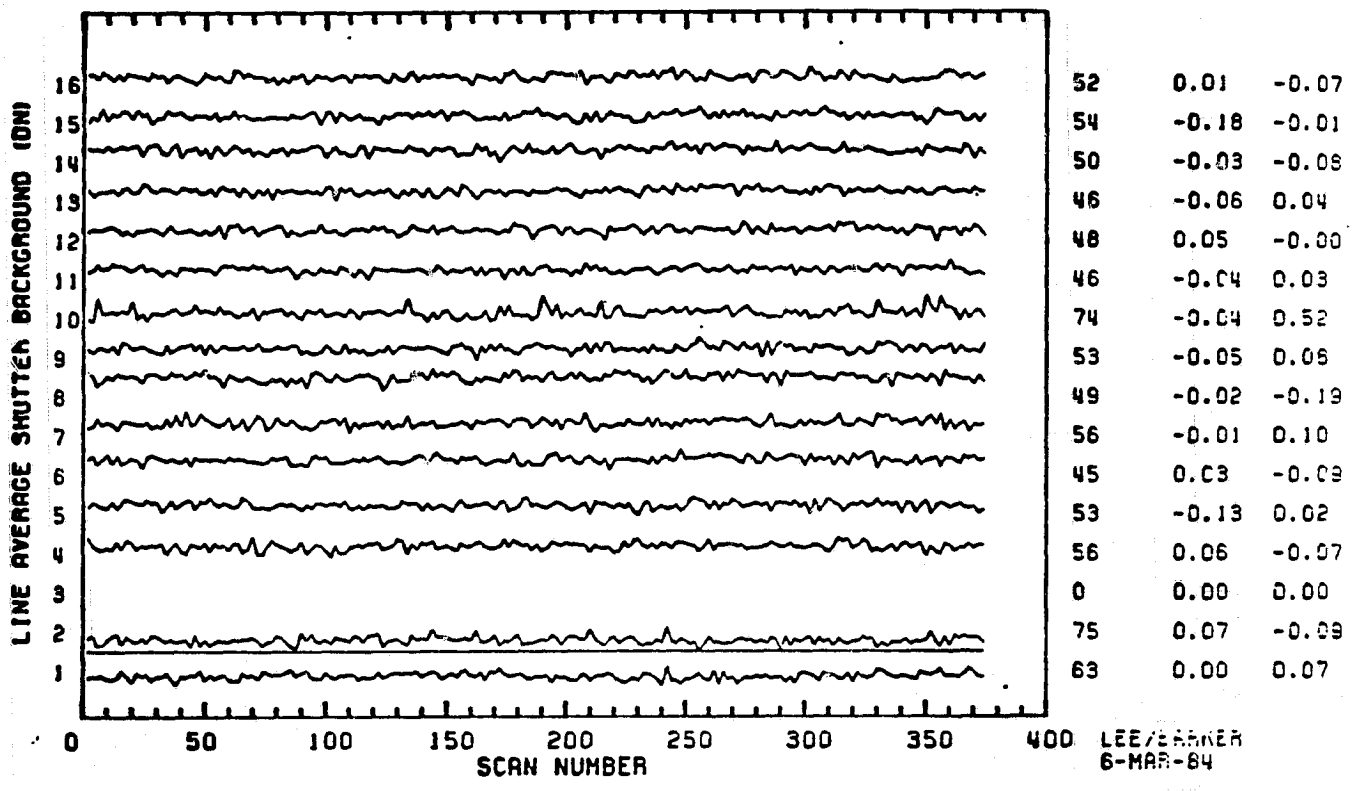

SCENE ID=40392-18152, BAND 5 (REVERSE)
SHUTTER BACKGROUND 1 SPECTRA AFTER CORRECTION

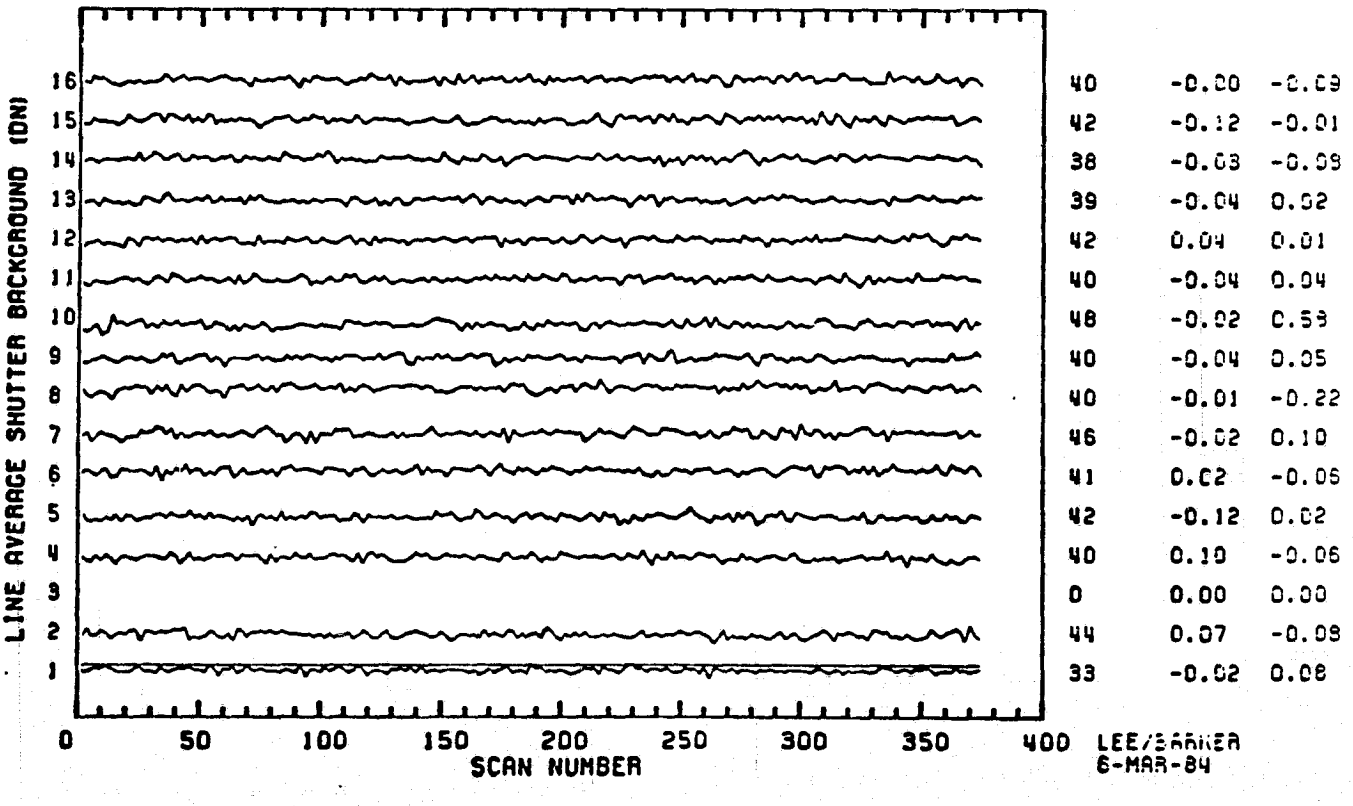

SCENE ID=40392-18152, BAND 5 (FORWARD)
SHUTTER BACKGROUND 2 SPECTRA AFTER CORRECTION

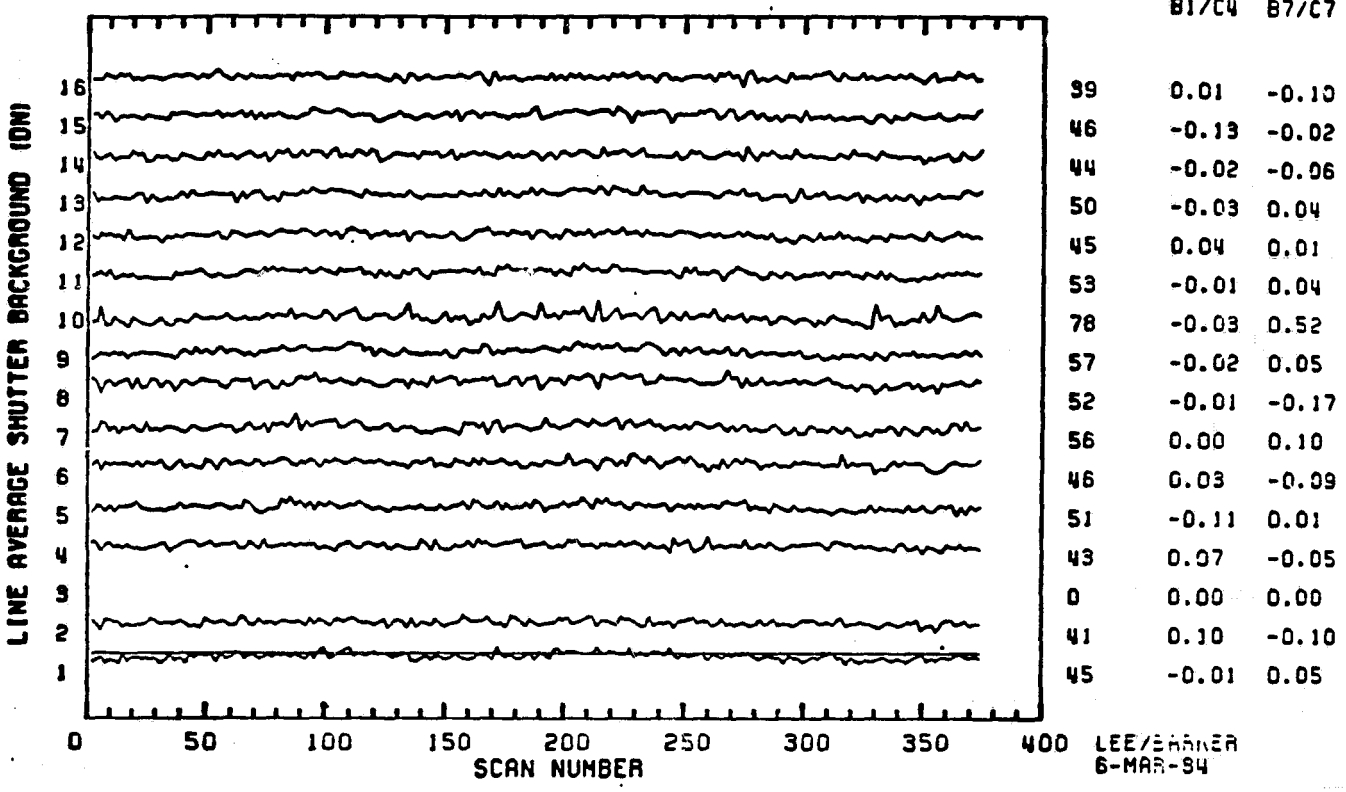

SCENE ID=40392-18152, BAND 5 (REVERSE)
SHUTTER BACKGROUND 2 SPECTRA AFTER CORRECTION

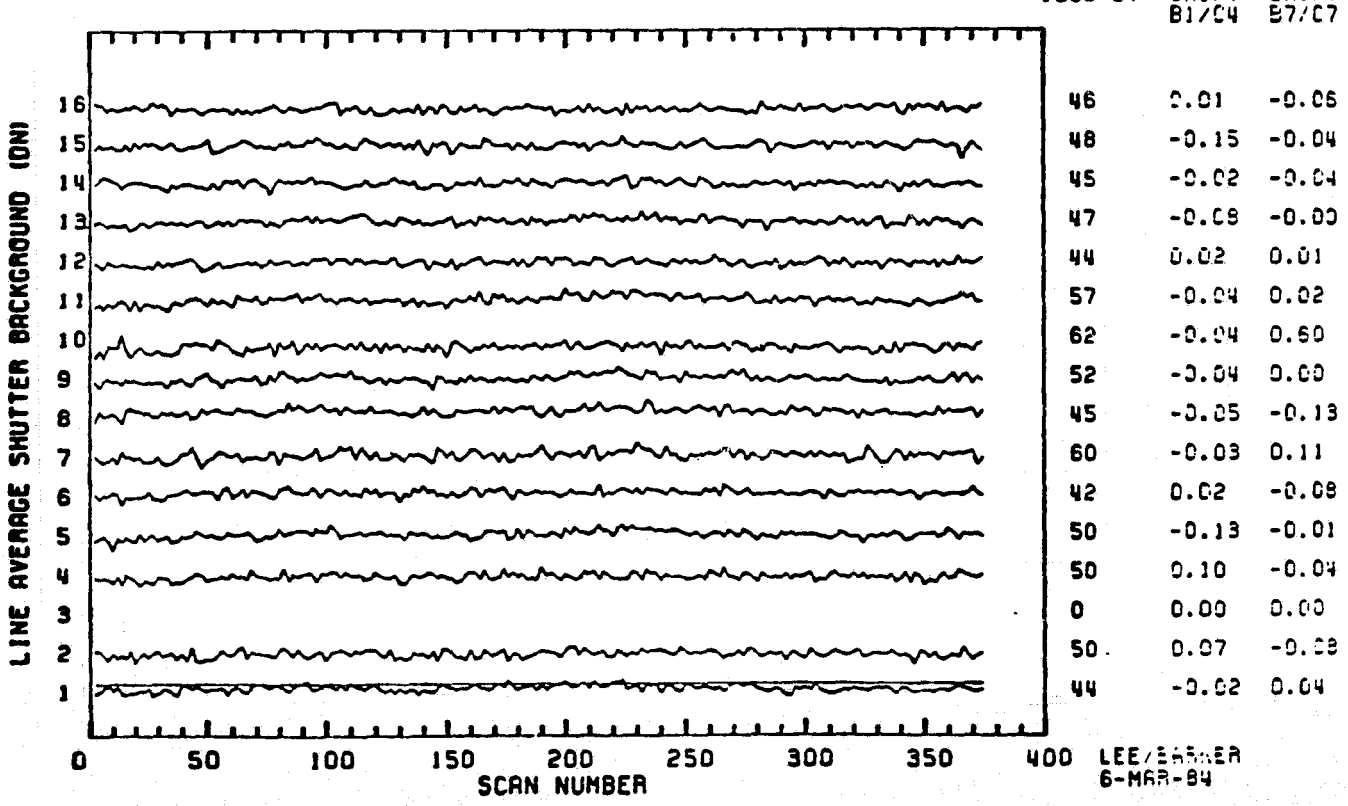

SCENE ID=40392-18152, BAND 7 (FORWARD)
SHUTTER BACKGROUND 1 SPECTRA AFTER CORRECTION

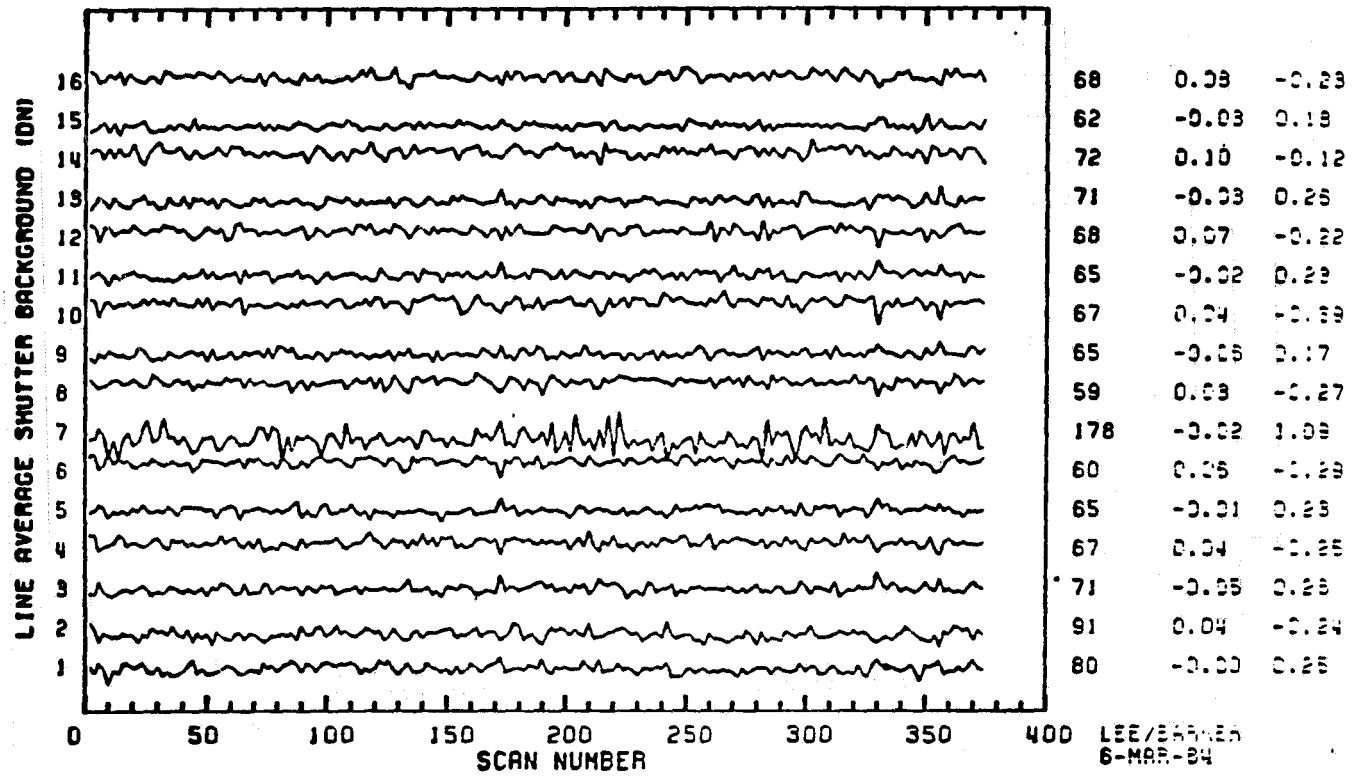

SCENE ID=40392-18152, BAND 7 (REVERSE)
SHUTTER BACKGROUND 1 SPECTRA AFTER CORRECTION

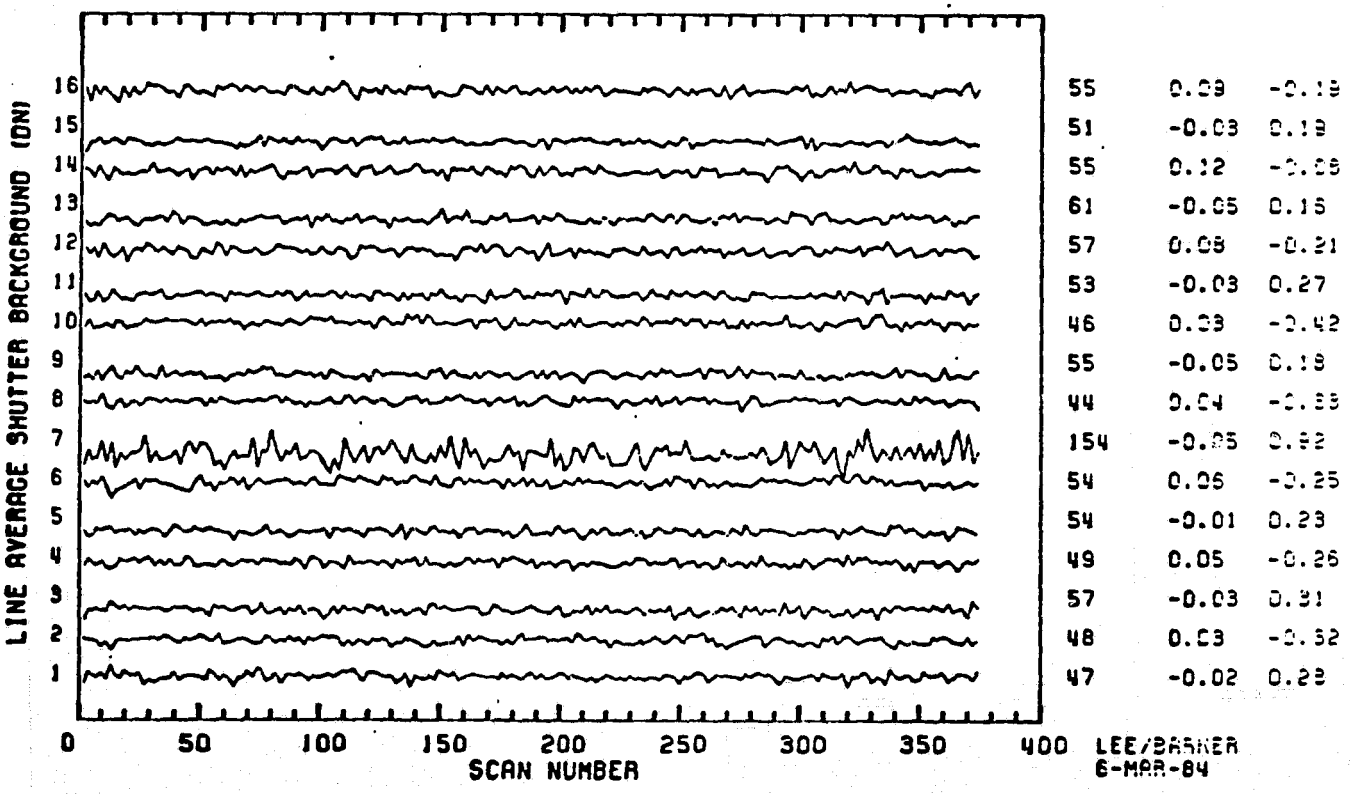

SCENE ID=40392-18152, BAND 7 (FORWARD)
SHUTTER BACKGROUND 2 SPECTRA AFTER CORRECTION

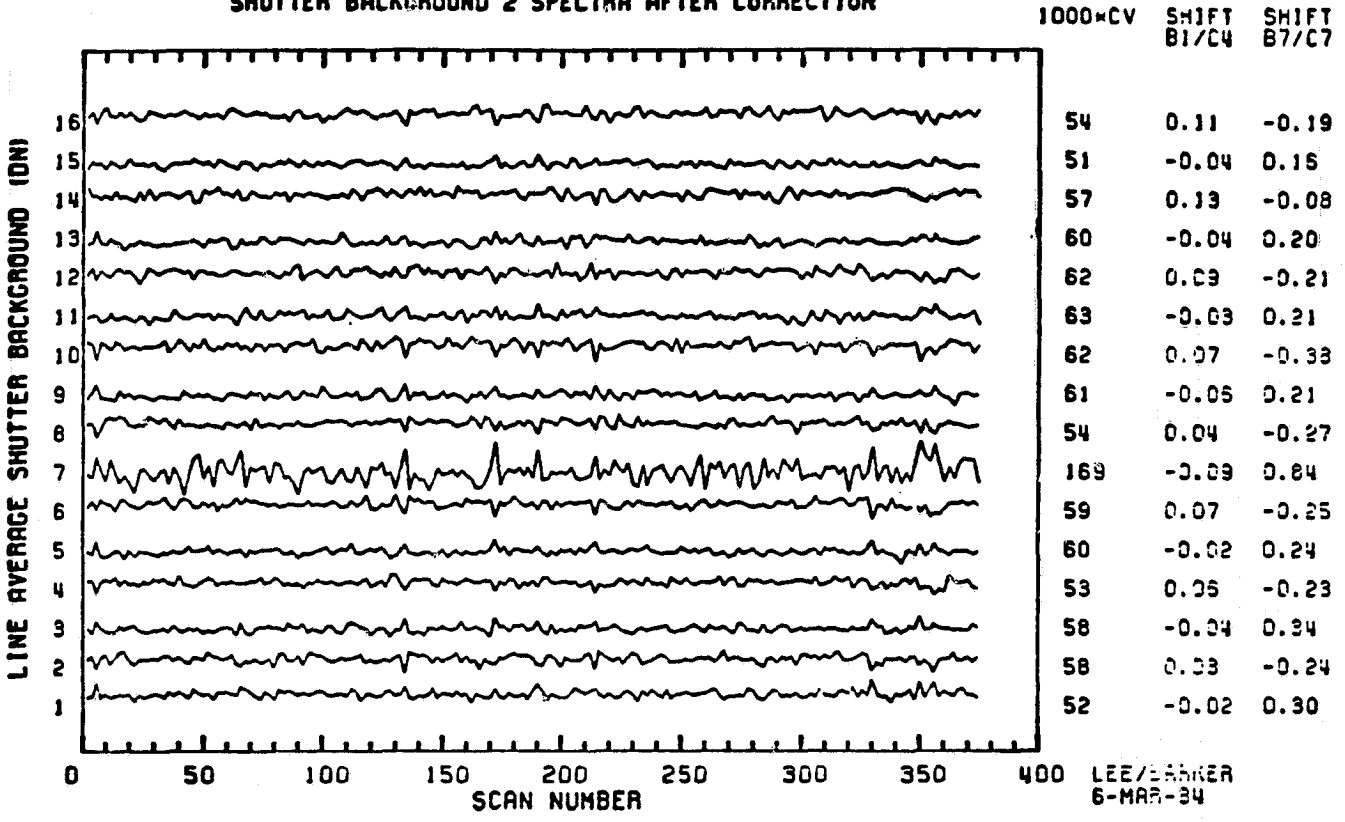

SCENE ID=40392-18152, BAND 7 (REVERSE)
SHUTTER BACKGROUND 2 SPECTRA AFTER CORRECTION

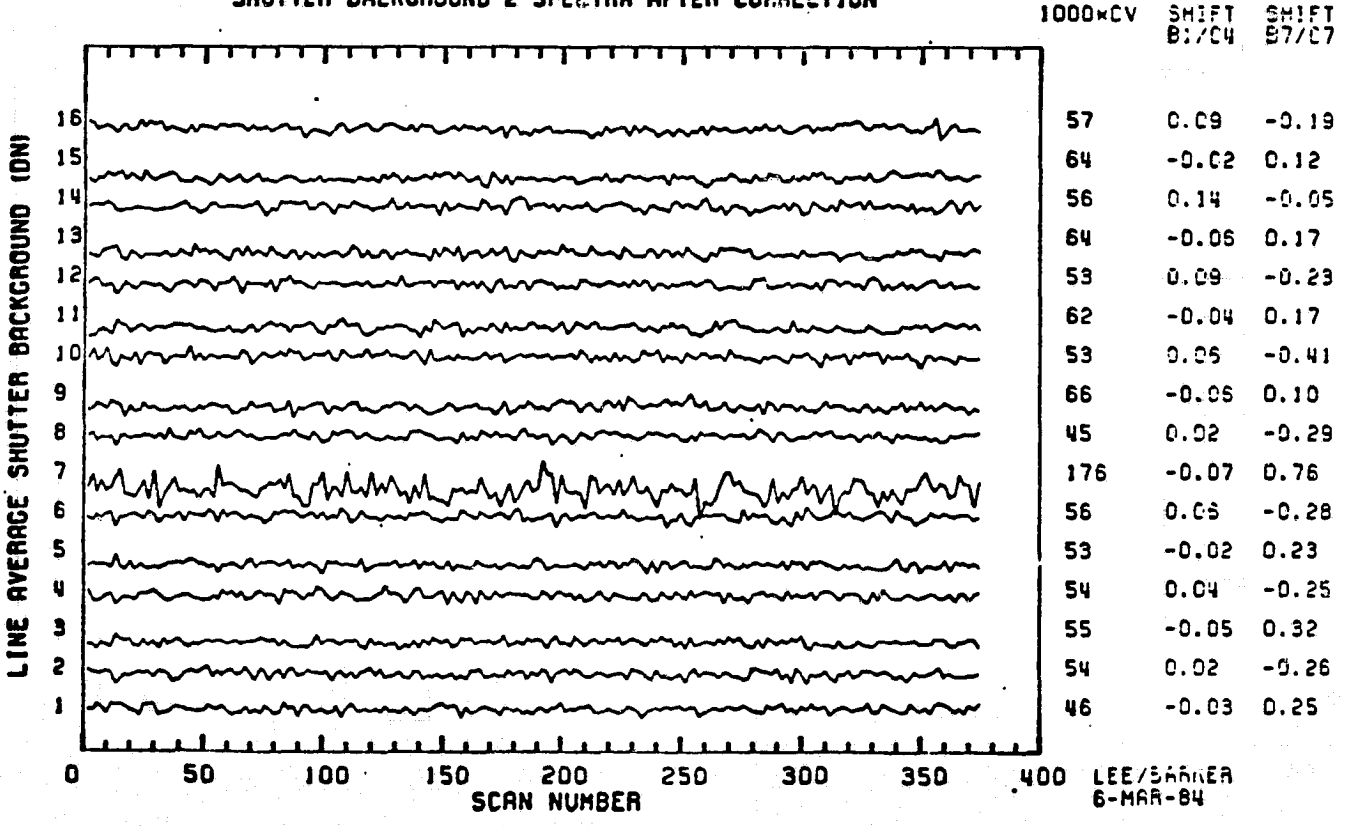

APPENDIX 9.10 - TM/F PLOTS OF "SHIFTED" BACKGROUND VERSUS SCAN

Landsat-5 TM/F averaged shutter backgrounds before DC restoration are plotted versus scan number for illustrative forward scans before and after being corrected (Section 4.5) for scan-correlated shifts of type 5-3 (Landsat-5 Band 3, Channel 1) for in-orbit data (NASA ID 50005-16221) and prelaunch data (5-596-13285). These plots are included as follows:

9.10.1	50005-16221	Band 1
9.10.2	50005-16221	Band 2
9.10.3	50005-16221	Band 3
9.10.4	50005-16221	Band 4
9.10.5	50005-16221	Band 5
9.10.6	5-596-13285	Band 5
9.10.7	5-596-13285	Band 7
9.10.8	5-596-13285	Band 6 (FWD/REV).

SCENE ID=50005-16221, BAND 1 (FORWARD)
SHUTTER BACKGROUND 1 SPECTRA BEFORE CORRECTION

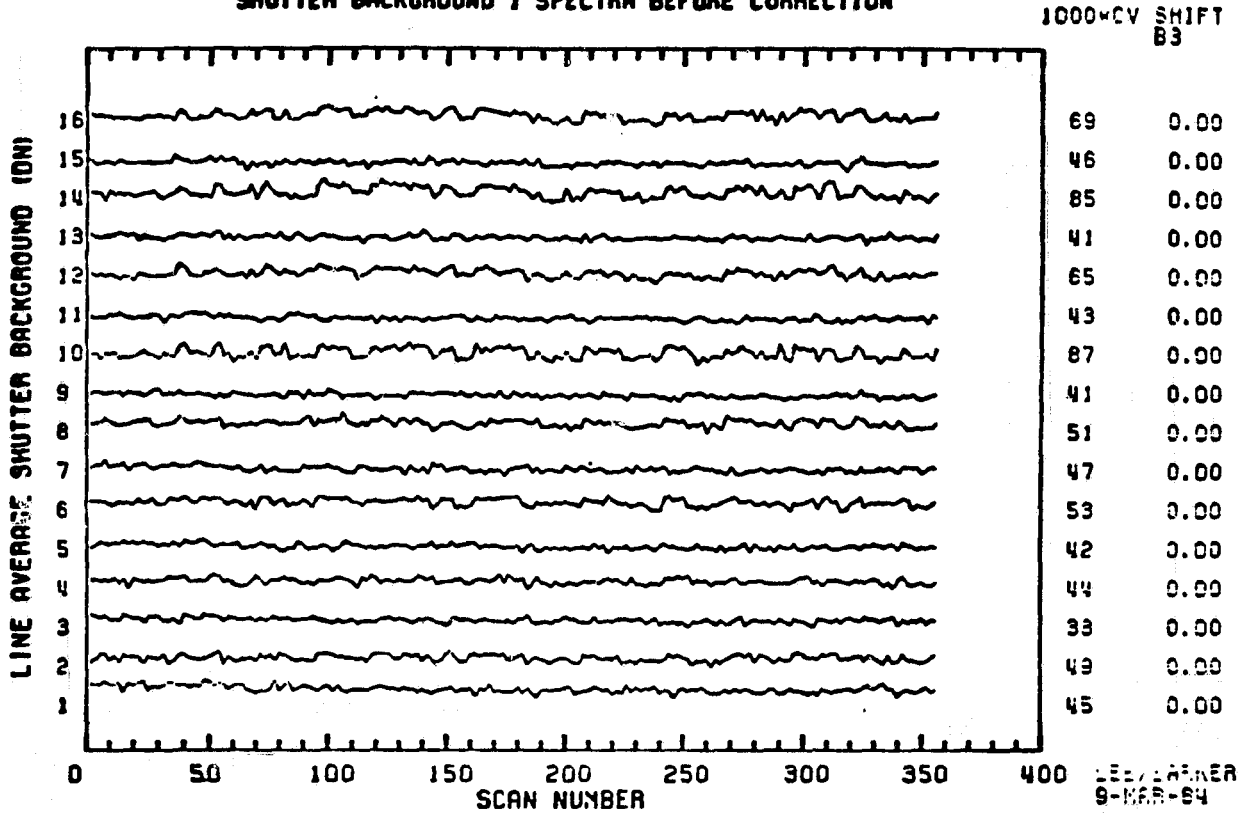

SCENE ID=50005-16221, BAND 1 (FORWARD)
SHUTTER BACKGROUND 1 SPECTRA AFTER CORRECTION

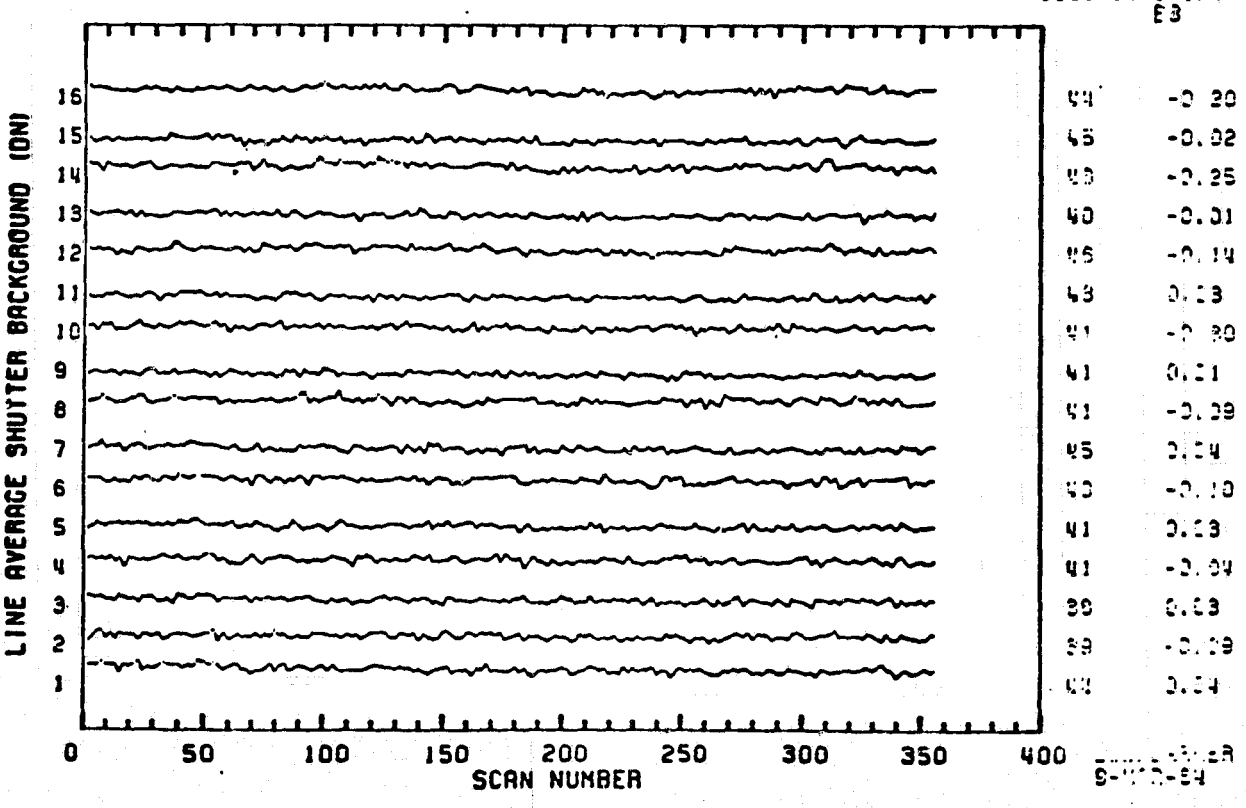

SCENE ID=50005-16221, BAND 2 (FORWARD)
SHUTTER BACKGROUND 1 SPECTRA BEFORE CORRECTION

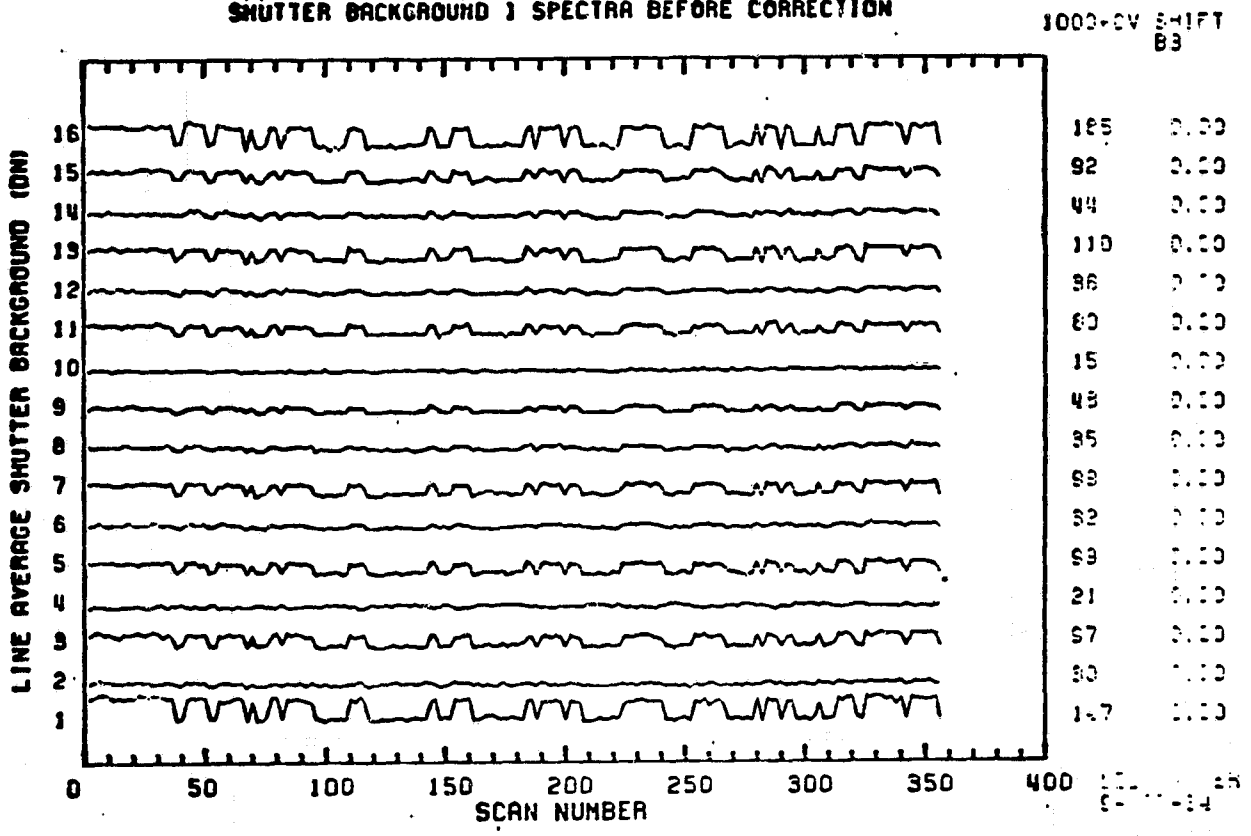

SCENE ID=50005-16221, BAND 2 (FORWARD)
SHUTTER BACKGROUND 1 SPECTRA AFTER CORRECTION

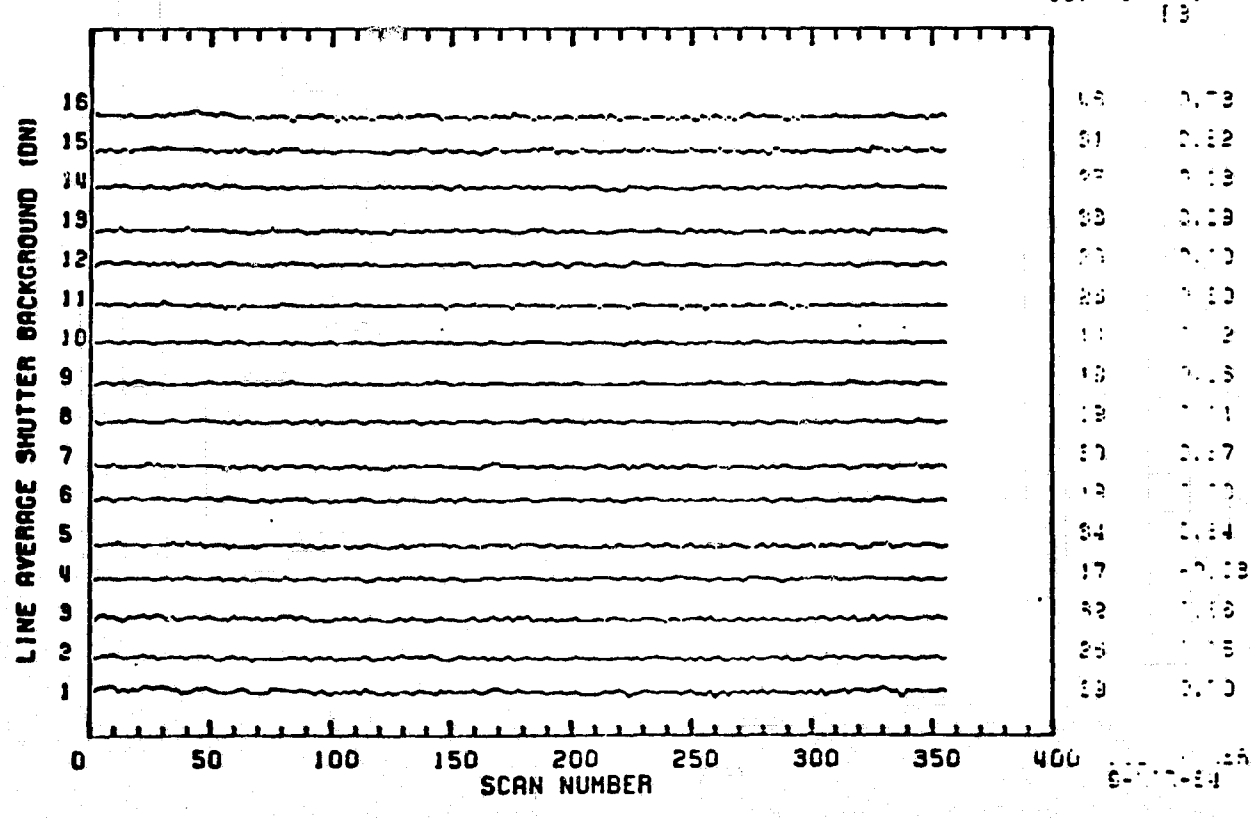

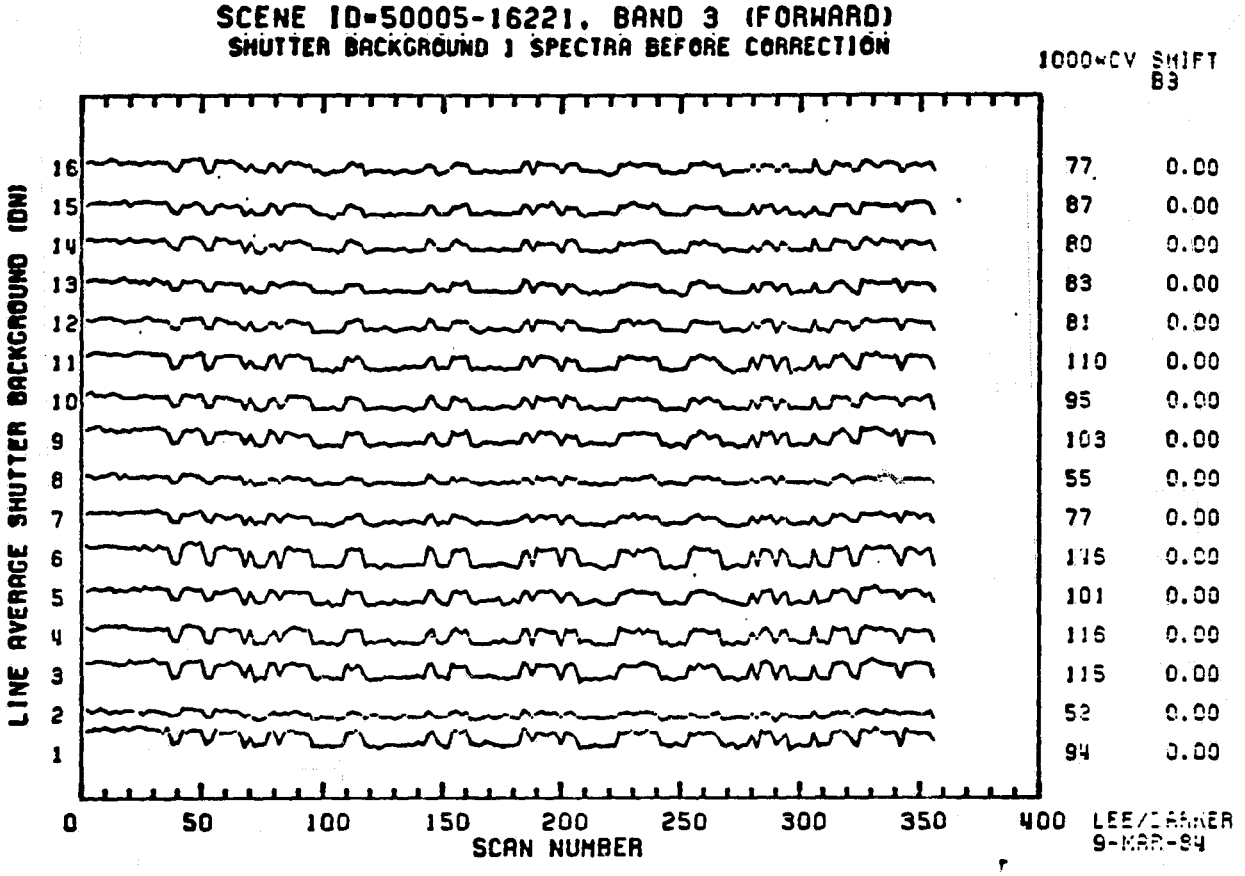

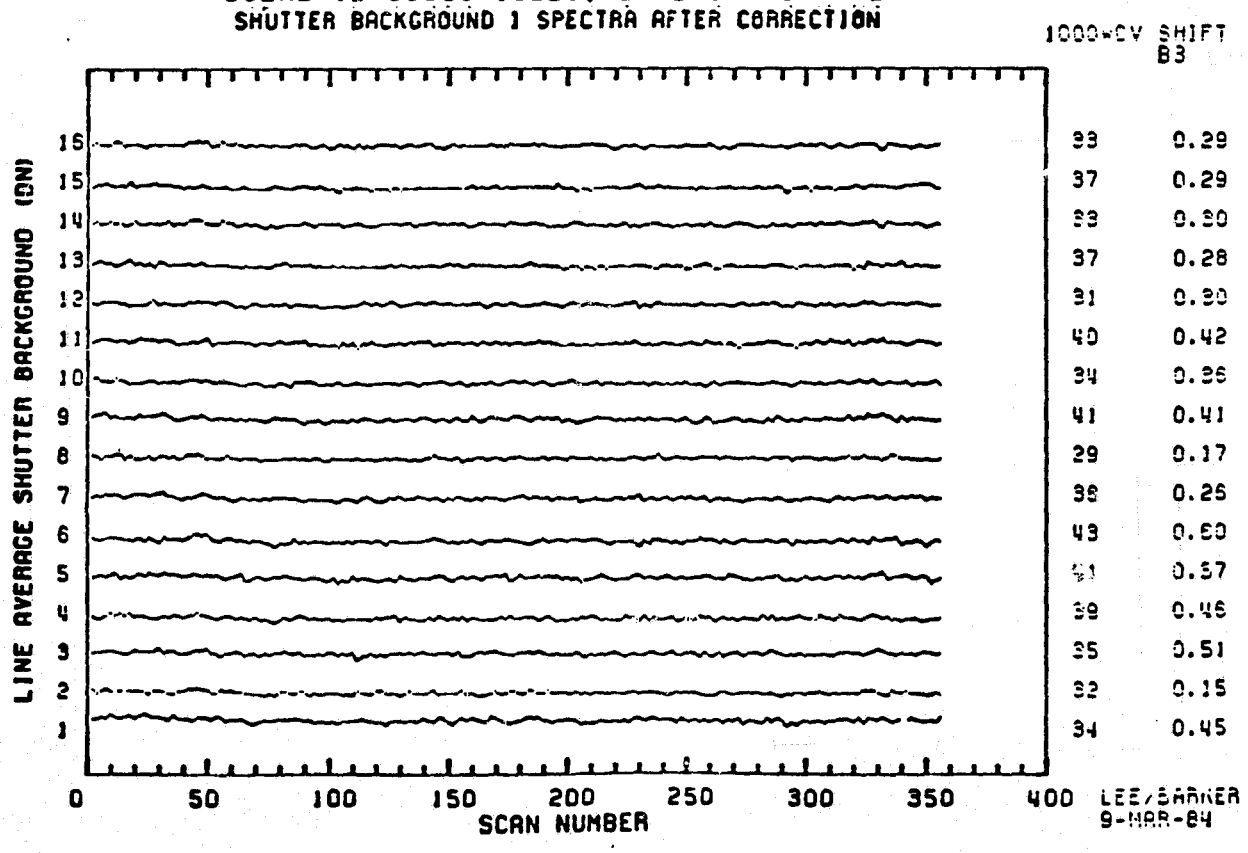

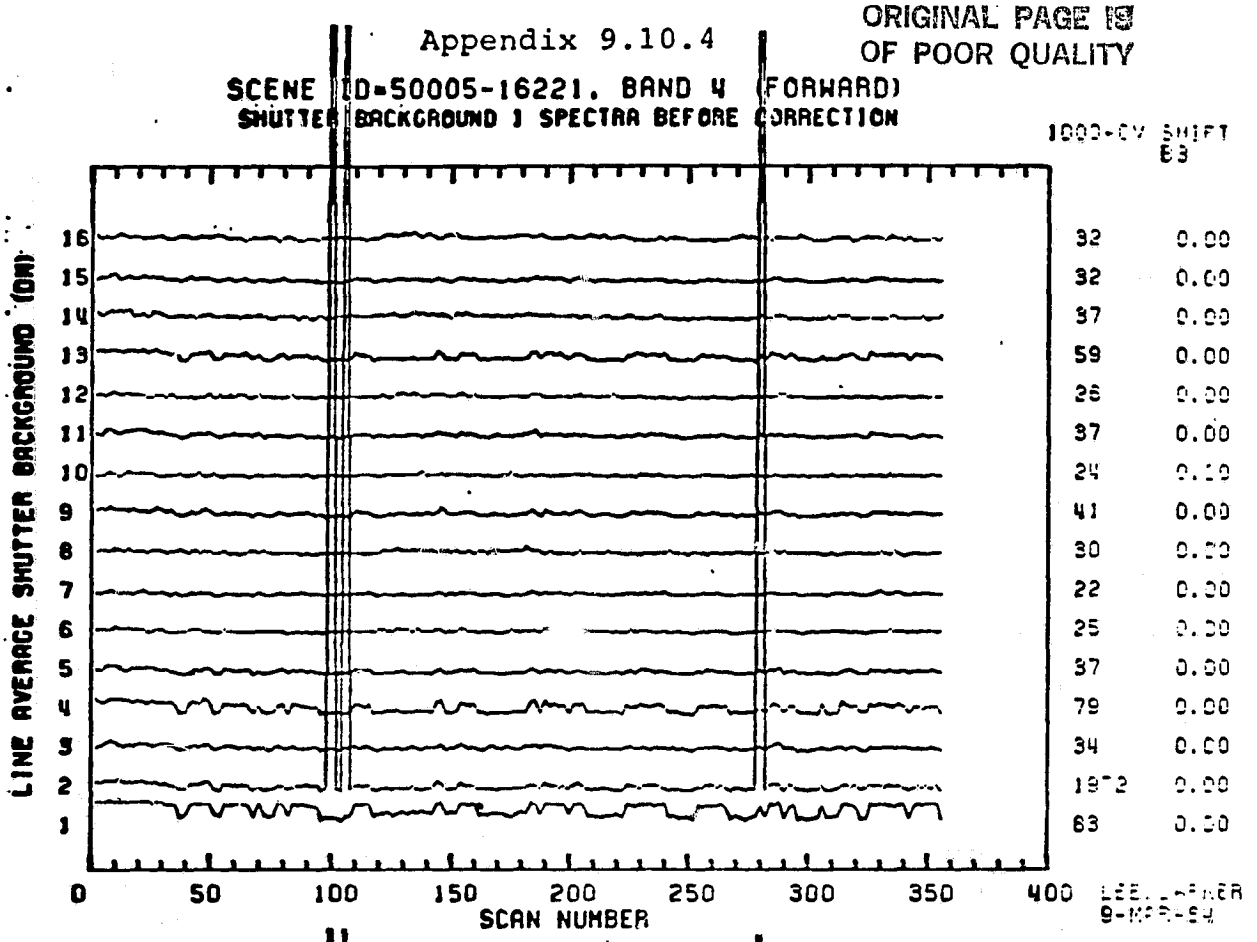

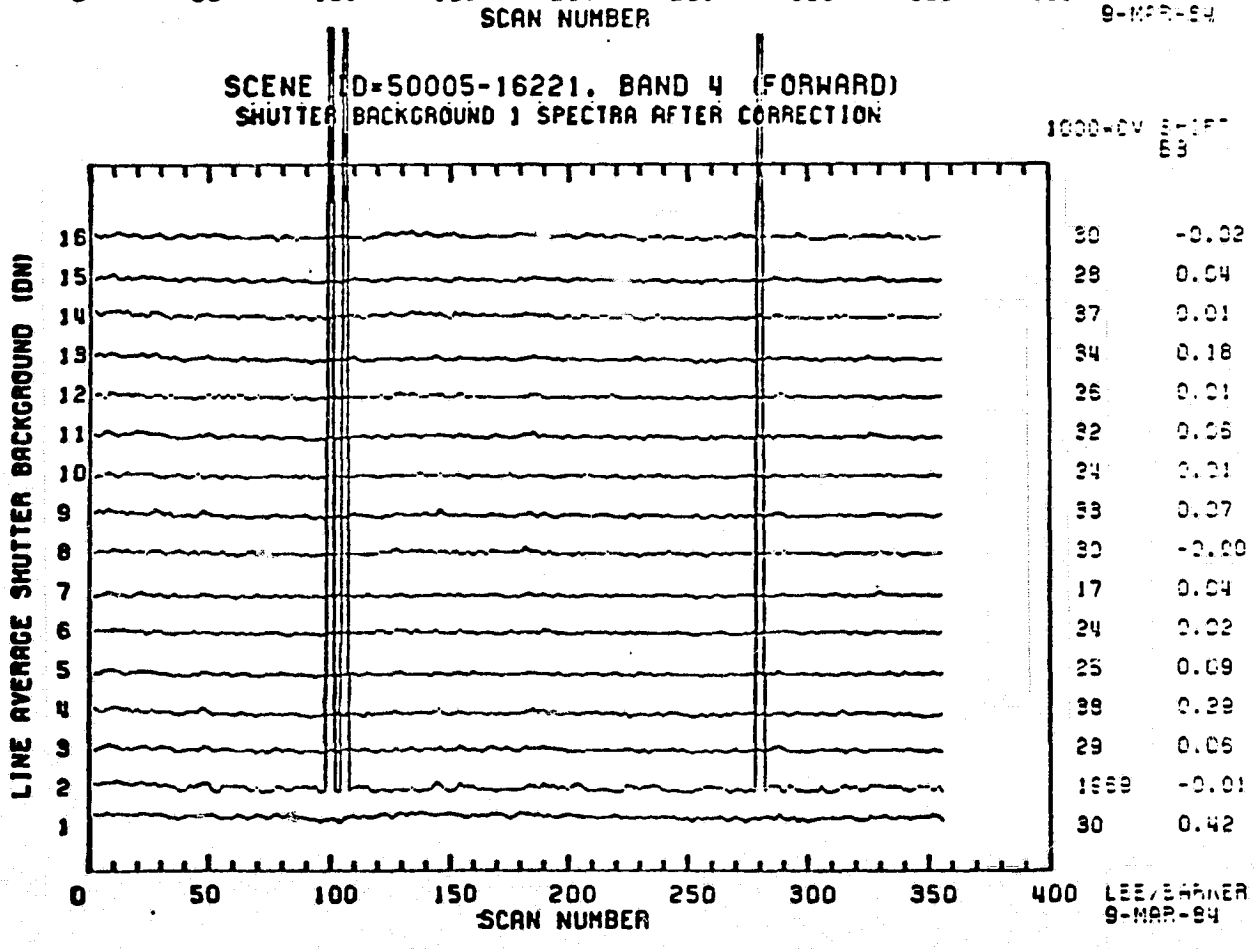

SCENE ID=50005-16221, BAND 5 (FORWARD)
SHUTTER BACKGROUND 1 SPECTRA BEFORE CORRECTION

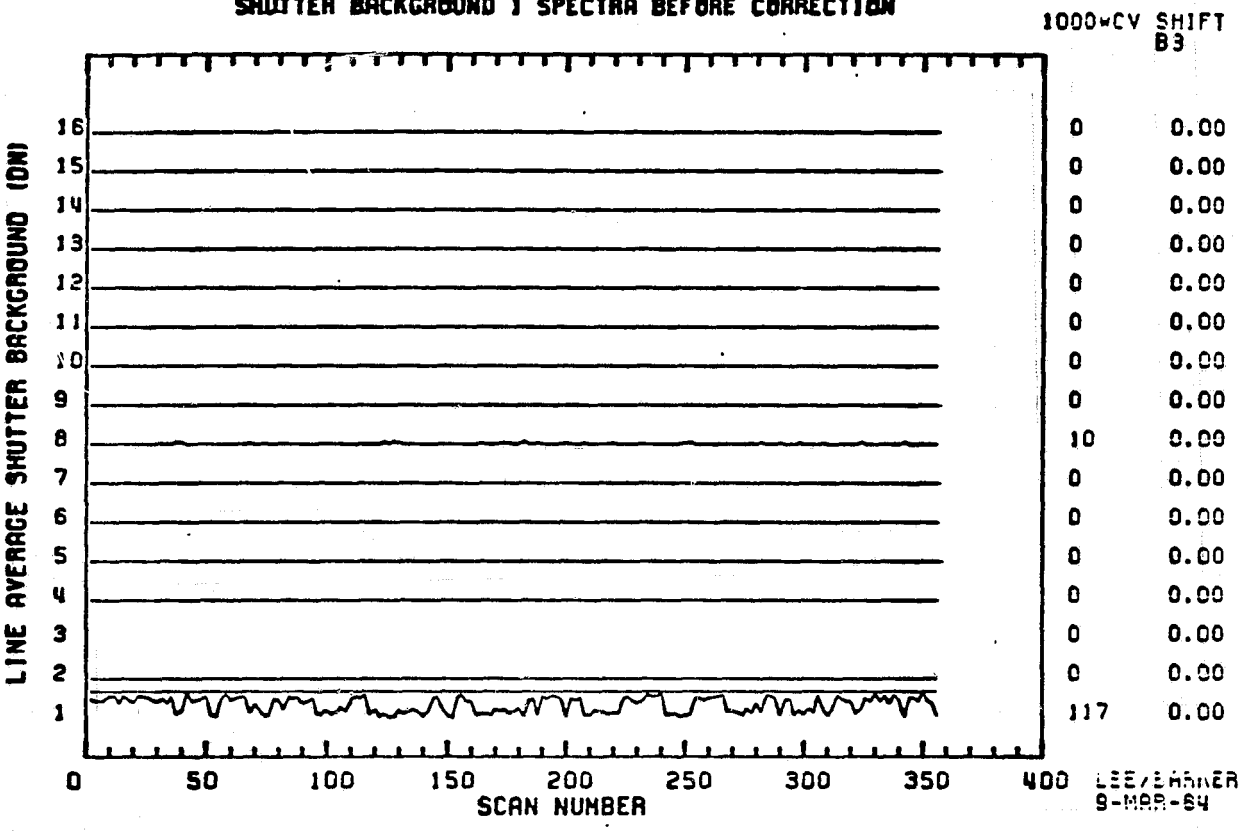

SCENE ID=50005-16221, BAND 5 (FORWARD)
SHUTTER BACKGROUND 1 SPECTRA AFTER CORRECTION

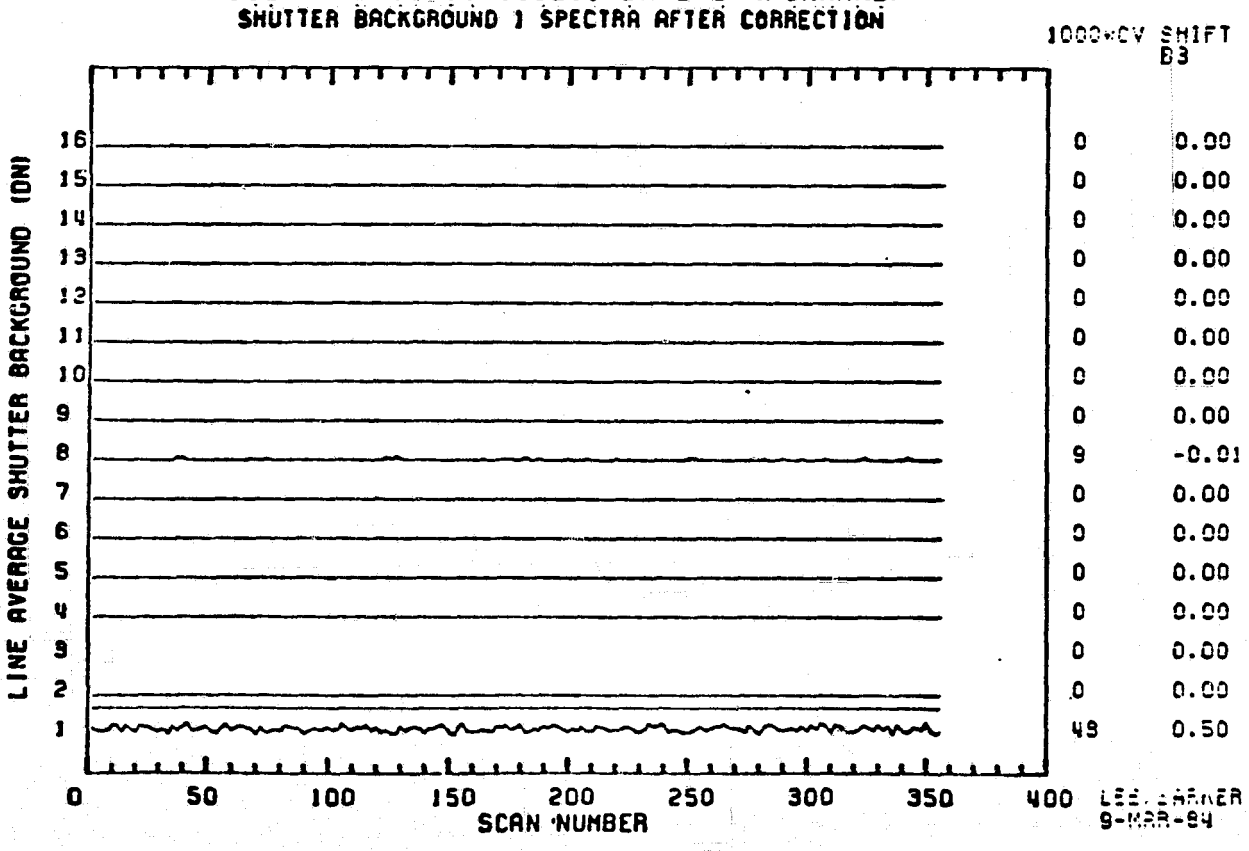

SCENE ID=5-596-13285, BAND 5 (FORWARD)
SHUTTER BACKGROUND : SPECTRA BEFORE CORRECTION

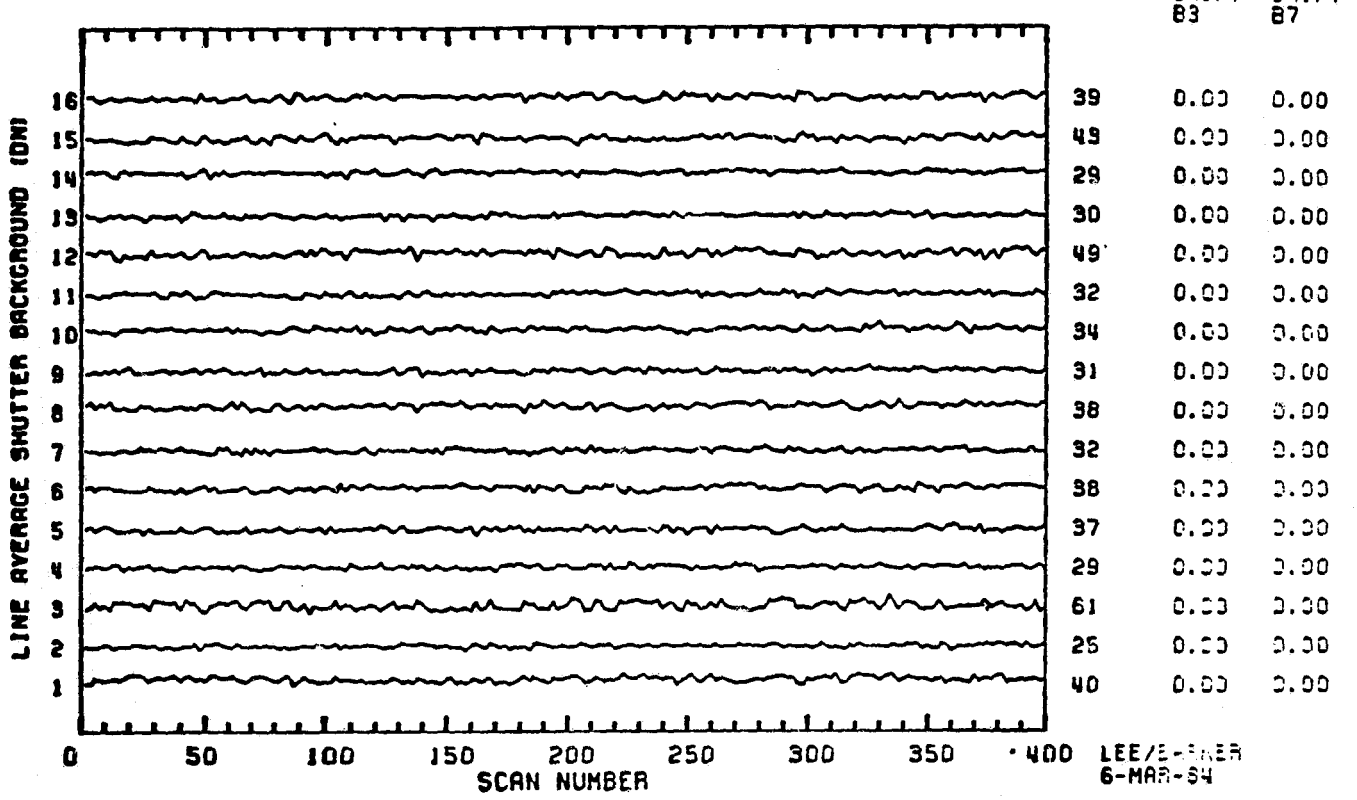

	1000×CV	SHIFT B3	SHIFT B7
16	39	0.00	0.00
15	49	0.00	0.00
14	29	0.00	0.00
13	30	0.00	0.00
12	49	0.00	0.00
11	32	0.00	0.00
10	34	0.00	0.00
9	31	0.00	0.00
8	38	0.00	0.00
7	32	0.00	0.00
6	38	0.00	0.00
5	37	0.00	0.00
4	29	0.00	0.00
3	61	0.00	0.00
2	25	0.00	0.00
1	40	0.00	0.00

LEE/BARNER
6-MAR-94

SCENE ID=5-596-13285, BAND 5 (FORWARD)
SHUTTER BACKGROUND) SPECTRA AFTER CORRECTION

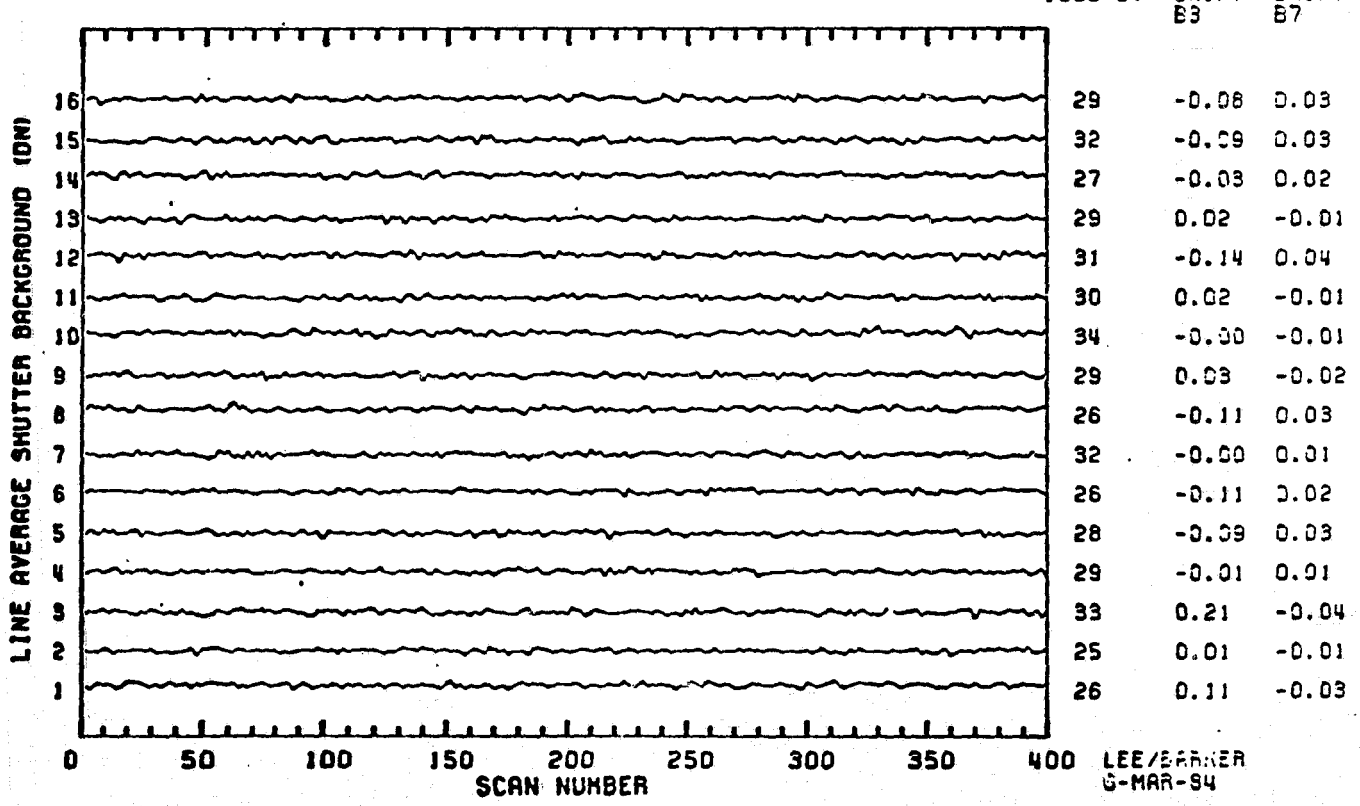

	1000×CV	SHIFT B3	SHIFT B7
16	29	-0.08	0.03
15	32	-0.09	0.03
14	27	-0.03	0.02
13	29	0.02	-0.01
12	31	-0.14	0.04
11	30	0.02	-0.01
10	34	-0.00	-0.01
9	29	0.03	-0.02
8	26	-0.11	0.03
7	32	-0.00	0.01
6	26	-0.11	0.02
5	28	-0.09	0.03
4	29	-0.01	0.01
3	33	0.21	-0.04
2	25	0.01	-0.01
1	26	0.11	-0.03

LEE/BARNER
6-MAR-94

SCENE ID=5-596-13285, BAND 7 (FORWARD)
SHUTTER BACKGROUND 1 SPECTRA BEFORE CORRECTION

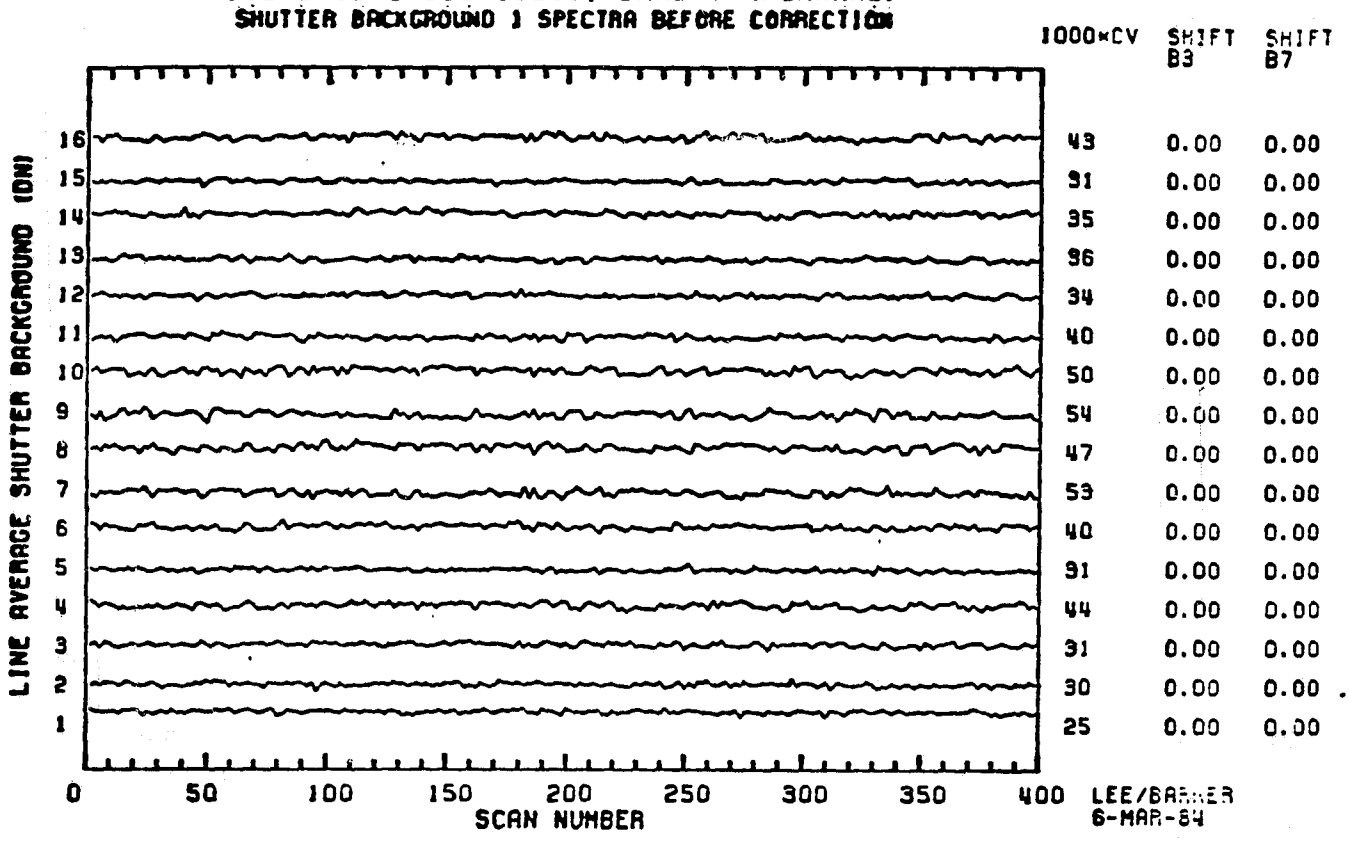

SCENE ID=5-596-13285, BAND 7 (FORWARD)
SHUTTER BACKGROUND 1 SPECTRA AFTER CORRECTION

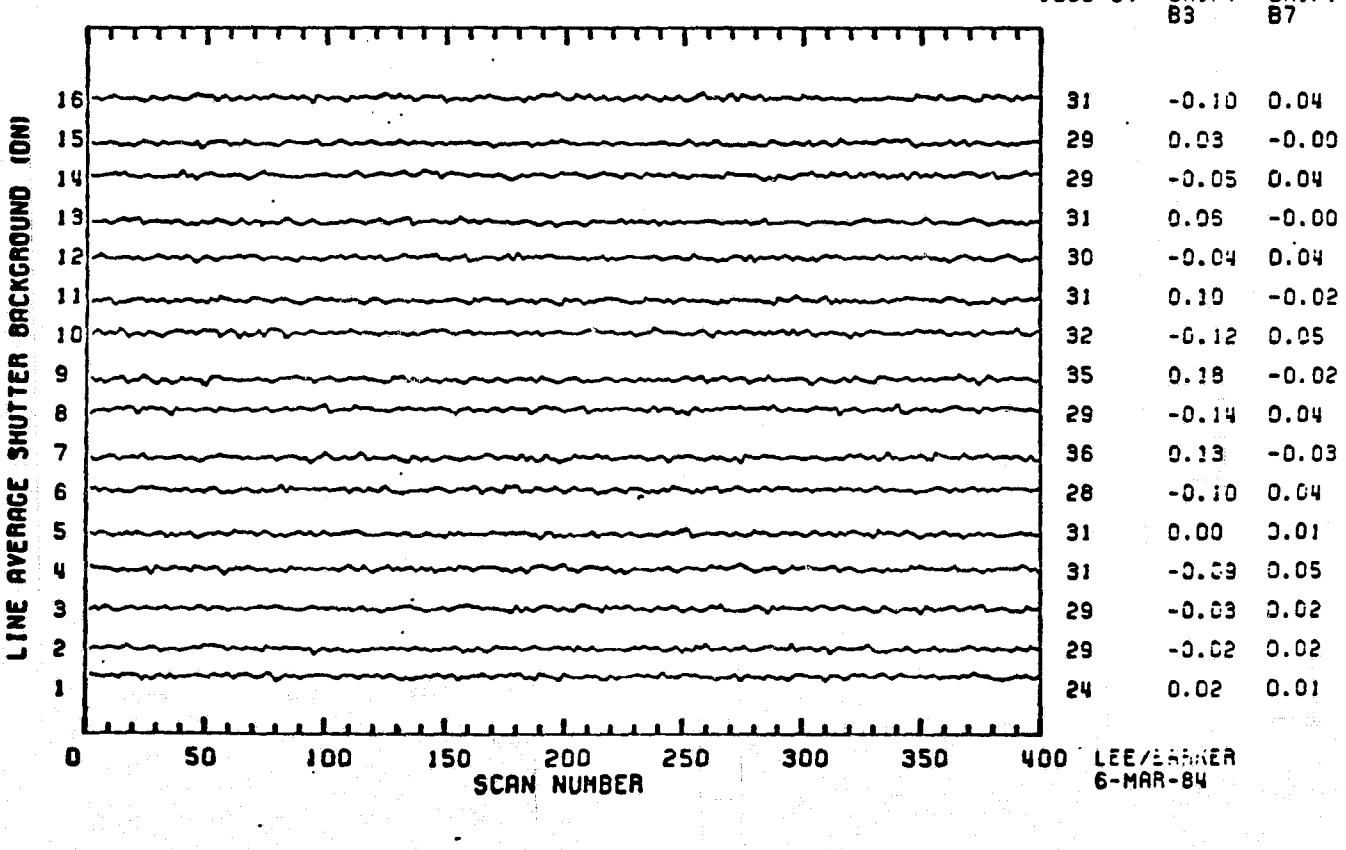

SCENE ID=5-596-13285, BAND 6 (FORWARD)
SHUTTER BACKGROUND) SPECTRA BEFORE CORRECTION

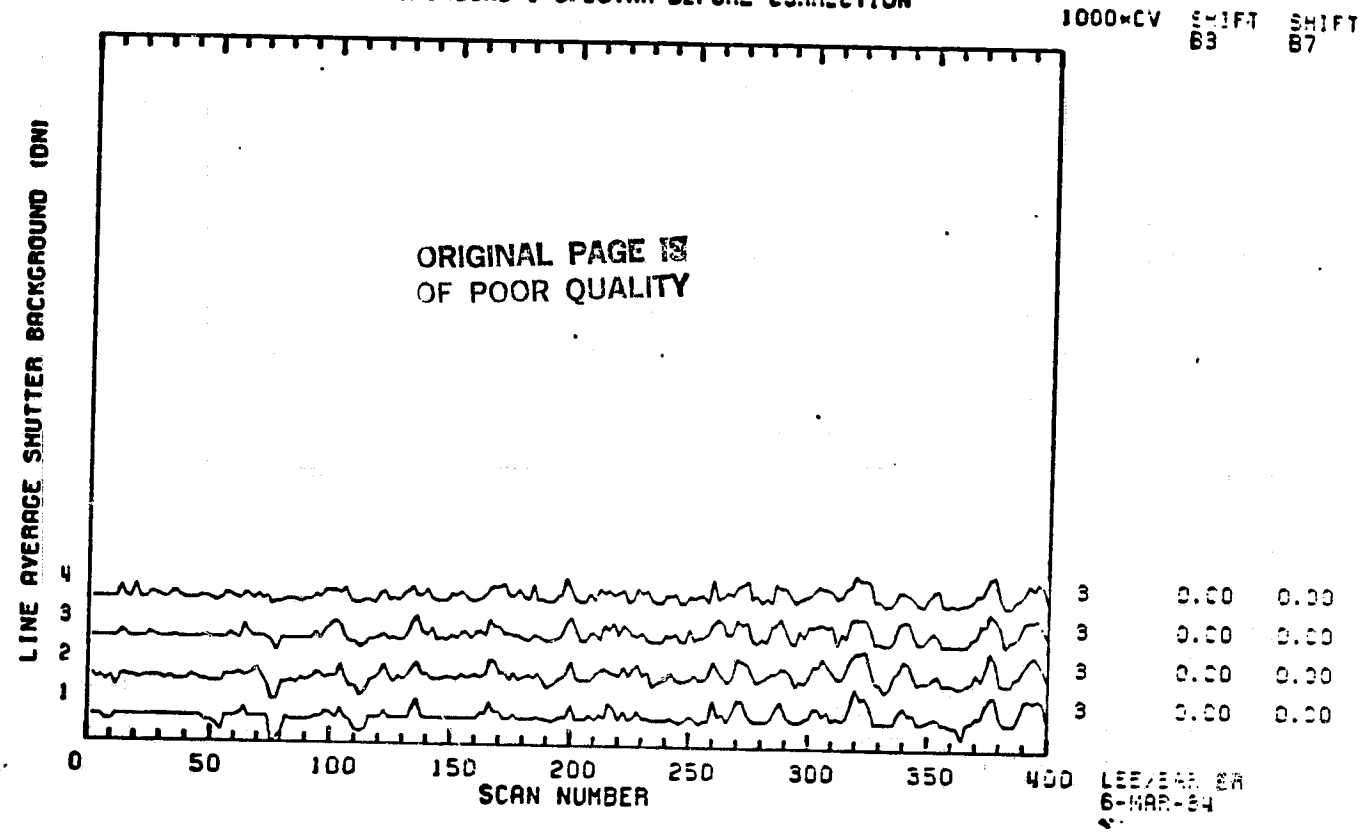

SCENE ID=5-596-13285, BAND 6 (REVERSE)
SHUTTER BACKGROUND) SPECTRA BEFORE CORRECTION

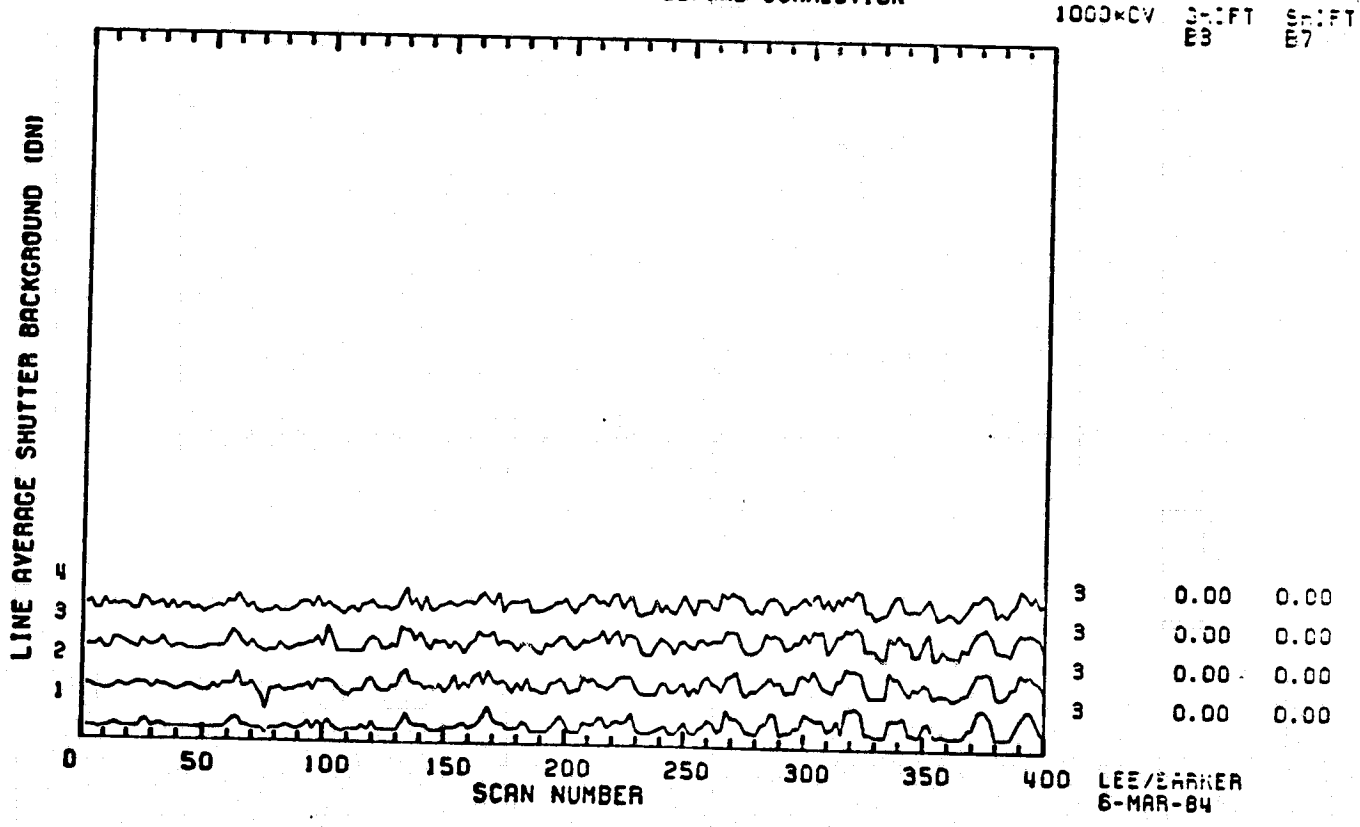

APPENDIX 9.11 - TM/F TABLES OF SCAN-CORRELATED SHIFTS

Landsat-5 TM/F within-scene tabulations (Section 4.5) of scan-correlated shifts by forward and reverse scans for type 5-3 (Landsat-5 Band 3, Channel 1) in Shutter regions before (shutter 1) and after (shutter 2) DC restoration for in-orbit data (NASA ID 50005-16221) and pre-launch tests (5-596-13285 and "golden tape" 5-198-10563) are included in this Appendix as follows:

9.11.1 TM/F Band 1 Shift 5-3
9.11.2 TM/F Band 2 Shift 5-3
9.11.3 TM/F Band 3 Shift 5-3
9.11.4 TM/F Band 4 Shift 5-3
9.11.5 TM/F Band 5 Shift 5-3
9.11.6 TM/F Band 7 Shift 5-3.

TYPE 5-3 SCAN-CORRELATED SHIFTS
BAND 1 LANDSAT-5 TM/F

	PRE-LAUNCH 5-596-13285		PRE-LAUNCH 5-198-10563				IN-ORBIT 50005-16221		
	SHUTTER 1		SHUTTER 1		SHUTTER 2		SHUTTER 1		
CH	FWD	REV	FWD	REV	FWD	REV	FWD	REV	CH
16	−.13	−.21	−.21	−.20	−.17	−.18	−.20	−.23	16
15	−.05	−.07	−.01	−.01	−.00	−.02	−.02	−.02	15
14	−.20	−.20	−.25	−.24	−.23	−.20	−.25	−.31	14
13	−.03	−.04	−.01	−.01	−.00	−.02	−.01	−.03	13
12	−.22	−.25	−.20	−.18	−.17	−.19	−.14	−.20	12
11	.01	.00	.00	−.01	.01	.01	.03	.02	11
10	−.16	−.19	−.25	−.25	−.23	−.19	−.30	−.34	10
9	−.00	−.01	.02	.03	.01	.04	.01	−.01	9
8	−.13	−.10	−.12	−.16	−.15	−.10	−.09	−.09	8
7	.04	.04	.08	.05	.11	.08	.04	.02	7
6	−.19	−.17	−.20	−.19	−.17	−.16	−.10	−.13	6
5	−.02	−.02	.01	.00	.01	.02	.03	−.01	5
4	−.12	−.09	−.09	−.10	−.12	−.12	−.04	−.10	4
3	−.14	−.01	.04	.04	.04	.02	.03	.00	3
2	−.14	−.16	−.13	−.13	−.13	−.17	−.09	−.15	2
1	−.04	−.03	.03	.01	.02	.00	.04	−.01	1

J. Barker/Y. Lee MAR 84 GSFC

9622(641/84

Appendix 9.11.2

TYPE 5-3 SCAN-CORRELATED SHIFTS
BAND 2 LANDSAT-5 TM/F

	PRE-LAUNCH 5-596-13285		PRE-LAUNCH 5-198-10563				IN-ORBIT 50005-16221		
	SHUTTER 1		SHUTTER 1		SHUTTER 2		SHUTTER 1		
CH	FWD	REV	FWD	REV	FWD	REV	FWD	REV	CH
16	.15	.16	.23	.21	.22	.23	.73	.75	16
15	.07	.07	.12	.13	.16	.12	.32	.37	15
14	.06	.07	.05	.05	.07	.07	.13	.20	14
13	.07	.08	.14	.14	.15	.12	.39	.41	13
12	−.02	−.02	.01	.00	.00	−.00	.10	.15	12
11	.05	.04	.10	.07	.11	.07	.30	.34	11
10	.00	.00	.00	.00	.00	.00	.02	.03	10
9	.03	.02	.07	.05	.07	.05	.16	.21	9
8	.03	.03	.04	.02	.03	.02	.11	.15	8
7	.09	.09	.13	.15	.16	.15	.37	.37	7
6	.04	.02	.04	.03	.04	.03	.08	.14	6
5	.12	.13	.17	.22	.20	.22	.34	.35	5
4	−.01	−.01	−.00	−.00	−.00	−.00	−.03	−.04	4
3	.18	.16	.23	.19	.23	.20	.38	.42	3
2	.02	.06	.06	.09	.06	.05	.05	.03	2
1	.55	.50	.54	.48	.55	.52	.70	.73	1

J. Barker/Y. Lee MAR 84 GSFC

Appendix 9.11.3

TYPE 5-3 SCAN-CORRELATED SHIFTS
BAND 3 LANDSAT-5 TM/F

	PRE-LAUNCH 5-596-13285		PRE-LAUNCH 5-198-10563				IN-ORBIT 50005-16221		
	SHUTTER 1		SHUTTER 1		SHUTTER 2		SHUTTER 1		
CH	FWD	REV	FWD	REV	FWD	REV	FWD	REV	CH
16	.23	.22	.24	.25	.29	.23	.29	.32	16
15	.24	.24	.26	.30	.34	.27	.29	.39	15
14	.20	.20	.21	.24	.24	.20	.30	.36	14
13	.25	.24	.29	.35	.33	.28	.28	.33	13
12	.17	.19	.30	.31	.33	.32	.30	.30	12
11	.27	.22	.25	.32	.35	.24	.42	.49	11
10	.20	.21	.20	.24	.23	.18	.36	.42	10
9	.28	.28	.29	.30	.30	.25	.41	.47	9
8	.14	.14	.12	.13	.14	.09	.17	.22	8
7	.25	.20	.24	.27	.28	.25	.26	.30	7
6	.27	.26	.31	.35	.31	.31	.60	.65	6
5	.27	.24	.28	.29	.32	.26	.37	.42	5
4	.29	.28	.38	.41	.39	.38	.46	.50	4
3	.38	.39	.42	.45	.48	.45	.51	.52	3
2	.12	.14	.17	.20	.20	.15	.15	.18	2
1	.46	.46	.49	.50	.52	.44	.45	.45	1

J. Barker/Y. Lee MAR 84 GSFC

9822(64)/84

Appendix 9.11.4

TYPE 5-3 SCAN-CORRELATED SHIFTS
BAND 4 LANDSAT-5 TM/F

	PRE-LAUNCH 5-596-13285		PRE-LAUNCH 5-198-10563				IN-ORBIT 50005-16221		
	SHUTTER 1		SHUTTER 1		SHUTTER 2		SHUTTER 1		
CH	FWD	REV	FWD	REV	FWD	REV	FWD	REV	CH
16	.02	.01	.03	.01	.03	.02	−.02	−.03	16
15	.04	.03	.13	.05	.12	.07	.04	.07	15
14	.02	.03	.04	.02	.04	.03	.01	.02	14
13	.06	.10	.18	.09	.16	.09	.18	.27	13
12	.01	.01	.01	.00	.01	.02	.01	.00	12
11	.06	.06	.15	.10	.19	.12	.06	.06	11
10	.00	.00	.00	−.00	.01	.00	.01	.01	10
9	.03	.04	.11	.04	.12	.05	.07	.11	9
8	.00	.01	.01	.01	.01	.01	−.00	−.01	8
7	.00	.01	.03	.02	.03	.02	.04	.06	7
6	.01	.01	.03	.02	.04	.03	.02	.03	6
5	.01	.02	.06	.03	.06	.03	.09	.13	5
4	.11	.17	.26	.12	.23	.17	.29	.33	4
3	.10	.11	.21	.14	.20	.14	.06	.06	3
2	.08	.11	.21	.08	.18	.13	−.01	.16	2
1	.35	.32	.18	.31	.24	.29	.42	.34	1

J. Barker/Y. Lee MAR 84 GSFC

9622(641)/84

Appendix 9.11.5

TYPE 5-3 SCAN-CORRELATED SHIFTS
BAND 5 LANDSAT-5 TM/F

	PRE-LAUNCH 5-596-13285		PRE-LAUNCH 5-198-10563 (NOISY)				IN-ORBIT 50005-16221		
	SHUTTER 1		SHUTTER 1		SHUTTER 2		SHUTTER 1		
CH	FWD	REV	FWD	REV	FWD	REV	FWD	REV	CH
16	−.08	−.10	−.23	−.21	−.26	−.14	.00	.00	16
15	−.09	−.08	−.01	.01	.01	.08	.00	.00	15
14	−.03	−.04	−.23	−.24	−.25	−.16	.00	.00	14
13	.02	.01	.10	.11	.11	.18	.00	.00	13
12	−.14	−.13	−.29	−.29	−.29	−.20	.00	.00	12
11	−.00	.02	.16	.12	.16	.23	.00	.00	11
10	−.00	.02	−.21	.18	−.11	−.06	.00	.00	10
9	.03	.03	.24	.22	.23	.34	.00	.00	9
8	−.09	−.11	−.30	−.33	−.32	−.19	−.01	−.00	8
7	−.00	−.08	.25	.22	.23	.33	.00	.00	7
6	−.11	−.08	−.23	−.22	−.25	−.14	.00	.00	6
5	−.09	−.06	.07	.06	.06	.13	.00	.00	5
4	−.01	−.01	−.18	−.17	−.18	−.11	.00	.00	4
3	.21	.21	—	—	—	—	.00	.00	3
2	.01	.01	−.18	−.13	−.14	−.08	.00	.00	2
1	.11	.14	.14	.12	.15	.18	.50	.55	1

J. Barker/Y. Lee MAR 84 GSFC

9622(64a1/84

Appendix 9.11.6

TYPE 5-3 SCAN-CORRELATED SHIFTS
BAND 7 LANDSAT-5 TM/F

	PRE-LAUNCH 5-596-13285		PRE-LAUNCH 5-198-10563 (NOISY)			
	SHUTTER 1		SHUTTER 1		SHUTTER 2	
CH	FWD	REV	FWD	REV	FWD	REV
16	−.10	−.10	−.21	−.23	−.25	−.14
15	.03	.02	.09	.08	.09	.13
14	−.05	−.07	−.27	−.27	−.29	−.16
13	.06	.08	.11	.10	.11	.16
12	−.04	−.05	−.34	−.32	−.36	−.20
11	.10	.09	.13	.15	.13	.18
10	−.12	−.12	−.53	−.46	−.56	−.32
9	.18	.17	.16	.18	.16	.25
8	−.14	−.13	−.47	−.41	−.49	−.29
7	.13	.17	.16	.18	.17	.22
6	−.10	−.08	−.27	−.29	−.35	−.16
5	.00	.02	.09	.09	.09	.14
4	−.09	−.09	−.27	−.29	−.29	−.17
3	−.03	−.04	.05	.04	.04	.12
2	−.02	−.01	−.23	−.24	−.26	−.16
1	.02	.02	.09	.08	.09	.16

J. Barker/Y. Lee MAR 84 GSFC

9622(64a)/84

APPENDIX 9.12 - SHUTTER BACKGROUNDS

This appendix contains selected background counts in DN for the shutter region of both the TM/PF and TM/F sensors. These data are taken from runs of the TRAPP software on the following scenes:

APPENDIX	SENSOR	ID	DATE	LOCATION	BACKGROUND
9.2.1	TM/PF	40109-15140	2 NOV 82	Washington, DC	BDC
9.2.2	TM/PF	40392-18152	12 AUG 82	San Francisco, CA	B-BC
9.2.3	TM/PF	40392-18152	12 AUG 82	San Francisco, CA	B-ADC
9.2.4	TM/F	5-596-13285	30 AUG 83	Pre-Launch, Ambient	B-BDC
9.2.5	TM/PF	40037-02243	22 AUG 82	Washington, D.C. PM	BDC.

Each page is from a TRAPP output. There are four sets of numbers and statistical summaries for the 96 reflective channels. These in-orbit scenes both have solid formations of could; the Washington scene has clouds on the eastern edge of the lower quarter of the scene, and this San Francisco scene has clouds on the western edge increasing to about 75% cloud cover. Bright-target for the saturation effects presumbably account for the non-zero differences in forward and reverse scans.

DATA COLLECT: 4010915140/ DCGFSC RUN ON DATE: 7-FEB-83 AT TIME: 17:30:27

SHUTTER AVERAGE

CHANNEL	BAND 1	BAND 2	BAND 3	BAND 4	BAND 5	BAND 7
1	2.830	2.858	2.897	2.792	2.676	2.725
2	2.335	2.366	2.362	2.169	2.511	2.326
3	2.305	2.355	2.479	2.359	-99999.0	2.315
4	2.340	2.432	2.337	2.161	2.544	2.336
5	2.350	2.234	2.273	2.099	2.519	2.199
6	2.438	2.444	2.345	2.362	2.697	2.360
7	2.214	2.167	2.230	2.068	2.613	2.446
8	2.405	2.236	2.403	2.418	2.703	2.437
9	2.124	2.099	2.180	2.065	2.494	2.191
10	2.315	2.095	2.346	2.115	2.562	2.418
11	2.069	2.138	2.053	2.069	2.512	2.227
12	2.421	2.146	2.210	2.181	2.538	2.333
13	2.078	2.144	2.159	2.039	2.545	2.113
14	2.446	2.151	2.386	2.077	2.560	2.399
15	2.086	2.128	2.113	2.067	2.531	2.118
16	2.428	2.230	2.523	2.215	2.581	2.426
MEANODD	2.257	2.265	2.298	2.195	2.556	2.292
MEANEVN	2.391	2.263	2.364	2.212	2.587	2.379
MEANALL	2.324	2.264	2.331	2.204	2.572	2.335
MEANODD SD	0.255	0.253	0.274	0.262	0.065	0.206
MEANEVN SD	0.052	0.135	0.087	0.118	0.073	0.046
MEANALL SD	0.191	0.196	0.199	0.197	0.069	0.151
MEAN SPSD	0.038	0.049	0.050	0.049	0.018	0.038
MEANALL CV	8.212	8.650	8.537	8.934	2.672	6.470

DIFFERENCE BETWEEN FORWARD AND REVERSE AVERAGES

CHANNEL	BAND 1	BAND 2	BAND 3	BAND 4	BAND 5	BAND 7
1	-1.178	-0.326	-0.228	-0.125	-0.165	-0.104
2	-1.195	-0.354	-0.273	-0.122	-0.165	-0.123
3	-1.113	-0.342	-0.312	-0.186	-99999.0	-0.004
4	-1.033	-0.225	-0.255	-0.104	-0.040	-0.025
5	-0.835	-0.238	-0.327	-0.070	-0.025	0.002
6	-1.193	-0.300	-0.282	-0.140	-0.018	-0.016
7	-0.876	-0.198	-0.258	-0.049	0.012	-0.200
8	-1.087	-0.271	-0.283	-0.074	-0.013	-0.037
9	-0.982	-0.153	-0.261	-0.071	-0.018	0.000
10	-1.054	-0.125	-0.343	-0.036	-0.007	-0.030
11	-1.122	-0.178	-0.181	-0.054	-0.003	0.005
12	-0.798	-0.207	-0.305	-0.033	-0.027	-0.038
13	-1.078	-0.186	-0.236	-0.016	-0.019	-0.001
14	-0.899	-0.152	-0.230	-0.014	-0.017	-0.023
15	-1.168	-0.161	-0.240	-0 035	-0.087	-0.050
16	-0.892	-0.184	-0.238	-0.020	-0.097	-0.093
MEANODD	-1.044	-0.223	-0.255	-0.076	-0.044	-0.044
MEANEVN	-1.019	-0.227	-0.276	-0.068	-0.048	-0.048
MEANALL	-1.031	-0.225	-0.266	-0.072	-0.046	-0.046
MEANODD SD	0.132	0.073	0.047	0.055	0.052	0.074
MEANEVN SD	0.145	0.077	0.037	0.049	0.055	0.039
MEANALL SD	0.134	0.073	0.042	0.050	0.056	0.057
MEAN SPSD	0.034	0.018	0.011	0.013	0.015	0.014
MEANALL CV	-13.020	-32.323	-15.840	-70.033	-122.384	-123.245

STANDARD DEVIATION OF SHUTTER

CHANNEL	BAND 1	BAND 2	BAND 3	BAND 4	BAND 5	BAND 7
1	1.289	0.503	0.790	0.472	0.805	0.985
2	1.445	1.009	0.548	0.381	0.755	0.991
3	1.195	0.490	0.578	0.481	-99999.0	0.854
4	1.449	0.690	0.726	0.385	0.823	1.031
5	1.084	0.432	0.534	0.305	0.878	0.916
6	1.430	0.521	0.528	0.483	0.880	1.015
7	1.264	0.376	0.496	0.259	1.084	1.945
8	1.312	0.426	0.856	0.531	0.811	0.926
9	1.093	0.308	0.452	0.247	0.852	0.960
10	1.184	0.302	0.575	0.320	0.878	1.050
11	1.242	0.352	0.393	0.254	0.912	0.935
12	1.321	0.377	0.478	0.411	0.847	1.006
13	1.149	0.359	0.521	0.202	0.830	0.809
14	1.352	0.360	0.597	0.268	0.792	1.090
15	1.260	0.340	0.517	0.255	0.824	0.786
16	1.600	0.437	0.848	0.412	0.785	0.956
MEANODD	1.197	0.395	0.535	0.310	0.884	1.024
MEANEVN	1.387	0.515	0.644	0.399	0.821	1.008
MEANALL	1.292	0.455	0.590	0.354	0.850	1.016
MEANODD SD	0.090	0.072	0.117	0.107	0.095	0.379
MEANEVN SD	0.124	0.232	0.146	0.083	0.045	0.052
MEANALL SD	0.140	0.177	0.140	0.103	0.077	0.261
MEAN SPSD	0.035	0.044	0.035	0.026	0.020	0.065
MEANALL CV	10.863	38.949	23.729	29.211	9.050	25.723

MAXIMUM AND MINIMUM

CHANNEL	BAND 1	BAND 2	BAND 3	BAND 4	BAND 5	BAND 7
1	8/ 0	5/ 2	5/ 1	4/ 2	5/ 0	6/ 0
2	8/ 0	6/ 0	5/ 1	4/ 1	5/ 0	6/ 0
3	7/ 0	4/ 1	4/ 1	4/ 2	*** /***	6/ 0
4	7/ 0	5/ 0	4/ 1	3/ 1	6/ 0	6/ 0
5	6/ 0	4/ 1	4/ 1	4/ 1	6/ 0	6/ 0
6	8/ 0	4/ 1	4/ 1	4/ 1	6/ 0	6/ 0
7	8/ 0	4/ 1	4/ 1	3/ 1	8/ 0	11/ 0
8	6/ 0	4/ 1	5/ 1	4/ 1	5/ 0	6/ 0
9	6/ 0	4/ 1	4/ 1	3/ 1	6/ 0	6/ 0
10	6/ 0	4/ 1	5/ 1	4/ 1	6/ 0	7/ 0
11	6/ 0	4/ 1	4/ 1	3/ 1	6/ 0	6/ 0
12	8/ 0	4/ 1	4/ 1	4/ 1	5/ 0	6/ 0
13	6/ 0	4/ 1	4/ 1	3/ 1	6/ 0	5/ 0
14	8/ 0	4/ 1	4/ 1	3/ 1	5/ 0	7/ 0
15	6/ 0	4/ 1	4/ 1	4/ 1	6/ 0	5/ 0
16	8/ 0	4/ 1	5/ 1	4/ 2	5/ 0	6/ 0
MEANODD	6.63/.00	4.13/1.1	4.13/1.0	3.50/1.3	6.14/.00	6.38/.00
MEANEVN	7.38/.00	4.38/.75	4.50/1.0	3.75/1.1	5.38/.00	6.25/.00
MEANALL	7.00/.00	4.25/0.9	4.31/1.0	3.63/1.2	5.73/.00	6.31/.00
MEANODD SD	0.92/.00	.354/.35	.354/.00	.535/.46	.900/.00	1.92/.00
MEANEVN SD	0.92/.00	.744/.46	.535/.00	.463/.35	.518/.00	.463/.00
MEANALL SD	0.97/.00	.577/.44	.479/.00	.500/.40	.799/.00	1.35/.00
MEAN SPSD	.242/.00	.144/.11	.120/.00	.125/.10	.206/.00	.338/.00
MEANALL CV	13.8/***	13.6/47.	11.1/.00	13.8/34.	13.9/***	21.4/***

SHUTTER1 AVERAGE

CHANNEL	BAND 1	BAND 2	BAND 3	BAND 4	BAND 5	BAND 7
1	3.053	3.140	3.322	2.986	2.487	2.538
2	2.361	2.605	2.617	2.343	2.327	2.171
3	2.418	2.661	2.823	2.527	-99999.0	2.321
4	2.528	2.653	2.499	2.251	2.583	2.408
5	2.464	2.605	2.615	2.288	2.563	2.309
6	2.428	2.705	2.687	2.517	2.863	2.493
7	2.617	2.563	2.649	2.289	2.830	2.496
8	2.445	2.571	2.606	2.532	2.934	2.544
9	2.302	2.467	2.616	2.215	2.660	2.270
10	2.436	2.406	2.666	2.290	2.715	2.519
11	2.287	2.478	2.439	2.209	2.667	2.338
12	2.558	2.427	2.531	2.269	2.702	2.374
13	2.284	2.563	2.548	2.150	2.677	2.179
14	2.414	2.484	2.746	2.308	2.723	2.492
15	2.320	2.496	2.507	2.209	2.591	2.114
16	2.416	2.565	2.775	2.378	2.658	2.440
MEANODD	2.468	2.622	2.690	2.359	2.639	2.321
MEANEVN	2.448	2.552	2.641	2.361	2.688	2.430
MEANALL	2.458	2.587	2.665	2.360	2.665	2.375
MEANODD SD	0.263	0.220	0.279	0.278	0.108	0.143
MEANEVN SD	0.064	0.106	0.097	0.109	0.183	0.119
MEANALL SD	0.185	0.170	0.204	0.204	0.150	0.139
MEAN SPSD	0.046	0.043	0.051	0.051	0.039	0.035
MEANALL CV	7.527	6.590	7.637	8.639	5.623	5.867

DIFFERENCE BETWEEN FORWARD AND REVERSE AVERAGES

CHANNEL	BAND 1	BAND 2	BAND 3	BAND 4	BAND 5	BAND 7
1	-0.396	1.319	1.445	0.456	-0.727	-0.571
2	-0.692	1.091	0.929	0.273	-0.722	-0.569
3	-0.564	1.333	1.102	0.413	-99999.0	-0.073
4	-0.471	1.117	1.006	0.191	-0.101	-0.063
5	-0.386	1.344	1.227	0.469	-0.055	-0.047
6	-1.259	1.289	1.364	0.364	-0.089	-0.046
7	-0.448	1.232	1.224	0.410	-0.087	-0.246
8	-1.082	1.291	1.249	0.311	-0.066	-0.062
9	-0.458	1.303	1.522	0.320	-0.115	-0.061
10	-0.598	1.196	1.444	0.442	-0.092	-0.019
11	-0.369	1.273	1.329	0.344	-0.124	-0.049
12	-0.432	1.293	1.378	0.397	-0.086	-0.025
13	-0.198	1.452	1.426	0.366	-0.115	-0.055
14	-0.564	1.237	1.606	0.590	-0.119	-0.058
15	-0.060	1.330	1.411	0.442	-0.309	-0.162
16	-0.591	1.477	1.344	0.478	-0.306	-0.228
MEANODD	-0.360	1.323	1.336	0.402	-0.219	-0.158
MEANEVN	-0.711	1.249	1.290	0.381	-0.197	-0.134
MEANALL	-0.536	1.286	1.313	0.392	-0.207	-0.146
MEANODD SD	0.159	0.064	0.141	0.054	0.238	0.181
MEANEVN SD	0.298	0.121	0.225	0.125	0.225	0.188
MEANALL SD	0.294	0.101	0.183	0.094	0.223	0.179
MEAN SPSD	0.073	0.025	0.046	0.024	0.058	0.045
MEANALL CV	-54.830	7.865	13.913	24.019	-107.664	-122.500

STANDARD DEVIATION OF SHUTTER

CHANNEL	BAND 1	BAND 2	BAND 3	BAND 4	BAND 5	BAND 7
1	1.365	1.253	1.718	0.722	0.919	1.041
2	1.632	1.354	0.979	0.795	0.871	1.059
3	1.225	1.113	1.238	0.732	-99999.0	0.879
4	1.795	1.087	1.059	0.792	0.905	1.067
5	1.154	1.045	1.243	0.690	0.941	0.958
6	1.574	1.051	1.047	0.746	0.943	1.037
7	1.355	1.000	1.179	0.633	1.103	1.825
8	1.510	1.073	1.250	0.895	0.921	0.979
9	1.200	1.043	1.252	0.592	0.930	1.003
10	1.361	1.004	1.126	0.698	0.953	1.096
11	1.395	1.029	1.227	0.592	0.950	0.972
12	1.601	1.105	1.061	0.684	0.926	1.022
13	1.368	1.191	1.325	0.579	0.924	0.863
14	1.474	1.007	1.163	0.768	0.888	1.132
15	1.513	1.134	1.410	0.652	0.887	0.814
16	1.737	1.213	1.491	0.742	0.879	1.013
MEANODD	1.322	1.101	1.324	0.649	0.951	1.044
MEANEVN	1.586	1.112	1.147	0.765	0.911	1.051
MEANALL	1.454	1.106	1.236	0.707	0.929	1.048
MEANODD SD	0.119	0.088	0.174	0.061	0.070	0.325
MEANEVN SD	0.140	0.118	0.162	0.066	0.030	0.049
MEANALL SD	0.185	0.101	0.186	0.086	0.055	0.224
MEAN SPSD	0.046	0.025	0.047	0.021	0.014	0.056
MEANALL CV	12.748	9.108	15.074	12.116	5.867	21.403

MAXIMUM AND MINIMUM

CHANNEL	BAND 1	BAND 2	BAND 3	BAND 4	BAND 5	BAND 7
1	10/ 0	10/ 0	14/ 0	6/ 0	6/ 0	7/ 0
2	11/ 0	9/ 0	7/ 0	6/ 0	6/ 0	6/ 0
3	8/ 0	8/ 0	10/ 0	6/ 0	*** /***	6/ 0
4	13/ 0	6/ 0	6/ 0	6/ 0	6/ 0	8/ 0
5	8/ 0	6/ 0	9/ 0	5/ 0	6/ 0	6/ 0
6	8/ 0	7/ 0	5/ 0	6/ 0	6/ 0	6/ 0
7	9/ 0	6/ 0	9/ 0	5/ 0	7/ 0	10/ 0
8	7/ 0	8/ 0	8/ 0	6/ 0	7/ 0	6/ 0
9	9/ 0	6/ 0	9/ 0	5/ 0	8/ 0	7/ 0
10	9/ 0	6/ 0	5/ 0	6/ 0	6/ 0	9/ 0
11	11/ 0	6/ 0	9/ 0	5/ 0	6/ 0	6/ 0
12	10/ 0	8/ 0	5/ 0	6/ 0	6/ 0	6/ 0
13	11/ 0	8/ 0	10/ 0	5/ 0	6/ 0	6/ 0
14	9/ 0	6/ 0	6/ 0	6/ 0	6/ 0	6/ 0
15	12/ 0	8/ 0	11/ 0	6/ 0	6/ 0	6/ 0
16	9/ 0	9/ 0	11/ 0	6/ 0	6/ 0	6/ 0
MEANODD	9.8/.00	7.25/.00	10.1/.00	5.38/.00	6.43/.00	6.75/.00
MEANEVN	9.5/.00	7.38/.00	6.63/.00	6.00/.00	5.13/.00	6.63/.00
MEANALL	9.6/.00	7.31/.00	8.38/.00	5.69/.00	6.27/.00	6.69/.00
MEANODD SD	1.49/.00	1.49/.00	1.73/.00	.518/.00	.787/.00	1.39/.00
MEANEVN SD	1.85/.00	1.30/.00	2.07/.00	.000/.00	.354/.00	1.19/.00
MEANALL SD	1.63/.00	1.35/.00	2.58/.00	.479/.00	.594/.00	1.25/.00
MEAN SPSD	.197/.00	.338/.00	.645/.00	.120/.00	.153/.00	.313/.00
MEANALL CV	16.9/***	18.5/***	30.8/***	8.42/***	9.5/***	18.7/***

SHUTTER2 AVERAGE

CHANNEL	BAND 1	BAND 2	BAND 3	BAND 4	BAND 5	BAND 7
1	2.841	2.635	2.778	2.789	2.874	2.785
2	2.287	2.160	2.296	2.269	2.676	2.417
3	2.329	2.210	2.404	2.406	-99999.0	2.334
4	2.428	2.258	2.141	2.123	2.649	2.401
5	2.396	2.164	2.234	2.160	2.610	2.261
6	2.502	2.311	2.267	2.414	2.777	2.422
7	2.227	2.094	2.203	2.114	2.757	2.465
8	2.504	2.158	2.259	2.408	2.846	2.498
9	2.216	1.993	2.184	2.181	2.631	2.232
10	2.398	1.952	2.274	2.230	2.628	2.473
11	2.170	2.041	2.039	2.157	2.650	2.311
12	2.499	1.965	2.140	2.203	2.620	2.354
13	2.114	2.054	2.161	2.045	2.645	2.150
14	2.403	2.077	2.327	2.291	2.616	2.454
15	2.102	2.007	2.097	2.108	2.569	2.091
16	2.454	2.100	2.309	2.376	2.570	2.436
MEANODD	2.299	2.150	2.263	2.245	2.677	2.328
MEANEVN	2.434	2.123	2.252	2.289	2.673	2.432
MEANALL	2.367	2.136	2.257	2.267	2.675	2.380
MEANODD SD	0.241	0.210	0.234	0.244	0.104	0.217
MEANEVN SD	0.074	0.127	0.072	0.104	0.093	0.044
MEANALL SD	0.186	0.168	0.168	0.183	0.095	0.161
MEAN SPSD	0.046	0.042	0.042	0.046	0.024	0.040
MEANALL CV	7.841	7.876	7.421	8.059	3.535	6.745

DIFFERENCE BETWEEN FORWARD AND REVERSE AVERAGES

CHANNEL	BAND 1	BAND 2	BAND 3	BAND 4	BAND 5	BAND 7
1	1.278	2.600	1.970	1.289	0.084	0.074
2	1.680	2.613	2.092	1.654	0.073	0.079
3	1.387	2.595	1.980	1.897	-99999.0	0.010
4	1.638	2.234	2.202	1.550	0.013	0.020
5	0.980	2.419	2.370	1.711	-0.053	-0.011
6	1.229	2.668	2.568	1.801	0.001	-0.004
7	1.392	2.321	2.265	1.488	-0.048	0.156
8	1.278	2.672	2.558	1.608	0.009	0.043
9	1.405	2.580	2.818	1.826	-0.056	0.001
10	1.769	2.451	3.017	1.597	-0.033	-0.004
11	1.983	2.404	2.289	1.405	-0.043	0.014
12	1.311	2.673	2.813	1.763	-0.011	0.018
13	1.960	2.787	2.341	1.308	-0.007	0.026
14	1.568	2.484	2.742	1.921	0.016	0.029
15	2.494	2.579	2.304	1.693	0.116	0.112
16	1.152	2.850	2.653	1.446	0.167	0.184
MEANODD	1.611	2.536	2.292	1.577	-0.001	0.048
MEANEVN	1.453	2.581	2.581	1.667	0.030	0.046
MEANALL	1.532	2.558	2.437	1.622	0.015	0.047
MEANODD SD	0.492	0.147	0.264	0.236	0.071	0.060
MEANEVN SD	0.236	0.187	0.307	0.152	0.063	0.062
MEANALL SD	0.382	0.164	0.314	0.197	0.067	0.059
MEAN SPSD	0.095	0.041	0.079	0.049	0.017	0.015
MEANALL CV	24.918	6.417	12.889	12.157	436.003	126.056

STANDARD DEVIATION OF SHUTTER2

CHANNEL	BAND 1	BAND 2	BAND 3	BAND 4	BAND 5	BAND 7
1	1.251	1.544	1.326	0.833	0.857	1.011
2	1.610	1.679	1.264	1.031	0.817	0.988
3	1.211	1.508	1.221	1.132	-99999.0	0.861
4	1.568	1.438	1.399	1.023	0.874	1.029
5	1.049	1.433	1.412	1.036	0.905	0.912
6	1.513	1.538	1.494	1.086	0.907	1.016
7	1.309	1.385	1.363	0.902	1.094	1.800
8	1.490	1.536	1.591	1.101	0.843	0.939
9	1.178	1.503	1.616	1.099	0.896	0.969
10	1.438	1.437	1.708	1.036	0.898	1.069
11	1.488	1.421	1.383	0.893	0.928	0.940
12	1.430	1.546	1.608	1.120	0.885	1.004
13	1.356	1.598	1.418	0.843	0.884	0.830
14	1.537	1.460	1.587	1.167	0.862	1.096
15	1.595	1.505	1.413	1.053	0.856	0.753
16	1.716	1.625	1.615	0.940	0.817	0.967
MEANODD	1.297	1.487	1.394	0.974	0.917	1.009
MEANEVN	1.538	1.532	1.533	1.063	0.863	1.013
MEANALL	1.417	1.510	1.464	1.018	0.888	1.011
MEANODD SD	0.167	0.070	0.111	0.119	0.082	0.330
MEANEVN SD	0.095	0.088	0.142	0.070	0.034	0.051
MEANALL SD	0.181	0.080	0.143	0.105	0.065	0.228
MEAN SPSD	0.045	0.020	0.036	0.026	0.017	0.057
MEANALL CV	12.735	5.306	9.749	10.328	7.361	22.526

MAXIMUM AND MINIMUM

CHANNEL	BAND 1	BAND 2	BAND 3	BAND 4	BAND 5	BAND 7
1	7/ 0	5/ 0	5/ 0	4/ 1	5/ 0	6/ 0
2	8/ 0	8/ 0	5/ 0	4/ 0	5/ 0	6/ 0
3	6/ 0	5/ 0	5/ 0	4/ 0	*** /***	5/ 0
4	8/ 0	6/ 0	5/ 0	4/ 0	5/ 0	6/ 0
5	6/ 0	5/ 0	5/ 0	4/ 0	6/ 0	5/ 0
6	7/ 0	5/ 0	5/ 0	4/ 0	6/ 0	6/ 0
7	6/ 0	4/ 0	5/ 0	4/ 0	8/ 0	10/ 0
8	7/ 0	5/ 0	5/ 0	5/ 0	6/ 0	5/ 0
9	6/ 0	5/ 0	5/ 0	4/ 0	6/ 0	6/ 0
10	7/ 0	5/ 0	5/ 0	4/ 0	5/ 0	6/ 0
11	6/ 0	4/ 0	5/ 0	4/ 0	5/ 0	6/ 0
12	6/ 0	5/ 0	5/ 0	5/ 0	5/ 0	6/ 0
13	6/ 0	5/ 0	5/ 0	4/ 0	5/ 0	5/ 0
14	7/ 0	5/ 0	5/ 0	4/ 0	5/ 0	6/ 0
15	6/ 0	5/ 0	5/ 0	4/ 0	5/ 0	5/ 0
16	7/ 0	5/ 0	5/ 0	4/ 0	5/ 0	6/ 0
MEANODD	6.13/.00	4.75/.00	5.00/.00	4.00/.13	5.71/.00	6.00/.00
MEANEVN	7.13/.00	5.50/.00	5.00/.00	4.25/.00	5.25/.00	5.88/.00
MEANALL	6.63/.00	5.13/.00	5.00/.00	4.13/.06	5.47/.00	5.94/.00
MEANODD SD	.354/.00	.463/.00	.000/.00	.000/.35	1.11/.00	1.69/.00
MEANEVN SD	.641/.00	1.07/.00	.000/.00	.463/.00	.463/.00	.354/.00
MEANALL SD	.719/.00	.885/.00	.000/.00	.342/.25	.834/.00	1.18/.00
MEAN SPSD	.180/.00	.221/.00	.000/.00	.085/.06	.215/.00	.295/.00
MEANALL CV	10.8/***	17.3/***	.000/***	8.28/***	15.3/***	19.9/***

SHUTTER1 AVERAGE

CHANNEL	BAND 1	BAND 2	BAND 3	BAND 4	BAND 5	BAND 7
1	2.868	2.589	2.836	2.955	2.729	3.019
2	2.522	2.021	2.194	2.260	2.361	2.445
3	2.434	2.175	2.400	2.309	2.440	2.502
4	2.472	1.998	2.156	2.152	2.365	2.410
5	2.330	1.962	2.237	2.102	2.254	2.340
6	2.557	2.041	2.154	2.159	2.329	2.443
7	2.269	1.992	2.226	2.137	2.266	2.280
8	2.683	2.023	2.219	2.220	2.528	2.423
9	2.189	2.046	2.320	2.167	2.299	2.289
10	2.302	2.017	2.170	2.124	2.377	2.352
11	2.143	2.008	2.193	2.191	2.288	2.271
12	2.303	2.011	2.198	2.132	2.274	2.256
13	2.202	1.985	2.122	2.096	2.207	2.180
14	2.418	2.006	2.160	2.193	2.359	2.416
15	2.129	2.020	2.108	2.136	2.167	2.163
16	2.386	2.010	2.220	2.312	2.297	2.394
MEANODD	2.320	2.097	2.305	2.262	2.331	2.381
MEANEVN	2.455	2.016	2.184	2.194	2.361	2.392
MEANALL	2.388	2.056	2.245	2.228	2.346	2.386
MEANODD SD	0.243	0.209	0.235	0.288	0.179	0.278
MEANEVN SD	0.131	0.013	0.028	0.066	0.076	0.063
MEANALL SD	0.201	0.149	0.173	0.205	0.134	0.195
MEAN SPSD	0.050	0.037	0.043	0.051	0.034	0.049
MEANALL CV	8.426	7.255	7.726	9.197	5.715	8.171

DIFFERENCE BETWEEN FORWARD AND REVERSE AVERAGES

CHANNEL	BAND 1	BAND 2	BAND 3	BAND 4	BAND 5	BAND 7
1	0.089	0.206	0.081	0.018	0.229	0.268
2	0.087	0.115	0.041	0.052	0.185	0.205
3	0.021	0.132	0.063	0.041	0.197	0.194
4	0.061	0.069	0.030	0.013	0.168	0.175
5	0.069	0.081	0.065	0.018	0.166	0.158
6	0.056	0.044	0.018	0.006	0.089	0.134
7	0.034	0.061	0.058	0.015	0.124	0.118
8	0.045	0.019	0.020	-0.014	0.088	0.083
9	0.039	0.049	0.034	0.015	0.115	0.084
10	0.030	0.015	0.010	-0.020	0.071	0.071
11	0.034	0.036	0.009	0.010	0.048	0.054
12	0.009	0.015	-0.008	-0.025	0.028	0.022
13	0.018	0.022	0.016	-0.002	0.037	-0.008
14	0.022	0.007	-0.014	-0.037	-0.004	-0.011
15	0.011	0.027	0.008	0.010	0.000	0.005
16	0.026	0.011	0.001	-0.045	-0.004	-0.008
MEANODD	0.039	0.077	0.042	0.016	0.115	0.109
MEANEVN	0.042	0.037	0.012	-0.009	0.078	0.084
MEANALL	0.041	0.057	0.027	0.003	0.096	0.097
MEANODD SD	0.027	0.063	0.029	0.012	0.081	0.095
MEANEVN SD	0.025	0.038	0.019	0.031	0.072	0.082
MEANALL SD	0.025	0.054	0.028	0.026	0.076	0.087
MEAN SPSD	0.006	0.014	0.007	0.007	0.019	0.022
MEANALL CV	61.523	95.388	102.885	778.120	79.542	89.825

STANDARD DEVIATION OF SHUTTER

CHANNEL	BAND 1	BAND 2	BAND 3	BAND 4	BAND 5	BAND 7
1	0.973	0.524	0.645	0.240	0.820	0.906
2	0.967	0.428	0.450	0.439	0.828	0.959
3	0.940	0.409	0.587	0.462	0.916	0.893
4	1.009	0.296	0.486	0.359	0.933	0.908
5	0.846	0.321	0.559	0.303	0.869	0.835
6	0.930	0.207	0.427	0.366	0.841	0.941
7	0.829	0.295	0.506	0.344	1.265	0.862
8	0.993	0.163	0.451	0.414	0.865	1.000
9	0.772	0.267	0.571	0.373	1.036	1.263
10	0.853	0.157	0.426	0.330	1.303	0.972
11	0.854	0.329	0.453	0.393	0.825	0.882
12	0.867	0.172	0.736	0.339	0.955	0.977
13	0.811	0.294	0.484	0.295	0.855	0.772
14	0.975	0.156	0.410	0.395	0.833	0.942
15	0.762	0.308	0.433	0.343	0.815	0.787
16	0.909	0.306	0.523	0.465	0.849	0.897
MEANODD	0.849	0.343	0.530	0.344	0.925	0.900
MEANEVN	0.938	0.236	0.488	0.388	0.926	0.919
MEANALL	0.893	0.290	0.509	0.366	0.926	0.925
MEANODD SD	0.075	0.084	0.073	0.068	0.155	0.154
MEANEVN SD	0.058	0.099	0.106	0.048	0.159	0.035
MEANALL SD	0.079	0.105	0.091	0.061	0.152	0.111
MEAN SPSD	0.020	0.026	0.023	0.015	0.038	0.028
MEANALL CV	8.890	36.121	17.784	16.751	16.425	12.017

MAXIMUM AND MINIMUM

CHANNEL	BAND 1	BAND 2	BAND 3	BAND 4	BAND 5	BAND 7
1	6/ 0	4/ 1	5/ 1	4/ 2	6/ 0	6/ 0
2	6/ 0	4/ 0	4/ 1	3/ 2	7/ 0	35/ 0
3	6/ 0	4/ 1	5/ 0	4/ 1	7/ 0	19/ 0
4	6/ 0	4/ 1	4/ 1	3/ 1	6/ 0	5/ 0
5	5/ 0	4/ 1	4/ 0	3/ 2	6/ 0	5/ 0
6	6/ 0	3/ 1	4/ 1	3/ 2	5/ 0	5/ 0
7	5/ 0	3/ 1	4/ 1	3/ 2	6/ 0	6/ 0
8	6/ 0	4/ 1	4/ 1	4/ 2	6/ 0	6/ 0
9	5/ 0	4/ 1	5/ 1	3/ 2	78/ 0	130/ 0
10	6/ 0	3/ 1	4/ 1	3/ 2	8/ 0	6/ 0
11	5/ 0	3/ 1	4/ 1	3/ 2	6/ 0	6/ 0
12	6/ 0	3/ 1	4/ 0	3/ 2	6/ 0	6/ 0
13	5/ 0	3/ 1	4/ 1	3/ 2	6/ 0	5/ 0
14	7/ 0	3/ 1	4/ 1	3/ 2	6/ 0	6/ 0
15	6/ 0	4/ 1	4/ 1	3/ 2	5/ 0	5/ 0
16	7/ 0	4/ 0	4/ 1	4/ 1	5/ 0	5/ 0
MEANODD	5.38/.00	3.63/1.0	4.38/.75	3.25/1.9	15.0/.00	22.8/.00
MEANEVN	6.25/.00	3.50/.75	4.00/.88	3.25/1.8	6.13/.00	9.3/.00
MEANALL	5.81/.00	3.56/.88	4.19/.81	3.25/1.8	10.6/.00	16.0/.00
MEANODD SD	.518/.00	.518/.00	.518/.46	.463/.35	25.5/.00	43.6/.00
MEANEVN SD	.463/.00	.515/.46	.000/.35	.463/.46	0.99/.00	10.4/.00
MEANALL SD	.555/.00	.512/.34	.403/.40	.447/.40	18.0/.00	31.4/.00
MEAN SPSD	.164/.00	.128/.09	.101/.10	.112/.10	4.50/.00	7.85/.00
MEANALL CV	11.3/***	14.4/39.	9.6/50.	13.8/22.	170./***	196./***

SHUTTER AVERAGE

CHANNEL	BAND 1	BAND 2	BAND 3	BAND 4	BAND 5	BAND 7
1	2.921	2.858	2.847	2.739	2.820	2.763
2	2.430	2.349	2.228	2.125	2.548	2.389
3	2.483	2.477	2.486	2.310	-99999.0	2.365
4	1.596	2.378	2.329	2.177	2.580	2.361
5	2.488	2.266	2.249	2.078	2.674	2.222
6	2.502	2.449	2.241	2.224	2.757	2.346
7	2.352	2.220	2.254	2.060	2.720	2.531
8	2.253	2.248	2.493	2.440	2.878	2.454
9	2.288	2.134	2.304	2.055	2.632	2.249
10	2.010	2.105	2.214	2.056	2.644	2.416
11	2.250	2.232	2.098	2.046	2.617	2.269
12	1.747	2.137	2.130	2.054	2.565	2.296
13	2.216	2.188	2.137	2.032	2.659	2.166
14	2.462	2.137	2.268	2.048	2.560	2.363
15	2.299	2.165	2.085	2.041	2.665	2.113
16	2.496	2.200	2.279	2.029	2.614	2.363
MEANODD	2.413	2.317	2.308	2.170	2.684	2.335
MEANEVN	2.187	2.250	2.273	2.144	2.656	2.374
MEANALL	2.300	2.284	2.290	2.157	2.669	2.354
MEANODD SD	0.228	0.242	0.254	0.247	0.068	0.215
MEANEVN SD	0.360	0.128	0.106	0.138	0.111	0.047
MEANALL SD	0.314	0.190	0.189	0.194	0.092	0.152
MEAN SPSD	0.078	0.048	0.047	0.049	0.024	0.038
MEANALL CV	13.648	8.338	8.250	8.995	3.436	6.454

DIFFERENCE BETWEEN FORWARD AND REVERSE AVERAGES

CHANNEL	BAND 1	BAND 2	BAND 3	BAND 4	BAND 5	BAND 7
1	0.221	0.156	0.259	0.114	0.024	0.005
2	0.153	0.104	0.054	0.089	0.064	0.059
3	0.212	0.171	0.171	0.193	-99999.0	-0.002
4	0.166	0.056	0.057	0.105	0.037	0.040
5	0.182	0.124	0.177	0.101	-0.038	-0.014
6	0.143	0.108	0.050	0.130	0.018	0.031
7	0.208	0.135	0.137	0.080	-0.032	0.044
8	0.132	0.125	0.082	0.093	0.026	0.019
9	0.234	0.118	0.197	0.079	-0.037	-0.034
10	0.132	0.071	0.082	0.058	0.007	0.030
11	0.299	0.139	0.139	0.073	-0.046	-0.008
12	0.155	0.082	0.052	0.061	0.028	0.043
13	0.332	0.149	0.186	0.059	-0.025	0.003
14	0.111	0.079	0.042	0.065	0.015	0.038
15	0.346	0.142	0.207	0.072	0.054	0.053
16	0.091	0.095	0.133	0.043	0.100	0.122
MEANODD	0.255	0.142	0.184	0.096	-0.014	0.006
MEANEVN	0.135	0.090	0.070	0.081	0.037	0.048
MEANALL	0.195	0.116	0.127	0.089	0.013	0.027
MEANODD SD	0.062	0.017	0.039	0.043	0.038	0.029
MEANEVN SD	0.025	0.022	0.029	0.029	0.031	0.032
MEANALL SD	0.077	0.033	0.068	0.036	0.042	0.037
MEAN SPSD	0.019	0.008	0.017	0.009	0.011	0.009
MEANALL CV	39.281	28.407	53.155	40.927	323.843	137.313

STANDARD DEVIATION OF SHUTTER

CHANNEL	BAND 1	BAND 2	BAND 3	BAND 4	BAND 5	BAND 7
1	1.259	0.681	1.278	0.590	0.844	1.017
2	1.326	0.985	0.587	0.440	0.768	1.022
3	1.148	0.627	0.845	0.558	-99999.0	0.867
4	1.155	0.680	0.706	0.493	0.847	1.055
5	1.115	0.549	0.757	0.370	0.910	0.917
6	1.290	0.553	0.468	0.493	0.913	1.010
7	1.297	0.491	0.688	0.320	1.095	1.965
8	1.152	0.523	0.877	0.594	0.890	0.951
9	1.120	0.453	0.675	0.304	0.891	0.984
10	0.960	0.392	0.468	0.318	0.913	1.065
11	1.327	0.524	0.670	0.320	0.918	0.961
12	1.121	0.472	0.381	0.285	0.889	0.989
13	1.296	0.592	0.796	0.378	0.873	0.829
14	1.269	0.387	0.546	0.335	0.873	1.091
15	1.425	0.592	0.906	0.401	0.856	0.792
16	1.553	0.461	0.988	0.277	0.828	0.961
MEANODD	1.248	0.564	0.827	0.405	0.912	1.042
MEANEVN	1.228	0.557	0.628	0.404	0.865	1.018
MEANALL	1.238	0.560	0.727	0.405	0.887	1.030
MEANODD SD	0.111	0.074	0.201	0.110	0.085	0.381
MEANEVN SD	0.175	0.197	0.213	0.117	0.049	0.050
MEANALL SD	0.142	0.144	0.225	0.110	0.070	0.263
MEAN SPSD	0.035	0.036	0.056	0.027	0.018	0.066
MEANALL CV	11.485	25.701	30.953	27.077	7.888	25.524

MAXIMUM AND MINIMUM

CHANNEL	BAND 1	BAND 2	BAND 3	BAND 4	BAND 5	BAND 7
1	10/ 0	7/ 0	13/ 0	6/ 0	6/ 0	6/ 0
2	8/ 0	6/ 0	5/ 0	5/ 1	6/ 0	7/ 0
3	9/ 0	6/ 0	9/ 0	5/ 0	*** /***	6/ 0
4	11/ 0	5/ 0	5/ 0	5/ 0	6/ 0	7/ 0
5	9/ 0	5/ 0	8/ 0	5/ 0	6/ 0	5/ 0
6	6/ 0	5/ 1	4/ 1	5/ 1	7/ 0	6/ 0
7	10/ 0	5/ 0	7/ 0	5/ 1	7/ 0	11/ 0
8	6/ 0	6/ 1	5/ 0	5/ 1	8/ 0	7/ 0
9	9/ 0	5/ 0	7/ 0	5/ 1	6/ 0	6/ 0
10	8/ 0	5/ 0	4/ 1	5/ 1	6/ 0	7/ 0
11	10/ 0	5/ 0	8/ 0	5/ 0	6/ 0	6/ 0
12	11/ 0	6/ 0	4/ 1	5/ 1	6/ 0	6/ 0
13	13/ 0	6/ 0	9/ 0	5/ 0	5/ 0	5/ 0
14	6/ 0	5/ 1	5/ 0	5/ 1	6/ 0	8/ 0
15	13/ 0	6/ 0	9/ 0	5/ 0	5/ 0	5/ 0
16	9/ 0	5/ 0	9/ 0	5/ 1	6/ 0	6/ 0
MEANODD	10.4/.00	5.63/.00	8.75/.00	5.13/.25	5.86/.00	6.25/.00
MEANEVN	8.13/.00	5.38/.38	5.13/.38	5.00/.88	6.38/.00	6.75/.00
MEANALL	9.3/.00	5.50/.19	6.94/.19	5.06/.56	6.13/.00	6.50/.00
MEANODD SD	1.69/.00	.744/.00	1.91/.00	.354/.46	.690/.00	1.98/.00
MEANEVN SD	2.10/.00	.518/.52	1.64/.52	.000/.35	.744/.00	.707/.00
MEANALL SD	2.18/.00	.632/.40	2.54/.40	.250/.51	.743/.00	1.46/.00
MEAN SPSD	.544/.00	.158/.10	.636/.10	.053/.13	.192/.00	.365/.00
MEANALL CV	23.5/***	11.5/***	36.6/***	4.94/91.	12.1/***	22.5/***

APPENDIX 9.13

RECOMMENDATIONS

TM RADIOMETRIC CHARACTERIZATION

6.1 ENGINEERING CHARACTERIZATION OF THE TM SENSOR

6.1.1 RECALIBRATE INTEGRATING SPHERE USED IN PRE-LAUNCH CALIBRATION

- ●.1 48" TM Integrating Sphere
  - o.1 SBRC
  - o.2 GSFC
  - o.3 NBS
- ●.2 Two 30" MSS Spheres
- ●.3 MMR 8-Band Field Radiometer

6.1.2 ANALYZE RELATIVE RADIOMETRY OF PRE-LAUNCH DATA ON 42 TRACK TAPES

6.1.3 EMPLOY ENGINEERING MODEL TM TESTS TO INVESTIGATE SOURCE OF:

- ●.1 Bin-Radiance Dependence (Unequal Bins)
- ●.2 Coherent Noise (Stationary and Time-Dependent)
- ●.3 Within-Line Droop
- ●.4 Bright Target Saturation (Recovery)
- ●.5 Scan-Correlated Shifts
- ●.6 IC Pulse Temperature-Dependence
- ●.7 "Secondary" Light Pulse in Calibration Region
- ●.8 Apparent Gain Changes with Time

6.1.4 PRODUCE FINAL REPORT DESCRIBING TM PERFORMANCE CHARACTERISTICS

6.2 FLIGHT SEGMENT OPERATIONS

6.2.1 INSTITUTE CHANGES IN OPERATIONAL PROCEDURES

- ●.1 Stop Routine Operation of IC Automatic Sequencer

- .2 Alternate Black Body Temperatures "T2" and "T3"
- .3 Set Outgassing Strategy at 20% Band 6 Gain Loss

6.2.2 PERFORM IN-ORBIT CALIBRATION TESTS

- .1 Calibrate Temperature-Dependence of IC Pulses

6.2.3 PERFORM IN-ORBIT CHARACTERIZATION TESTS

- .1 Redundant Power Supply Noise
- .2 Manual IC Operation with Automatic Sequencer off
- .3 "Override" Back-Up IC Operation
- .4 Coherent Noise Phasing Relative to Midscan Pulse
- .5 Noise with DC Restoration off

6.2.4 PERFORM IN-ORBIT SCIENTIFIC MISSION TESTS

- .1 Subsampled Extension of Swath Width, No Shutter
- .2 Bidirectional Reflectance by Off-Nadir Pointing
- .3 Intensive Single Site Acquisition by Pointing
- .4 TM/F and TM/PF Stereo by Pointing
- .5 TM/F and MSS/F (High Gain) Bathymetry
- .6 TM Single S/C Stereo
  - o.1 Fore/Aft
  - o.2 Side-to-Side

6.3 TIPS GROUND PROCESSING

6.3.1 PROVIDE FOR FUTURE CHANGE IN RADIOMETRIC CALIBRATION PARAMETERS

- .1 Post-Calibration Dynamic Range (RMIN, RMAX)
- .2 Spectral Radiance for each IC Lamp level
- .3 Averaged Pulse for each IC Lamp Level
- .4 Pre-Launch Gains and Offsets
- .5 Calculated Pre-Launch Nominal IC Pulses

6.3.2 PROVIDE FOR CHANGES IN IC SYSTEMATIC RADIOMETRIC CORRECTION PROCEDURES INVOLVING:

- ●.1 Two Background Shutter Collects (avoid DC Restore)
- ●.2 Within-Scene Corrections
  - o.1 Bin-Radiance Dependence
  - o.2 Coherent Noise
  - o.3 Scan-Correlated Shifts
- ●.3 Background Outliers (Incomplete Obscuration)
- ●.4 "Secondary" Light Pulse in Calibration Region
  - o.1 Search 80 to 148 mf Collect Window
- ●.5 Pulse Integration Parameters
  - o.1 Optimize Integration Width (near 39 mf)
- ●.6 Pulse Averaging
  - o.1 Separate Forward and Reverse Scans
- ●.7 Lamp State Options
  - o.1 Reject 111 State for any Regression
  - o.2 Omit 000 State when possible
  - o.3 Omit Shutter Background when possible
  - o.4 Permit any States and Background
- ●.8 IC Pulse Temperature-Dependence
- ●.9 Between-Channel Correlations
  - o.1 Between-Band Absolute Radiometry
  - o.2 Quality Assurance Redundancy Check
- ●.10 Within-Pulse Smoothing
- ●.11 Between-Date Smoothing
- ●.12 Reference Channels or Variance Weighting
- ●.13 Statistical Quality Indices

6.3.3 MODIFY HISTOGRAM EQUALIZATION PROCEDURE TO PROVIDE FOR:

- ●.1 Optional 1st pass HDT-RT Histogram
- ●.2 Line-by-line Systematic Correction
- ●.3 2nd Pass HDT-RT 11-Bit Histogram
- ●.4 HDT-AT 11-Bit Histogram and File
- ●.5 Histogram Reference to "Quiet" Channel
- ●.6 Histogram Monitoring of IC Quality
- ●.7 Weighting of IC and Histogram Constants
- ●.8 HDT-PT Histogram File for each Band

6.3.4 MODIFY GEOMETRIC PROCESSING PROCEDURES TO PROVIDE FOR:

- ●.1 Single Pass Image Rectification (Geodetic) Product
- ●.2 Geocoded Map Compatibility
  - o.1 UTM Resampling as Standard
- ●.3 Single Pass Cubic Spline Resampling
- ●.4 Image Co-ordinate File for GCPs
- ●.5 Relative GCPs
- ●.6 Alternative Global GCP Library Build

6.3.5 PROVIDE THREE-SECTIONED POST-CALIBRATION DYNAMIC RANGE

6.3.6 MODIFY IMAGE CALIBRATION PROCEDURE TO PROVIDE FOR:

- ●.1 Non-Adjacent Channel Replacement Algorithm
- ●.2 Probabilistic Approach

6.3.7 PROVIDE THE FOLLOWING PRODUCTS

- ●.1 Semi-weekly Tapes of Raw Calibration Data
- ●.2 Semi-weekly "Unity" CCT-AT
- ●.3 Special "Unity" CCT-AT of Calibration Region
- ●.4 Reprocessed "Reference" Scenes
- ●.5 History Tapes Tapes of Calibration Constants
- ●.6 Selected HDT-RT Copies
- ●.7 Extra Band(s) of Binary Data
- ●.8 Extra Band(s) of 8-Bit Data
- ●.9 Tapes at Reduced Resolution
- ●.10 Cloud-free Global TM Archive by Season
- ●.11 "Unity" HDT-AT and CCT-AT as Standard, with PCD

6.3.8 RESEARCH AND DEVELOP PROCEDURES FOR:

- ●.1 Within-Line Processing
- ●.2 Band 6 Processing
- ●.3 Ingestion of Foreign TM Tapes
- ●.4 Full Interval Radiometric Processing
- ●.5 Creation and Processing of Pre-Launch Data
- ●.6 GPS Test to Reduce Control Point Neighborhood Size

6.4 DEVELOP PROCEDURES FOR POSSIBLE CONTINGENCY EXPERIMENTS

●.1 SCIENTIFIC EXPERIMENTS

- ●.1 Lunar Radiometric Calibration
- ●.2 Stero and Bidirectional Reflectance
- ●.3 Time-of-Day Orbital Changes
- ●.4 Revisit Frequency Requirements
- ●.5 Utility of Mixed Spatial Resolution

- .2 ENGINEERING EXPERIMENTS
  - .1 Band 6 Sensitivity at70 K
  - .2 Focus Test on Inchworms over GCPs
  - .3 Tests of Global Position System Utility
  - .4 Tests of On-Board Computer Options
  - .5 Alternative Lamp and Power Supply Tests
  - .6 Recalibration Before and After In-Orbit Repair

APPENDIX 9.14 - KEY WORDS

Absolute Radiometry

Apparent Gain Changes

Archival TM Imagery of Globe, Recommendation

Atmospheric Peeling

Automatic Sequencer

Background from Shutter

Between-Band Gain Changes

Between-Date TM Radiometry

Between-Date Smoothing, Recommendations

Between-Scan Shifts, see Scan-Correlated Shifts

Between-Scene Gain Changes

Bidirectional Reflectance, Recommendations

Bin-Radiance Dependence

Bright Target Saturation (Recovery)

Calibration

Calibrator, Internal (IC)

Channel-Correlated Shifts, see Scan-Correlated Shifts

Coherent Noise

Contingency Experiments for TM on Landsat, Recommendations

Dark Current Restoration (DC Restore)

DC Restoration

"Droop" within a Line of TM Imagery

Dynamic Range after TM Radiometric Calibration, Post-Calibration